AD NUMBER: AD0895930
LIMITATION CHANGES
TO: Approved for public release; distribution is unlimited.
FROM: Distribution authorized to U.S. Government. agencies and their contractors; Administrative/Operational Use; 1 Aug 1949. Other requests shall be referred to Office of Naval Research, Arlington, VA 22203.
AUTHORITY
ST-A NTIS per ONR LTR dtd 26 OCT 1977

COLLINS RESEARCH REPORT

CRR 102

Copy No. 35

COLLINS

Contract No.: N7onr-414 Task I June 20, 1947

INTERIM REPORT ON

MICROWAVE RADIOMETRY PROJECT

1 August 1949

Department of Navy
Office of Naval Research

COLLINS RADIO COMPANY
CEDAR RAPIDS, IOWA, U. S. A.

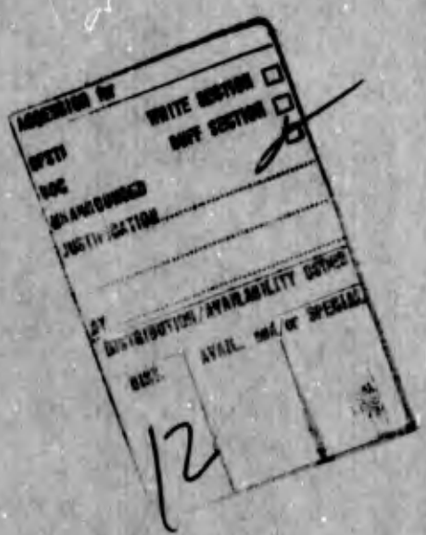
ACCESSION for
NTIS WHITE SECTION
DDC BUFF SECTION
UNANNOUNCED
JUSTIFICATION
BY
DISTRIBUTION/AVAILABILITY CODES
DIST. AVAIL. and/or SPECIAL
12

(14) CRR-102

[redacted]

(9) INTERIM REPORT,

ON THE

(6) MICROWAVE RADIOMETRY PROJECT.

OF THE

COLLINS RADIO COMPANY

This report is submitted in partial fulfillment of contract N7onr-414 Task I between the Collins Radio Company and the Office of Naval Research

(15) N7onr-414(01) (11) August 1949 (12) 177 p.

PREPARED BY:

(10) C. M. Hepperle, Project Leader
W. E. Giberson, Research Engineer
H. J. Malandrinos, Research Engineer
R. M. Ringoen, Research Engineer

APPROVED BY:

D. C. McCoy
Research Physicist

W. W. Forley 3rd
Asst. Director of Research

Asst. Inspector of
Naval Material

COLLINS RADIO COMPANY

Cedar Rapids, Iowa

MR 1087 800

TABLE OF CONTENTS

LIST OF ILLUSTRATIONS

NOMENCLATURE

Black Body Theory
Section 2.1

A	Effective area of collector - $cm.^2$
A_r	Area of isotropic reflector - $cm.^2$
a	Fractional power absorption $\frac{\text{(power absorbed by body)}}{\text{(power incident on body)}}$
a_o	Fractional power absorption for a unit atmosphere
C	Antenna factor $\left(\frac{1}{4\pi} \int_\Omega G(\theta, \phi) d\Omega\right)$
c	Velocity of light in a vacuum ($3 \cdot 10^{+10}$ cm/sec)
d	Depth of radiating body - cm.
Δf	Frequency interval - cycles per second
G	Antenna gain over an isotropic radiator
h	Planck's constant
i_λ	Rate at which a body radiates energy in a given direction per unit solid angle and per unit of its own area as projected on a plane perpendicular to the given direction
k	Boltzmann's constant - 1.381×10^{-23} joules/mol./deg. K.
m	Coefficient of reflectivity $\frac{\text{(power reflected)}}{\text{(power incident)}}$
m_s	Reflectivity of radiating surface
m_r	Reflectivity of reflecting surface
P	Power - watts
P_r	Power received by collector - watts
T	Temperature in degrees Kelvin
T_m	Temperature of atmosphere weighted against absorption (degrees K.)

T_r Equivalent antenna temperature - deg. K

T_s Temperature of radiating body - deg. K

T_θ Antenna temperature when pointed at atmosphere at angle θ - deg. K

a Attenuation constant - nepers per unit length

a_o Attenuation per unit atmosphere - nopers

θ Spherical coordinate angle; angle from the zenith

λ Wavelength in centimeters

ρ Distance from collector to radiating body - cm.

ψ_λ Density of Radiation - the radiant energy per unit volume in a stream of radiation at the wavelength, λ

Ω Solid angle - steradians

Ω_r Solid angle subtended by reflector at antenna

Ω_s Solid angle subtended by radiating surface at reflecting body

RECEIVER DESIGN
Section 2.2

b Bandwidth of low pass filter (sec^{-1})

C_A Total primary capacitance - farads

C_B Total secondary capacitance - farads

E_D D.C. voltage developed across diode load resistor with antenna looking at source - volts

E_o D.C. voltage developed across diode load resistor with reference connected - volts

Δf_{IF} I.F. amplifier bandwidth - cycles per second

f_o Center frequency of I.F. Amplifier - cycles per second

f_1 Open-circuited primary frequency - cycles per second

f_2	Open-circuited secondary frequency - cycles per second
G_A	Signal source conductance - mhos
G_B	Lumped conductance of secondary side of transformer - mhos
G_g	Conductive component of tube input impedance - mhos
G_s	Transformed source conductance - mhos
g_c	Conversion gain of crystal expressed as a power ratio
g_2	I.F. amplifier power gain expressed as a power ratio
K	Coefficient of Coupling
L_A	Primary inductance - henries
L_B	Secondary inductance - henries
L_c	Crystal conversion loss expressed as a power ratio
NF_c	Noise figure of the crystal converter - ratio
NF_{IF}	I.F. amplifier noise figure - ratio
NF_{REC}	Receiver noise figure - ratio
P_A	Noise power output of the attenuator - watts
P_C	Noise power output of the crystal - watts
P_{IF}	Noise Power output of the I.F. amplifier - watts
P_m	Minimum detectable signal power - watts
P_R	Power output of the antenna circuit - watts
R_A	Equivalent antenna resistance - ohms
R_g	Vacuum tube loading due to transit-time loading and lead inductance effects - ohms
R_s	Transformed source resistance - ohms
R_t	Equivalent noise resistance of the input tube - ohms
ΔT	R.M.S. temperature fluctuations of the output meter - degrees K.

T_{moon}	Black body temperature of moon - degrees K.
T_{sun}	Black body temperature of sun - degrees K.
T_o	The reference temperature
t_a	Ratio between antenna temperature and reference temperature
t_c	Noise temperature of crystal expressed as a ratio
β	A constant equating the noise due to active grid loading to Johnson noise from a resistor
n	Diode efficiency expressed as a fraction

SERVO DESIGN
Section 3.2.4.5

A	Azimuth angle - degrees
h	Elevation angle - degrees
t	Hour angle - degrees
δ	Declination - degrees
ϵ_A	Azimuth tracking error - degrees
ϵ_h	Elevation tracking error - degrees
ϕ	Latitude of observer - degrees
ω_A	Velocity of sun in azimuth - deg/hr.
ω_h	Velocity of sun in elevation - deg/hr.

ABSTRACT

The following report presents the results of work done on the theory, design and application of microwave radiometry equipment. In the first section a brief historical outline and a delineation of the purpose of the work is given. The second section is devoted to the development of microwave black body and detection theory that is pertinent to the design and application of microwave radiometers.

The third section is devoted to discussions of the basic components of microwave radiometers and to the description of the work done on four radiometer systems. The quality of the data from two of these systems -- the K-Band Radio Telescope and the Automatic Radio Sextant -- is presented. The Automatic Radio Sextant utilizes the thermal emission at microwave frequencies from the sun as a means of continuously tracking the sun under all weather conditions. For the weather conditions encountered during tests the sextant tracked the sun in elevation with following errors ranging from 0.005° to 0.018° for elevation angles in excess of 5°.

The fourth and last section is a discussion of astronomical observations and military applications of microwave radiometry. Measurements of the sun and moon at a wavelength of 1.25 cm. indicate that the black body temperatures of these two bodies are 11,600° K and 260° K respectively. Data taken during a total eclipse of the moon reveals that the radiation from the eclipsed moon at a wavelength of 1.25 cm. is essentially the same as that from the full moon.

It is concluded that the Automatic Radio Sextant for all-weather navigation is a practical application of microwave radiometry. Calculated results are presented which show the detection of small targets such as aircraft and vessels by microwave radiometry methods is not feasible at the present state of the art.

SECTION 1

FINAL REPORT ON

MICROWAVE RADIOMETRY RESEARCH

1. INTRODUCTION

1.1. History

The effort directed toward the study of microwave radiometry under this contract was begun in July of 1947. Prior to this time the Collins Radio Company had sponsored a project for construction of a K-band radiometer. The work was started along three main channels: A study of the literature, an investigation of noise in receivers, and a consideration of equipment. By November of 1947 refinements in the construction of a K-band radiometer and the initial construction of a ten-centimeter radiometer were under way. An automatic radio sextant was envisioned, and test equipment for noise figure measurement was installed. In August of 1948, the RF components for the ten-centimeter radiometer were completed and adequate I.F. strip and R.F. assemblies had been constructed; research on a three-millimeter radiometer had been initiated; a K-band radiometer was operating satisfactorily, and the ground work for the radio sextant was completed. In the months since August 1948, the work consisted of completing the automatic radio sextant and compiling a considerable amount of data on the performance of the sextant and the K-band radiometer.

At the termination of the contract, sufficient theory had been derived or investigated to support the experimental conclusions obtained from the constructed equipment. A theoretical analysis of the reception of thermal radiation at radio frequencies with highly directional antennas, an analysis of the over-all limiting sensitivity of a radiometer, and an investigation of the thermal radiation received from various types of bodies have been completed.

1.2. Purpose

The scope of the work was made rather broad; it was, however, to include:

a. Studies of the generation, propagation, and reception of microwave emission due to temperature, particularly associated with propagation through the atmosphere, and consideration of problems encountered with electronic measurements at extremely low power levels.

b. The design and construction of equipment for possible military application and to facilitate the associated studies.

c. An investigation of the usefulness of microwave thermal emission from military objects; i.e. moon, sun, stars, earth, landmarks, aircraft and ships.

1.3. Scope of the Report

This report is accordingly divided into three major parts; the theory, the equipment, and the results. Contributions to the general knowledge are to be found in each: in the theoretical consideration of the overall response of a receiver to low-level noise power, in the successful development of an automatic radio sextant; and in the result that the sun is at present the sole useful source for military application.

SECTION 2

2. THEORY OF RADIOMETRY

2,1. Microwave Black Body Theory

It has long been known that all bodies emit thermal radiation throughout the frequency spectrum, and that the intensity of this radiation is some function of the temperature of the body and the wavelength of the radiation. Considerable work, both theoretical and experimental, has been done to determine what law or function this radiation follows. Until recently, the emphasis in experimental work was placed on the ultra-violet, optical, and infrared spectrums, for measuring techniques had been developed for these frequencies which permitted the accurate determination of intensities and wavelengths. The experimental results indicated that the law governing radiation which was introduced by Planck at the turn of the century gave correct answers for the spectral ranges mentioned above.

Planck's radiation law predicted that some energy, although of a much lower level, should be radiated at wavelengths much longer than infrared. The incorporation of new microwave techniques and special electronic circuitry in modern receivers has permitted the investigation of this low power thermal radiation. Its study in the wavelength range from 12 cm down to the shortest wavelength where microwave techniques may be employed is called microwave radiometry.

For the purpose of studying this radiation, which is but one of many possible forms of radiation from a given body, an ideally perfect emitter, the black body, has been conceived. Such a body will absorb all of the energy incident upon it at the wavelengths for which it is black, and thereby become capable of the maximum possible thermal radiation.

Although this radiation, which is customarily called black body radiation, is in the form of noise, its random polarization and fluctuating amplitude may be averaged over a sufficiently long period of time to maintain a constant level for a given set of conditions. Thermal, or black body radiation, thus received from any body may best be divided into two parts; That which originates from the body itself, and that which is generated elsewhere and reflected from the surface of the body. In the theory that follows, the former will be considered first.

2.1.1. Direct Sources

Planck's radiation law will be used as a basis for deriving an expression for the energy that a microwave antenna will intercept when directed at a given object.

Planck's radiation law states that for a black body,

$$\psi_\lambda = \frac{8\pi ch}{\lambda^5} \frac{1}{e^{\frac{ch}{\lambda kT}} - 1} \qquad \text{(joules cm}^{-3}\text{)}$$

where:

ψ_λ = density of radiation - the radiant energy per unit volume in a stream of radiation at the wavelength, λ

λ = wavelength (centimeters)

h = Planck's constant

c = velocity of light ($3 \cdot 10^{10}$ cm/sec.)

k = Boltzmann's constant (1.38×10^{-23} joules/mol./deg. K)

T = temperature of black body (degrees Kelvin)

Expansion of the denominator in Planck's law in a series yields:

$$\psi_\lambda = \frac{8\pi ch}{\lambda^5} \left[\frac{1}{\frac{ch}{\lambda kT} + \frac{c^2 h^2}{2\lambda^2 k^2 T^2} + \cdots} \right]$$

For the wavelengths of interest in microwave radiometry, λT is large enough to justify retaining only the first term of the series expansion.

Hence:

$$\psi_\lambda = \frac{8\pi kT}{\lambda^4} \qquad 2.1$$

Equation 2.1 is the well-known Rayleigh-Jeans formula. It states that the radiation density is directly proportional to the absolute temperature of the body and inversely proportional to the fourth power of the wavelength.

Equation 2.1 may be put into a more convenient form by multiplying both sides by $\Delta\lambda$ and making the substitution, valid for very small $\Delta\lambda$,

$$\Delta\lambda = -\frac{\lambda^2}{c} \Delta f$$

where Δf = frequency interval or bandwidth.

thus:

$$\psi_\lambda \Delta\lambda = \frac{-8\pi kT \Delta f}{c\lambda^2} \qquad \text{(joules/cm}^3\text{)} \qquad 2.2$$

For an isothermal enclosure,

$$\psi_\lambda = \frac{4\pi\, i_\lambda}{c}$$

where i_λ = rate at which a body radiates energy in a given direction per unit solid angle and per unit of its own area as projected on a plane perpendicular to the given direction.

Substituting this relation for ψ_λ in Equation 2.2, it is found that,

$$i_\lambda\, \Delta\lambda = -\frac{2kT\, \Delta f}{\lambda^2} \qquad \text{watts/cm}^2\text{/unit solid angle.}$$

Now, let

$$P = |i_\lambda\, \Delta\lambda|$$

so that

$$P = \frac{2kT\, \Delta f}{\lambda^2} \qquad 2.3$$

Equation 2.3 expresses the power radiated into a unit solid angle per square centimeter of radiating surface.

This analysis may be altered so that it may be applied to any body, regardless of its characteristics. From basic black body theory it is known that a body at temperature T which is not black will radiate as though it were a black body at temperature aT where "a" is the fractional power absorption; i.e.,

$$a = \frac{\text{(Power absorbed by the body)}}{\text{(Power incident on the body)}} .$$

For example, through a section of material of depth Δz and incident power P_0, the power transmitted will be $P_0 e^{-2a\Delta z}$ where a is the usual attenuation per unit length for the material at the wavelength being considered.* The power absorbed will be $P_0 (1-e^{-2a\Delta z})$. Consequently, $a = 1-e^{-2a\Delta z}$ by definition.

For a general body, then, T in equation 2.3 must be replaced by aT. Thus

$$P = \frac{2k\, aT\, \Delta f}{\lambda^2} \qquad \text{(watts/cm}^2\text{/unit solid angle)} \qquad 2.4$$

* a represents the voltage or current attenuation per unit length.

It may be assumed now that the temperature within the body and the attenuation per unit length for the wavelength of interest are functions of position. With reference to Fig. 2.1 let $a(x, y, z)$ be the attenuation factor (nepers per unit length) for the material at the point (x, y, z) and let $T(x, y, z)$ be the temperature in degrees Kelvin at the same point.

Consider first the radiation from the i^{th} section. For this section, $a = a(x, y, z_i)$, $T = T(x, y, z_i)$ and $\alpha = 1 - e^{-2a(x, y, z_i)\Delta z}$. Equation 2.4 gives, for the power radiated from one square centimeter of surface into a unit solid angle,

$$2\left(1 - e^{-2a(x, y, z_i)\Delta z}\right) \frac{kT(x, y, z_i)\,\Delta f}{\lambda^2} \qquad 2.5$$

Since the magnitude of the power radiated to the left of $z = 0$ is desired, the absorbing material between the i^{th} section and $z = 0$ must be taken into consideration. The power radiated by the i^{th} section will be attenuated by each intervening incremental volume. Therefore, the power at $z = 0$ is that expressed by equation 2.5 times the product of the incremental attenuations due to the intervening sections, or:

$$2\left[e^{-2a(x, y, z_1)\Delta z}\, e^{-2a(x, y, z_2)\Delta z} \cdots e^{-2a(x, y, z_2)\,\Delta z}\right] \left[1 - e^{-2a(x, y, z_i)\Delta z}\right] kT(x, y, z_i)\,\frac{\Delta f}{\lambda^2}$$

In summation form, this becomes

$$2e^{-2\sum_{j=1}^{i-1} a(x, y, z_j)\Delta z}\left[1 - e^{-2a(x, y, z_i)\Delta z}\right] \frac{kT(x, y, z_i)\Delta f}{\lambda^2};$$

so that the limit of the summation as $\Delta z \to 0$ is

$$2e^{-2\int_0^{z_{i-1}} a(x, y, z)\,dz}\left(1 - e^{-2a(x, y, z_i)\Delta z}\right)\frac{kT(x, y, z_i)\Delta f}{\lambda^2} \qquad 2.6$$

To obtain the total power at $Z = 0$ it is only necessary to sum equation 2.6 from $Z = 0$ to $Z = d$. In doing this, however, it will be more convenient to expand $1 - e^{-2a(x, y, z_i)\Delta z}$ in a power series; i.e.,

$$1 - e^{-2a(x, y, z_i)\Delta z} = 2a(x, y, z_i)\Delta z - \frac{\left[2a(x, y, z_i)\,\Delta z\right]^2}{2!} +$$

FIG 2.1

A GENERAL RADIATING BODY

DIVIDED INTO INCREMENTAL VOLUMES

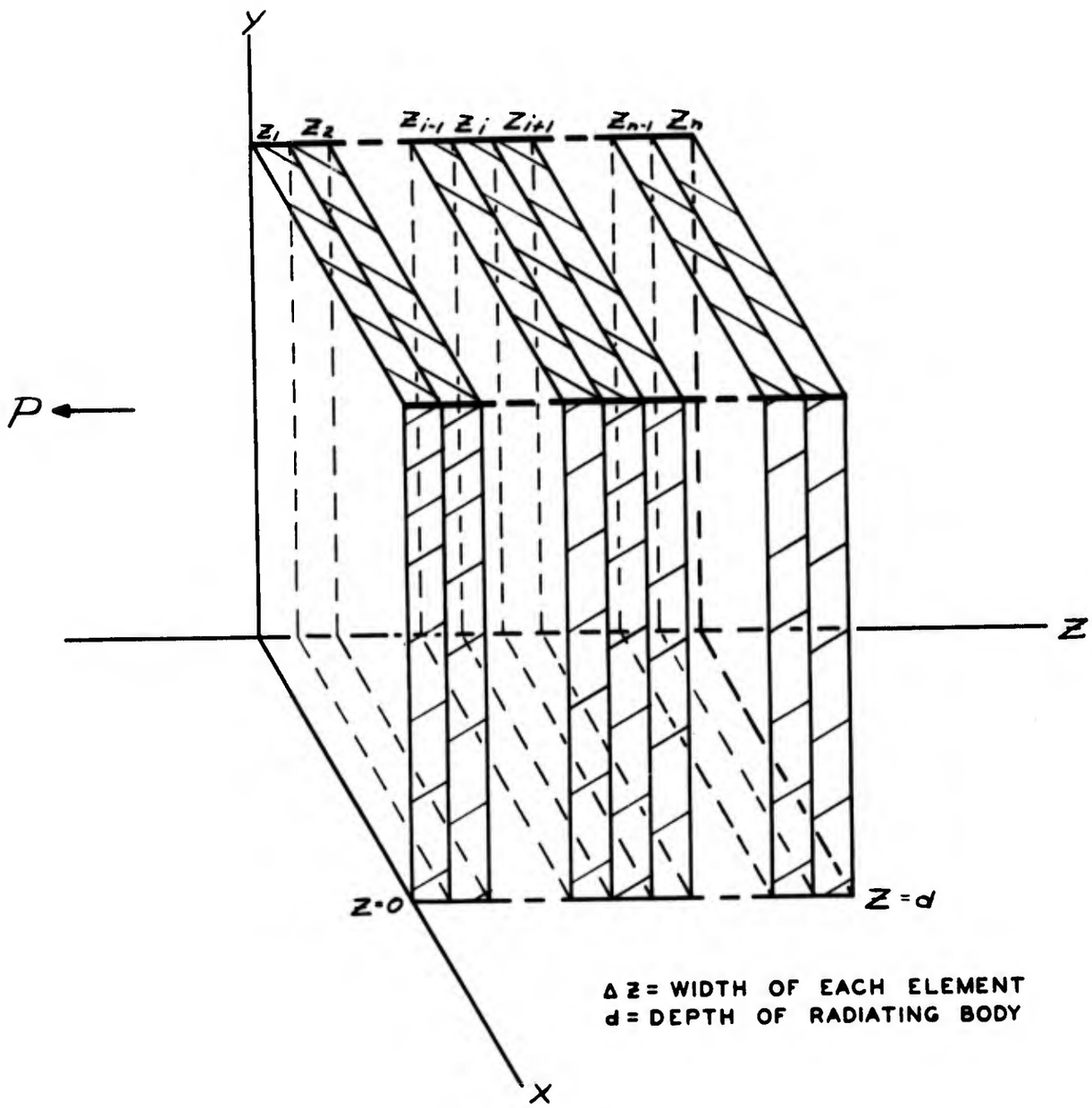

Δz = WIDTH OF EACH ELEMENT

d = DEPTH OF RADIATING BODY

from which it can be seen that for very small ΔZ, only the first term of the series need be retained. The power at $Z = 0$ due to the power radiated by the i^{th} section is therefore

$$4e^{-2\int_0^{z_{i-1}} a(x, y, z)dz}\, a(x, y, z_i)\; kT(x, y, z_i)\; \frac{\Delta f\; \Delta z}{\lambda^2} \qquad 2.7$$

Now, summing equation 2.7 from $Z = 0$ to $Z = d$, as follows,

$$P_0 = \frac{4k\;\Delta f}{\lambda^2} \sum_{i=1}^{n} e^{-2\int_0^{z_{i-1}} a(x, y, z)dz}\, a(x, y, z_i)\; T(x, y, z_i)\Delta Z,$$

and taking the limit as $\Delta Z \to 0$ and $n \to \infty$, it is seen that;

$$P_0 = \frac{4k\;\Delta f}{\lambda^2} \int_0^d e^{-2\int_0^{z} a(x, y, z)dz}\, a(x, y, z)\; T(x, y, z)dz$$

watts/cm^2/unit solid angle 2.8

Equation 2.8 gives the power radiated into a unit solid angle per square centimeter of radiating surface at $Z = 0$. However, part of this power may be reflected back into the body due to a difference in conductivity and dielectric constant between the materials to the right and left of $Z = 0$. Let $m(x, y)$ be the function representing the fraction of the power reflected back into the body at the point, x, y, o. Then,

$$P_0 = \frac{4k\;\Delta f}{\lambda^2} \left[1 - m(x, y)\right] \int_0^d e^{-2\int_0^{z} a(x, y, z)dz}\, a(x, y, z)\; T(x, y, z)dz$$

watts/cm^2/unit solid angle 2.9

Equation 2.9 may now be used to determine the amount of power incident on a collector separated a given distance from the radiating body. Consider a collector located a distance ρ_0 from the body on a line perpendicular to the surface of the body. To find the power incident upon the collector as contributed by one square centimeter of radiating surface, equation 2.9 must be integrated over the solid angle subtended by the collector. No terms in equation 2.9 are a function of this solid angle, however, and the integration is performed by a simple multiplication. Hence:

$$P = \frac{4k\,\Delta f}{\lambda^2}\,[1 - m(x, y)] \int_0^d e^{-2\int_0^z a(x, y, z)\,dz}\, a(x, y, z)\, T(x, y, z)\,dz \left[\frac{A(x, y)}{\rho_0^2}\right] \left(\frac{\text{watts}}{\text{cm}^2}\right) \qquad 2.10$$

where $A(x, y)$ is the effective area the collector presents to the point x, y on the radiating body

and $\frac{A(x, y)}{\rho_0^2}$ is the solid angle subtended by the collector at the source.

But, to obtain the total power incident upon the collector, equation 2.10 must be integrated over the area of the radiating surface. If P_r be the total power intercepted, then

$$\Delta P_r = \frac{4k\,\Delta f}{\lambda^2}\,[1 - m(x, y)] \left[\int_0^d e^{-2\int_0^z a(x, y, z)\,dz}\, a(x, y, z)\, T(x, y, z)\,dz\right] \frac{A(x, y)}{\rho_0^2}\,\Delta y\,\Delta x \quad \text{(watts)}$$

By letting Δy and Δx approach zero, and integrating over the surface, S, of the radiator it is found that,

$$P_r = \frac{4k\,\Delta f}{\lambda^2} \iint_s [1 - m(x, y)] \left[\int_0^d e^{-2\int_0^d a(x, y, z)\,dz}\, a(x, y, z)\, T(x, y, z)\,dz\right] \frac{A(x, y)}{\rho_0^2}\,dy\,dx \qquad 2.11$$

For microwave radiometry purposes, equation 2.11 is not in a convenient form. It would be preferable to have an equation which expressed the power incident upon the collector as a function of the area of the collector and the solid angle subtended by the radiating surface as viewed from the collector.

Equation 2.11 may be transformed into this type of expression with the aid of Fig. 2.2. In the figure the point x, y is defined by the angles θ and ϕ and the distance ρ_0. Since ρ_0 is a constant for a given separation between the radiator and collector, $T(x, y, z)$ and $a(x, y, z)$ may be expressed as functions of θ, ϕ and z which, when integrated with respect to z, become functions of θ and ϕ alone. Similarly, $m(x, y)$ and $A(x, y)$ may be expressed as functions of θ and ϕ.

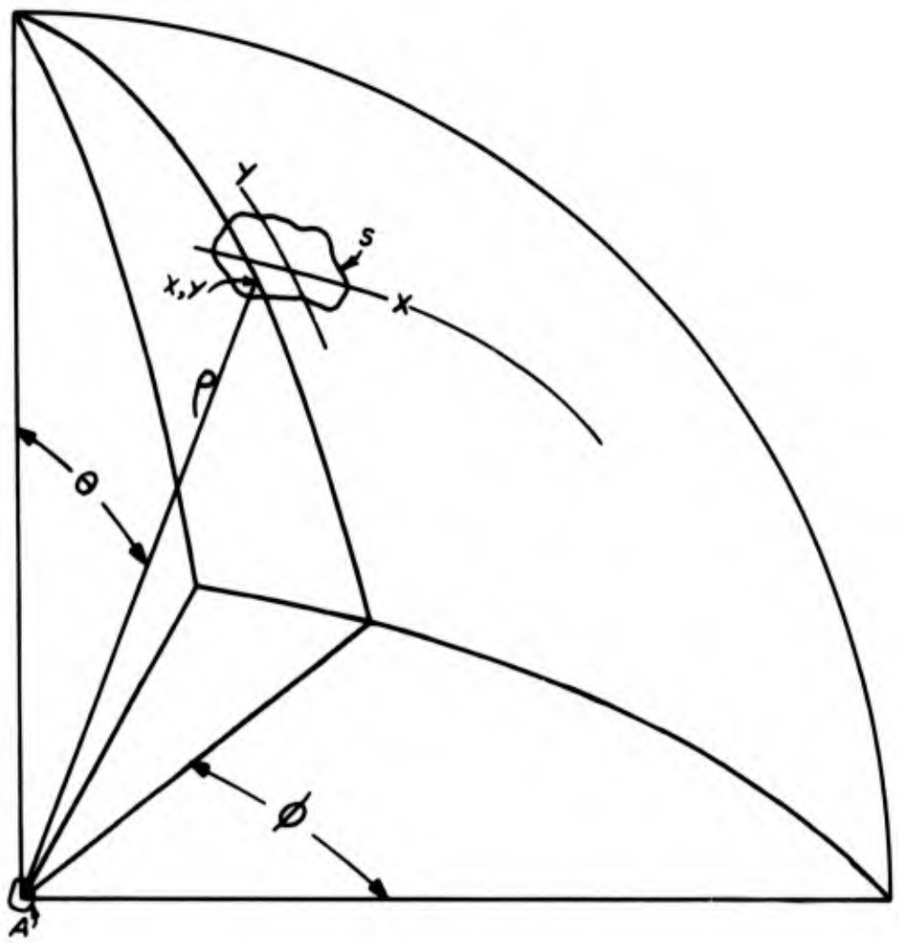

TRANSFORMATION FROM RECTANGULAR TO SPHERICAL COORDINATES FOR DEFINING A AND S

FIG 2.2

With the aid of Fig. 2.2, it is evident that $dy = \rho_0 d\theta$ and $dx = \rho_0 \sin\theta\, d\phi$

Making these substitutions in equation 2.11 and expressing the functions of x and y as functions of θ and ϕ, equation 2.11 becomes

$$P_r = \frac{4k\,\Delta f}{\lambda^2} \iint_s \left[1 - m(\theta,\phi)\right] \left[\int_0^d e^{-2\int_0^z a(\theta,\phi,z)dz} a(\theta,\phi,z)\, T(\theta,\phi,z)dz\right] A(\theta,\phi)\sin\theta\, d\theta\, d\phi$$

The double integral is now the integral over the solid angle subtended by the radiator because $\sin\theta\, d\theta\, d\phi$ is a differential solid angle, $d\Omega$: it may be written,

2.12

$$P_r = \frac{4k\,\Delta f}{\lambda^2} \int_\Omega \left[1 - m(\theta,\phi)\right] \left[\int_0^d e^{-2\int_0^z a(\theta,\phi,z)dz} a(\theta,\phi,z)\, T(\theta,\phi,z)dz\right] A(\theta,\phi)\, d\Omega \text{ watts}$$

where Ω = solid angle subtended by radiating body.*

In microwave radiometry, the collector is an antenna which has an effective area of $\frac{\lambda^2}{4\pi} G(\theta, \phi)$, where $G(\theta, \phi)$ is the gain of the antenna over an isotropic radiator. Also, an antenna will accept only one-half the total power incident upon it because of the random polarization of the thermal radiation and the plane polarization of the antenna. Hence, for an antenna as a collector, equation 2.12 becomes:

$$P_r = 2k\,\Delta f \frac{1}{4\pi} \int_\Omega \left[1 - m(\theta,\phi)\right] \left[\int_0^d e^{-2\int_0^z a(\theta,\phi,z)dz} a(\theta,\phi,z)\, T(\theta,\phi,z)dz\right] G(\theta,\phi)\, d\Omega \quad 2.13$$

The above relation is at the same time general and limited. It holds for wavelengths in the microwave region and longer. It furthermore assumes no absorbing medium between the source and the antenna. The effect of such an absorbing medium will be considered later.

It does, however, consider cases where the temperature of the source varies, where the attenuation within the source varies, and where the solid angle subtended by the source is not limited in relation to the beam width of the antenna at microwave frequencies. As such, this relation

*The nature of the transformation yielding equation 2.12 requires that d be small in comparison with ρ_0 and that either the radiating body or the antenna beam width be of small angular size. However, these restrictions may be removed by carrying out the work in spherical coordinates. This results in

$$P_R = \frac{4k\,\Delta f}{\lambda^2} \int_\Omega \left[1 - m(\theta,\phi)\right] \left[\int_{\rho_0}^{\rho_0+d} e^{-2\int_{\rho_0}^{\rho} a(\theta,\phi,\rho)d\rho} a(\theta,\phi,\rho)\, T(\theta,\phi,\rho)\, d\rho\right] A(\theta,\phi)\, d\Omega$$

which is the same as equation 2.12 except that z of the integrand has been replaced by the spherical coordinate ρ. The limits of the integration, though changed, are such that the integration is still carried out through the depth of the medium.

between the received power and the temperature and characteristics of the source is the basis for the important special derivations and applications which form the body of this report.

In general, all of the functions in equation 2.13 are not known. In most cases certain assumptions may be made in order to reduce the complexity of the relation. For example, let the temperature in the source and the attenuation per unit length within the source be constant and assume no reflections to exist: i.e.,

$$\text{Let} \qquad T(\theta,\ \phi,\ z) = T$$
$$a(\theta,\ \phi,\ z) = a \qquad\qquad 2.14$$
$$n(\theta,\ \phi) \quad = \quad 0$$

Then equation 2.13 may be solved as follows:

$$P_r = 2k\,\Delta f\,\frac{1}{4\pi}\int_\Omega\left[\int_0^d e^{-2a\alpha}\,aT\,dz\right]\,G(\theta,\ \phi)\,d\Omega$$
$$= kT\,\Delta f\,\left[1 - e^{-2ad}\right]\frac{1}{4\pi}\int_\Omega G(\theta,\ \phi)\,d\Omega \qquad 2.15$$
$$= kaT\,\Delta f\,\frac{1}{4\pi}\int_\Omega G(\theta,\ \phi)\,d\Omega$$

The integral $\frac{1}{4\pi}\int_\Omega G(\theta,\ \phi)\,d\Omega$ is easily evaluated if the antenna beam width is either much smaller or much larger than the solid angle subtended by the source. For the case where the source completely encloses the beam, the integral has a value of unity. If the source is much smaller than the beam, the gain may be considered constant over the solid angle, and the integral has the value $\frac{G\Omega}{4\pi}$ where "G" is the peak gain of the antenna. When the beam width and the source are of comparable size, the evaluation becomes involved. Collins Engineering Report 149, which accompanies this report, is concerned with the evaluation of this integral for symmetrical beams and sources of circular cross section.

Further use of the relation 2.15 can be made in extending the theory to a more general case; that is, where an absorbing medium exists between the source and the antenna. If the medium absorbs, it must also radiate. Considering, then, that the medium is itself a source, having a fractional power absorption, a_2, a constant temperature, T_2, and subtending the total solid angle of the antenna, equation 2.15 yields:

$$P_2 = ka_2T_2\,\Delta f \qquad \text{(watts)} \qquad 2.16$$

The power from the source transmitted through the medium will be $e^{-2a_2 d_2} P_{source}$ or $(1 - a_2) P_{source}$ so that the antenna will receive, from the source alone,

$$P_1 = ka(1 - a_2)\ T\ \Delta f\ \frac{1}{4\pi} \int_\Omega G(\theta, \phi)\ d\Omega \qquad \text{watts} \qquad 2.17$$

Ω = angle subtended by source

The total power received is the sum of the power from the medium and that from the source; thus

$$P_r = k\Delta f \left[a_2 T_2 + a(1 - a_2)\ T\ \frac{1}{4\pi} \int_\Omega G(\theta, \phi)\ d\Omega \right]. \qquad 2.18$$

Equation 2.18 may be applied directly to the most simple case arising in microwave radiometry. Consider an antenna completely surrounded by an isothermal enclosure which absorbs all the energy incident upon it. For this case $a = 1$, $\frac{1}{4\pi} \int_\Omega G(\theta, \phi)\ d\Omega = 1$, and $T = T_2$; thus,

$$P_r = kT\ \Delta f \qquad \text{watts} \qquad 2.19$$

It is interesting to note that this result, as well as those expressed in equations 2.18 and 2.13, shows wavelength independence and a direct variation of power with temperature. Such a result is not at all obvious from the mathematical statement of Planck's law.

The discussion of the theory of direct sources will be completed with a conversion of the power received, as in equation 2.18, to an equivalent antenna temperature. The latter is defined as the temperature that an isothermal black body enclosure would have to assume in order to present a power at the antenna equal to the power being considered. Denoting the equivalent antenna temperature by T_r and employing equation 2.19, it can be seen that

$$P_r = kT_r \Delta f; \quad T_r = \frac{P_r}{k\ \Delta f}. \qquad 2.20$$

Or, letting a_2 take the general form a and assuming a black body source,

$$T_r = aT_2 + (1 - a)\ T_s\ \frac{1}{4\pi} \int_\Omega G(\theta, \phi)\ d\Omega \qquad 2.21$$

T_s = temperature of the black body source

The above relation is very useful; in fact, it has formed the direct basis for most of the work which was done under this project.

2.1.2. Reception of Reflected Thermal Radiation

Thermal radiation may also be intercepted from reflecting bodies on which radiation from another source is incident. The amount of energy received by an antenna looking at the reflecting body will be a function of the area and reflecting properties of the body as well as the characteristics of the source and antenna.

For the particular cases of reflected thermal energy treated in the remainder of this report it will be sufficient to assume that the reflecting body acts as an isotropic reflector. Also, the assumption that the radiating surface is uniform in temperature, absorption, and reflectivity will be made. Atmospheric absorption will not be considered.

Under the conditions listed above, equation 2.12 may be used to compute the total power incident upon the isotropic reflector of area A_r; that is,

$$P_r = \frac{4k\ \Delta f}{\lambda^2} \left[1 - m_s\right] \left[\frac{aT}{2}\right] A_r\ \Omega_s \quad \text{watts} \qquad 2.22$$

T = temperature of radiator

a = fractional absorption of radiator

m_s = reflectivity of radiating surface

A_r = area of isotropic reflector

Ω_s = solid angle subtended by radiating surface at reflecting body

If m_r is the reflectivity factor for the surface of the reflecting body, the total reflected power will be

$$P = \frac{4k\ \Delta f}{\lambda^2}\ m_r \left[1 - m_s\right]\ \frac{aT}{2}\ A_r\ \Omega_s \quad \text{watts} \qquad 2.23$$

As the reflecting body is assumed to reflect isotropically, the power reflected from a sq. cm. of surface into one unit solid angle is given by the quotient of the right side of equation 2.23 and $4\pi A_r$, or;

$$P = \frac{k\ \Delta f}{2\pi\lambda^2}\ m_r \left[1 - m_s\right]\ \left[aT\right]\ \Omega_s \quad \text{watts/cm}^2\text{/unit solid angle} \qquad 2.24$$

In the last section it was shown that integrating an equation in the form and units of equation 2.25 over the solid angle subtended by the antenna and over the area of the source gave the same result as integrating over the area of the antenna and over the solid angle subtended by the source (equation 2.11 and 2.12). In this case, it will be more expedient to handle the equation by the latter method to find the total power received by an antenna directed at the reflecting body.

None of the terms in equation 2.24 is a function of position on the cross-section of the antenna so the total power received may be obtained by multiplying the equation by the effective antenna area, $\frac{\lambda^2}{4\pi} G(\theta,\phi)$, and integrating the result over the solid angle subtended by the reflecting body, Ω_r. The power must also be divided by two to take into account the effect of the random polarization of the thermal radiation. Hence, the total received power is

$$P_r = \frac{k\,\Delta f}{4\pi}\, m_r \left[1 - m_s\right]\, aT\Omega_s \cdot \frac{1}{4\pi} \int_{\Omega_r} G(\theta,\ \phi)\, d\Omega_r \quad \text{watts} \qquad 2.25$$

It is interesting to note that if the source is a black body which subtends the total solid angle about a perfectly reflecting body and the reflecting body completely fills the antenna beam, the received power is again $kT\Delta f$.

The results of these reflection considerations for isotropic reflectors will be given further consideration in the balance of this report.

2.1.3. Atmospheric Absorption Measurement Theory

The theory which has been derived in the past two sections can be made directly applicable only when the absorption coefficient of the medium between the source and the antenna is known. It was one of the aims of the work under this contract to study the effects of the atmosphere so that the above theory could be used to interpret experimental results.

The equations suggest several means of determining the fractional absorption constant of the atmosphere. The first of two such methods to be considered consists of forming the difference of two atmospheric readings at different antenna elevation angles. As one angle must result in a different path length from the other, the atmosphere will absorb a different amount of power for one angle than for the other.

A radiating body situated outside the earth's atmosphere is considered. If the atmosphere absorbs energy at the wavelength of interest, the energy received from the body by an antenna will be less than that indicated by equation 2.13. However, if the atmosphere absorbs energy at this wavelength, it must also radiate; and as a consequence, some energy

will be received from the atmosphere itself. Equation 2.13 may be used to compute the energy received from the absorbing atmosphere.

Assume that the antenna beam width is small enough so that within the beam, the temperature, T, and the attenuation constant, a, do not vary with respect to θ and ϕ, that reflections between the various stratified layers of the atmosphere are negligibly small and further, that the atmosphere will completely fill the antenna beam. Then

$$P_r = 2k\,\Delta f \int_0^d e^{-2\int_0^z a(z)dz}\, a(z)\, T(z)\, dz. \qquad 2.26$$

From temperature measurements at various altitudes, it is known that T does not vary greatly with z in the absorbing atmosphere. Therefore, to a good approximation, it may be further assumed that T is constant at some weighted value, T_m.

With these restrictions equation 2.26 gives, for the equivalent antenna temperature due to the atmosphere,

$$T_r = 2T_m \int_0^d e^{-2\int_0^z a(z)dz}\, a(z)\, dz \qquad 2.27$$

The integral from 0 to d, being of the form $e^x dx$, is readily evaluated; thus,

$$T_r = \left[1 - e^{-2\int_0^d a(z)dz}\right] T_m \qquad 2.28$$

In order to measure the fractional absorption of the atmosphere with a radiometer, measurements of T_r must be made for at least two tipping angles. Although absolute measurements of T_r are difficult to obtain, differences in T_r for two tipping angles may be made with considerable accuracy. Therefore an equation expressing a_0 (the fractional absorption per unit atmosphere) as a function of the difference in T_r must be derived.

Let the height of the atmosphere be d and let z vary from 0 to d on a line perpendicular to the horizon plane. Then, for an elevation other than 90^0, the attenuation per unit length should be multiplied by $\sec\theta$, where θ is the angle measured from the zenith to the center of the beam, and the integration performed for 0 to d as before. Letting T_θ be the antenna temperature at the angle θ, equation 2.28 becomes

$$\frac{T_\theta}{T_m} = 1 - e^{-2\sec\theta\int_0^d a(z)dz} \qquad 2.29$$

or

$$\frac{T_\theta}{T_m} = 1 - \left[e^{-2\int_0^d a(z)\,dz}\right]^{\sec\theta} \qquad 2.30$$

but from equation 2.30, with $\theta = 0$, it is seen that,

$$\frac{T_o}{T_m} = 1 - e^{-2\int_0^d a(z)\,dz}$$

and

$$e^{-2\int_0^d a(z)\,dz} = 1 - \frac{T_o}{T_m} \qquad 2.31$$

Substituting this relation into equation 2.30, it is found that

$$\frac{T_\theta}{T_m} = 1 - \left[1 - \frac{T_o}{T_m}\right]^{\sec\theta} \qquad 2.32$$

where $\frac{T_o}{T_m}$ is equal to the fractional absorption per unit atmosphere, a_o.

Let θ take on values θ_1 and θ_2. Then,

$$\frac{T_{\theta_1} - T_{\theta_2}}{T_m} = \left[1 - \frac{T_o}{T_m}\right]^{\sec\theta_2} - \left[1 - \frac{T_o}{T_m}\right]^{\sec\theta_1} \qquad 2.33$$

If T_m is known and $T_{\theta_1} - T_{\theta_2}$ is measured, equation 2.33 may be used to solve for a_o. The algebra involved is simplified if $\theta_1 = 60^\circ$ and $\theta_2 = 0^\circ$. For this case, equation 2.33 may be solved for a_o directly; yielding,[1]

$$a_o = \frac{1}{2} \pm \frac{1}{2}\sqrt{1 - \frac{4(T_{60} - T_o)}{T_m}} \qquad 2.34$$

Another method for determining the fractional absorption of the atmosphere is evident from Equation 2.21. In this method, a radiometer is

[1]R. H. Dicke, KYHL, Vane and Beringer. "The Absorption of Atmospheric Water Vapor in the K-Band Region" M.I.T. Radiation Laboratory Report 1002, Jan. 1946.

used to record the apparent temperature of a given source; for example, the sun, at two different elevation angles. The situation is expressed mathematically by assuming a variable fractional absorption constant, i.e.,

$$a(\theta) = 1 - e^{-2a_0 \sec \theta} \qquad 2.35$$

valid only for $\theta < 70^\circ$ due to the curvature of the earth's surface

where $a_0 = \int_0^d a(z)dz$ nepers/unit atmosphere

so that Equation 2.21 can be rewritten in the form:

$$T_r = \left(1 - e^{-2a_0 \sec \theta}\right) T_m + e^{-2a_0 \sec \theta} \frac{T_s}{4\pi} \int_\Omega G(\theta, \phi)\, d\Omega \qquad 2.36$$

Now let $\frac{1}{4\pi} \int_\Omega G(\theta, \phi)\, d\Omega$ take on two definite values, c_1 and c_2.

so that:

$$T_1 = \left(1 - e^{-2a_0 \sec \theta}\right) T_m + e^{-2a_0 \sec \theta} T_s c_1$$

$$T_2 = \left(1 - e^{-2a_0 \sec \theta}\right) T_m + e^{-2a_0 \sec \theta} T_s c_2$$

then

$$(T_1 - T_2)_\theta = (c_1 - c_2)\, e^{-2a_0 \sec \theta} T_s \qquad 2.37$$

If the above measurements were made at two values of θ for the same constant radiating body, then,

$$\frac{(T_1 - T_2)_{\theta_1}}{(T_1 - T_2)_{\theta_2}} = \frac{e^{-2a_0 \sec \theta_1}}{e^{-2a_0 \sec \theta_2}} = \left[e^{-2a_0}\right]^{\sec \theta_1 - \sec \theta_2}$$

and

$$a_0 = \frac{1}{2(\sec \theta_2 - \sec \theta_1)} \ln \frac{(T_1 - T_2)_{\theta_1}}{(T_1 - T_2)_{\theta_2}} \text{ nepers/unit atmosphere} \qquad 2.38$$

Equation 2.38 may be used to compute a_0 when $(T_1 - T_2)$ is known for two values of θ. The method is not well suited for measuring low absorptions, for the detection of any significant difference in $T_1 - T_2$ requires that one measurement be made for a large value of θ. Large values of θ

invalidate the analysis, for Equation 2.35 assumes that the tipping angle will not exceed 70°.

Another disadvantage of this method is that atmospheric conditions must be presumed to remain constant while the radiating body moves from one angle to the other. The method has an advantage, however, if the radiating body is the sun for here the instrument need not be as sensitive as that required for making absorption measurements utilizing atmospheric temperature measurements alone. And, finally, this latter method has an important advantage in that knowledge of T_m is not required.

2.2. DETECTION THEORY

2.2.1. Minimum Detectable Signal and Noise Figure Relations

In the microwave region below 10 cm., the superheterodyne receiver is possibly the most sensitive detector available. Unfortunately, at these wavelengths good amplifiers are not readily available and receivers generally have noise figures considerably greater than unity.

It is often required in the practice of radiometry to detect signals that are much less than the inherent noise power output of the receiver itself. When this condition occurs, it is usually advantageous to modulate the received signal and employ special methods for discriminating against receiver noise.

It is the purpose of this section on Detection Theory to present analysis of a special[2] receiver which has proved helpful not only in actual design of equipment for radiometry but also in its application. The analysis first discusses the minimum detectable signal, and its limitation, the output meter fluctuations. In the course of this discussion the noise figure of the IF amplifier and of the overall receiver are defined and their use in analysis made clear. It is concluded that the limit on the minimum detectable signal is the crystal in use today rather than the IF amplifier noise figure.

Finally, an overall view of the detection process is presented. The input signal is traced from the antenna to the audio circuits, and an expression for the R.M.S. modulation voltage as a function of the equivalent antenna temperature is presented in Equation 2.51.

A block diagram of a Dicke radiometer is shown in Figure 2.3. In this system a reference attenuator is periodically inserted in the antenna line. This attenuator, which is matched to the line for all depths of

[2] Dicke, Kyhl, Vane, Beringer, "The Absorption of Atmospheric Water Vapor in the K-Band Region", Report 1002, M.I.T. Rad. Labs. Jan. 1946.

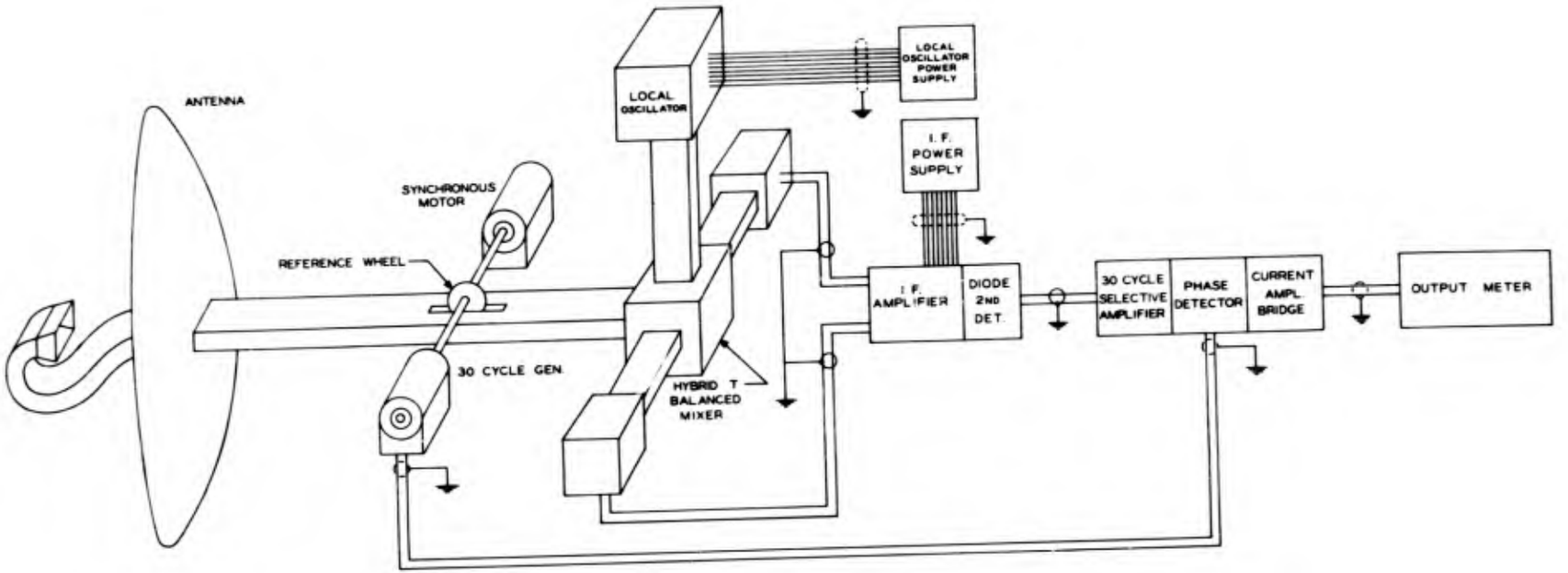

FIG 2.3

BLOCK DIAGRAM OF GENERAL RADIOMETER

insertion, effectively terminates the line when completely inserted. Under the latter condition, the voltage output of the diode detector of the I.F. amplifier is due to the receiver noise plus the noise generated by the attenuator. When the attenuator is removed, the diode output is due to the antenna noise plus the receiver noise. Consequently, if the attenuator is inserted and removed at a given frequency, the diode output will be modulated at that frequency. This modulation can be extracted and amplified in a band pass amplifier which is tuned to the modulation frequency. The amplified modulation voltage can then be rectified in a phase sensitive rectifier, the reference phase being provided by a generator rotating synchronously with the reference attenuator. The output of the phase sensitive rectifier is presented on a milliameter.

It is seen that the output meter reading is proportional to:

(Antenna Noise + Receiver Noise) - (Reference attenuator noise + Receiver Noise) = Antenna Noise - Reference attenuator Noise.

The receiver noise averaged over a finite time interval is subtracted from that of the preceding time interval. Since noise is of a statistical nature, the two powers will not be exactly equal. Consequently, after each subtraction there will be a small quantity of receiver noise remaining which will appear as fluctuation of the output meter. These fluctuations limit the maximum sensitivity that can be attained with this type of receiver.

Dicke[3] has derived an expression for the root-mean square temperature fluctuations in the output meter as a function of the system parameters:

$$\Delta T = \frac{T_o \pi^{3/2} NF_{rec}}{8} \left(\frac{b}{\Delta\omega}\right)^{1/2} \qquad 2.39$$

where: NF_{rec} = overall receiver noise figure expressed as a ratio

$\Delta\omega$ = Rec. I.F. bandwidth in radians per sec.

b = bandwidth of low-pass filter in radians per sec.

T_o = temperature of modulating wheel in degrees Kelvin

ΔT = RMS temperature fluctuations of the output meter in degrees centigrade.

[3] R. H. Dicke, "The Measurement of Thermal Radiation", Rev. Sci. Inst. Vol. 17, July 1946, pp. 268-275.

Equation 2.39 is based on the assumption that the frequency versus amplitude response of both I.F. and low-pass filter pass bands are rectangular, that the second detector has linear I-V operating characteristics, (For an ideal linear detector, the output fluctuation is just 0.50 that of the square law detector.) and that the signal modulation is square wave.

Figure 2.4 is a plot of the RMS temperature fluctuations of the output meter as a function of low-pass filter bandwidth for various values of receiver noise figure. The bandwidth is fixed at 50.2×10^7 sec^{-1} and the modulator wheel is assumed to be at room temperature, 300° K.

In equation 2.39 it is shown that the minimum detectable radiation varies directly as the receiver noise figure, and inversely as the square root of the I.F. bandwidth. However, the overall receiver noise figure is a function of the I.F. noise figure, which, in turn, generally increases with increasing I.F. bandwidth due to I.F. input circuit considerations. Consequently, instead of making the I.F. bandwidth as wide as possible, it is necessary to reach a compromise between receiver noise figure and I.F. bandwidth.

The noise figure of an amplifier or receiver can be defined simply as the ratio of the noise of the receiver or amplifier to that of the theoretically perfect receiver or amplifier ($NF = 1$). In the microwave region, a receiver noise figure of from 10-20 times is considered fairly good. An intermediate frequency amplifier noise figure in the region of 1-1/2 to 2 times is considered good for a bandwidth of 8 mc/s at a center frequency of 30 mc/s.

Equation 2.40 from Friis[4], gives the noise figure of two networks connected in cascade as:

$$NF_{1+2} = NF_1 + \frac{(NF_2 - 1)}{G_1} \qquad 2.40$$

where: NF_{1+2} = noise figure of the combination

NF_1 = noise figure of the first network

NF_2 = noise figure of the second network

G_1 = available power gain of the first network.

(All quantities are expressed as ratios.)

[4]H. T. Friis, "Noise Figures Of Radio Receivers", PROC IRE (1944) pp. 419-423.

FIG 2.4

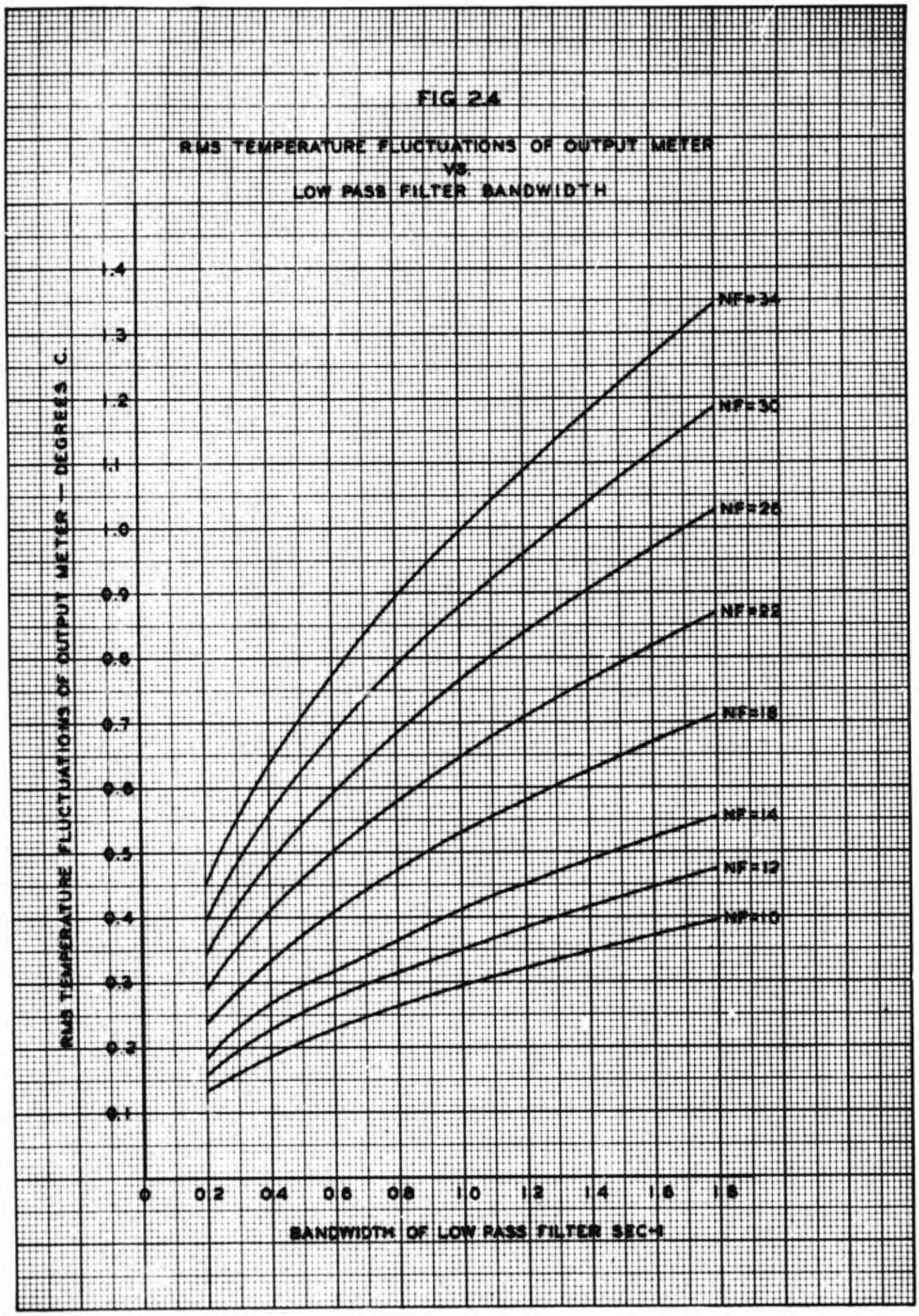
RMS TEMPERATURE FLUCTUATIONS OF OUTPUT METER
VS.
LOW PASS FILTER BANDWIDTH
RMS TEMPERATURE FLUCTUATIONS OF OUTPUT METER — DEGREES C.
1.4
1.3
1.2
1.1
1.0
0.9
0.8
0.7
0.6
0.5
0.4
0.3
0.2
0.1
NF=34
NF=30
NF=26
NF=22
NF=18
NF=14
NF=12
NF=10
0
0.2
0.4
0.6
0.8
1.0
1.2
1.4
1.6
1.8
BANDWIDTH OF LOW PASS FILTER SEC-1

An examination of equation 2.40 shows that if the gain of the first network is high, any source of noise in the second network will not materially affect the overall noise figure, and consequently, it would be unprofitable to devote much effort in reducing the noise figure of the second network. If the gain of the first network is small, then the reverse would be true. If the first network consists of a crystal converter and the second network is the I.F. amplifier of a receiver, the term g_1 is very small and the noise figure of the second network is important. According to convention, when discussing microwave receivers employing crystal converters or mixers, the noise figure of the crystal is written as the product of the loss ratio $1/g_c$ and another term called the equivalent crystal noise temperature, t_c; that is

$$NF_c = \frac{t_c}{g_c} \qquad 2.41$$

$1/g_c$ is also written as L_c and is given in decibels. It is necessary to convert it to a ratio, however, before using it in the formula for noise figure.

The expression for overall receiver noise figure then becomes:

$$NF_{rec} = \frac{(t_c + NF_{IF} - 1)}{g_c}$$

or

$$NF_{rec} = L_c(t_c + NF_{IF} - 1). \qquad 2.42$$

where: L_c = conversion loss of crystal

t_c = ratio of the noise power available from the crystal to the available noise power from a resistor, $(KT\,\Delta f)$, at the reference temperature 293° K, measured at the I.F. frequency used.

NF_{IF} = intermediate frequency amplifier noise figure

NF_{rec} = overall receiver noise figure

(All values are again expressed as pure ratios)

Since L_c and t_c are essentially fixed in production crystals,* it appears that the only term left in which an improvement might be effected is the I.F. noise figure. There is, however, a practical limit to the value which NF_{IF} can assume without undue expenditure of time and effort. For an I.F. amplifier of 8 or 10 mc/s bandwidth, at 30 mc/s it is very hard to achieve a noise figure as low as 1.5 times using existing techniques. Furthermore, if the I.F. noise figure starts in the region of 2 to 3 times and is subsequently reduced to 1.5 times, the minimum detectable signal will not improve in proportion. This is shown in the following examples.

The JAN specifications for the IN26 crystal give a maximum conversion loss of 8.5 db and a maximum noise ratio of 2.7 times. Using the maximum values of L_c and t_c and assuming an I.F. noise figure of 3.1 times, the resulting overall receiver noise figure is, from equation 2.42,

$$NF_{rec} = 7.07\ (3.1 + 2.7 - 1)$$

$$= 34 \text{ times}$$

Using the same values of L_c and t_c, but decreasing the value of the noise figure to 1.55 yields an overall receiver noise figure of:

$$NF_{rec} = 7.07\ (1.55 + 2.7 - 1)$$

$$= 23 \text{ times}$$

Although a change in the I.F. noise figure has a noticeable effect on the overall receiver noise figure, such a change manifests little reduction in the minimum detectable signal. It is seen in Figure 2.4 (Equation 2.39), that the RMS temperature fluctuations of the output meter are only reduced from $\Delta T = 0.45^\circ$ C to $\Delta T = 0.30^\circ$ C as a result of improving the I.F. noise figure 3 db, when, for example, the audio bandwidth is 0.2 sec^{-1}. The associated minimum detectable signal will only change from

*In general terms, the noise temperature t_c of the crystal converter is influenced by the noise originating in the medium toward which the antenna is directed. If the antenna is looking at a very cold region, the noise temperature of the converter decreases, simply because the noise power converted from the antenna terminals to the output terminals of the converter is less than when the antenna looks at a warm object. This is analogous to the thermo dynamic case in which a "hot" object radiates to a cooler object. Actually the noise power converted from the antenna terminals of the mixer to the I.F. terminals is usually small compared to other noise components in the overall receiver due to the conversion gain of the converter being of the order of 0.1 to 0.2 times.

$$P_m = KT\,\Delta f = 1.38 \times 10^{-23} \times 0.45 \times 16 \times 10^6$$

$$= 0.98 \times 10^{-16} \text{ watts}$$

to

$$P_m = KT\,\Delta f = 1.38 \times 10^{-23} \times 0.30 \times 16 \times 10^6$$

$$= 0.66 \times 10^{-16} \text{ watts.}$$

If the I.F. amplifier noise figure could be reduced to unity, (the perfect amplifier), the overall receiver noise figure would be 19.1 times, but the minimum detectable signal would only drop to 0.55×10^{-16} watts.

The increase in sensitivity is desirable, but it has been made clear in the discussion above that there is no apparent justification for devoting the time and energy necessary for the achievement of a very low I.F. noise figure in order to realize such a slight increase in sensitivity. Progress, if it is to be made, must be made by improving the noise figure of the R.F. section.

The relations above define the conditions which determine the minimum detectable signal of a radiometer. These conditions dictate that use be made of the best crystals available mounted in an r.f. mixer which yields the minimum noise figure possible, and finally that the I.F. amplifier have as wide a bandwidth as is consistent with a good noise figure. (For a center frequency of 30 mc, the optimum bandwidth of the I.F. amplifier for radiometers is in the neighborhood of 10 mc.)

2.2.2. Receiver Design

To further facilitate the design, calibration and understanding of the radiometer receiver, it was necessary to predict the amount of voltage output which could be expected for a given antenna temperature. The preceeding sections have presented a means of determining the expected antenna temperature for a given source; that is, Equation 2.21. The following derivation has as its goal a relation between T_r of Equation 2.21 and the output voltage, E_{rms}.

The magnitude and quality of the radiometer output will depend on the noise power received at the input terminals of the receiver, the noise power generated in the crystal mixer, the noise power generated in the I.F. amplifier, the bandwidth of the I.F. and audio amplifiers, the gain of both, and the time constant of the meter.

To facilitate the analysis, consider the block diagram of Figure 2.5 in which the antenna has been replaced by an equivalent resistance, R_a, at a temperature $t_a\ T_o$, and in which the rotating attenuator or modulator wheel has been replaced by a fixed, switchable attenuator, A, of

large attenuation at a temperature T_o. Both A and R_a are matched to the input line of the mixer.

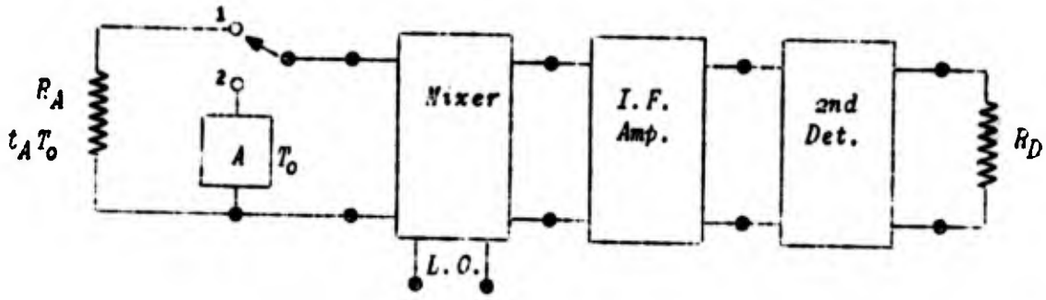

Figure 2.5

It is assumed that the local oscillator drive incident upon the converter is of such a value that the noise figure of the converter is optimized. This assumption is easily realized in practice if the rectified crystal current, for good crystals, is in the region of 0.5 ma. It is also assumed that noise contributions from the local oscillator have been eliminated.

The various noise contributions can be examined in a more detailed manner by referring again to the diagram of Figure 2.5.

The available noise power from R_a is:

$$P_R = K t_a T_o \Delta f \qquad 2.43$$

where: t_a = the ratio of the actual temperature of R_a to the reference temperature T_o

T_o = the reference temperature

K = Boltzman's Constant

and Δf = R.F. acceptance bandwidth of the receiving device.

The available I.F. noise power from the crystal converter when it is connected to R_a is composed of the inherent noise generated by the crystal plus the converted noise power from R_a.

Thus:

P_c = inherent converter noise + converted signal noise

$$P_c = K \Delta f_{if} T_o \mathcal{G}_c (NF_c - 2) + 2 t_a T_o \mathcal{G}_c K \Delta f_{if} \qquad 2.44$$

But $NF_c = \frac{t_c}{g_c}$ by equation 2.41 ; so that,

$$P_c = KT_o \Delta f_{if} \left[2g_c (t_a - 1) + t_c\right] \qquad 2.45$$

The factor 2 enters the equations since both the "image" and the "signal" frequency bands are converted by the crystal.

The process is cumulative; for the I.F. amplifier, it can be written that:

P_{IF} = inherent noise + amplified signal noise

$$P_{IF} = KT_o \Delta f_{if} g_2 (NF_{IF} - 1) + g_2 P_c$$

$$P_{IF} = g_2 KT_o \Delta f_{if} \left[2g_c (t_a - 1) + t_c + NF_{IF} - 1\right] \qquad 2.46$$

In equation 2.46, P_{IF} is the noise power incident upon the I.F. amplifier second detector when the antenna termination, R_a, has a temperature $t_a T_o$.

There remains the problem of converting this incident noise power to a voltage developed across the diode load resistor, R_D. The output load resistance of the amplifier is determined by the equivalent resistance of the tank circuit in parallel with the diode resistance and R_D in series.

An equivalent circuit of the output of the I.F. amplifier is shown in Figure 2.6.

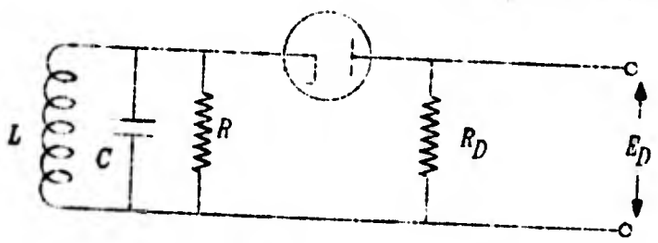

Figure 2.6

For a circuit of this type, the equivalent load resistance, R_e, can be obtained from the expression,

$$R_e = \frac{Q_L}{\omega C}$$

where Q_L is the loaded Q of the tank

and ω is the center angular frequency of the amplifier.

Next, considering the relation,

$$E = \sqrt{\text{Power x Resistance}}$$

and in view of the assumption that the diode is operating in a linear section of its characteristics (it has been mentioned that in such operation, a diode will have only one half the inherent noise that a square law operating diode would have), it can be seen that

$$E_D = (P_{IF}\, R_e)^{1/2}\, n \qquad 2.47$$

where n is the diode efficiency.

In more complete form and using the relation;

$$NF_{rec} = \frac{NF_{IF} + t_c - 1}{\mathcal{G}_c}$$

$$E_D = \left\{ \mathcal{G}_c\, \mathcal{G}_2\, KT_o\, \Delta f_{if} \left[2(t_a - 1) + NF_{rec} \right] \frac{Q_L}{\omega c} \right\}^{1/2} n \qquad 2.48$$

It is appropriate at this point to digress long enough to compute the amount of I.F. gain needed to supply a typical diode with a sufficient noise level to assure linear operation. A common diode, such as the 6AL5 requires that the DC voltage developed across the load be on the order of 2 volts for such operation. Using 2 volts for E_D in Equation 2.48 then, it is seen that the I.F. gain,

$$\mathcal{G}_2 = \frac{4}{\mathcal{G}_c\, n^2\, KT_o\, \Delta f_{if} \left[2(t_a - 1) + NF_{rec} \right] \frac{Q_L}{\omega c}} \qquad 2.49$$

To complete the analysis, it is only necessary to consider the audio section. For this purpose the modulation voltage produced by the attenuator or reference wheel is the required unknown. When the radiometer receives its input from the antenna, at temperature $t_a\, T_o$, there is a voltage at the diode given by Equation 2.48. Similarly, when the wheel replaces the antenna, the voltage, E_o is that given by Equation 2.48 with $t_a = 1$. The difference in these voltages, $E_D - E_o$ represents the peak to peak modulation voltage. For a sine wave modulation

$$E_{rms} = \frac{.707(E_D - E_o)}{2} = \frac{.707n}{2} \left(\frac{\mathcal{G}_2\, \mathcal{G}_c\, KT_o\, \Delta f_{if}\, Q_L}{\omega c} \right)^{1/2} \left\{ \left[2(t_a - 1) + NF_{rec} \right]^{1/2} - \left[NF_{rec} \right]^{1/2} \right\} \qquad 2.50$$

Equation 2.50 can be reduced to an approximate relation which is very useful. Let

$$a = \frac{.707n}{2}\left(\frac{\xi_c\ \xi_2\ KT_0\ \Delta f_{if}\ Q_L}{\omega c}\right)^{1/2}$$

$$b = NF_{rec}$$

$$c = 2(t_a - 1);$$

Then

$$E_{rms} = a\left[(c+b)^{1/2} - b^{1/2}\right]$$

or

$$E_{rms} = ab^{1/2}\left[\left(1+\frac{c}{b}\right)^{1/2} - 1\right]$$

But to a sufficient approximation (since $NF_{rec} \geq 25$ and $t_a < 4$ in the general case)

$$E_{rms} \approx \frac{ac}{2b^{1/2}}$$

or, finally,

$$E_{rms} \approx \frac{.707n}{2}\left(\frac{\xi_c\ \xi_2\ KT_0\ \Delta f_{if}\ Q_2}{\omega c\ NF_{rec}}\right)^{1/2}(t_a - 1) \qquad 2.51$$

Equation 2.51 is the desired quantitative expression for the expected input to the audio section. It is to be noted that for a given radiometer, the coefficient of $(t_a - 1)$ is a constant. The output voltage, therefore is proportional to the difference in equivalent temperature between the source and the modulator wheel reference.

In the general case, the reference can be considered to exist at a temperature t_{a1} T_o. It is easy to show that the radiometer, under these conditions, again measures the difference in the signals produced by each source; that is,

$$E_{rms} = \frac{.707n}{2}\left[\frac{\xi_2\ \xi_c\ KT_0\ \Delta f_{if}\ Q_L}{\omega c}\right]^{1/2}\left\{\left[2(t_a - 1) + NF_{rec}\right]^{1/2} - \left[2(t_{a1} - 1) + NF_{rec}\right]^{1/2}\right\} \qquad 2.52$$

SECTION 3

3. EQUIPMENT FOR RADIOMETRY

3.1. Components

3.1.1. R.F. Section

The R.F. section of the general radiometer comprises an antenna, a modulator or reference section, and a mixer. The design of a suitable antenna is not unique to a general radiometer; hence, no discussion is required here.

The reference section has two requirements imposed on it other than the fact that it must accomplish the switching action which alternately connects the receiver to the antenna and then to the reference attenuator.* The requirements are that the V.S.W.R. looking into the reference section should be as nearly unity as possible for any position of the disc, and the attenuation of the section should be at least 10 db. and preferably more when the disc is completely inserted in the waveguide.

In Section 2.2.2., the equations predicting the modulation voltage developed at the I.F. second detector were given. This analysis was made assuming that the only source of second detector output was the difference of the noise powers from the antenna and reference wheel. Unless special precautions are taken, however, this assumption is not valid.

Any variation of admittance in the R.F. portion of the receiver will also affect the output voltage of the second detector. The minimization of this effect requires a more elaborate R.F. mixer than is commonly employed. The discussion given here will, therefore, be concerned mainly with the R.F. mixer.

*A common way of accomplishing this action is to dip a lossy disc periodically in and out of the waveguide connecting the antenna to the receiver. The disc is usually mounted eccentrically on a shaft so that rotation of the shaft causes the disc to dip in and out of the guide.

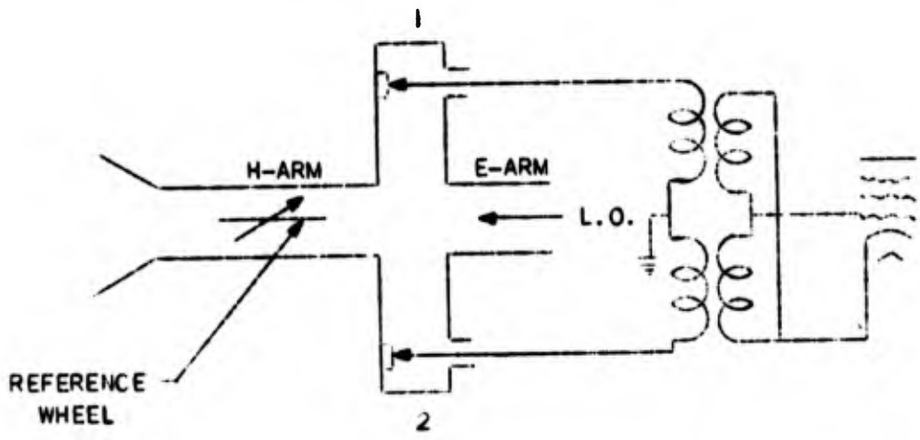

Figure 3.1

Fig. 3.1 is a simplified diagram of the R.F. mixer and the input to the first I.F. amplifier tube. It will be observed that a balanced mixer utilizing a magic tee is employed. This type of mixer has been discussed thoroughly by Pound[5] for radar applications, but its application to radiometers has not been discussed in detail.

The familiar advantages of the magic tee balanced mixer are:

1. Reduces local oscillator noise contribution to overall receiver noise.

2. Prevents received signal from being absorbed by local oscillator coupling line.

3. Reduces coupling of local oscillator signal to antenna line.

A few remarks concerning the magic tee itself may be in order. Power introduced in the L. O. arm divides equally between the co-planar arms 1 and 2, whereas essentially none of the L. O. power appears in the antenna line. There is a phase difference of 180° between the L. O. wave in arm 1 and the wave in arm 2. Power introduced at the antenna arm also divides equally between arms 1 and 2 with no phase difference existing between the waves in these arms.

In the conventional operation of the balanced mixer the signal from the antenna beats with the L. O. signal in the crystals to generate a

[5]R. V. Pound, "MICROWAVE MIXERS", Vol. 16, MIT RAD. LAB. SERIES McGraw Hill Book Co, New York, 1948

signal at the beat frequency. Since the phase of the L. O. signal incident on one crystal is different by 180° from that incident on the other, the beat frequencies generated in each crystal will also differ in phase by 180°. The two beat frequency voltages are added in a push-pull transformer which couples the two crystals to the single ended beat frequency or I.F. amplifier.

In general, local oscillator noise power which is also incident on each crystal, beats with the fundamental frequency of the oscillator to generate noise sidebands. These would contribute noise at the desired beat frequency, unless the beat frequency chosen is sufficiently large compared to the noise spectrum of the local oscillator. In this type of mixer, however, the beat frequency voltage arising from local oscillator noise will be in phase, thereby cancelling in the push-pull transformer circuit.

Referring again to Fig. 3.1, the admittance presented to the input terminals of the mixer when the reference wheel is terminating the antenna line may be slightly different than the admittance presented when the wheel is removed and the antenna terminates the line. In practice it is difficult to maintain a V.S.W.R. less than 1.08 looking from the mixer toward the antenna-reference wheel combination for all positions of the wheel. The R.F. admittance presented to the input terminals of the mixer will, therefore, vary in synchronism with the reference wheel.

This variation of R.F. admittance at the input terminals produces a variation of the I.F. admittance at the output terminals of the mixer, which, in turn, causes the noise power input to the I.F. amplifier to vary. Since the admittance variation occurs in synchronism with the insertion and removal of the reference wheel, the reading of the output meter on the radiometer will be influenced. Unfortunately, this effect is serious enough to cause large errors in the measurement of the noise power incident on the mixer.

This effect can be minimized, and in some cases entirely eliminated, by the addition of a phase shifter between one crystal and the symmetry plane of the magic tee. In practice, the phase shifter is adjusted until the electrical length from one crystal to the symmetry plane is one quarter wave longer than the electrical length from the other crystal to the symmetry plane.

A possible explanation of the effect of the phase shifter will now be presented.

Fig. 3.2 is a simplified diagram of the mixer with the addition of the quarter wave section between one crystal and the symmetry plane of the magic tee. The addition of the quarter wavelength section does not affect the phase of the I.F. voltage produced at the crystal since the increase in line length is small compared to a wavelength at the I.F. frequency.

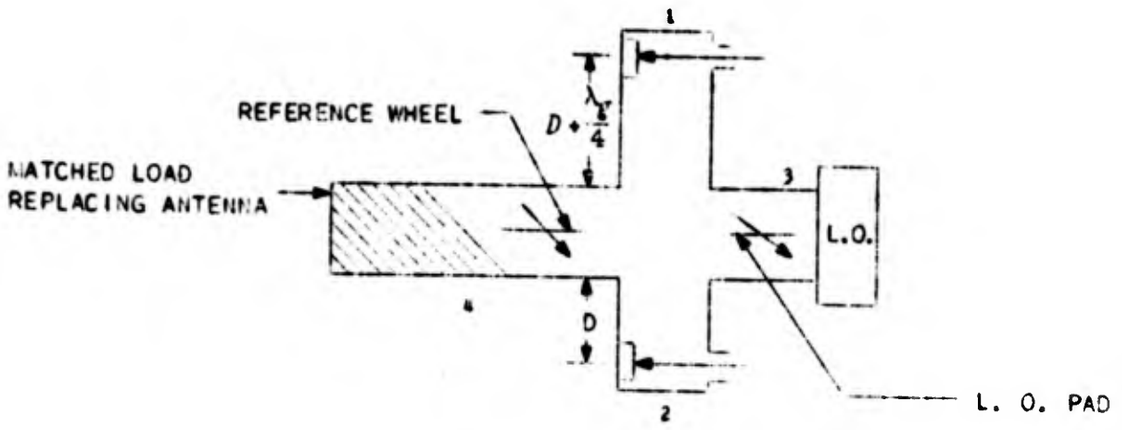

Figure 3.2

The power present in arm 4 of the mixer consists of noise generated by the matched termination and the reference wheel. Since the bandwidth of the R.F. components is many times greater than the bandwidth of the I.F. amplifier, there will be two bands of energy converted to the I.F. frequency. Although the R.F. frequencies of interest completely cover these two bands, it will be sufficient to consider a single frequency in each band.

Let the local oscillator frequency be ω; the signal frequency, α; the image frequency, γ; and the I.F. frequency, β

Then $\alpha = \omega + \beta$

$\gamma = \omega - \beta$

It is an established fact that the I.F. voltages produced at the crystals, as a result of the beat between α and ω and between γ and ω will cause the R.F. admittance of the crystals to vary at a frequency β. This admittance variation will cause part of the incident power to be reflected from the crystal at each of the three frequencies α, γ, and ω, and since the crystal admittance is being modulated at a frequency β each of the reflected components will also be modulated at the frequency β.

The power incident on the crystals at frequencies α and γ is very small initially and the percentage of this power reflected at the crystals is also small. In view of this, it seems quite acceptable to neglect the reflected components at these frequencies. The local oscillator power incident on either crystal is very large compared to the signal and image power. In fact, for the case of reference wheel and matched load at room temperature (293°K) the local oscillator power delivered to each crystal is 10^{10} times greater than the power generated by the reference wheel or matched load. Therefore, the most important reflected component will be that at the local oscillator frequency ω. Since the reflected component of ω is modulated at frequency β, there will be two frequencies in the reflected wave which must be considered, namely $\omega+\beta$ and $\omega-\beta$, which from the definitions above, are equivalent to α and γ.

It will be considered, then, that as a result of the modulation of the R.F. admittance of the crystal, the local oscillator wave incident on each crystal will produce two new waves of frequency α and γ traveling toward the symmetry plane of the mixer. If these waves are again reflected toward the crystals by some discontinuity in the mixer plumbing they will again beat with the local oscillator wave to produce a voltage at the I.F. frequency β. The phase of this voltage may be such as to add to or subtract from the I.F. voltage resulting from the power generated in the antenna line.

It is felt that this is the phenomenon which gives rise to spurious output meter indications. Specifically, the waves reflected from the crystals return to the antenna line of the mixer. The admittance at the input terminals of the mixer varies at a frequency determined by the speed of the reference wheel; hence, the re-reflected waves will have a low frequency modulation imposed on them corresponding to the rate of variation of the input admittance. This will give rise to a voltage at the output terminals of the mixer which will be of the same nature as the desired voltage.

The addition of the quarter wavelength section between crystal (1) and the symmetry plane is such that the reflected waves from the crystals arrive at the symmetry plane with a phase difference of 180°, thereby cancelling the unwanted effect. This can be shown with the aid of vector diagrams.

The vectors representing the local oscillator and signal voltages at two points in the crystal arms equidistant from the symmetry plane are shown in Fig. 3.3a.

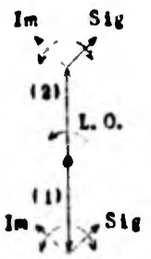

Figure 3.3a

The two vectors representing the local oscillator voltage differ by 180° since the local oscillator is connected to the E-arm of the magic tee. The small vectors representing the signal and image frequencies point in the same directions since these signals are introduced at the H or shunt arm of the magic tee. The image and signal vectors rotate in opposite directions at the intermediate frequency, f, since both the image and signal frequency differ from the local oscillator frequency by this amount.

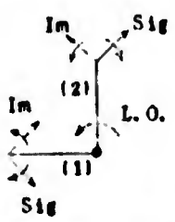

Figure 3.3b

In Fig. 3.3b the conditions existing at the crystals are shown. The local oscillator wave at crystal (1) has been retarded by 90° because of the quarter wavelength section. As pointed out previously, the I.F. voltage developed at the crystals as a result of the signal and image waves beating with the local oscillator wave results in a portion of the local oscillator wave being reflected with a modulation at the I.F. frequency imposed on it. This state of affairs

Figure 3.3c

is the same as shown in Fig. 3.3b. By the time the reflected waves reach the symmetry plane of the mixer, the phase of the waves from crystal (1) have been delayed another 90° with respect to the waves from crystal (2). Thus, the signal and image waves generated by each crystal reach the symmetry plane 180° out of phase, as shown in Fig. 3.3c.

There is no assurance that the waves generated by each of the two crystals will be of equal amplitude, neither will the electrical length of various crystals be equal. The latter effect can be compensated by substituting a line stretcher or phase shifter for the quarter wavelength section. Since the waves are not necessarily of equal amplitude, the proper adjustment of the phase shifter will, in general, only minimize the spurious output meter readings.

Fig. 3.4 demonstrates the effectiveness of choosing the proper line length between the symmetry plane of the mixer and the crystals. The data for this curve were taken by inserting a mismatch (V.S.W.R. = 1.3) between the antenna termination and the modulating wheel. The upper and lower curves represent the maxima of the radiometer output as the phase of the mismatch was varied over a half wavelength.

The abscissa of the curve represents arbitrary settings of the phase shifter. At the proper setting of the phase shifter indicated by the minima of the curves, the effect of varying the mismatch by a half wavelength is very small.

To simplify the adjustment of the phase shifter, the crystal cartridges should be well matched to the mixer. Otherwise, adjustment of the phase shifter will vary the local oscillator power to the crystal, causing a wide admittance variation.

Fig. 3.5 is a photograph of a representative radiometer mixer such as described in this section. Both crystal holders are tunable and can be detached from the magic tee for tuning. A variable matched attenuator is provided for adjustment of local oscillator drive.

3.1.2. I.F. Amplifiers

The work done on intermediate frequency amplifiers was centered around the design of input circuits for coupling from a push-pull, or balanced crystal converter configuration, to the input tube of an I.F. amplifier. The main reason for concentrating effort on this section of the I.F. amplifier was an attempt to realize as low an I.F. noise figure as possible, consistent with the wide bandwidth desired. As was shown in Section 2.2.1., it is rather doubtful if there is justification in concentrating too much

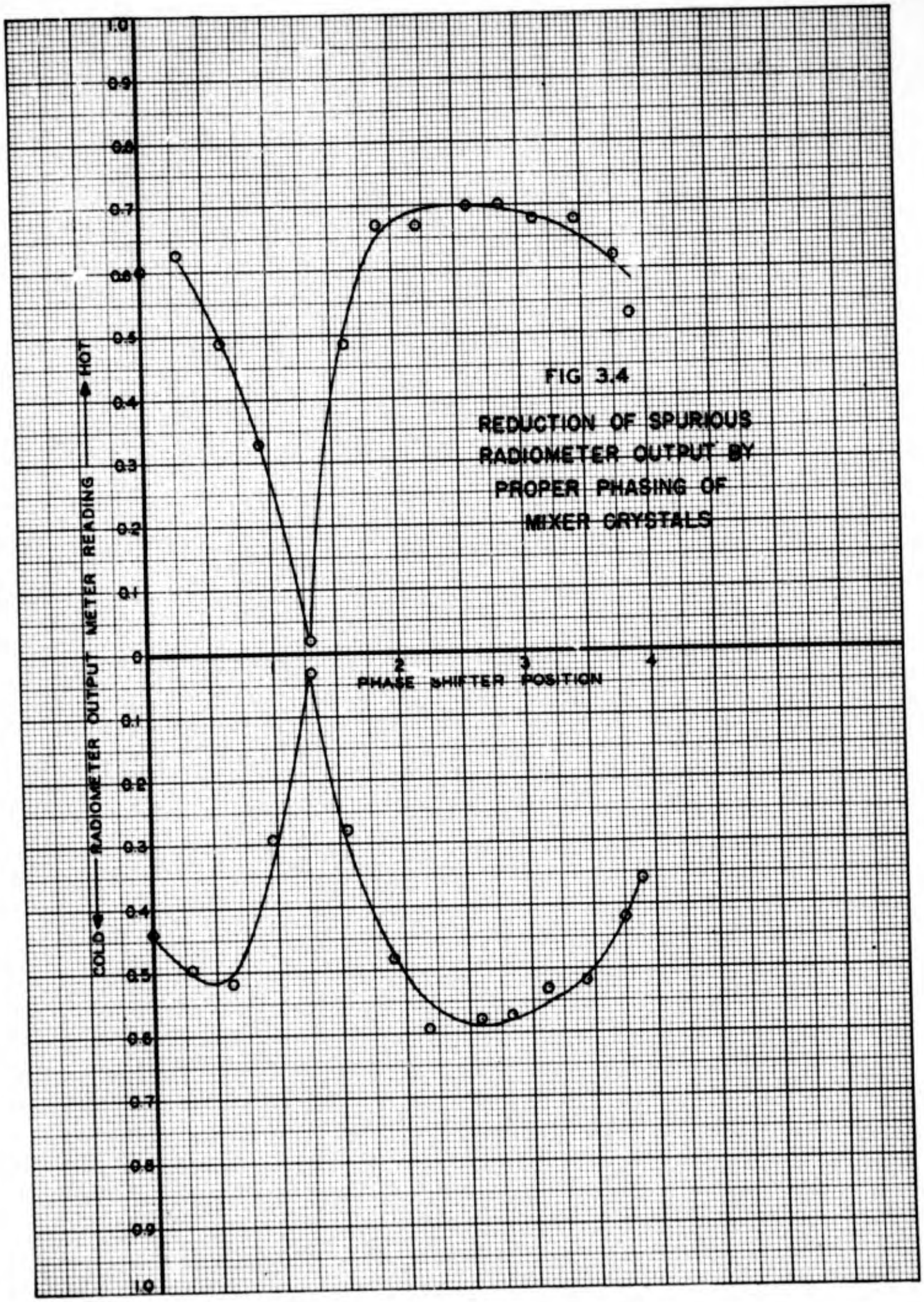

FIG 3.4

REDUCTION OF SPURIOUS RADIOMETER OUTPUT BY PROPER PHASING OF MIXER CRYSTALS

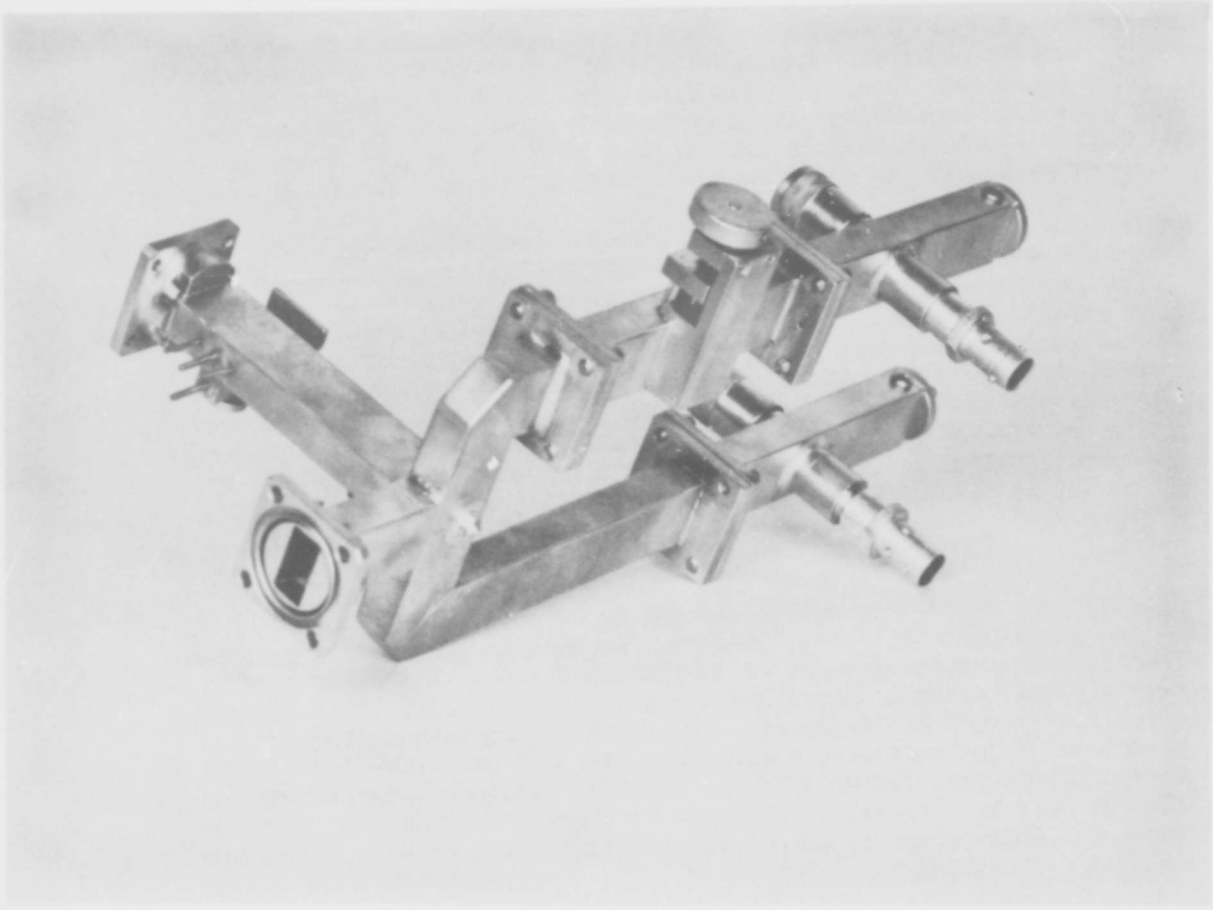

Figure 3.5 Representative Radiometer Mixer

effort towards improving the noise figure beyond 1.5 times, especially when the quality of crystals obtainable for operation in the K-Band region is considered. However, as might be surmised, it does require some time and effort before it is possible to realize even an I.F. noise figure of 2 times when the I.F. bandwidth is of the order of 8 mc/s centered at 30 mc/s.

The I.F. admittance of a typical microwave crystal converter may be represented by a parallel circuit containing a capacitance and a resistance. The capacitative component depends upon the mechanical design of the converter and generally ranges from 5 to 25 uuf. The conductive component is a function of the local oscillator drive and of the r.f. tuning of the converter; it varies over a fairly large range from one crystal to another. For usual operating conditions, that is, with local oscillator drive of such a value that the rectified crystal current is about 0.5 ma., the conductance, G_d, varies from 1600 to 5000 micromhos. For the IN 26 crystal, it is generally assumed to have a nominal value of 2200 micromhos.

The input admittance for conventional grounded-cathode amplifiers is determined by the grid-ground capacity, which is composed of actual tube, socket, and wiring capacities. The conductive component, G_g, consists of transit-time loading, cathode-lead-inductance feedback, and loading due to losses in the input circuit. Cathode-lead-inductance loading, which does affect the input bandwidth, can be considered to be zero for noise work. Loading due to losses in the input circuit can be kept low enough to be negligible by good design if the unloaded Q's of the windings are of the order of 100. Transit time loading, however, greatly exceeds all other loading at 30 mc. and higher. At 30 mc. the transit-time loading for a 6 AK5 tube is about 12 micromhos. (R_g = 83,000 ohms).

The primary purpose of an input coupling circuit is to supply the necessary impedance step-up between the crystals and the first amplifier tube to achieve as low a noise figure as possible, consistent with the desired bandwidth. The only input circuit configuration that is applicable for connecting push-pull crystals to a single-ended input amplifier is a transformer employing two series connected primaries whose associated secondaries are connected in parallel. The transformer should not be affected by a lack of balance in the I.F. admittances of the crystals and should possess sufficient balance in the primaries to allow suppression of local-oscillator noise.

The effect of shot-noise on amplifier noise figure decreases as the input-circuit impedance level is increased, whereas the effect of active grid loading on noise figure increases as the impedance level is increased. At frequencies where transit-time loading is not negligible the minimum noise figure will increase and the optimum transformed source impedance (that value required to make the noise figure a minimum) will decrease as the frequency increases.

The variation of noise figure with transformed source resistance, or step-up may be obtained from equation 3.1[6] e.g.,

$$NF = 1 + \beta \frac{R_s}{R_g} + \frac{R_t}{R_g}\left[1 + \frac{R_t}{R_g}\right]^2 \qquad 3.1$$

where: R_s = transformed source resistance

R_g = the vacuum tube loading due to transit-time and lead inductance effects.

R_t = equivalent noise resistance[7] of the input tube.

β = a constant equating the noise due to active grid loading to the noise from a resistor at the reference temperature T_0. It is generally assumed to be 5.

For a pentode connected 6 AK5, R_g equals approximately 83,000 ohms at 30 mc. and R_t equals 1880 ohms. Figure 3.6 is a plot of equation 3.1, using the values indicated above. As shown in Figure 3.6, the optimum transformed source resistance is approximately equal to 5000 ohms for the pentode connected 6 AK5. At 60 mc. this value is about 2500 ohms with the minimum noise figure being about 3.5 db. It should be noted at this point that the optimum transformed source resistance for a triode connected input tube is considerably lower; it consequently enables the attainment of a wider bandwidth and lower noise figure than does the same tube connected as a pentode.

Wallman has shown[8] that an input stage configuration consisting of a grounded-cathode triode followed by a grounded-grid triode yields a much lower noise figure (1.6 db for a 6 mc bandwidth at 30 mc) than can be obtained by using a pentode connected tube. Such a system was constructed, but due to the emphasis being directed towards the Radio Sextant this work was suspended before a satisfactory unit was finished.

---

[6] Hopper and Miller, "DESIGN OF RADAR I.F. AMPLIFIERS", Proc IRE, November, 1947

[7] D. O. North, "FLUCTUATIONS IN SPACE CHARGE CONNECTS AT MODERATELY HIGH FREQUENCIES", RCA Review, 1941-42.

[8] Wallman, Macnee, and Gadsen, "A LOW NOISE AMPLIFIER," IRE, Vol. 36, June 1948, pp. 700-708.

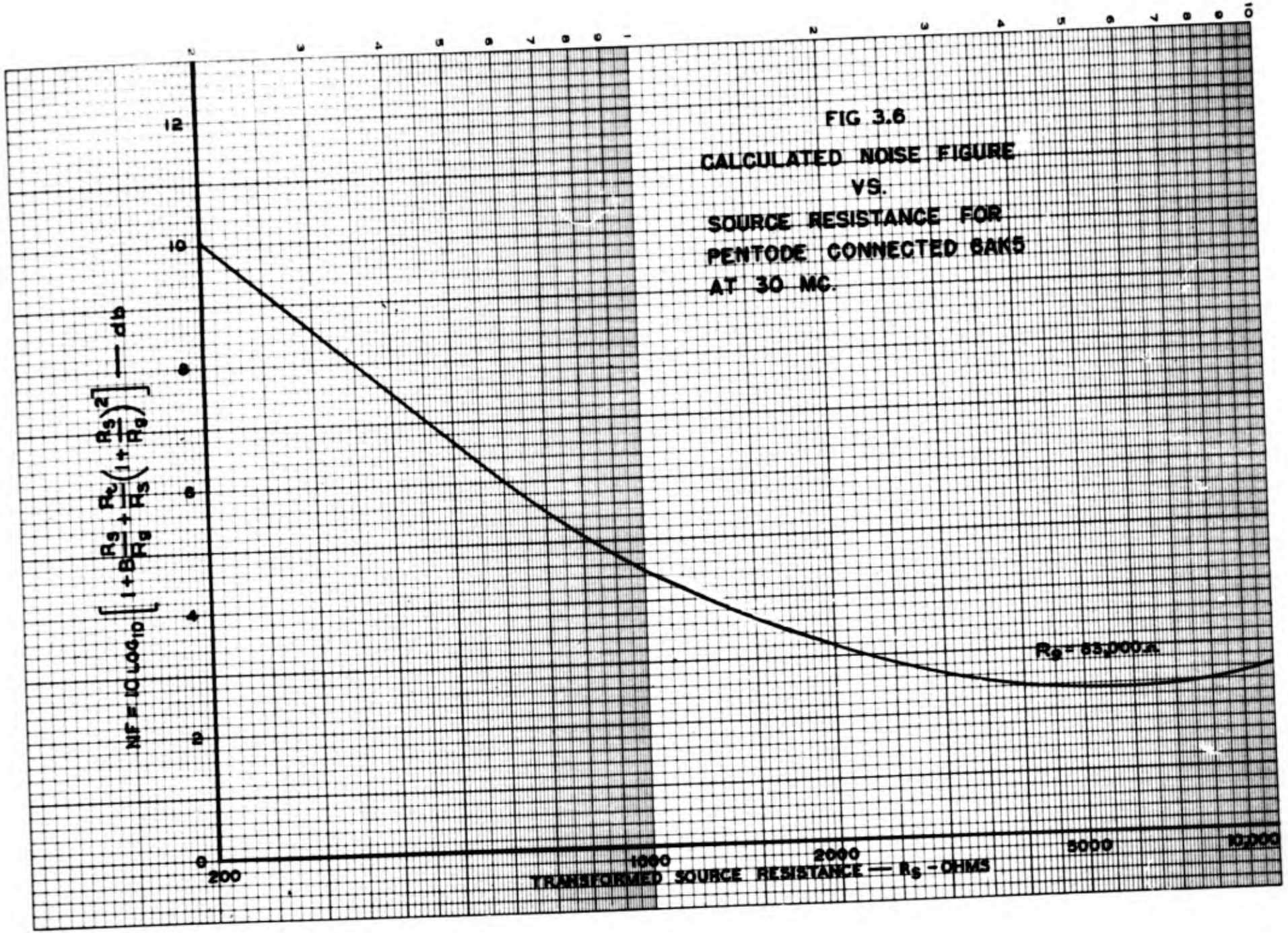
FIG. 3.6
CALCULATED NOISE FIGURE
VS.
SOURCE RESISTANCE FOR
PENTODE CONNECTED 6AK5
AT 30 MC.
$NF = 10 \log_{10}\left[1 + B\frac{R_s}{R_g} + \frac{R_e^2}{R_s}\left(1+\frac{R_s}{R_g}\right)^2\right]$ — db
12
10
8
6
4
2
0
200
1000
2000
5000
10,000
TRANSFORMED SOURCE RESISTANCE — R_s - OHMS
R_g = 65,000Ω

Equation 3.1 yields only the first order effects of changing transformed source impedance, but as such, it is valuable since it indicates an approximate value around which empirical adjustments may be made. Although the noise figure deteriorates rapidly for low values of R_s, it is sometimes necessary to operate at a value somewhat lower than the optimum in order to realize the bandwidth desired.

In the design of most interstage transformers for I.F. amplifiers of considerable bandwidth, both the primary and secondary are loaded with a resistance and generally the primary and secondary Q's are either equal or differ by a small ratio. It is undesirable from the standpoint of noise figure to incorporate any secondary loading in the input transformer and consequently it is not possible to employ the general high-Q theory in this type of design. For wide-band applications the transitionally coupled low-Q theory[9] is applicable. This theory has been developed for the case when the primary and secondary Q's are low and equal and for the case when one of the Q's is infinity. The latter case is applicable to the design of input transformers when the secondary Q is unloaded and very high (100 or so). Transitional coupling is that which yields a maximally flat pass-band; it is somewhat higher than critical coupling (the coupling which yields maximum secondary voltage).

The circuit arrangement shown in Figure 3.7 is the general form used for connecting a push-pull converter to the input of a single-ended amplifier. All the formulas for the conventional single-ended input transformer apply if L_B is twice the value calculated for the single-ended transformer. Under these circumstances it is necessary to consider only one-half of the transformer in the design procedure. It should be pointed out that G_B does not represent a physical resistor but represents all the conductances on the secondary side of the transformer lumped together.

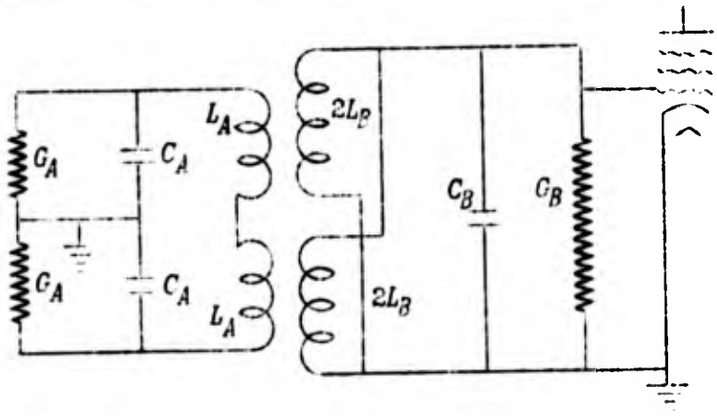

Figure 3.7

[9] Valley and Wallman, "VACUUM TUBE AMPLIFIERS", MIT Series, Vol. 18, Chap. 5, McGraw Hill Book Co., New York, 1948.

In the trial design of a balanced input transformer the value of the mixer conductance G_A and the value of primary and secondary capacitance will generally be known, and this is sufficient to start the design. For the IN 26 crystal, G_A has a mean value of 2000 micromhos and for the 6 AK5, the total secondary capacitance is about 7 uuf. Assume that the primary capacitance, C_A, equals 25 uuf and that the I.F. amplifier center frequency is to be 30 mc. The midband transformed source conductance G_s [10] then becomes,

$$G_s = \frac{C_B\ G_A}{2C_A} = \frac{7 \times 10^{-12} \times 2000 \times 10^{-6}}{2 \times 25 \times 10^{-12}} = 280\ \mu\text{mhos.} \qquad 3.2$$

or $R_s = \frac{1}{G_s} = 3600\ \Omega$

The 3 db bandwidth is then:

$$\Delta f = \frac{\sqrt{2}\ G_s}{2\pi\ C_B} = \frac{1.4 \times 280 \times 10^{-6}}{6.28 \times 7 \times 10^{-12}} \approx 9\ \text{mc} \qquad 3.3$$

If the input network is transitionally coupled, ($K^2\ Q_A^2 = 1/2$) the coefficient of coupling may be found from the following equation.

$$K = \frac{G_A}{f\ 2\pi\ C_A\ \sqrt{2}} = \frac{2000 \times 10^{-6}}{6.28 \times 30 \times 10^6 \times 25 \times 10^{-12} \times \sqrt{2}} = 0.294 \qquad 3.4$$

and the primary Q, Q_A becomes,

$$Q_A = \sqrt{\frac{0.5}{K^2}} = 2.36 \qquad 3.5$$

In a double tuned circuit, the optimum transformed source conductance can be achieved either by increasing C_A, as shown in equation 3.2, or by decreasing K. Increasing C_A has the disadvantage of increasing the primary coil loss conductance. If K has to be decreased much below transitional in order to increase the transformed source resistance to optimum, the shape of the response curve of the input circuit approaches that of a single tuned circuit. Under these conditions, for a given G_s, the bandwidth is appreciably less than when C_A is increased and the coupling kept transitional. The midband transformed source conductance can be written as

$$G_s = \frac{K^2\ (2\pi\ f_o)^2\ C_A\ C_B}{G_A}$$

[10] Loc. Cit., Section 13.14

so that as G_A increases, the bandwidth decreases, approaching that of a single tuned circuit, while the transformed source conductance decreases causing R_s to increase and approach the optimum value, consequently, the choice of either adjusting the transformer for minimum amplifier noise figure or maximum bandwidth is apparently presented. It is possible, however, to increase the bandwidth with but a small increase in the noise figure by adding cathode-lead inductance in the first stage.

In transitionally coupled, double-tuned, circuits of large fractional bandwidth, it is necessary to tune the primary and secondary coils to frequencies lower than the center frequency f_0. From the analysis of C. P. Gadsden[11] the ratio of primary frequency to center frequency, for the example above, is $f_1/f_0 = 0.99$ and the ratio of secondary frequency to center frequency is $f_2/f_0 = 0.96$. Therefore the primary, with the secondary open-circuited, will resonate at 30 x 0.99 = 29.7 mc/s and the secondary with the primary open-circuited will resonate at 30 x 0.96 = 28.8 mc/s. Using the known values of primary and secondary capacitance, the primary and secondary inductances will be $L_A = 1.14\ \mu h$ and $L_B = 4.35\ \mu h$. Since two secondaries are placed in parallel they should be made twice as large as the calculated value, or 8.7 μh. It should be realized that this design is only approximate at best, and empirical adjustments are necessary before a satisfactory transformer can be obtained.

The transformer assembly is shown in figures 3.8 and 3.9. To reduce capacitative coupling, adjacent ends of the primary and secondary coils are made to operate at RF ground potential. The by-pass condenser between the two ends of the primary coils insures their operation at the same potential, while isolating the d.c. returns for the two crystals.

Since the outer ends of the primary and secondary windings barely contribute to the mutual inductance, the self-inductance of the individual primary and secondary windings can be conveniently adjusted by varying the spacing of the outer (grounded) few turns. It is convenient to use a Q-meter for these adjustments since the actual frequency and capacitance can be simulated. The Q-meter also provides an easy means of empirically determining the coupling coefficient after the primary and secondary inductances are adjusted to their correct values.

The width of the dielectric fin separating the primary and secondary windings of each half of the transformer is determined experimentally for the coupling coefficient desired. Besides providing uniformity of coupling for both sections of the transformer (if the primary and secondary windings are started close to the fin), it also serves as a tie-point for the inside windings.

---

[11] Loc. Cit. Section 5.5

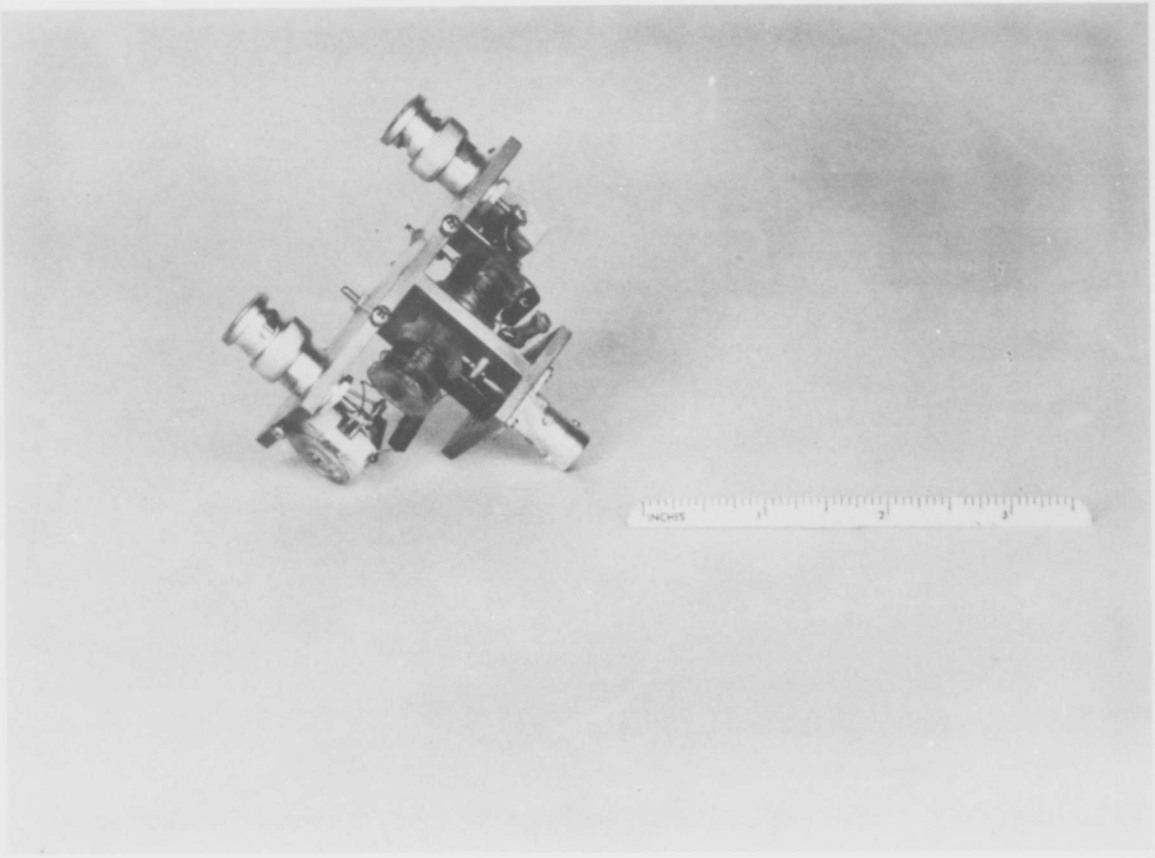

Figure 3.8 30 Mc Balanced Input Transformer

E.P. NO. 1485-9-18C

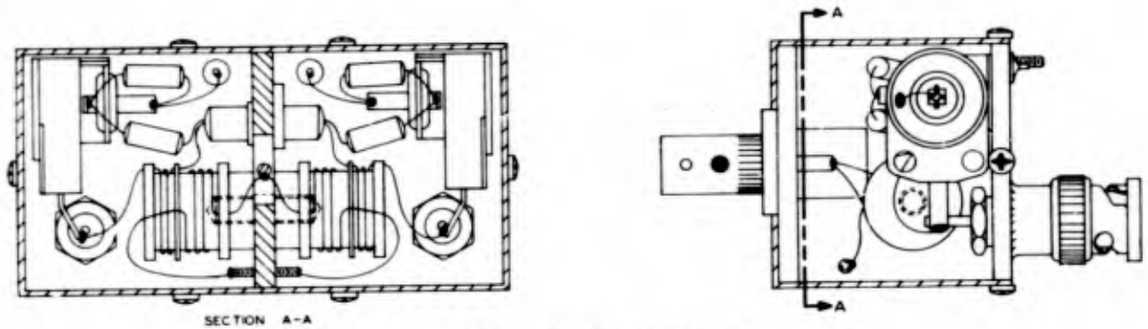

SECTION A-A

TRANSFORMER ASSEMBLY
(SCALE : 2" = 1")

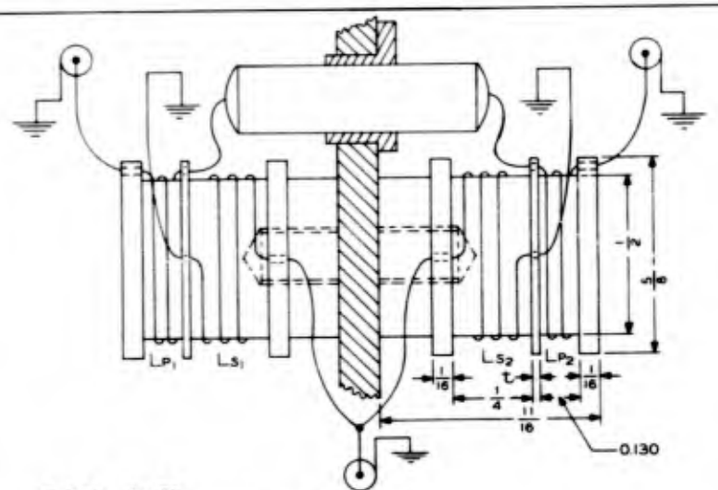

TYPICAL VALUES
L_{P_1} & L_{P_2} = 7T #30 ENAM. - CLOSE WOUND
L_{S_1} & L_{S_2} = 20T #30 ENAM. - CLOSE WOUND
L_{P_1} & L_{P_2} = 1.46 μh ; Q UNLOADED = 95
L_{S_1} & L_{S_2} = 4.24 μh ; Q UNLOADED = 95
t = 0.022 IN.

DETAIL DWG. OF 30 MC. BALANCED TRANSFORMER FOR COUPLING IN26 CRYSTALS TO PENTODE CONNECTED 6AK5 FOR A 7 MC. BANDWIDTH.
COIL MAT'L. - ACRYLIC
(SCALE : 4" = 1")

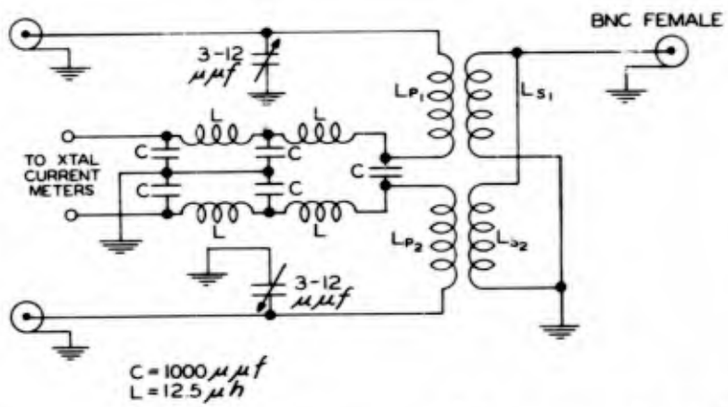

C = 1000 $\mu\mu f$
L = 12.5 μh

TRANSFORMER CIRCUIT DIAGRAM
FIG. 3.9

ALTERATIONS

COLLINS RADIO COMPANY
CEDAR RAPIDS, IOWA

30 MC BALANCED
INPUT TRANSFORMER

The filters in the ground potential ends of the two primaries prevent any I.F. signal power from being delivered to the crystal current meters and they also present a large attenuation to any signal that might be picked-up on the crystal current meter leads.

Figure 3.10 is the complete circuit diagram of the I.F. amplifier employed in the Radio Sextant and the 1.25 cm. radiometer. The amplifier employs 6AK5 pentode connected tubes arranged to form a pair of staggered-triples at a center frequency of 30 mc. and a bandwidth of about 8 mc. The amplifiers were originally constructed by the Galvin Co. and were modified in this laboratory to accommodate the balanced input transformer. The overall amplifier gain is around 90 db.

A matched line noise generator [12] and associated equipment were constructed for measuring the noise figure of I.F. amplifiers. The measured noise figures varied from 3 to 5 db, when the overall bandwidth was approximately 8 mc. These values are somewhat higher than the minimum obtainable, as shown in figure 3.5, and are a result of the transformed source resistance being too low. This is the penalty paid for the wide bandwidth.

The operation of the present I.F. amplifiers has disclosed several faults in their construction. Due to the extreme sensitivity of the I.F. amplifier and the relatively poor decoupling in the plate, gain control, and filament lines, considerable disturbances were present in the output meter of the radiometer when interfering signals lying in the I.F. pass-band were present. Any transient current, resulting from the switching of other devices, also affected the output meter. By adding more filtering in the plate, gain, and filament lines, in the form of pi-filters, the external disturbances were reduced to a negligible value. It was also found essential that all leads entering the amplifier be well shielded and well grounded at only one point, prior to entering the amplifier, to prevent ground current loops from being formed.

As a result of theoretical considerations made of the diode detector and of measurements made on its operating level, it is felt that more gain could profitably be incorporated prior to the detector in order to insure its operation in the linear region.

3.1.3 Audio and Meter

It has been pointed out in previous sections that the output of the second detector of the I.F. strip is an a.c. voltage which is proportional to the temperature difference existing between the reference

---

[12] Yardley Beers, "NOISE FIGURES AND THEIR MEASUREMENTS", RADIATION LABORATORY REPORT #746, July 1945.

EXP NO. 1485-9-2C

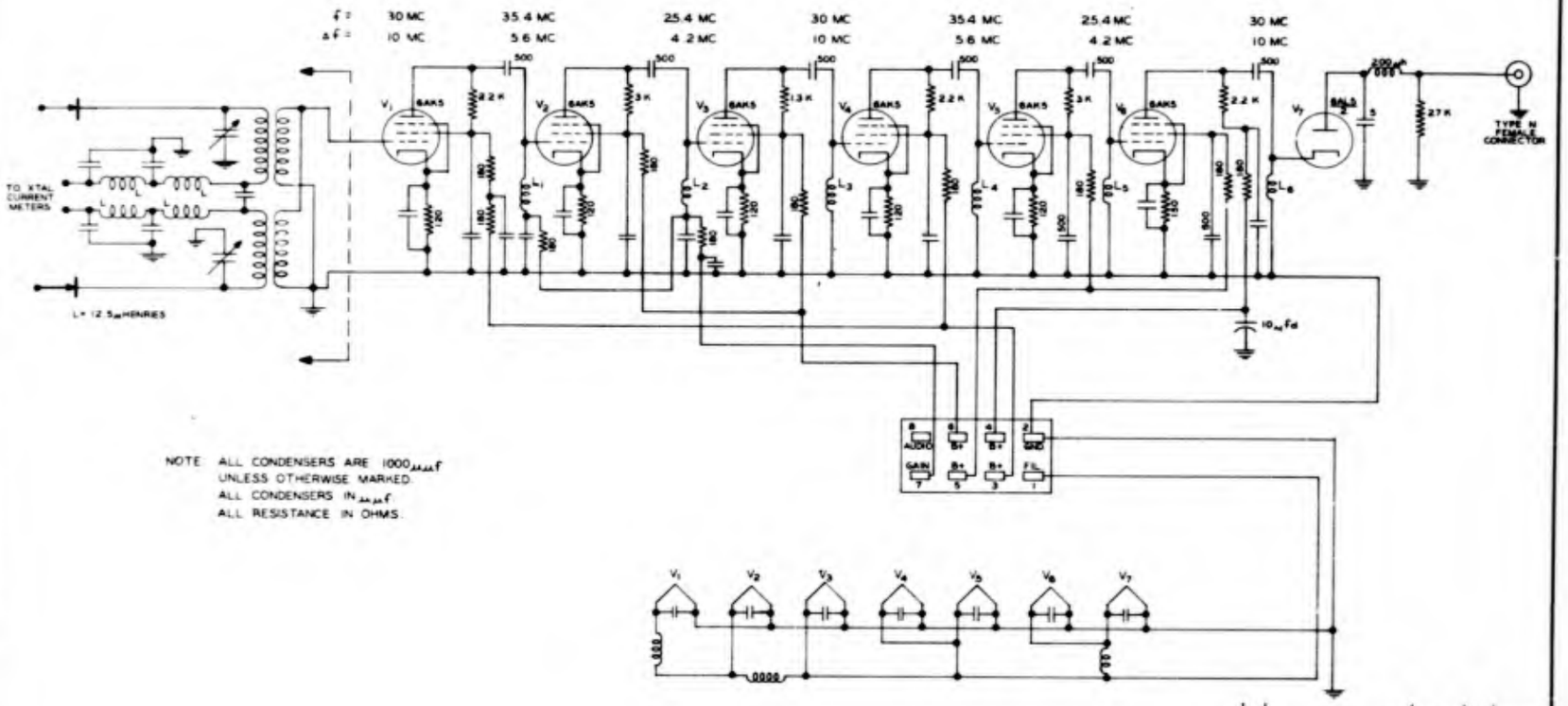

NOTE: ALL CONDENSERS ARE 1000 μμf UNLESS OTHERWISE MARKED.
ALL CONDENSERS IN μμf.
ALL RESISTANCE IN OHMS.

FIG. 3.10

NO.	DESCRIPTION	AUTHORITY	DATE	REVISION NO.

ALTERATIONS

COLLINS RADIO COMPANY
CEDAR RAPIDS, IOWA

MATERIAL:
ANGLES FINISH:
SCALE: x1
DRAWN BY | TRACED BY | APPROVED BY | DATE: 6-9-49

TITLE: BALANCED INPUT 30 MC I. F. AMPLIFIER

COLLINS PART NO. | ALTERATION NO.
GOVERNMENT PART NUMBER

UNLESS OTHERWISE SPECIFIED:
DECIMAL DIMENSIONS MAY VARY ±.010
FRACTIONAL DIMENSIONS MAY VARY ±1/32
MACHINED RIGHT ANGLES MAY VARY ±.1°
SHEARED RIGHT ANGLES MAY VARY ±.25°
BROKEN RIGHT ANGLES MAY VARY ±1°
ALL CONCENTRIC DIAMETERS MARKED WITH (*) SHALL BE HELD WITHIN ____ TOTAL INDICATOR READING.
ALL DIMENSIONS ARE FINISH DIMENSIONS INCLUDING APPLIED FINISH AND ARE GIVEN IN INCHES.

attenuator and the antenna termination. The frequency of this voltage is determined by the rate of switching from reference attenuator to antenna. The audio amplifier following the I.F. amplifier is therefore to be tuned to this modulation frequency so that other frequencies present in the noise output of the I.F. amplifier will be effectively removed.

Fig. 3.11 is a diagram of a suitable system for amplifying the desired modulation from the diode detector of the I.F. amplifier. Essentially, the unit consists of a band pass amplifier tuned to the modulation frequency, a phase detector, and a d.c. current amplifier for driving a 0-1 ma. meter.

In this particular amplifier, the band pass characteristic is obtained by degenerative feedback through a twin-T network connected between plate and grid of the first tube. By an appropriate design of the amplifier and twin-T network, the pass band can be readily controlled.

The twin-T network is a band rejection filter which can be tuned to a very sharp null. Since frequencies other than the null frequency are fed back out of phase to the grid of the first tube the amplifier response will be peaked at the null frequency. Fig. 3.12 is the response curve of the first stage of the amplifier shown in Fig. 3.11.

In general it is not desirable to make the pass band of the amplifier too narrow, since slight changes in the filter characteristic would then affect the output of the system. The bandwidth of this amplifier was controlled by simply varying the magnitude of the feedback voltage to the first grid. A bandwidth of 5 cycles to half power points proved satisfactory for this system.

Possibly the most important functions of the tuned stage are the rejection of 60 cps and odd harmonic voltages of the modulation frequency. Odd harmonics will cause an undesirable output from the phase detectors.

The phase detectors, consisting of the two 6SJ7 tubes following the 6SL7 phase inverter, give a d.c. output from the a.c. modulation voltage impressed on their control grid. This is accomplished by beating the input signal with the signal from the reference generator which is driven in synchronism with the reference wheel. Since the phase of the reference generator signal remains fixed, the d.c. output of the phase detector will reverse polarity for a reversal in phase of the input signal. This provides the "hot" and "cold" sense of the radiometer; an equivalent antenna temperature that is less than the reference wheel temperature will yield a modulation voltage differing in phase by 180° from the modulation voltage produced by an equivalent antenna temperature that is higher than the reference wheel temperature.

As the input signal has a random fluctuation imposed on it, the R.C. filter network following the phase detectors is used to smooth the d.c. output. The bandwidth of this low pass filter determines, in part,

EXP. NO. EP 1686-3-25C

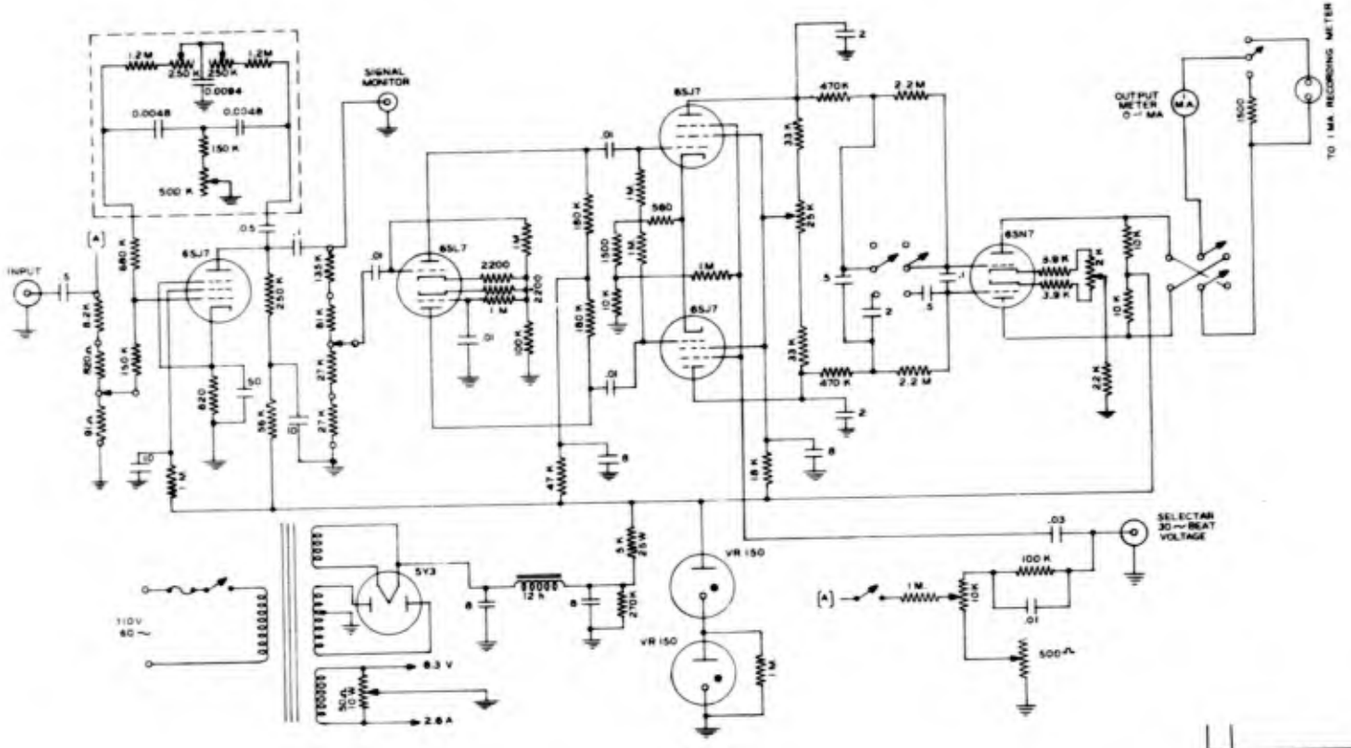

FIG. 3.11

NO.	DESCRIPTION	AUTHORITY	DATE	REVISION NO.

ALTERATIONS

COLLINS RADIO COMPANY
CEDAR RAPIDS, IOWA

MATERIAL
APPLIED FINISH
SCALE
DRAWN BY | CHECKED BY | APPROVED BY | DATE

TITLE
30 CYCLE
LOCK-IN AMPLIFIER

COLLINS PART NO. | ALTERATION NO.
GOVERNMENT PART NUMBER

UNLESS OTHERWISE SPECIFIED:
DECIMAL DIMENSIONS MAY VARY ±.010
FRACTIONAL DIMENSIONS MAY VARY ±1/32
MACHINED RIGHT ANGLES MAY VARY ±1°
SHEARED RIGHT ANGLES MAY VARY ±2°
BROKEN RIGHT ANGLES MAY VARY ±5°
ALL CONCENTRIC DIAMETERS MARKED WITH (*) SHALL BE HELD WITHIN ____ TOTAL INDICATOR READING.
ALL DIMENSIONS ARE FINISH DIMENSIONS INCLUDING APPLIED FINISH AND ARE GIVEN IN INCHES.

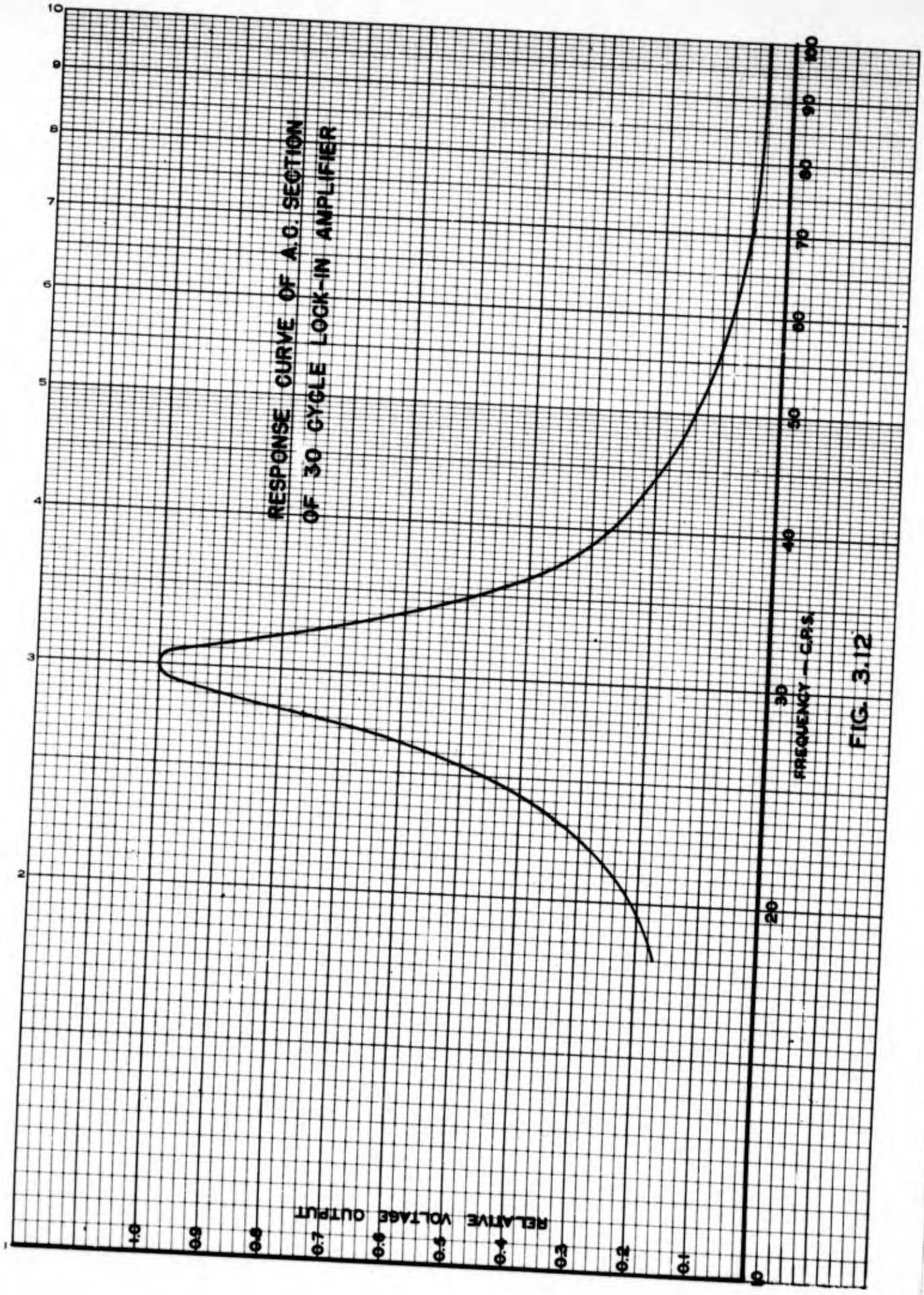
RESPONSE CURVE OF A.C. SECTION
OF 30 CYCLE LOCK-IN AMPLIFIER
RELATIVE VOLTAGE OUTPUT
FREQUENCY — C.P.S.
1.0
0.9
0.8
0.7
0.6
0.5
0.4
0.3
0.2
0.1
0
10
9
8
7
6
5
4
3
2
1
100
90
80
70
60
50
40
30
20

FIG. 3.12

the maximum sensitivity of the instrument. Reduction of the bandwidth lowers the minimum detectable signal, but at the expense of measuring time.

The current amplifier which drives the meter is a conventional vacuum tube voltmeter circuit. A reversing switch is provided at the meter terminals to allow the use of the complete meter scale for either "hot" or "cold" readings.

It will be observed that provision is made for introducing a small portion of the voltage from the reference generator to the input of the amplifier. By properly selecting its phase, the voltage introduced will tend to cancel the signal voltage supplied from the I.F. amplifier. This is equivalent to off-setting the "zero" of the output meter. It is accordingly very convenient for measuring small changes in equivalent antenna temperature when the background temperature is either very high or very low.

3.2 SYSTEMS

3.2.1 3.2 mm Radiometer

A radiometer operating in the millimeter wavelength range would have two virtues: Its antenna would be capable of great resolution with nominal antenna dimensions, and the operating wavelength of 3.2 mm would coincide with the next unexplored minimum of atmospheric absorption.

As no continuous wave 3.2 mm. oscillators were available for use as a signal generator or local oscillator, the first step in the construction of such a radiometer involved the generation of 3.2 mm. power. It seemed that the most simple way to obtain such power was to use the appropriate harmonic generated by a crystal that was being driven by a lower frequency oscillator.

The first experiments in this direction were made, using a IN26 crystal driven by a 2K-33 oscillator operating at a wavelength of 1.2 cm. Since the crystal unit in the IN26 is mounted in a co-axial cartridge the 1.2 cm. power was introduced through a co-axial line. The center conductor of the co-axial line passed through the wave-guide intended to propagate the 4th harmonic of 1.2 cm.

Two of these harmonic generators were constructed to facilitate inspection of the various harmonics produced. The method used was similar to the well-known spectrum analyzer technique employed at lower frequencies.

In this instance the small waveguides carrying the harmonic power were coupled together and the frequency of one of the fundamental oscillators was swept by applying a saw-tooth voltage to the reflector. The I.F. output terminals of one of the harmonic generators was attached to

the I.F. input terminals of a conventional K-band spectrum analyzer. The fundamental oscillator driving the other harmonic generator was not swept.

The waveguide carrying the harmonic power (dimensions 0.110" x .055" I.D.) passed the 3rd and higher harmonics. A pip could be expected on the screen of the spectrum analyzer for each harmonic above the second that was present, for at some part of its sweep the swept oscillator would produce a harmonic that differs from the harmonic produced in the other generator by the I.F. frequency.

Several IN26 crystals were tried as well as positive and negative d.c. bias on each generator, but no fourth harmonic of 1.2 cm. could be detected. The third harmonic and a small amount of second harmonic were easily detected, however.

The absence of fourth harmonic power may have been due to the effects of higher modes in the co-axial line of the crystal cartridge since the unit was designed for the 1.25 cm. wavelength region. At this time oscillator tubes operating in the wave-length range of 6 to 7 mm. became available and it was decided that better results could be obtained by utilizing the second harmonic of a 6.4 mm. oscillator.

Since the IN26 cartridge was not designed for shorter wavelengths, it seemed logical that better results could be obtained by mounting the crystal parts directly in the waveguides.

A sketch of the harmonic generator constructed for generating the second harmonic of 6.4 mm. power is shown in Fig. 3.13. A detector was also made by mounting the silicon and whisker assembly directly in a section of 0.100" x 0.050" I.D. waveguide.

To facilitate detection of the harmonic power, the fundamental oscillator was amplitude modulated with a 1000 cycle square wave. This allowed the use of an a.c. amplifier for detecting the 1000 cycle envelope of the harmonic power.

Using silicon slabs and whiskers (1.5 mil tungsten wire) from IN26 cartridges in the mount shown in Fig. 3.13, the 2nd harmonic r.m.s. voltage measured across a 500 ohm load connected to the detector crystal was 70 to 100 microvolts. As no facilities for measuring absolute power levels at either the fundamental or harmonic frequency were available, no estimate of efficiency could be made, except that it was obviously very low. The power from the fundamental 6 mm. oscillator was sufficient to yield one ma. of rectified crystal current at the generator crystal. Biasing the generator crystal with a battery in the direction which increased the crystal current increased the harmonic output by 2.5 db.

The type of construction described above is certainly limited to laboratory equipment. For field equipment the stability of the crystal

EXP. NO.

QUANTITY	USED ON	QUANTITY	ITEM NO.	QUANTITIES ARE FOR ONE ASSEMBLY: COLLINS PART NUMBER	GOVERNMENT PART NO.	PART NAME

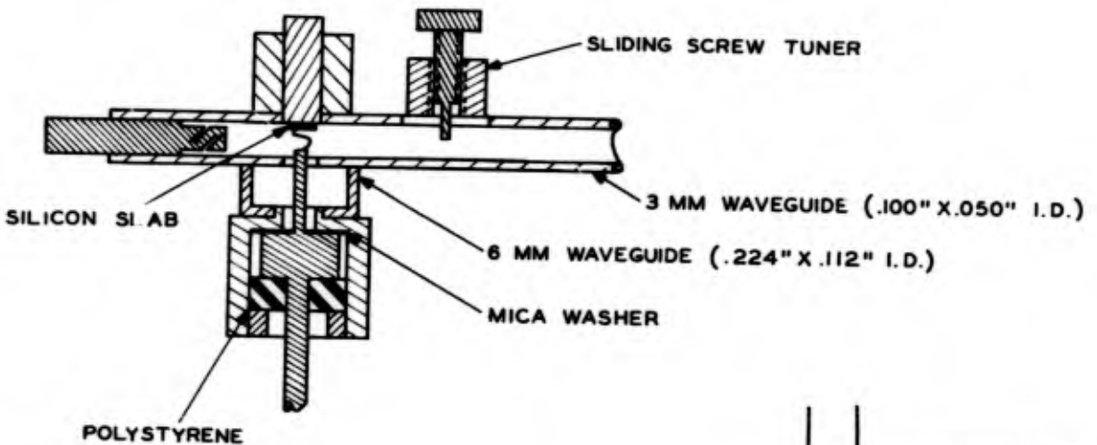

FIG. 3.13

NO.	DESCRIPTION	AUTHORITY	DATE	REVISION NO.

ALTERATIONS

COLLINS RADIO COMPANY
CEDAR RAPIDS, IOWA

MATERIAL:

APPLIED FINISH:

SCALE =1

DRAWN BY	CHECKED BY	APPROVED BY	DATE

TITLE

CRYSTAL MULTIPLIER FOR PRODUCING 3 MM POWER FROM A 6 MM OSCILLATOR

COLLINS PART NO. | ALTERATION NO.

GOVERNMENT PART NUMBER

UNLESS OTHERWISE SPECIFIED:
DECIMAL DIMENSIONS MAY VARY ±.010
FRACTIONAL DIMENSIONS MAY VARY ±1/32
MACHINED RIGHT ANGLES MAY VARY ±.1°
SHEARED RIGHT ANGLES MAY VARY ±.25°
BROKEN RIGHT ANGLES MAY VARY ±1.°
ALL CONCENTRIC DIAMETERS MARKED WITH (*) SHALL BE HELD WITHIN TOTAL INDICATOR READING.
ALL DIMENSIONS ARE FINISH DIMENSIONS INCLUDING APPLIED FINISH AND ARE GIVEN IN INCHES.

units and the oscillator would not be great enough for actual use. The fact that the whisker pressure on the silicon slab of the crystal unit must be very small complicates the problem of making a rugged system - also the 6 mm. oscillators at the present time are not very powerful or stable.

H. Q. North of the General Electric Company has described [13] some experiments involving the use of welded contact germanium crystals as harmonic generators. His results show that the welded contact germanium units produced ten to one hundred times more third harmonic than conventional silicon units. North's measurements were based on multiplication from a fundamental wavelength of 1.2 cm. to a wavelength of 4 mm.

On the basis of these results, the welded germanium unit seems to be the best third harmonic generator, as well as the most rugged, due to the fact that the whisker is welded to the germanium slab. In addition, the Klystron oscillators developed for the 9 mm. region are five to ten times more powerful than the 6 mm. oscillators as well as being more stable. Although the third harmonic produced by a crystal will be less intense than the second harmonic, the increased efficiency of the fundamental oscillator and added stability of the crystal unit would more than offset this disadvantage.

Time did not permit the investigation of these improvements, but it is recommended that future work include the suggestions outlined above.

3.2.2 S-Band Radiometer

The design* of a radiometer operating in the wavelength region from 9 to 11 cm. was undertaken. It was intended that this radiometer be used with the 8-foot paraboloid antenna furnished with a 615 B radar set.

At wavelengths in the vicinity of 10 cm., the noise spectrum of Klystron oscillators is narrow. At nominal I.F. frequencies of 30 mc. or more there is very little excess noise contributed by the local oscillator to over-all receiver noise. For this reason, a balanced magic tee mixer would have been unnecessary at this wavelength except for the fact that admittance variations in the antenna line, as discussed in Section 3.1.1, were still present. The spurious output caused by these admittance variations is probably more serious at this wavelength because the conversion loss of the crystals is less than at the shorter wavelengths.

---

[13] H.Q. North, "A COMPARISON OF SILICON AND GERMANIUM MICROWAVE CRYSTALS AS HARMONIC GENERATORS OF 4 mm. AND 6 mm. WAVES." G.E. Report 15, January 1946.

* This radiometer was designed according to the general design information given previously in Section 3.1

Fig. 3.14 is a photograph of the r.f. components constructed for the S-band radiometer. Waveguide was used throughout even though it made the over-all size much larger than it would have been if co-axial lines had been used. This was done to aid in the construction and tuning of the component parts.

A magic tee mixer was employed with an E-bend in each crystal arm so that a phase shifter* could be inserted between one crystal and the symmetry plane of the magic tee without separating the I.F. output terminals of the two crystals an undue amount. Each crystal holder was detachable and complete in itself so that it was matched easily before it was connected to the mixer.

The local oscillator assembly was all mounted on one piece of waveguide which was attached to the E-arm of the mixer magic tee. The local oscillator was a 2K41 Klystron which was coupled to the waveguide through a co-ax to waveguide transition. The attenuator which controlled the local oscillator drive was a section of IRC resistance strip mounted inside the waveguide in a manner which allowed motion of the strip across the guide. A wavemeter was attached to the remaining Klystron output co-ax for frequency monitoring.

The reference wheel shown in the photograph was made up of two circular sections of IRC resistance strip clamped together. The first section was made of 500 ohms per square and the second was made of 800 ohms per square material. The diameter of the wheel was 5 inches. The laminated construction was used to minimize the wheel diameter required to maintain a match for all wheel positions. This wheel resulted in the proper attenuation characteristic, but the V.S.W.R. looking into the reference wheel section was 1.25 in the worst position, a value too high for satisfactory operation. Further experiments indicated that a larger wheel diameter was required.

The r.f. components shown in the photograph were the only components specifically constructed for the S-band radiometer. No great emphasis was put on this radiometer because of the demands of the radio sextant.

3.2.3 K-Band Radiometer

The K-band radiometer was the first radiometer constructed; nearly all the designs were first tried in this set before they were incorporated into other equipment. The fact that this set operates at a wavelength that is near the peak of the water absorption band, with consequent contributions to the output from the atmosphere, makes reduction of data rather

* A phase shifter of the magic tee type, rather than the excessively long dielectric type, was used.

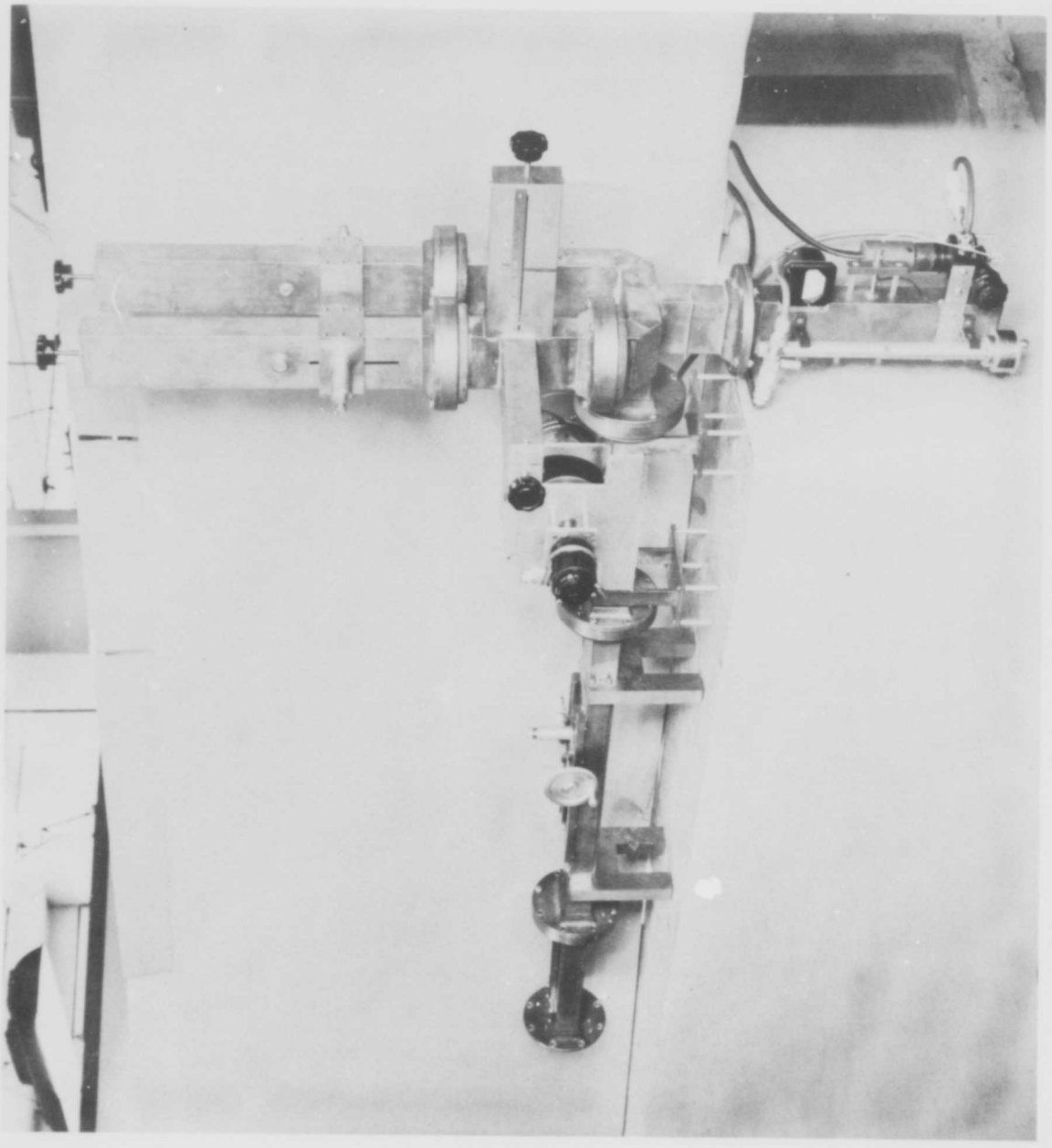

Figure 3.14 R.F. Components for 10 cm. Radiometer

complicated. This aspect is not always undesirable, however. A large amount of useful data have been obtained with this radiometer.

The design of the K-band radiometer follows that discussed in Section 3.1. All of the r.f. components were made in 1/2" x 1/4" O.D. standard waveguide. The mixer follows the special design outlined in Section 3.1.1; the phase shifter used consists of a tapered slab of polystyrene which can be moved across the waveguide. The reference wheel consists of a circular section of 400 ohms per square resistance strip which is 3 inches in diameter. This section is mounted eccentrically on a shaft so that at one position the wheel dips almost completely into the waveguide through a slot cut in the wide face of the guide. One-half revolution later the wheel is out of the guide with the edge of the wheel being even with the inside surface of the top of the waveguide. Since the wavelength is short, the 3-inch diameter wheel remains reasonably well-matched (Max. V.S.W.R. = 1.07) for all positions in the guide.

Fig. 3.15 is a photograph showing the radiometer r.f. and I.F. components mounted in a box. The box serves both as an electrical shield and a thermal insulator since it is desirable to maintain the reference wheel at a constant temperature.* It is also desirable to maintain the temperature of the local oscillator at a fixed value, since this, in conjunction with a well-regulated power supply, practically eliminates frequency drift.

It is extremely important that the I.F. amplifier be very well shielded and decoupled from its supply lines or that the entire box containing the radiometer act as a good shield, with all incoming leads filtered for frequencies that are passed by the I.F. amplifier.

The control console for this radiometer is shown in Fig. 3.16. The top panel contains two 0-1 ma. meters for monitoring the local oscillator drive to each crystal, and the center meter indicates resonance on the wavemeter. The second unit from the top is the 30-cycle lock-in amplifier. The two bottom units are the I.F. and local oscillator power supplies. On the left of the console is an audio amplifier and loud speaker which is very helpful in identifying extraneous noise.

Fig. 3.17 is a photograph of the radiometer connected to a 30-inch diamter paraboloid antenna and mounted on an equatorial mount. The hour angle axis of the mount can be driven by a synchronous motor for tracking celestial bodies.

---

* It will be observed that the local oscillator tuning knob and the wavemeter control shaft are brought out of the box so that control of the local oscillator frequency can be effected without disturbing the temperature equilibrium of the box.

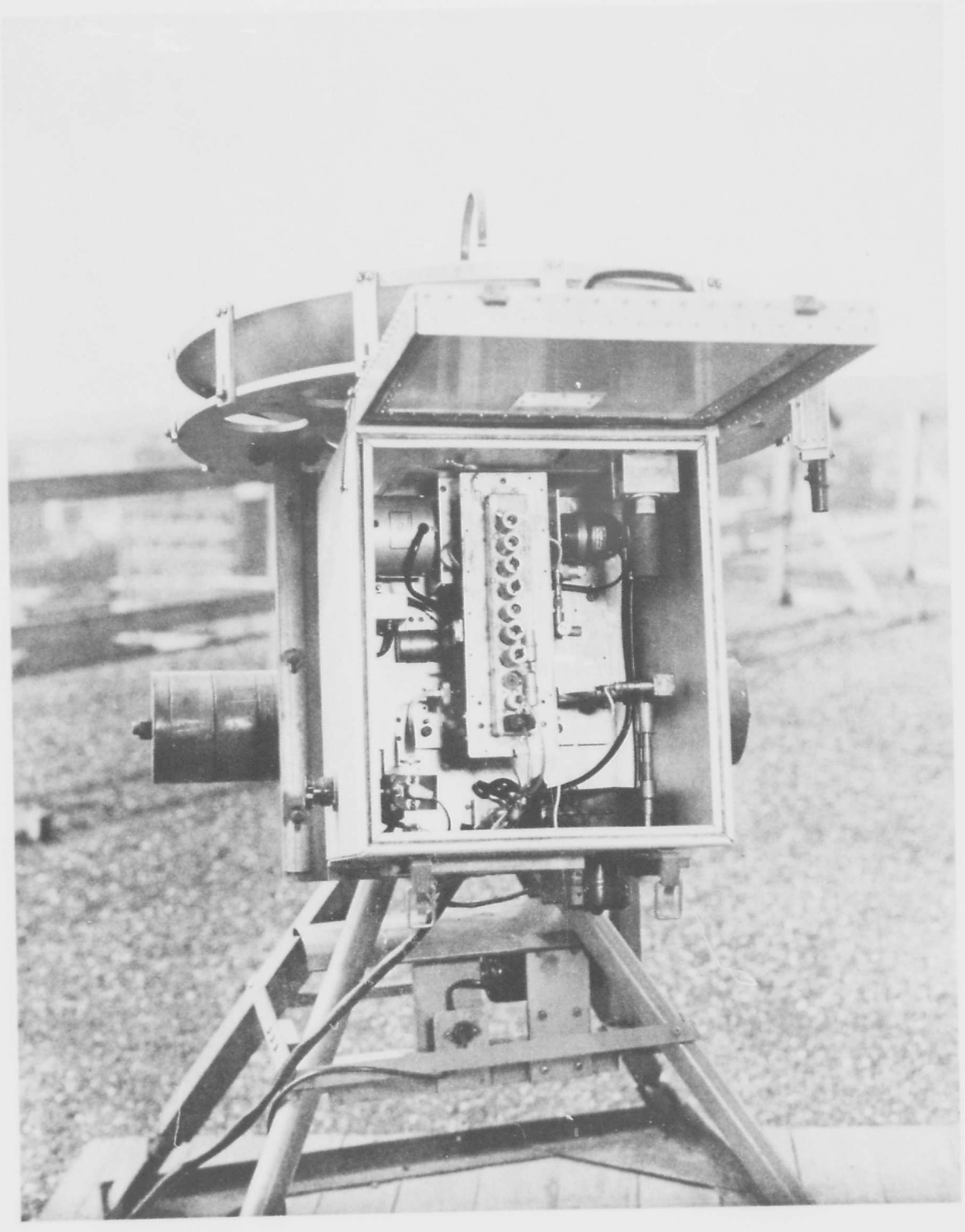

Figure 3.15 K-Band Radiometer

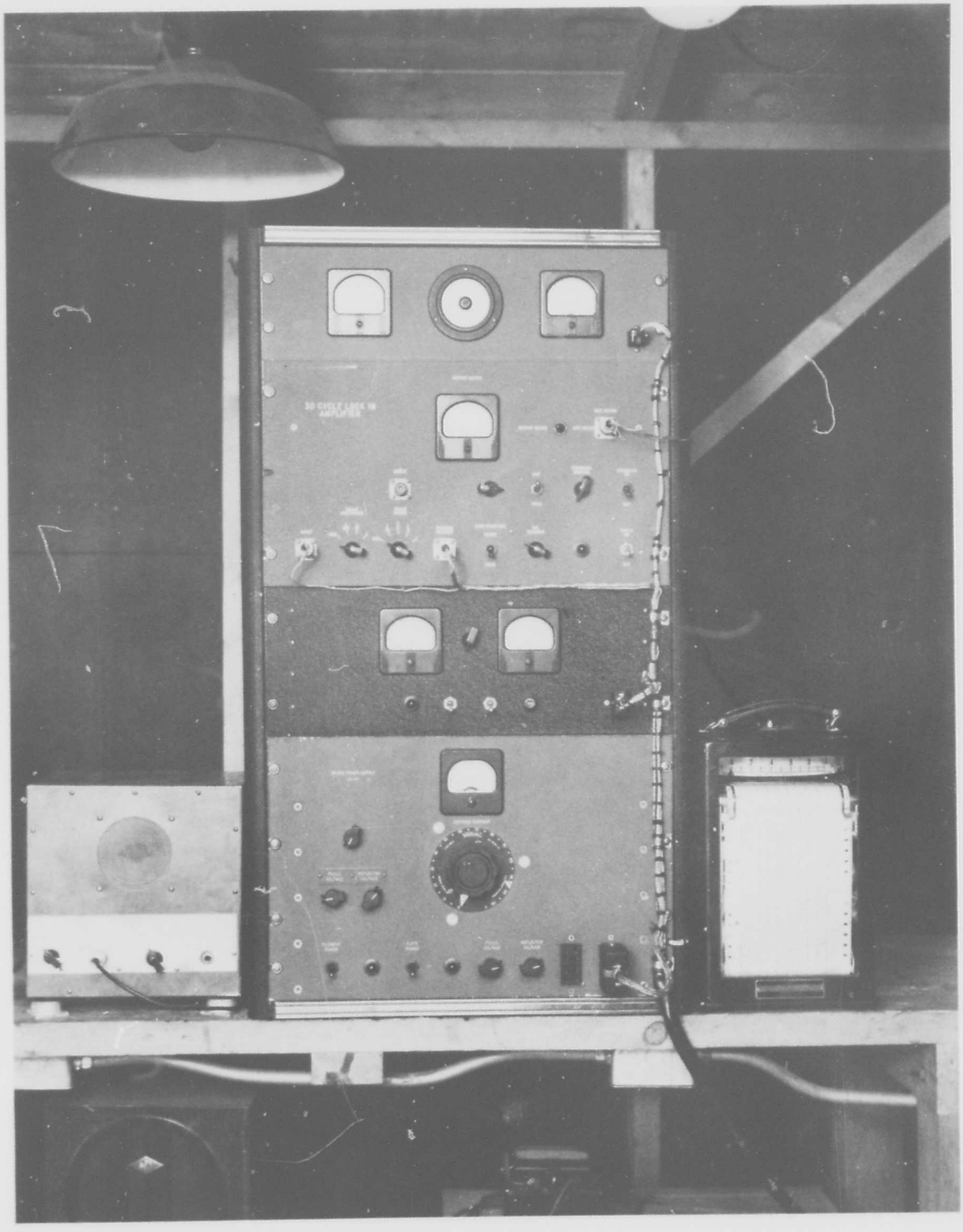

Figure 3.16 Radiometer Console

Figure 3.17 K-Band Radiometer and Equatorial Mount

The performance of this radiometer is essentially summed up by the data given in Fig. 3.18. The data were taken by substituting a matched termination for the antenna feed horn. The termination temperature was increased in steps and the radiometer output recorded on an Esterline Angus recording meter. A plot of the data shown in Fig. 3.18 is given in Fig. 3.19.

It is seen that the output meter reading is linear with respect to the difference between antenna temperature and reference wheel temperature. The linearity of this particular radiometer was checked for large signals corresponding to temperature differences of 3000 degrees, and the variation of output with temperature difference remained linear.

The maximum output meter fluctuation encountered in the run appears to be equivalent to a ± 3 degree temperature variation. The r.m.s. value of this fluctuation is approximately 1 degree which is higher than that predicted by the equation given in 2.2.1. The reason for this discrepancy is not understood.

The constants for the K-band radiometer are given below:

Operating Wavelength - 1.25 cm.

Type of Mounting - Equatorial

Antenna Diameter - 30 inches

Antenna 1/2 power beamwidths

E plane - - - - - - - - - - - - 1.28 degrees
H plane - - - - - - - - - - - - 1.17 degrees

Antenna Gain Relative
to isotropic - - - - - - - - - 42.3 db.
Receiver noise figure - - - - - 14.8 db.
Receiver bandwidth - - - - - - 14 mc.
Low pass filter bandwidth - - 0.1 cycle
Modulation frequency - - - - - 30 cycles

The greatest limitation of this and other radiometers, aside from the output meter fluctuations, arises when the system is used to measure absolute temperatures. Most of the difficulty arises in the calibration of the radiometer. If the calibration made with a test load is to apply when the antenna is connected, the admittance of the test load and that of the antenna must be the same, for the reasons mentioned in Section 3.1.1. One way to combat this difficulty is to use a high temperature calibrating source and a high gain antenna so that the admittance variation effects will represent only a small part of the total radiometer output.

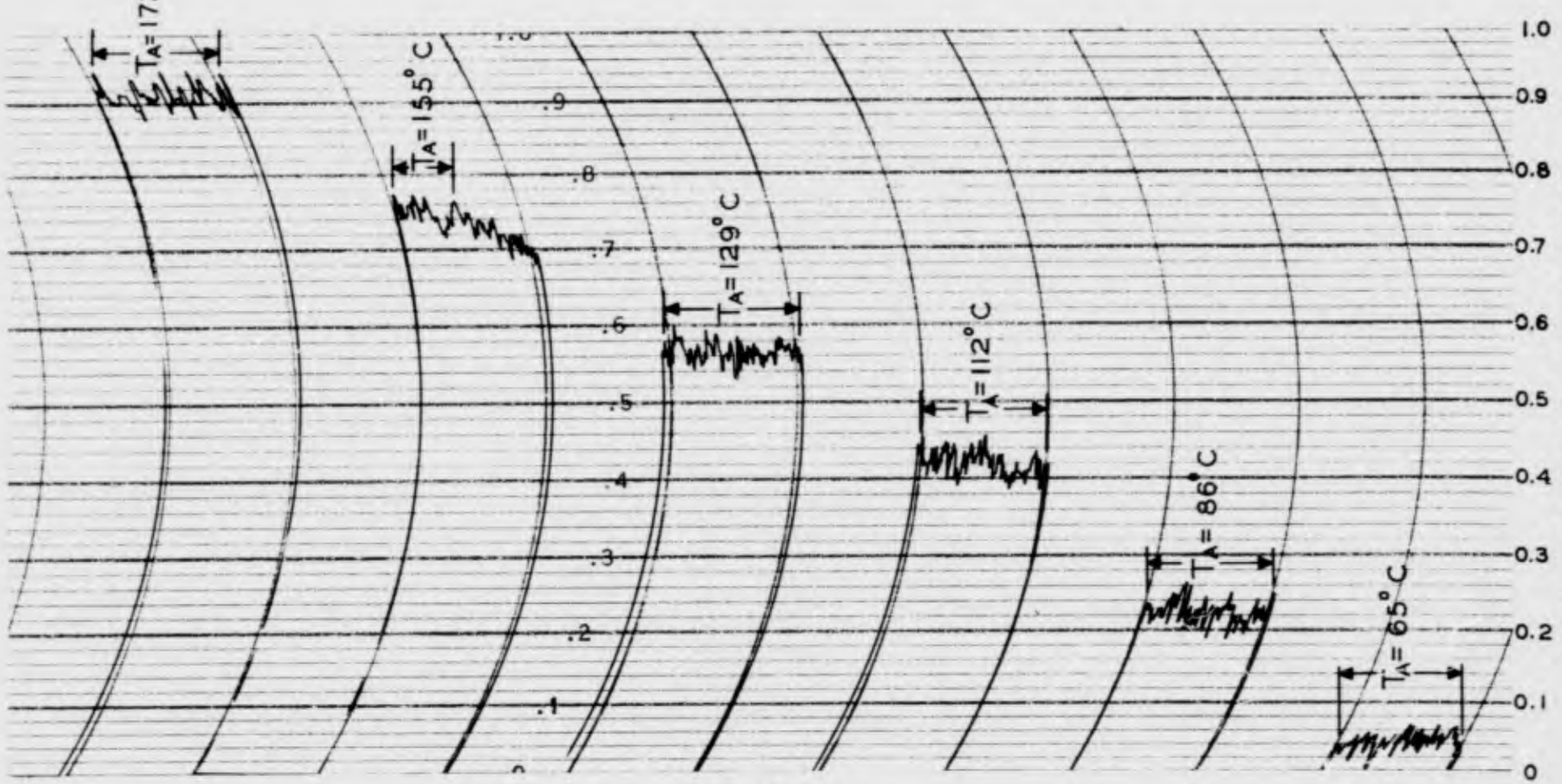

FIG. 3.18

RADIOMETER OUTPUT AS A FUNCTION OF ANTENNA TEMPERATURE

FIG. 3.19

CALIBRATION CURVE FOR 1.25 CM. RADIOMETER
ATTENUATOR SETTINGS 1, 1/10
REFERENCE WHEEL TEMPERATURE +60° C

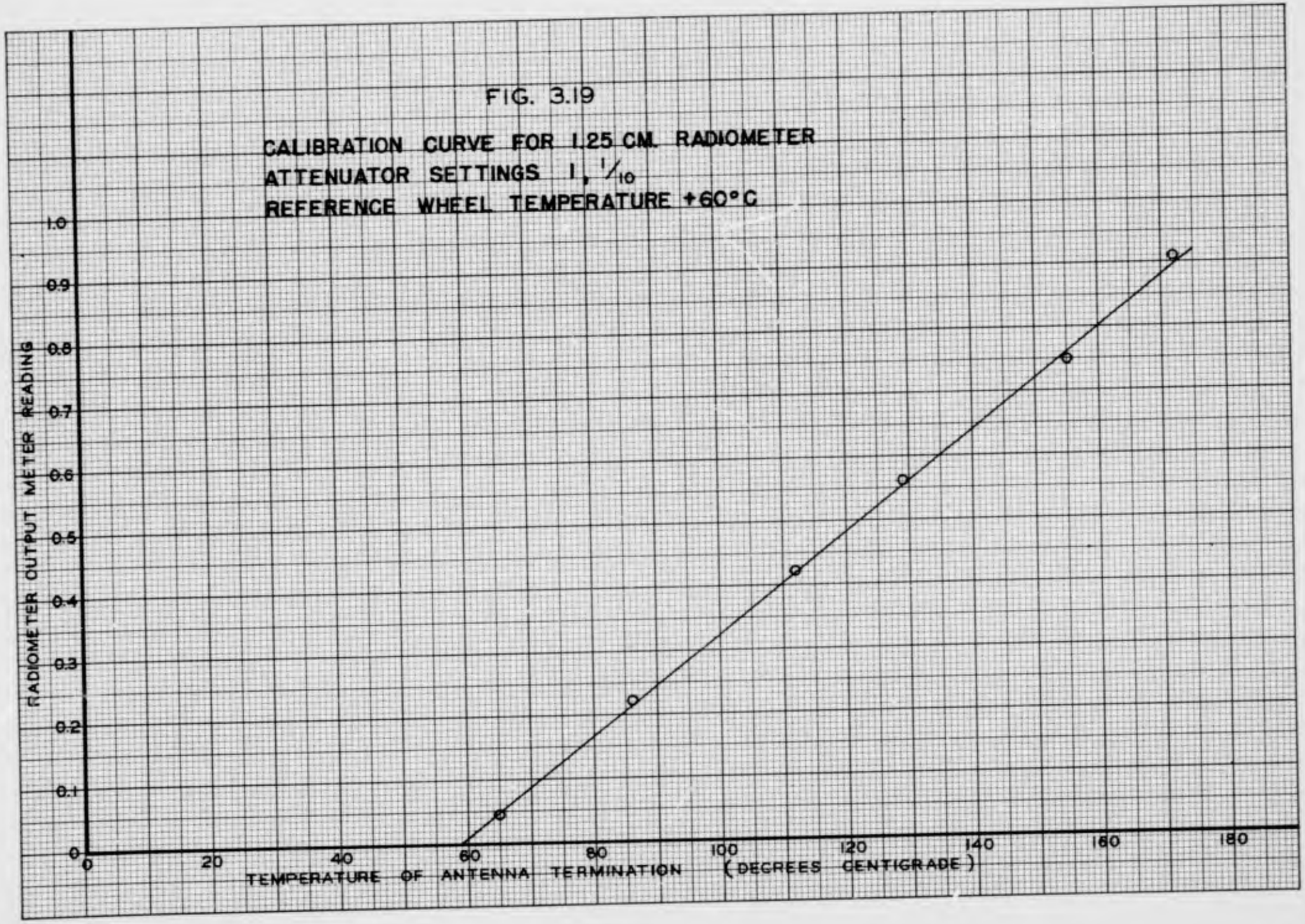

3.2.4 Automatic Radio Sextant

3.2.4.1 Introduction.

The purpose of this equipment is to provide a means for locating the sun under all weather conditions. The automatic feature permits continuous presentation of elevation and azimuth angles at a remote point.

The instrument was constructed about a 36-inch searchlight. The major modifications made on the searchlight were the removal of the arc assembly and the addition of a 48-inch diameter paraboloid reflector. Fig. 3.20 is a photograph of the modified searchlight.

An operating wavelength of 1.87 cm. was chosen for the experimental model since this wavelength seemed to be the best compromise between undesirable atmospheric absorption effects and excessive antenna dimensions.

3.2.4.2 Theory of Operation.

The problem is primarily one of making an antenna automatically follow the sun. To accomplish this, some method of obtaining error information which tells the direction that the antenna is displaced from the sun must be employed. The method chosen is similar to that used in one of the common types of Automatic Tracking Radars. The type of radar referred to employs a conically scanning antenna which modulates the reflected power from the target. The phase of the modulation imposed on the received signal is then continuously compared with voltages generated by a two-phase reference generator which is directly coupled to the scanning mechanism.

Instead of receiving reflected power from a target, the radio sextant receives directly radiated power from the sun, but the mechanism of modulation due to the conically scanning beam is the same as in the Automatic Tracking Radar. In order to obtain sufficient power from the sun to operate this system, it is necessary that the antenna beam width be of the same order of magnitude as the angle subtended by the sun. During the scanning cycle, the antenna beam will scan various areas on the sun depending on the orientation of the scan axis with respect to the sun. Thus, if the scan axis points directly toward the center of the sun, the received energy is essentially constant over the scanning cycle. If the scan axis is displaced from the center of the sun, the received energy will be greater at some points of the scan than at others. This results in the modulation of the received signal from the sun. It can be shown that this modulation will have a definite phase determined by the direction of the displacement of the scan axis from the center of the sun.

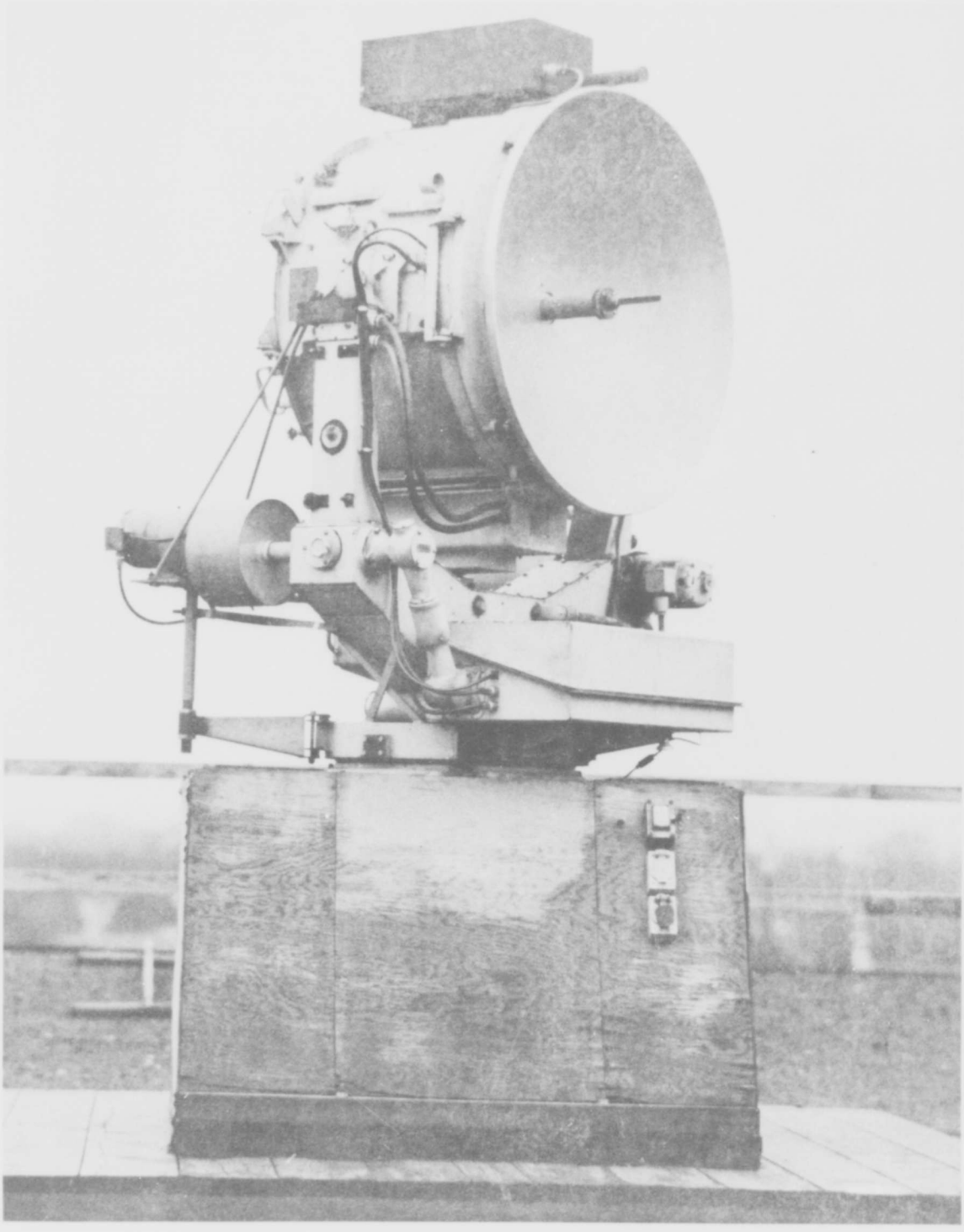

Figure 3.20 Automatic Radio Sextant

Fig. 3.21 is a block diagram of the radio sextant. The signal, received from the sun and modulated by the conically scanning antenna, is converted to an intermediate frequency by beating it with the signal from a local oscillator in a crystal mixer. The resulting I.F. signal is amplified and the modulation extracted by the second detector of the I.F. amplifier. The modulation voltage is amplified in a selective amplifier and its phase compared with that of a reference generator which is geared to the scanning mechanism. This comparison of signal and reference voltages results in a d.c. voltage that is proportional to the angular error in one plane. To get error voltages in two planes at right angles to each other, the modulation signal is split and compared with the voltages generated by a two-phase reference generator, the phases of which are 90° apart. The error voltages are used to control amplidyne generators which drive the motors positioning the antenna.

3.2.4.3 Antenna Design

The requirements of the antenna are that the gain and scan angle must be judiciously chosen so that an angular error of 0.1 degree in the system will yield a large enough modulation of the antenna temperature to permit operation of the automatic positioning devices in the sextant.

This problem was somewhat complicated by the fact that the beamwidth of the antenna must be comparable to the angle subtended by the sun. Therefore, the gain of the antenna is not constant over the desired solid angle and it becomes necessary to solve the integral $\int_{\Omega} G(\theta, \phi)\, d\Omega$ for the various positions of the beam as it scans the sun. This work was performed in a general manner and reported in Collins Engineering Report No. 149.

Fig. II of CER #149 is a plot of the power received by an antenna as the antenna beam is swept across a circular source. The calculations were made for a particular type of antenna, i.e., a paraboloid reflector illuminated by a symmetrical feed system which tapers the illumination so that at the edges of the reflector the illumination is down by 10 db from that at the center.

With the aid of this curve, the energy received by the antenna at every point of the conical scan for any chosen angular error can be determined. A sample plot of the received energy for two angular errors of the same magnitude but opposite directions is shown in Fig. 3.22. It will be observed that the phase of the modulation produced differs by 180° for errors that have opposite sense. The peak to peak modulation for various angular errors is plotted in Fig. 3.23.

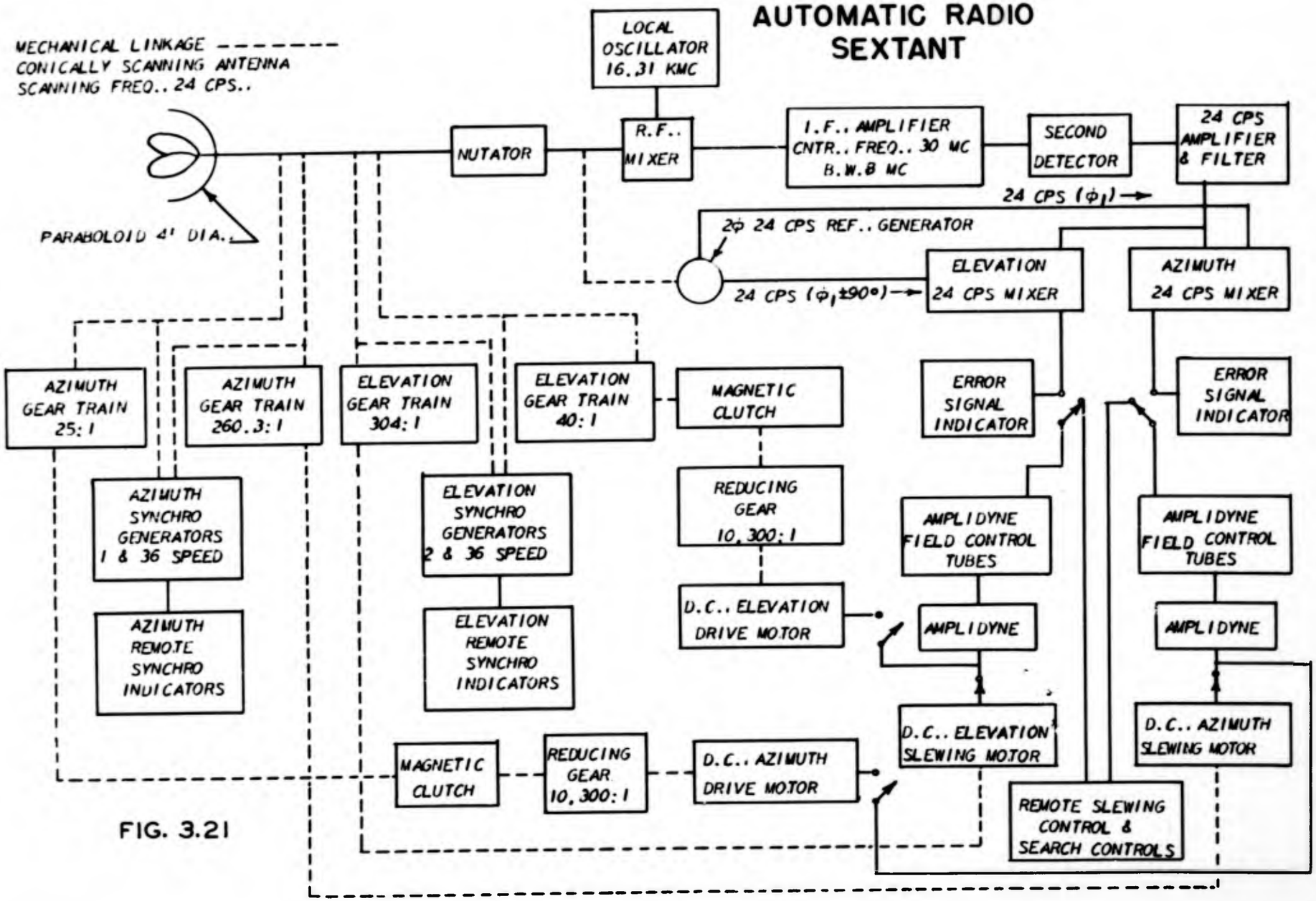
AUTOMATIC RADIO SEXTANT
MECHANICAL LINKAGE
CONICALLY SCANNING ANTENNA
SCANNING FREQ.. 24 CPS..
PARABOLOID 4' DIA.
LOCAL OSCILLATOR 16.31 KMC
NUTATOR
R.F.. MIXER
I.F.. AMPLIFIER CNTR.. FREQ.. 30 MC B.W.8 MC
SECOND DETECTOR
24 CPS AMPLIFIER & FILTER
24 CPS (φ1)
2φ 24 CPS REF.. GENERATOR
24 CPS (φ1±90°)
ELEVATION 24 CPS MIXER
AZIMUTH 24 CPS MIXER
AZIMUTH GEAR TRAIN 25:1
AZIMUTH GEAR TRAIN 260.3:1
ELEVATION GEAR TRAIN 304:1
ELEVATION GEAR TRAIN 40:1
MAGNETIC CLUTCH
ERROR SIGNAL INDICATOR
ERROR SIGNAL INDICATOR
AZIMUTH SYNCHRO GENERATORS 1 & 36 SPEED
ELEVATION SYNCHRO GENERATORS 2 & 36 SPEED
REDUCING GEAR 10,300:1
AMPLIDYNE FIELD CONTROL TUBES
AMPLIDYNE FIELD CONTROL TUBES
AZIMUTH REMOTE SYNCHRO INDICATORS
ELEVATION REMOTE SYNCHRO INDICATORS
D.C.. ELEVATION DRIVE MOTOR
AMPLIDYNE
AMPLIDYNE
D.C.. ELEVATION SLEWING MOTOR
D.C.. AZIMUTH SLEWING MOTOR
MAGNETIC CLUTCH
REDUCING GEAR 10,300:1
D.C.. AZIMUTH DRIVE MOTOR
REMOTE SLEWING CONTROL & SEARCH CONTROLS

FIG. 3.21

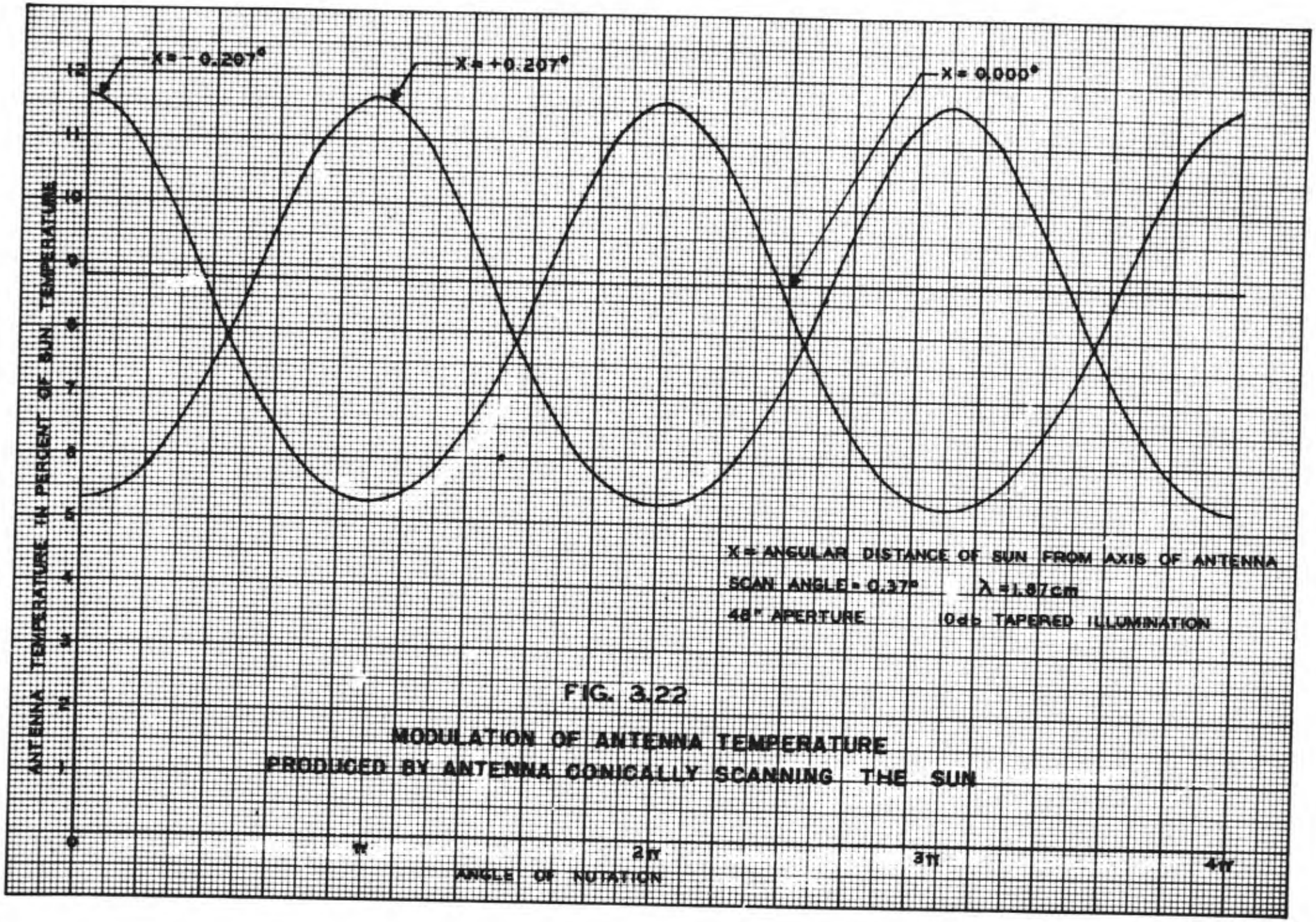

FIG. 3.22

MODULATION OF ANTENNA TEMPERATURE
PRODUCED BY ANTENNA CONICALLY SCANNING THE SUN

The choice of paraboloid diameter was made by plotting curves similar to Fig. 3.23 and selecting the minimum antenna diameter which would give at least 3 percent* modulation of the signal radiated by the sun. The paraboloid selected has a diameter of 48 inches and a focal length of 14.5 inches.

The choice of the scan angle is not critical. However, the scan angle should be approximately one half the half power beam width of the antenna pattern. The scan angle used here was 0.37 degrees.

The conical scan was effected by nutating the antenna feed inside the paraboloid reflector. Nutation of the double dipole feed is accomplished by rotating an off-set bearing near the dipole end of the feed line. The other end of the feed line which couples to the mixer is supported by gimbals. The r.f. connection between the mixer and antenna feed consists of a choke-flange joint with an air gap of .010 inches between the choke and flange. The feed line was made long in order to minimize the relative motion between choke and flange as the feed nutates. Fortunately, this nutation process introduces negligible admittance variations in the antenna line.

The scan angle is determined by the amount the center line of the feed is displaced from the axis of the paraboloid. For deep parabolas the angular shift of the beam is less than the angular displacement of the feed with respect to the paraboloid axis. The scan angle is approximated by

$$\left[1 - \frac{1}{2(1+q)}\right]\delta \quad \text{where } q = \left(\frac{4 \times \text{Focal Length}}{\text{Mirror Diameter}}\right)^2$$

and δ is the angular displacement of the feed with respect to the paraboloid axis.

The agreement between the calculated curve of angular error vs. relative modulation and the measured curve is shown in Fig. 3.24. To make this comparison, both the calculated and measured peak modulation values were normalized to unity. The agreement is fair although the distance between the measured peaks is slightly less than that between the calculated peaks.

---

* It has been determined by the method of Section 2.2.2 and Fig. 2.26 that a 3 percent change produced a sufficient audio signal.

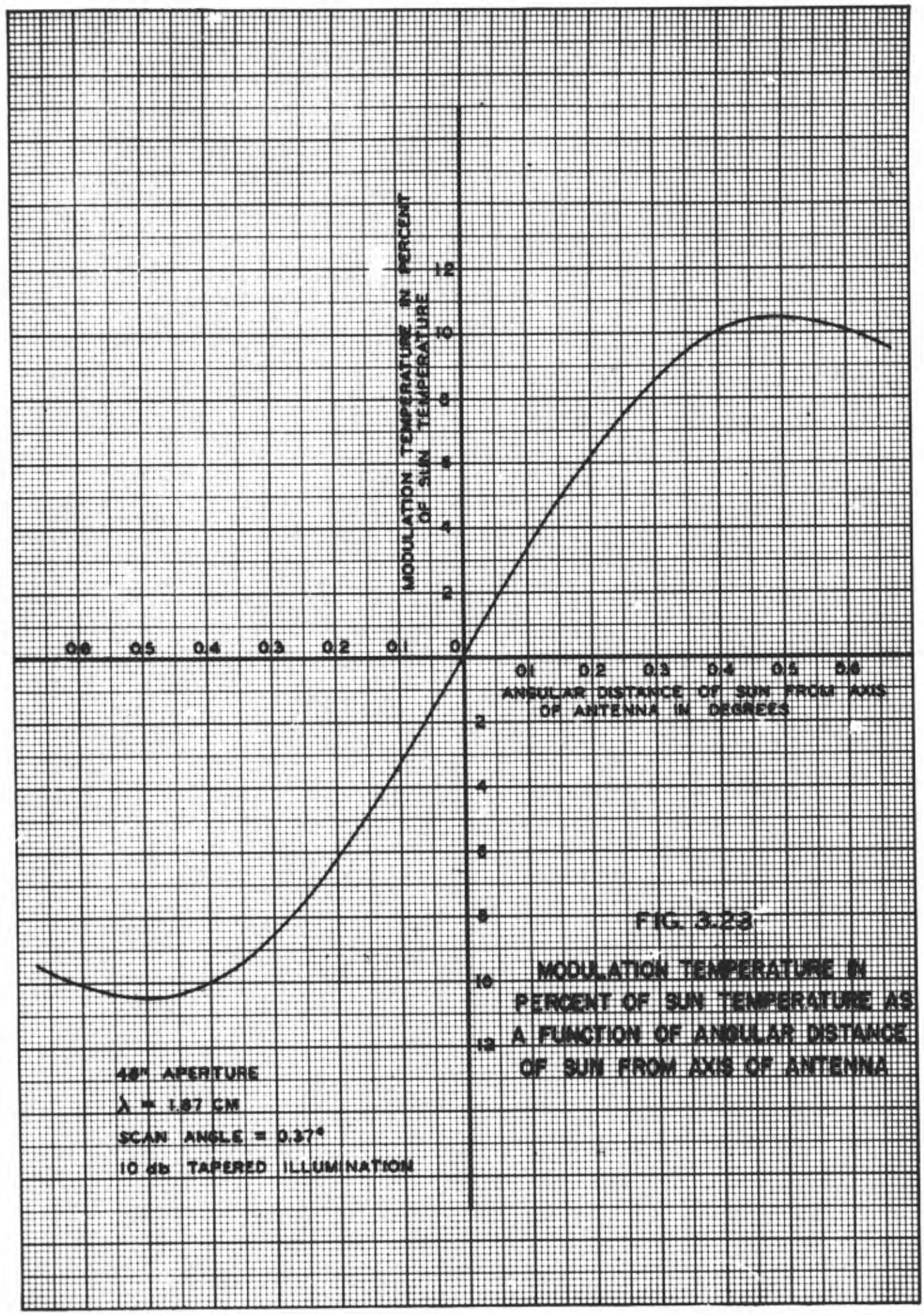

FIG. 3.2-3

MODULATION TEMPERATURE IN PERCENT OF SUN TEMPERATURE AS A FUNCTION OF ANGULAR DISTANCE OF SUN FROM AXIS OF ANTENNA

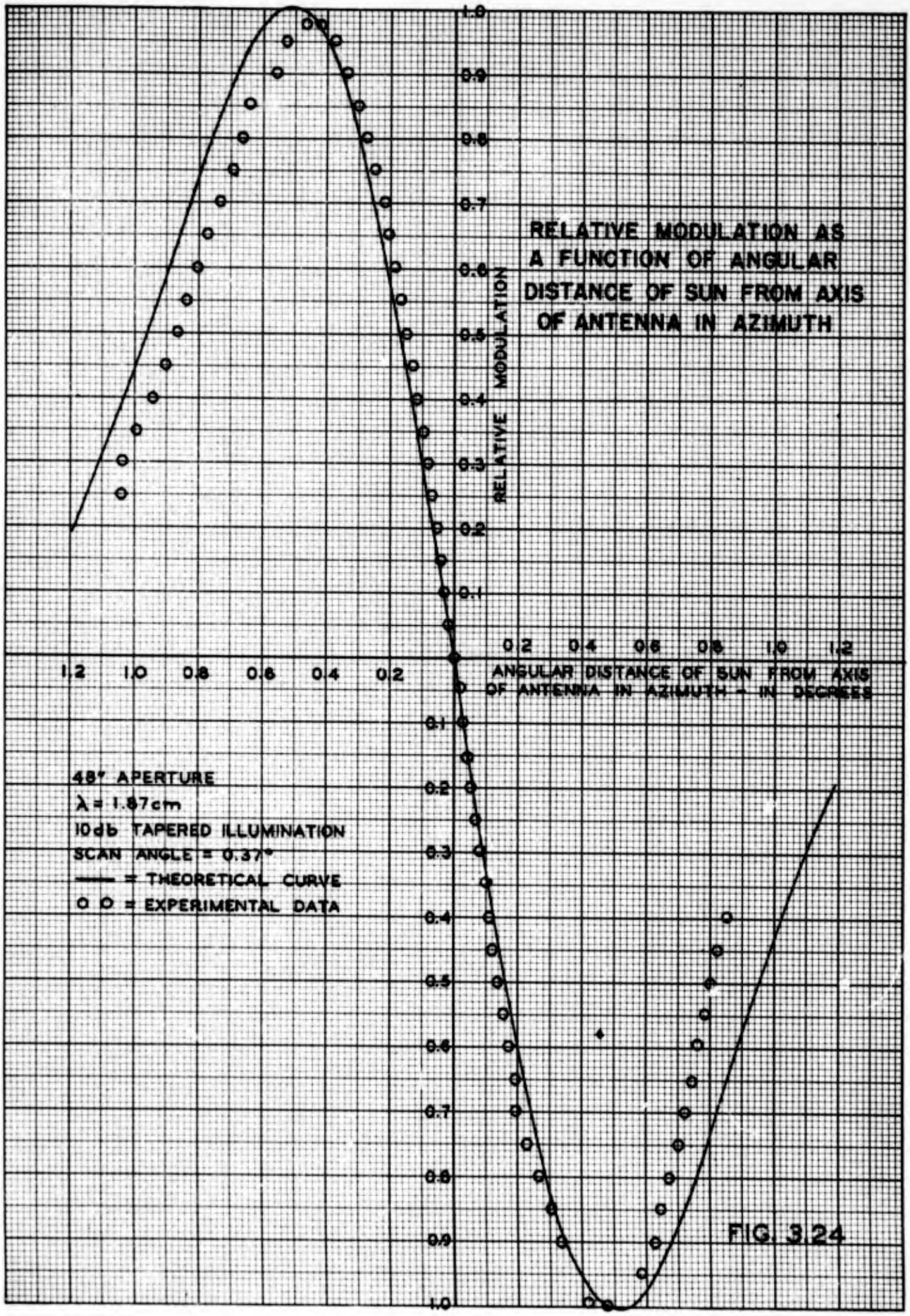
RELATIVE MODULATION AS A FUNCTION OF ANGULAR DISTANCE OF SUN FROM AXIS OF ANTENNA IN AZIMUTH
RELATIVE MODULATION
1.0
0.9
0.8
0.7
0.6
0.5
0.4
0.3
0.2
0.1
0.2
0.4
0.6
0.8
1.0
1.2
1.2
1.0
0.8
0.6
0.4
0.2
ANGULAR DISTANCE OF SUN FROM AXIS OF ANTENNA IN AZIMUTH - IN DEGREES
48" APERTURE
λ = 1.87cm
10db TAPERED ILLUMINATION
SCAN ANGLE = 0.37°
—— = THEORETICAL CURVE
o o = EXPERIMENTAL DATA

FIG. 3.24

3.2.4.4 Receiver Design

The receiver used in the radio sextant is essentially the same as used in all the radiometers except that no reference wheel is necessary since the modulation of the incoming noise power is accomplished by nutating the antenna feed. The design principles are the same as outlined in preceding sections, except that the mixer can be simplified somewhat. In Section 3.1.1 it was pointed out that admittance variations caused by the rotating reference wheel gave rise to a spurious receiver output. Since the nutating antenna feed does not cause any such admittance variations the phase shifter can be omitted from the mixer.

The complete receiver including mixer, local oscillator, I.F. amplifier and appropriate power supplies are all mounted in the searchlight drum as shown in Fig. 3.25.

It was intended throughout the design to strive for a maximum following error of 0.1 degree in both azimuth and elevation. From Fig. 3.26 the maximum and minimum antenna temperatures during one nutation cycle can be found. For example, the angle of conical scan is 0.37 degrees which indicates that the antenna temperature is 8.8 percent of the sun temperature when the sun is on the axis of the scanning system. When the sun is displaced from the scan axis by 0.1 degree the maximum antenna temperature will be $0.104 T_{sun}$ and a half nutation cycle later the antenna temperature will be $0.071 T_{sun}$. The sun temperature at 1.87 cm. wavelength is not known accurately but it is probably of the order of 10,000 degrees K. Thus, the minimum and maximum antenna temperatures encountered during one nutation cycle for an error of 0.1 degree are 710° K and 1040° K, respectively.

The r.m.s. modulation voltage developed at the output of the I.F. amplifier is given by equation 2.52 which is repeated here for convenience.

$$E_{rms} = \frac{0.707}{2}\left[E_{D_1} - E_{D_2}\right] \approx \frac{0.707}{2}\, n \left[\frac{\xi_2\, \xi_c\, KT_0\, \Delta f_{if}\, Q_L}{\omega C}\right]^{1/2} \left\{\left[2(t_a - 1) + NF_{REC}\right]^{1/2} - \left[2\,(t_{a_1} - 1) + NF_{REC}\right]^{1/2}\right\} \qquad 3.6$$

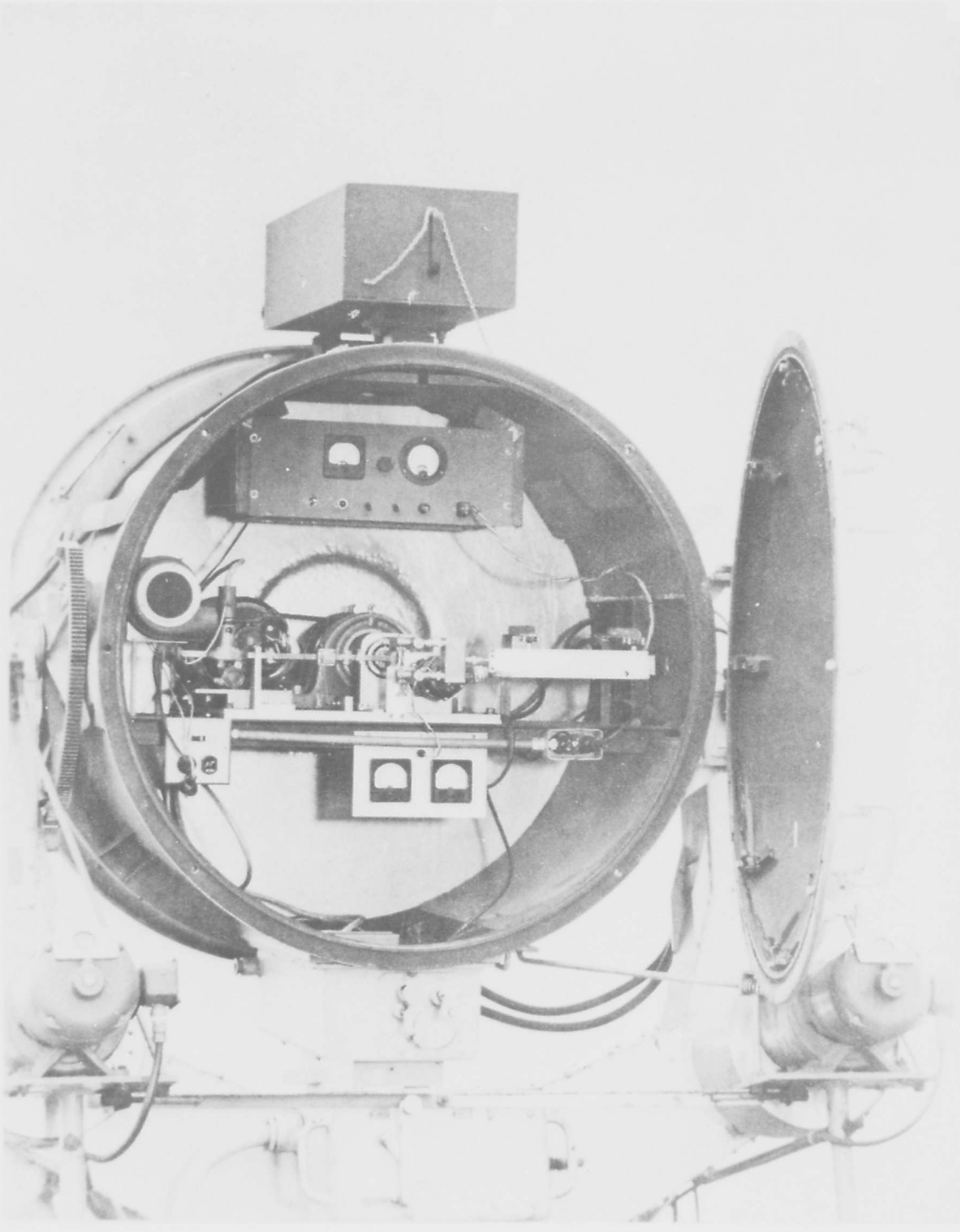

Figure 3.25 Rear View of Searchlight Drum Showing Receiver Components

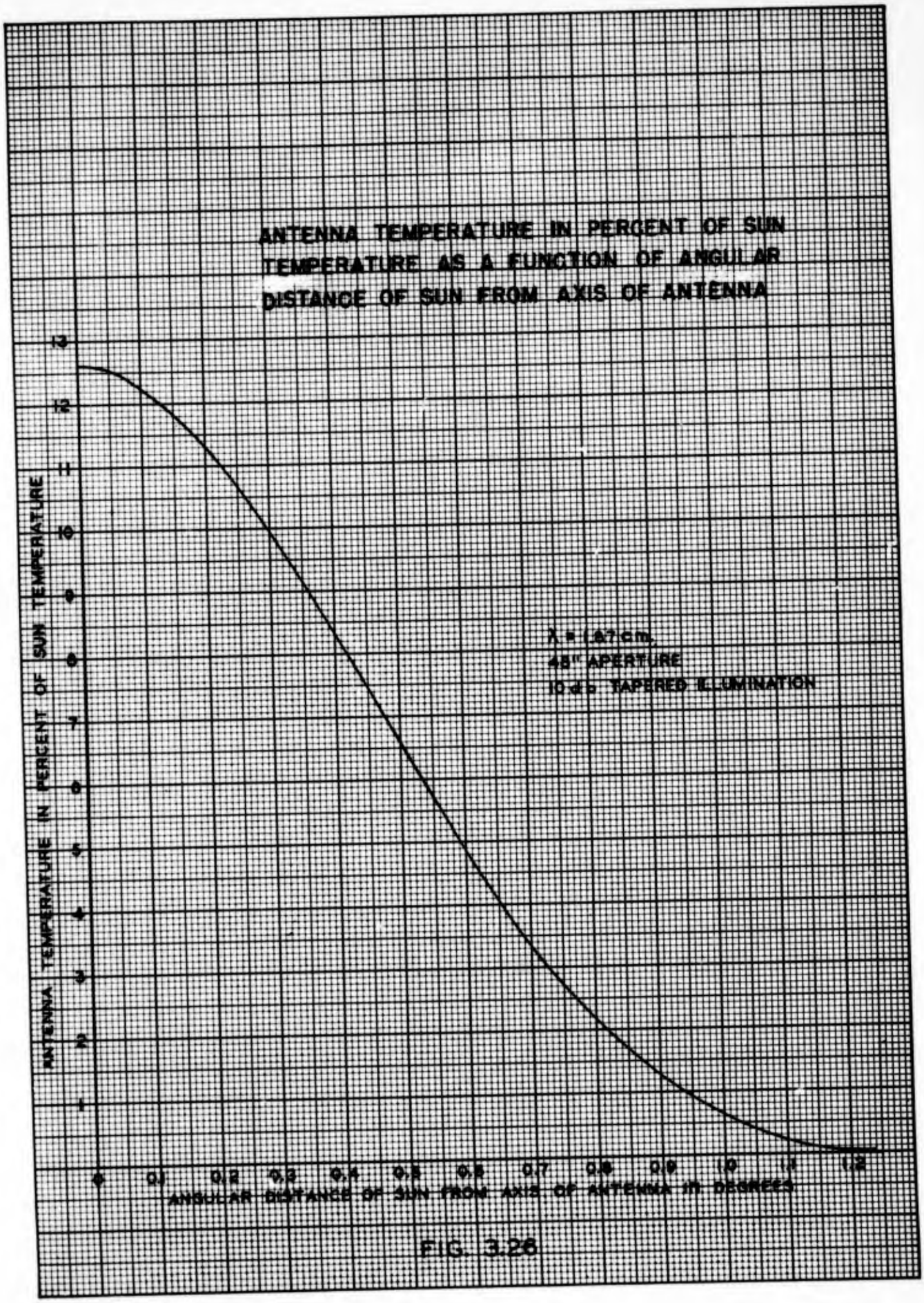
ANTENNA TEMPERATURE IN PERCENT OF SUN TEMPERATURE AS A FUNCTION OF ANGULAR DISTANCE OF SUN FROM AXIS OF ANTENNA
ANTENNA TEMPERATURE IN PERCENT OF SUN TEMPERATURE
13
12
11
10
9
8
7
6
5
4
3
2
1
λ = 1.67 cm.
48" APERTURE
10 db TAPERED ILLUMINATION
0
0.1
0.2
0.3
0.4
0.5
0.6
0.7
0.8
0.9
1.0
1.1
1.2
ANGULAR DISTANCE OF SUN FROM AXIS OF ANTENNA IN DEGREES

FIG. 3.26

The values of the various terms in equation 3.6 are:

$$t_a = 3.55$$

$$t_{a_1} = 2.42$$

$$g_2 = 90 \text{ db.}$$

$$k = 1.38 \times 10^{-23} \text{ Joules/mol./Deg. K}$$

$$T_o = 293^\circ K$$

$$\Delta f_{if} = 8 \times 10^6 \text{ cycles}$$

$$Q_L = 3$$

$$\omega = 2\pi(30 \times 10^6) \frac{\text{rad}}{\text{sec}}$$

$$C = 10 \times 10^{-12} \text{ farads}$$

$$g_c = 0.159$$

$$NF_{REC} = 28 \text{ times}$$

$$n = 0.5$$

Substituting these values in equation 3.6, it is found that

$$E_{rms} \approx 3.2 \text{ millivolts}$$

This is the magnitude of the desired a.c. output from the I.F. amplifier when the antenna is displaced 0.1 degree from the sun. Since the nutation frequency is 24 cycles, the modulation frequency is also 24 cycles.

3.2.4.5 Servo Design

a. Basic Considerations

The design of the servo system for the Radio Sextant was based on a maximum following error, in azimuth and elevation, of 0.1° when the sun's velocity in azimuth and elevation is a maximum at the latitude of 42° N (the latitude of this laboratory).

The sun's angular velocity in azimuth and elevation is not constant, except under special circumstances; it is therefore necessary to calculate the exact range of velocities that will be encountered in order to design a servo system that will have the dynamic speed range and stability required to follow the sun accurately.

The transformation between azimuth-elevation and hour angle-declination coordinates may be obtained by solving the "astronomical triangle." The following formulae are typical of those resulting from applying the general principles of spherical trigonometry to this triangle:

$$\sin \delta = \sin h \sin \phi - \cos h \cos \phi \cos A \qquad 3.7$$

$$\cos \delta \cos t = \sin h \cos \phi + \cos h \sin \phi \cos A \qquad 3.8$$

$$\cos \delta \sin t = \cos h \sin A \qquad 3.9$$

where δ = the declination

t = the hour angle

h = the altitude or elevation of the sun

ϕ = the latitude of the observer

A = the azimuth angle

Equations 3.7 and 3.8 are solved simultaneously and "A" is eliminated. Differentiating the resulting expression with respect to t yields the elevation velocity. By a similar process, "h" may be eliminated and an expression for the azimuthal velocity obtained. From the final expression, the maximum azimuthal angular velocity may be obtained as a function of latitude for various declination angles.

The maximum azimuthal velocity $\omega_{A_{max}}$, which occurs at local apparent noon, is

$$\omega_{A_{max}} = 15 \csc \phi; \text{ when } \delta = 0^\circ$$

and

$$\omega_{A_{max}} = \frac{15}{\sin \phi - 0.425 \cos \phi}; \text{ when } \delta = \pm 23^\circ.$$

Fig. 3.27 shows the maximum values of azimuthal angular velocity, as a function of latitude, for declination angles of 0° and $+23^\circ$. It can be seen from these curves that $\omega_{A\ max}$ becomes infinite, at local apparent noon, whenever the declination is equal to the latitude. During certain parts of the year, noon observations would be difficult to take if the observer were located in the region between the Tropic of Cancer and the Tropic of Capricorn and if the declination were equal to the latitude. It is felt, however, that a satisfactory solution to this problem can be obtained at no sacrifice to the quality of the Radio Sextant under other conditions, if such discontinuities are objectionable.

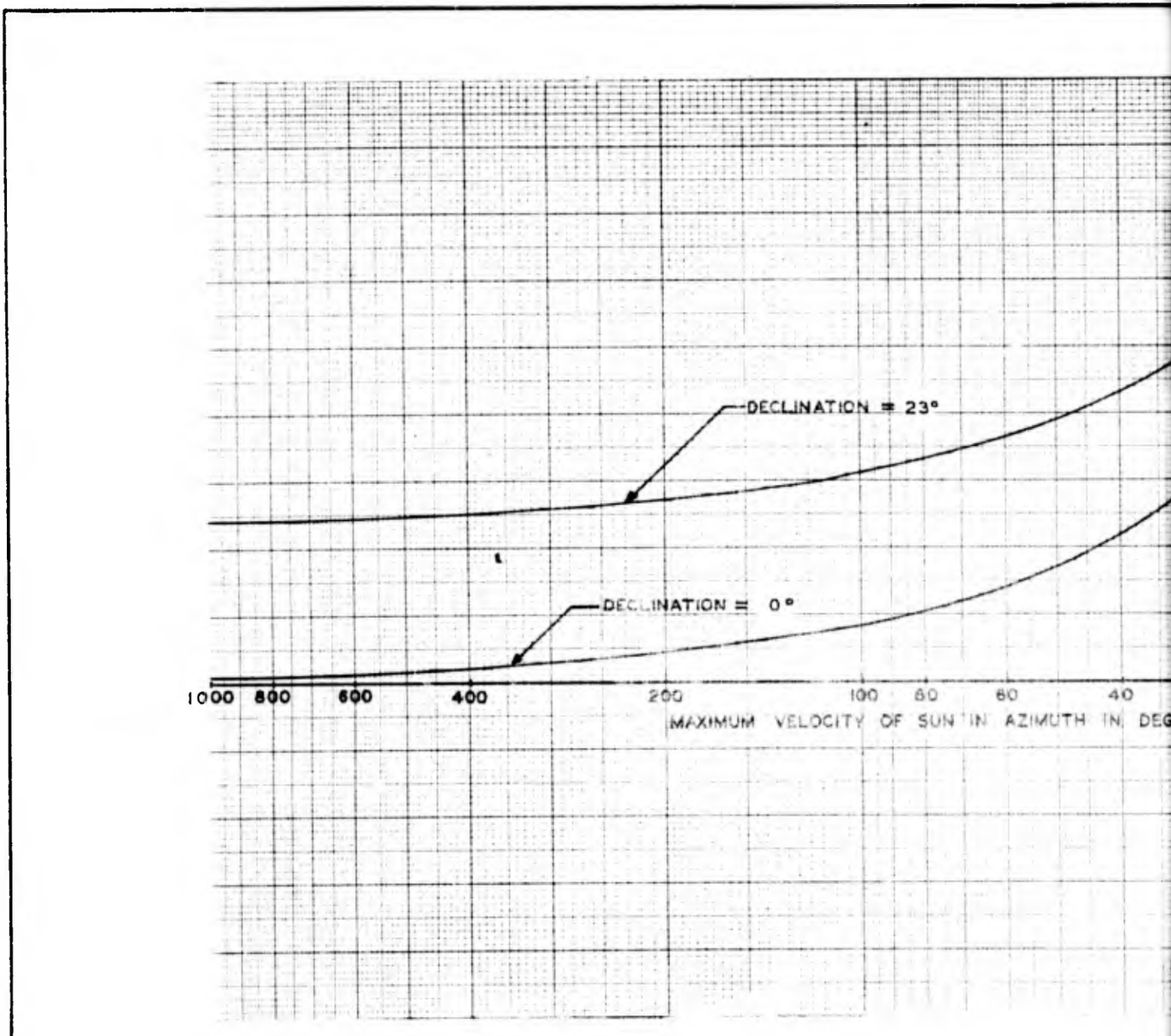

MAXIMUM
AS A FUNCTI

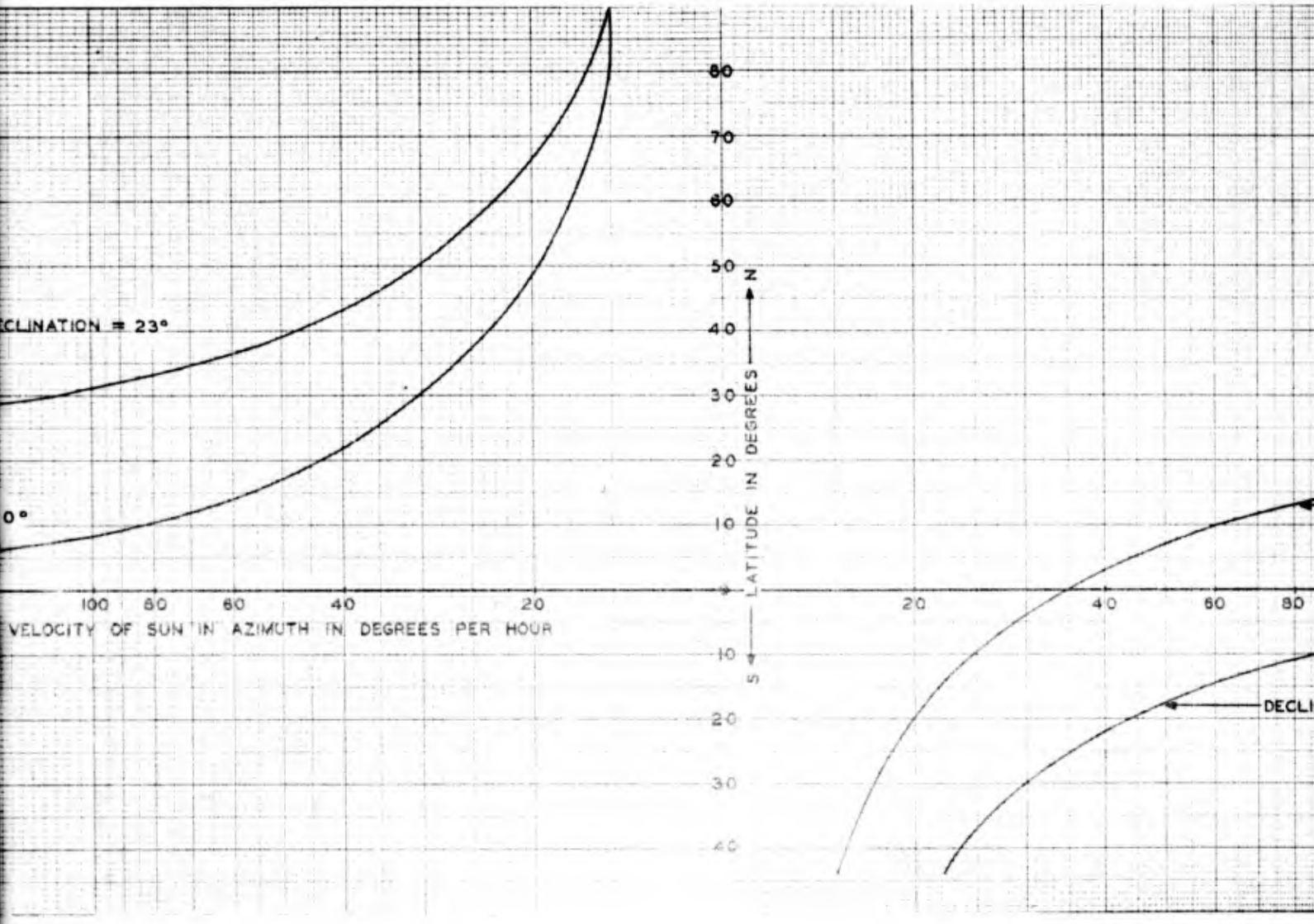

FIG. 3.27

MAXIMUM VELOCITY OF THE SUN IN AZIMUTH AT LOCAL APPARENT NOON AS A FUNCTION OF LATITUDE FOR DECLINATION ANGLES 0 AND 23 DEGREES

2

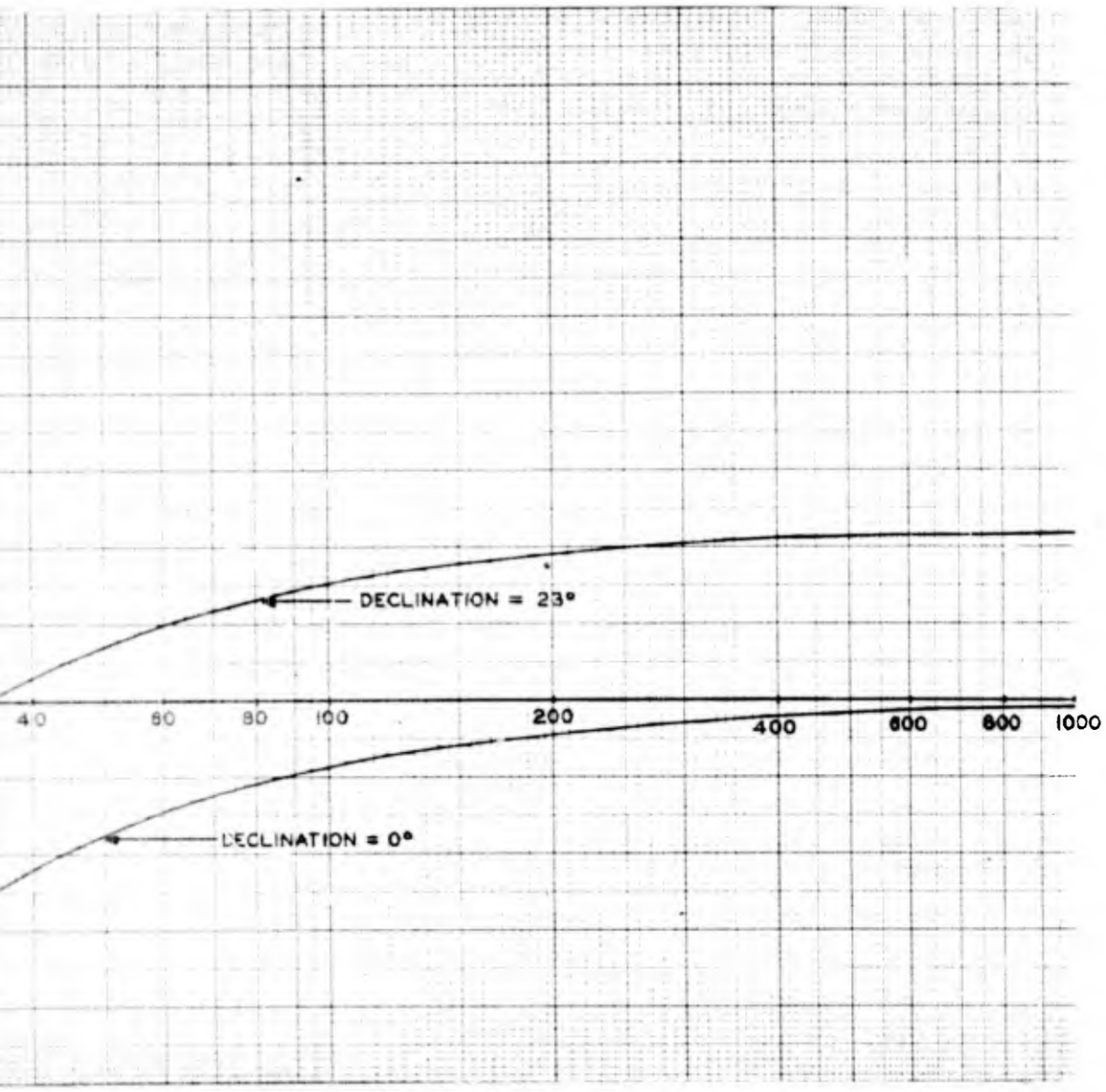

NT ION
3 DEGREES

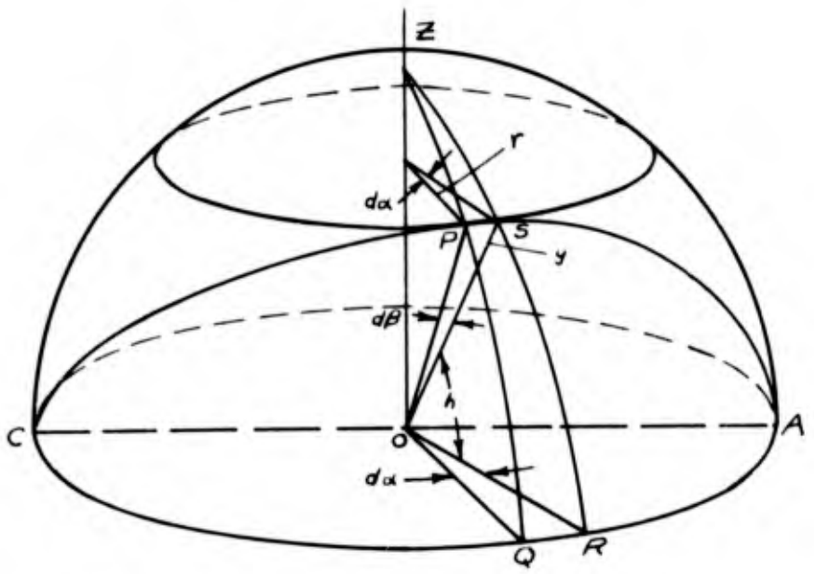

FIG. 3.28

ILLUSTRATION SHOWING SUN'S PATH WITH RESPECT TO OBSERVER'S HORIZON PLANE

The range of elevation velocities has a maximum of 15° per hour and a minimum of 0° per hour and possesses no discontinuities such as does the azimuth velocity. For the latitude of this laboratory, the azimuthal angular velocity of the sun varies between a maximum of 42.5° per hour and a minimum of 9° per hour and the elevation angular velocity varies from a maximum of 11.2° per hour to a minimum of 0° per hour.

When dealing with azimuthal velocities of an antenna, there is a subtle distinction which must be made between the horizontal component of the motion of the antenna beam and the rotation of the azimuth axis. If the horizontal component of the angular displacement of the antenna beam is θ, then the azimuth axis on which the antenna is mounted must be moved through an angle $\frac{\theta}{\cos h}$ where h is the elevation angle of the antenna beam.

This fact can be proved very simply with the aid of Fig. 3.28 which is drawn for the conditions occurring at one of the equinoxes. Let AQC in Fig. 3.28 represent the horizon plane for the observer at point O and let APC define the path of the sun, at an elevation angle h, then $d\beta/dt$ represents the horizontal component of the sun's actual angular velocity and da/dt represents the azimuthal angular velocity of the sun. Then,

$$\cos h = r/y$$

$$\text{or} \qquad y = r/\cos h \qquad 3.10$$

$$\text{but } y \frac{d\beta}{dt} = r \frac{da}{dt} \qquad 3.11$$

and so, by substitution of y from equation 3.10:

$$\frac{r}{\cos h} \cdot \frac{d\beta}{dt} = r \frac{da}{dt} ,$$

$$\text{or} \qquad \frac{d\beta}{dt} = \cos h \frac{da}{dt} \qquad 3.12$$

For this latitude the maximum elevation angle is 71° (90° - Lat. + δ). If the maximum azimuthal angular velocity is 42.5° per hour then the horizontal angular velocity of the antenna beam, when h = 71° is:

$$\cos h \times 42.5^\circ = 0.325 \times 42.5^\circ = 13.8^\circ/\text{hr}$$

It can also be shown that the angle subtended by POS is less, by cos h, than the angle subtended by QCR, which indicates that the angular displacement of the antenna beam from the center of the

sun, resulting from a finite following error, will be smaller, by cos h, than the angular displacement projected onto the horizon plane.

By a similar derivation, it can also be shown that if the antenna is directed ahead of the sun along the path described by the sun's motion, the velocity at which the sun will pass through the antenna beam will be 15 cos δ degrees per hour.

The angular velocities in azimuth and elevation (excluding the azimuth velocity discontinuities) are very low in comparison to standard drive motor speeds and consequently it is necessary to insert a large gear reduction between the drive motors and the mount in order to obtain stable servo operation. The standard drive motor speed may be taken as 1725 RPM. It is desirable to operate at a speed lower than maximum, when the angular velocity is a maximum, to have sufficient speed reserve to allow pulling in on the sun after the sun has been located during the search scan. Assume that it is desired to operate at 1/3 maximum motor speed when tracking the sun at its maximum azimuthal angular velocity of 42.5° per hour. The gear reduction needed would then be

$$\frac{1725 \times 60 \times 360}{3 \times 42.5} = 292{,}000 \text{ to } 1$$

And in elevation where $\omega_h(max) = 11.2^\circ$ per hour the gear reduction would need to be

$$\frac{1725 \times 60 \times 360}{3 \times 11.2} = 1{,}100{,}000 \text{ to } 1$$

The 36-inch searchlight furnished as a mount for the Radio Sextant was driven in azimuth and elevation by a pair of 1200 RPM D.C. motors with a total gear reduction of 260.3 to 1 in azimuth and 304 to 1 in elevation. Since this gear reduction is much lower than that needed, it was decided to employ these motors for slewing and search operation and replace the manually operated hand cranks with motors possessing the necessary gear reduction. The gear reduction between the mount drive rings in azimuth and elevation and their respective hand cranks was 25 to 1 and 40 to 1. The gear reduction needed between slow speed tracking motors and their respective hand crank shafts will be $\frac{292{,}000}{25} = 11{,}700$ in azimuth and $\frac{1{,}100{,}000}{40} = 27{,}500$ in elevation.

A servo drive system employing amplidyne generators and D.C. drive motors was considered to be the most practical since this was the system employed in the searchlight and could be

most easily adapted to the Radio Sextant. The motors obtained for slow speed tracking were multiple parallel gearhead 115 V D.C. motors having a counter-shaft speed of 10 RPH which is a gear reduction of 10,300 to 1. The motors are rated at 1/8 H.P. which is much greater than needed, as far as the torque requirements are concerned, but were the smallest ones available with such a high integral gear reduction. This value of gear reduction is very close to that desired in azimuth but is 0.375 as large as that desired in elevation, which means the maximum motor speed will be 0.375 that value chosen or $(\frac{1725}{3})$ (0.375) or 216 R.P.M. when the maximum elevation velocity is 11.2° per hour. This was not considered objectionable.

The presence of noise or undesired disturbances in the servo input signal is an important consideration in the design of the servo loop characteristic. Input noise causes spurious output position fluctuations and can also cause overloading in the power stages of the servo system.

Both of these effects are reduced by narrowing the frequency band of the servo transfer characteristic by the insertion of an R.C. network or time constant. When such a network is inserted in a servo system, it is desirable to use the maximum amount of time constant that will still allow stable servo performance. Nyquist's criterion of stability states that for a system to be absolutely stable, the gain curve must cross the zero-db. axis at a frequency lower than that at which the phase curve crosses the -180° phase axis. However, a stability phase margin of from 30° to 60° at the crossover point and a gain margin of 10-20 db. at the phase cross-over point is generally considered good practice. The design and analysis of the servo system used was based on the frequency response method. This method depends essentially on the construction and interpretation of graphs representing the steady-state response of the system to sinusoidal inputs covering an appropriate frequency range.

Figure 3.29 is a block diagram of the servo loop used in the Radio Sextant.

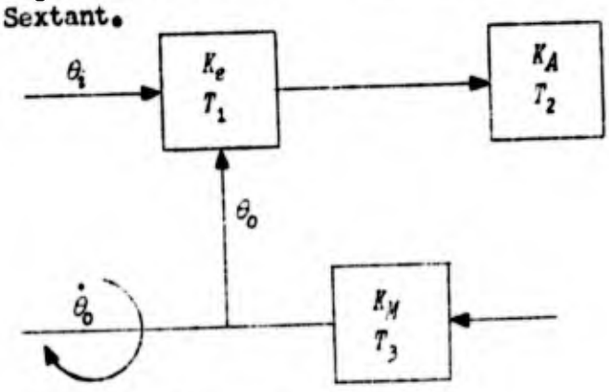

Fig. 3.29

where θ_i = input signal function

θ_o = output signal function

$\dot{\theta}_o = d\theta_o/dt$ = output shaft velocity

K_e = gain of error detector and amplifier in volts/deg.

K_a = gain of power amplifier in ma./volt

K_m = gain of amplidyne and motor in rad/sec/ma.

The feedback transfer function of this loop is:

$$\frac{\theta_o}{\epsilon} = \frac{K_v}{j\omega(j\omega T_1 + 1)(j\omega T_2 + 1)(j\omega T_3 + 1)} = KG(j\omega) \qquad 3.13$$

where $KG(j\omega)$ equals the loop gain, in terms of the velocity error constant K_v, the system time constants, and the angular frequency. The time constants, T_2 and T_3, associated with K_a and K_m respectively, are approximately 0.1 seconds maximum, and as such, are essentially negligible with respect to T_1. The maximum allowable time constant in the error detector and amplifier T_1 is to be determined. The required velocity error constant, K_v, for a given input velocity and a given following error ϵ, is given by the following relationship:

$$K_v = \frac{V}{\epsilon} \qquad 3.14$$

If the maximum following error is to be 0.1° when the maximum azimuthal angular velocity is 42.5° per hour, then:

$$K_v = \left[\frac{42.5^\circ/\text{hr}}{0.1^\circ}\right]\left[\frac{1}{3600}\right] = 0.118 \text{ sec}^{-1}. \qquad 3.15$$

Figure 3.30 is a plot of loop gain and phase shift versus frequency for two values of velocity error constant, $K_v = 0.118$ and 0.236 sec^{-1} corresponding to following errors of 0.1° and 0.05° respectively, when the azimuthal angular velocity is taken as 42.5° per hour. Since the time constants, T_2 and T_3, are essentially negligible, equation 3.13 becomes

$$KG(j\omega) = \frac{K_v}{j\omega(j\omega T_1 + 1)} \qquad 3.16$$

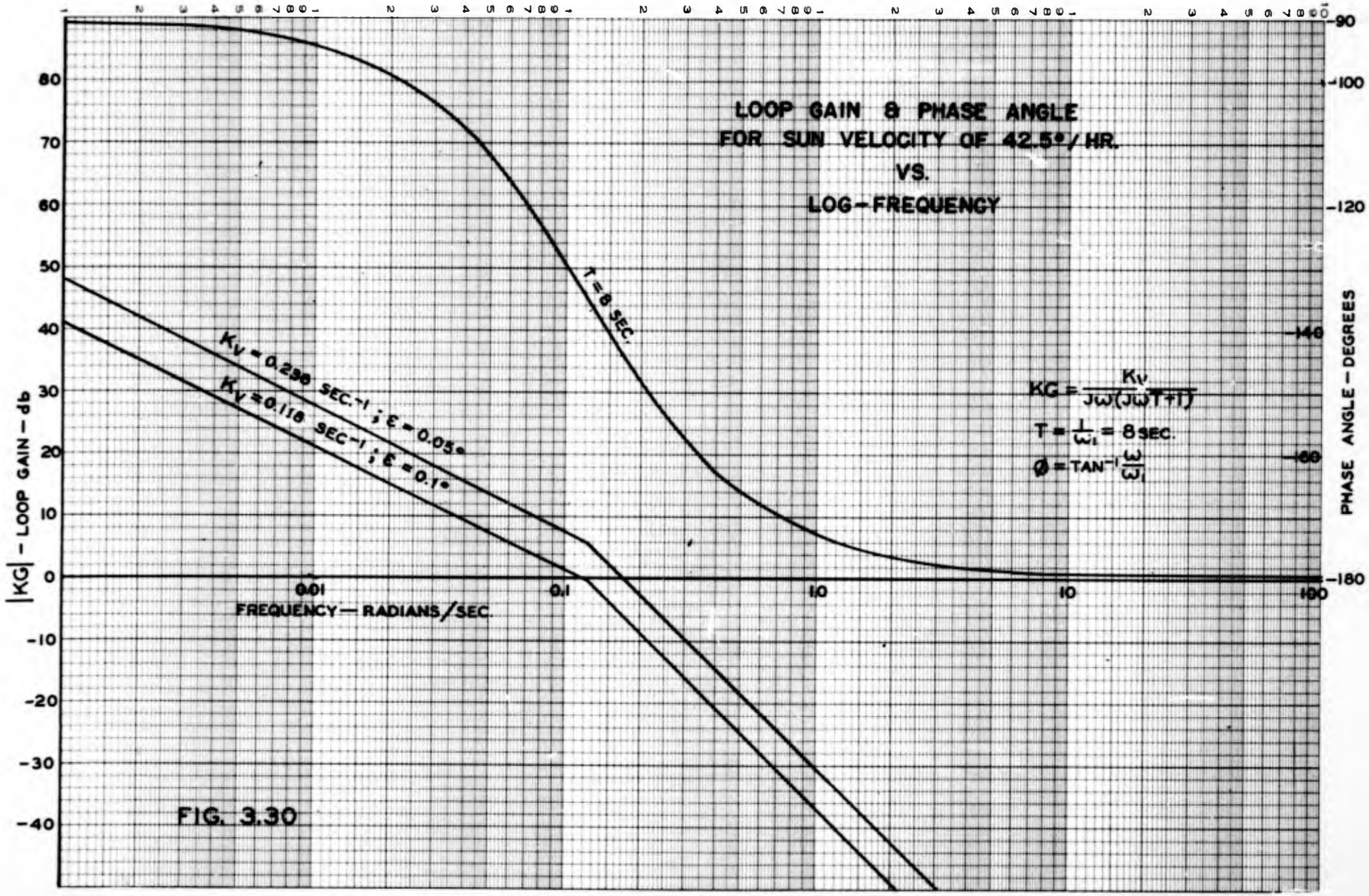
LOOP GAIN & PHASE ANGLE
FOR SUN VELOCITY OF 42.5°/HR.
VS.
LOG-FREQUENCY
T=8 SEC.
K_V = 0.236 SEC.$^{-1}$; ε = 0.05°
K_V = 0.118 SEC.$^{-1}$; ε = 0.1°
$KG = \frac{K_V}{J\omega(J\omega T+1)}$
$T = \frac{1}{\omega_1} = 8$ SEC.
$\phi = \tan^{-1}\frac{\omega}{\omega_1}$
|KG| - LOOP GAIN - db
PHASE ANGLE - DEGREES
FREQUENCY - RADIANS/SEC.
0.01
0.1
1.0
10
100
80
70
60
50
40
30
20
10
0
-10
-20
-30
-40
-90
-100
-120
-140
-160
-180

FIG. 3.30

The time constant in the error detector amplifier was taken as 8 seconds, since this value yielded a 45° phase margin when K_v = 0.118 sec^{-1}. When K_v is taken as 0.236 sec^{-1} the phase margin is 36°, which indicates that the system will be stable.

From equation 3.14 the required velocity error constant for a given error and maximum velocity can be obtained. After this value has been determined, the total amplifier gain may then be calculated from the following expression:

$$K_v = \frac{K_c \; K_a \; K_m}{N} \qquad 3.17$$

where N is the total gear reduction in a given channel (azimuth or elevation) of the system.

As shown in equation 3.17, the loop gain is a constant for a particular value of K_v. If the velocity should increase, then of course the following error would increase. It is important to realize that the gain is defined by K_v.

Measurement made on the azimuth tracking motor indicated that for fixed excitation, the slope of the R.P.M. versus armature volts curve was 14.6. Since the total gear reduction in the system was 10,300 x 25 = 257,500 to 1, the azimuth axis would be driven at 1.226 deg/hr/armature volt. Tests on the azimuth amplidyne showed that a differential current of one milliampere yielded a generator output of 6.91 volts. The motor-amplidyne combination would then drive the antenna mount in azimuth at 8.46 deg/hr/ma differential current. This value includes gear reduction in the system. Using the notation of Figure 2.29, where K_m is given in units of rad/sec/ma,

$$\frac{K_{m_a}}{N} = 8.46 \text{ deg/hr/ma} = 41 \times 10^{-6} \text{ rad/sec/ma}$$

for the azimuth channel.

Similar measurements on the elevation motor-amplidyne combination, including total gear reduction from motor armature shaft to elevation drive ring, showed that the antenna mount would be driven in elevation at 7.6 deg/hr/ma.

Measurements made on the power amplifier, K_a, showed that a D.C. voltage of one volt on the grids of the power amplifiers yielded a one-milliampere differential current in the amplidyne control field. Then, from equation 3.17, K_e will be:

$$K_e = \left[\frac{K_v}{K_a}\right]\left[\frac{K}{K_m}\right]$$

$$= \frac{0.118}{1 \times 41 \times 10^{-6}} = 0.00286 \times 10^6 \text{ volts/rad}$$

$$\text{or} \quad K_e = \frac{0.00288 \times 10^6}{57.3} = 50.2 \text{ volts/deg}$$

From equation 3.6 the calculated output of the second detector, in the I.F. amplifier, for an antenna following error of 0.1°, is 3.2 millivolts. However, if the elevation angle is 71°, which is the largest value encountered at this latitude, a 0.1° following error of the antenna corresponds to a following error of $0.1^\circ/\cos h$ or 0.307° at the azimuth ring. Consequently, the calculated value of error voltage from the second detector is higher than the value that would be obtained had the calculation been based on a following error of 0.1° at the azimuth ring.

The gain of the error detector amplifier will then need to be:

$$\frac{5.02}{3.2 \times 10^{-3} \times 0.325} = 4840$$

for a following accuracy at the azimuth ring of 0.1° when $\omega_{A_{max}} = 42.5^\circ/\text{hr}$, and the elevation angle is 71°.

3.2.4.5 Servo Design

b. Servo Amplifier

A necessary voltage gain of 4840x in the servo amplifier, as arrived at in the previous section, was considered to be less than the gain for which the servo amplifier should be designed. Allowances for small errors in the calculations plus the fact that greater tracking accuracies might possibly be obtained than the specified 0.1 degrees led to the design of a servo amplifier with a maximum gain of approximately two times the calculated amount.

In all previous radiometers, a twin "T" feedback amplifier had been used to obtain the narrow bandwidth necessary to suppress most of the noise components present in the output of the second detector. However, tests showed that the output meter fluctuations were not increased by broadening the bandwidth of the feedback amplifiers to 5 cycles. The twin "T" feedback

amplifiers, when slightly detuned, have a tendency to become unstable. Also, temperature and humidity changes affect the tuning of the twin *T*, and hence the gain. Another bad feature is that the phase shift through a feedback amplifier of this type is a rapid function of frequency; this is undesirable for a stable servo mechanism. For these reasons, it was decided to obtain the desired response by employing RC shaping circuits in the amplifier. To eliminate any 60 cycles present, a twin *T* tuned to that frequency was placed in cascade with the amplifier. Figure 3.3.1 shows the circuit diagram of the 4 stage, 24 cycle/second amplifier consisting of a 6SL7 twin triode and a 6SN7 twin triode. Five RC shaping circuits, three high pass, and two low pass filters, each designed to attenuate 24 cycles approximately 3 db. were used to shape the pass band. The twin *T* in cascade was designed to produce very little attenuation at 24 cps and maximum attenuation at 60 cps. This was done by making the series impedances on the input side 20 times those on the output side. The resulting twin *T* attenuation at 24 cps is 3.3 db. and at 60 cps, 61.3 db.

The total voltage gain of the amplifier is 12,000 and the bandwidth is 20 cycles, as indicated by its response curve, Fig. 3.32. The amplifier is linear up to 50 volts rms output. A 5 step gain control which is accurate to better than 1% is incorporated into the design.

The 24 cps output of the amplifier section had to be compared with each phase of the reference voltage in such a way as to produce d.c. voltages proportional to the elevation and azimuth angular errors. This required two phase sensitive detectors. As the type of detector chosen operated on a balanced signal input, a phase inverter, using a 6J5 tube, was used to convert the unbalanced voltage output of the amplifier to balanced voltages. This balanced output is paralleled and fed into 4 cathode followers, incorporating 2-6SN7 tubes. These cathode follower stages provide the necessary low driving impedance for the phase detectors and serve to isolate the detectors so that no interaction of the two reference voltages can take place. The voltage gain of the phase inverter is 0.915 and that of the cathode follower is 0.91.

The phase detector which is used consists of two diodes in opposition into which the signal is fed out of phase and the reference voltage fed in phase. This particular type of phase detector was chosen because it is relatively insensitive to signal wave shape, its d.c. output is compared to ground, and it is very easily balanced. The 200K ohm potentiometers in the output allow the detectors to be balanced so as to give zero d.c. output with no signal applied.

The phase detectors also provide excellent output voltage limiting. Their operation is such that the d.c. output is linear with the product of the signal input and the cosine of the phase angle between the reference voltage and the signal until the latter reaches the same level as the reference voltage. Any signal amplitude larger than this cancels in the output network, thereby holding the d.c. output voltage constant at the same magnitude as the rms reference voltage at the diodes. As the reference voltage at this point is 15 volts, a maximum d.c. output of 15 volts is assured. This permits operation of the sextant at very high gain without overdriving any part of the system following the phase detectors.

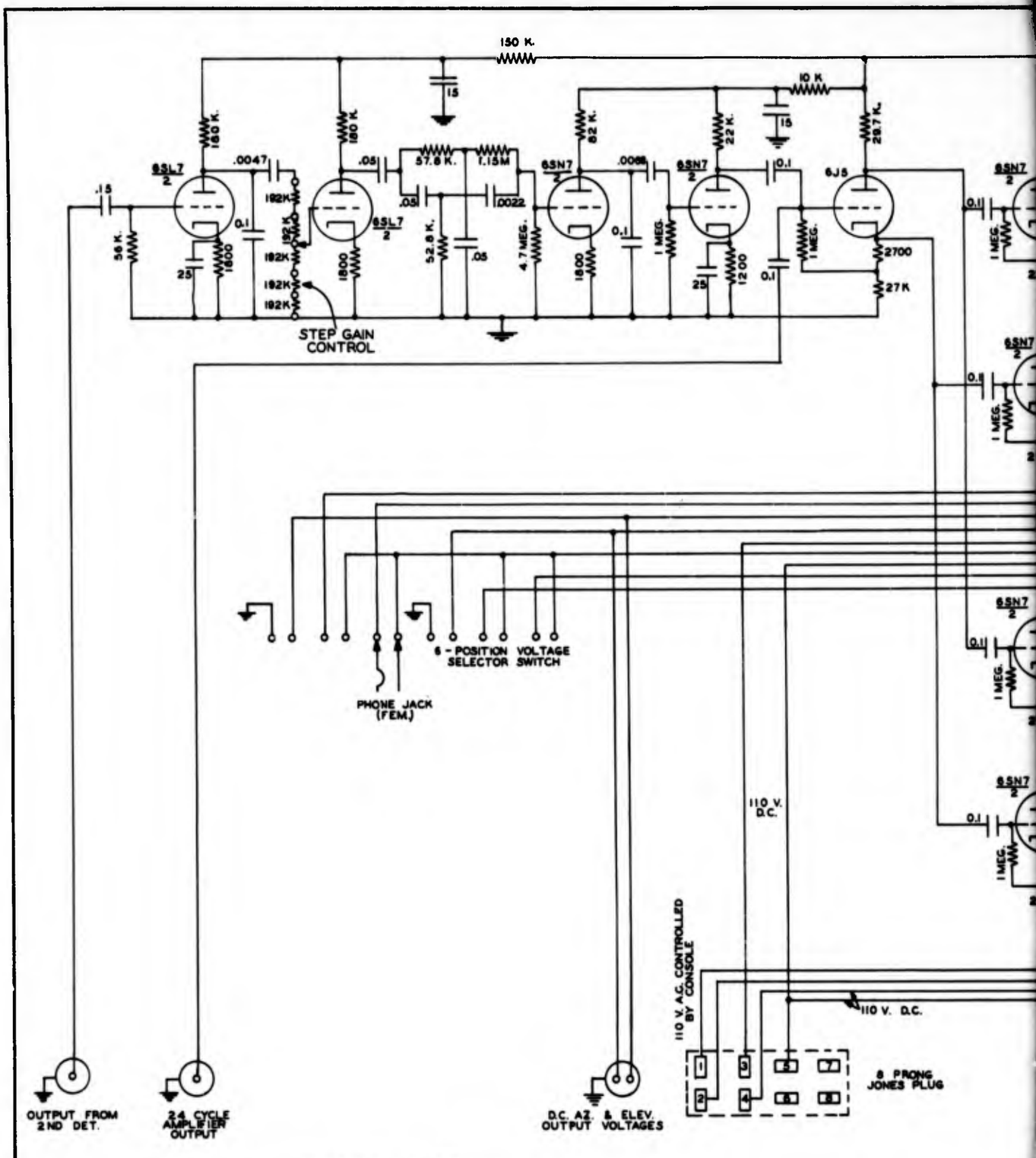

NOTE:- - - - - - - MECHANICAL LINKAGE.
ALL CONDENSER VALUES IN MICROFARADS.
ALL RESISTORS 1 WATT UNLESS OTHERWISE SPECIFIED.

FIG. 3.31

EXP. NO. 1485-9-3C

QUAN. TITY	USED ON	QUANTITY	ITEM NO.	QUANTITIES ARE FOR ONE ASSEMBLY: COLLINS PART NUMBER	GOVERNMENT PART NO.	PART NAME

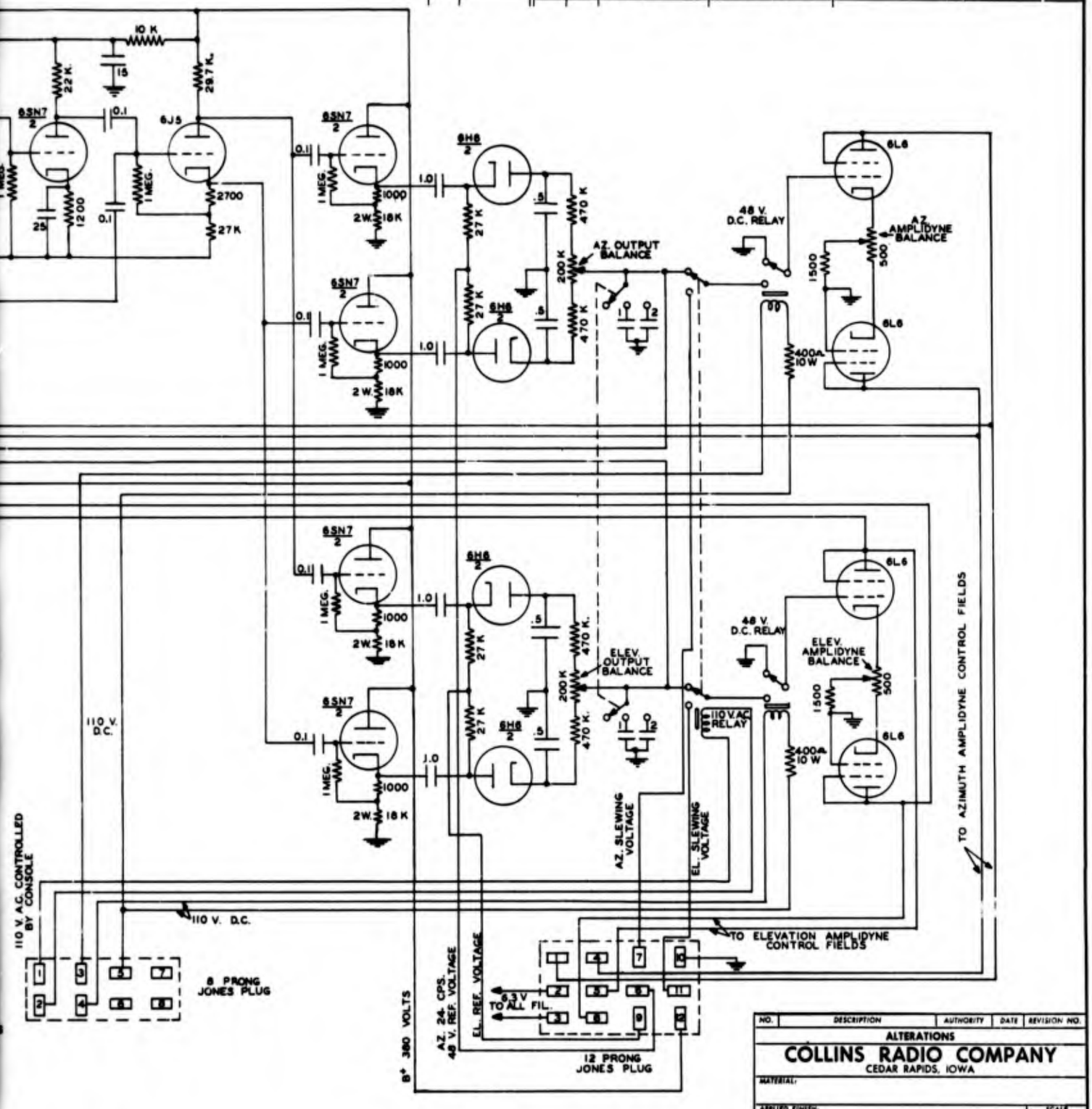

FIG. 3.31

NO.	DESCRIPTION	AUTHORITY	DATE	REVISION NO.
	ALTERATIONS			

COLLINS RADIO COMPANY
CEDAR RAPIDS, IOWA

MATERIAL:

APPLIED FINISH: SCALE =1

DRAWN BY	CHECKED BY	APPROVED BY	DATE
			6-13-49

TITLE
SERVO AMPLIFIER SCHEMATIC DIAGRAM

COLLINS PART NO. ALTERATION NO.

GOVERNMENT PART NUMBER

UNLESS OTHERWISE SPECIFIED:
DECIMAL DIMENSIONS MAY VARY ±.010
FRACTIONAL DIMENSIONS MAY VARY ±1/32
MACHINED RIGHT ANGLES MAY VARY ±.1°
SHEARED RIGHT ANGLES MAY VARY ±.25°
BROKEN RIGHT ANGLES MAY VARY ±1.°
ALL CONCENTRIC DIAMETERS MARKED WITH (*) SHALL BE HELD WITHIN TOTAL INDICATOR READING.
ALL DIMENSIONS ARE FINISH DIMENSIONS INCLUDING APPLIED FINISH AND ARE GIVEN IN INCHES.

2

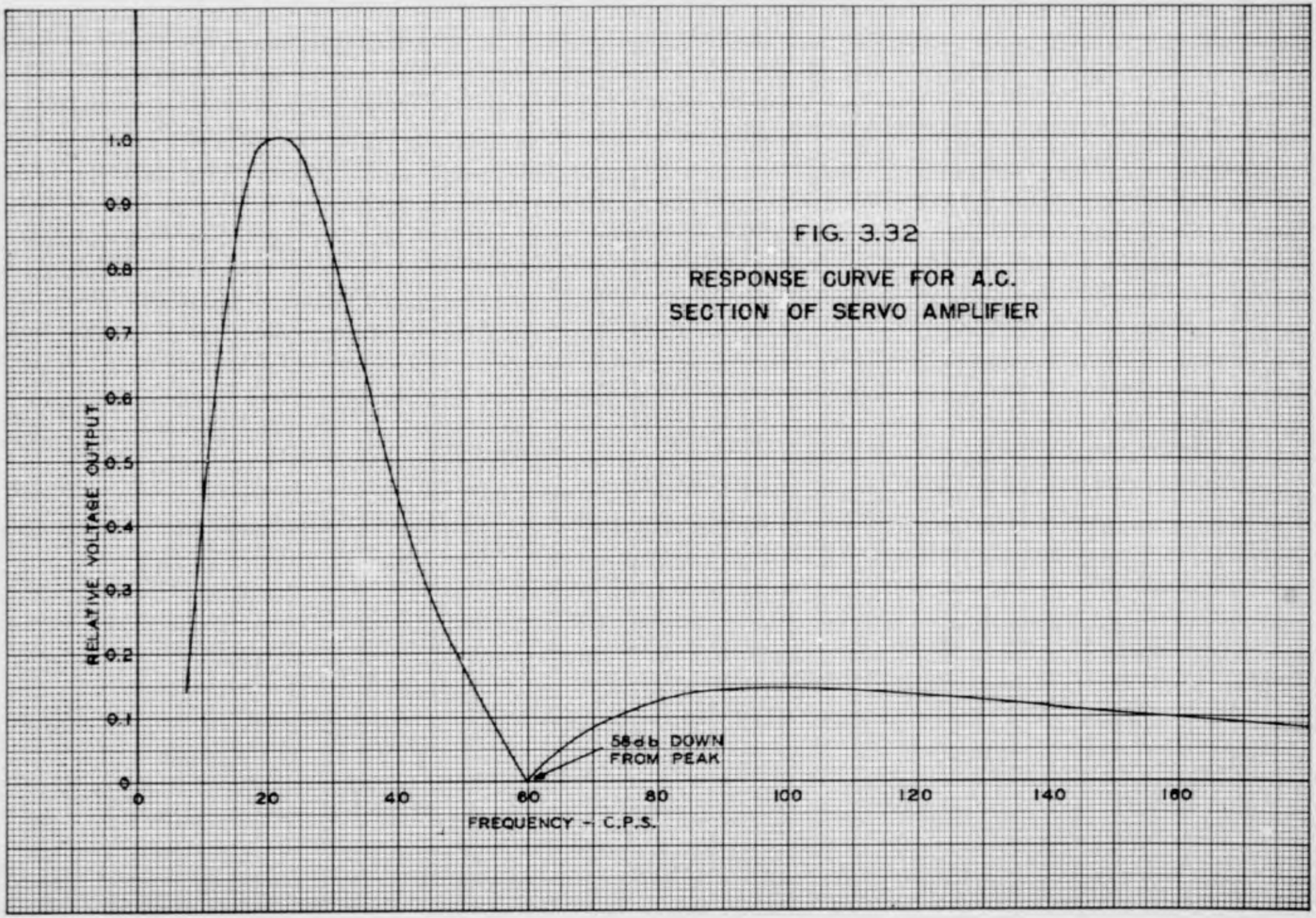

FIG. 3.32

RESPONSE CURVE FOR A.C.
SECTION OF SERVO AMPLIFIER

Provisions were made for inserting various values of capacitance to ground in the output of the phase detectors to provide low pass filtering. As the output impedance of the detector is approximately 0.5 megohms, each microfarad to ground results in a time constant of about 0.5 seconds.

The d.c. output of each phase detector is fed into a power amplifier designed to control the amplidyne fields. Each power amplifier consists of two triode connected 6L6's as shown in Figure 3.31. The grid of one 6L6 is grounded and the d.c. signal is placed on the grid of the other. The small (1000 ohm) resistance of each half of the amplidyne field necessitated a large bias, 40 volts, on the tubes in order to limit the quiescent field current to 12 ma. with a plate supply voltage of 380 volts. The common 1500 ohm resistor in the cathode circuits causes the current through the two tubes to change in opposite directions when a signal is applied. The 500 ohm potentiometer was placed in the circuit to balance the amplidyne fields; that is, zero output when no signal is present. As mentioned in the previous section, a d.c. signal of one volt on the grid of the 6L6 produced a differential current of 1 ma. in the field windings of the amplidyne.

The 6 position voltage selector switch, shown in Fig. 3.31 allows the two output voltages and the voltages across the amplidyne fields to be measured. The 4 balance adjustments are situated on the front of the servo amplifier chassis along with the voltage selector switch, voltmeter jack, and step gain control as shown in Fig. 3.33. This arrangement facilitates the initial balancing of the system.

The filament transformer for the servo amplifier is mounted on the relay chassis next to the servo amplifier in the control box, as shown in the photograph, Fig. 3.33. The power supply was located below the base of the searchlight and was connected to the servo amplifier through slip rings. It is an electronically regulated 380 volt, 200 milliampere supply.

3.2.4.6 Sextant Operation and Control

The radio sextant is remotely controlled by a console which is connected to the sextant through slip rings. Portable error voltage meters and positioning controls are also employed to allow the sextant to be operated from any point in its vicinity. Fig. 3.34 is a schematic diagram of the console and the sextant drive circuitry which it controls.

The functions of the console, pictured in Fig. 3.35 are as follows: The error voltages on which the sextant is operating are metered. Recording milliammeters may be connected to record the voltages against time. The antenna position is indicated by means of 1 and 36 speed synchros in azimuth and 2 and 36 speed synchros in elevation. The searchlight may be manually positioned using either

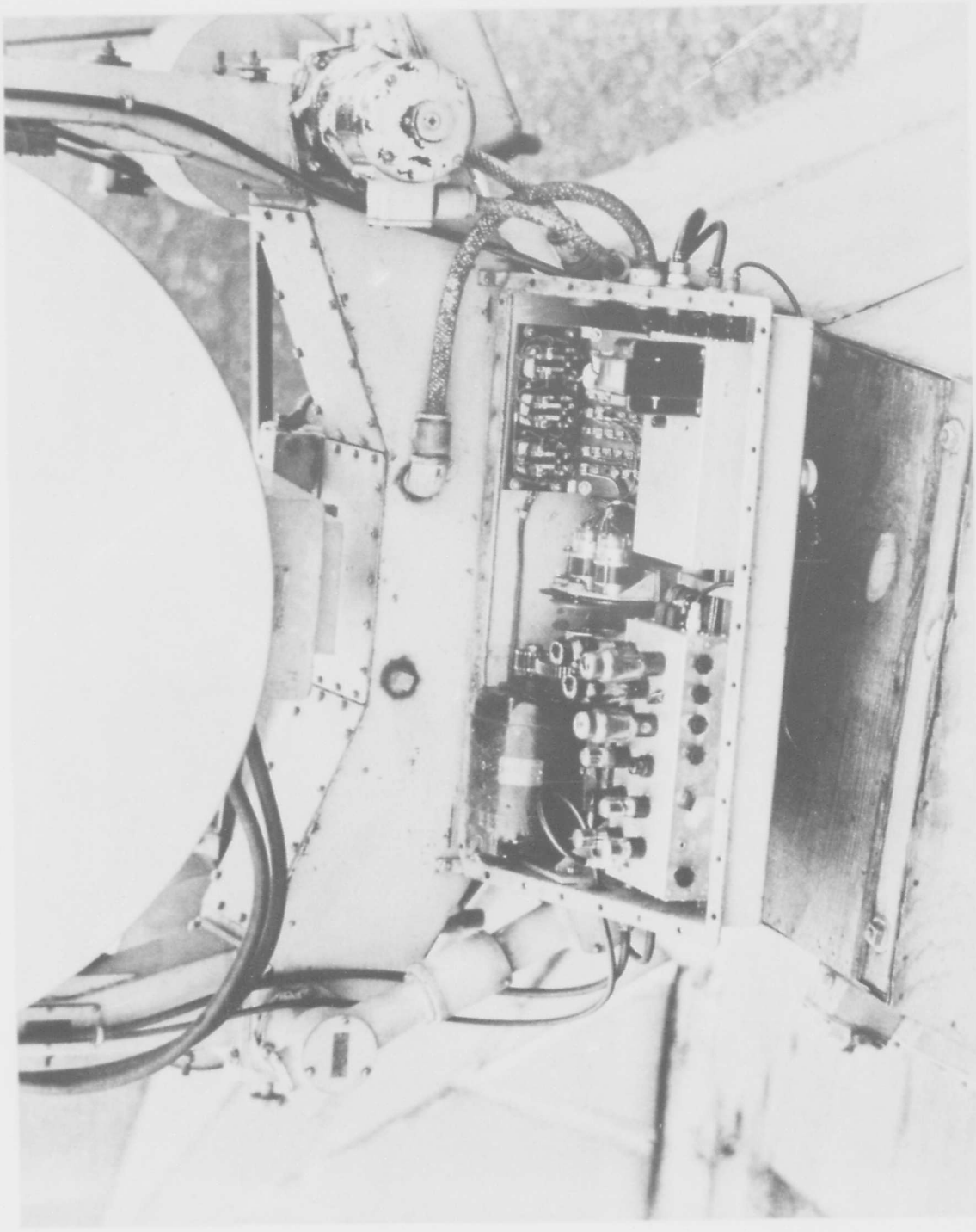

Figure 3.33 Control Box

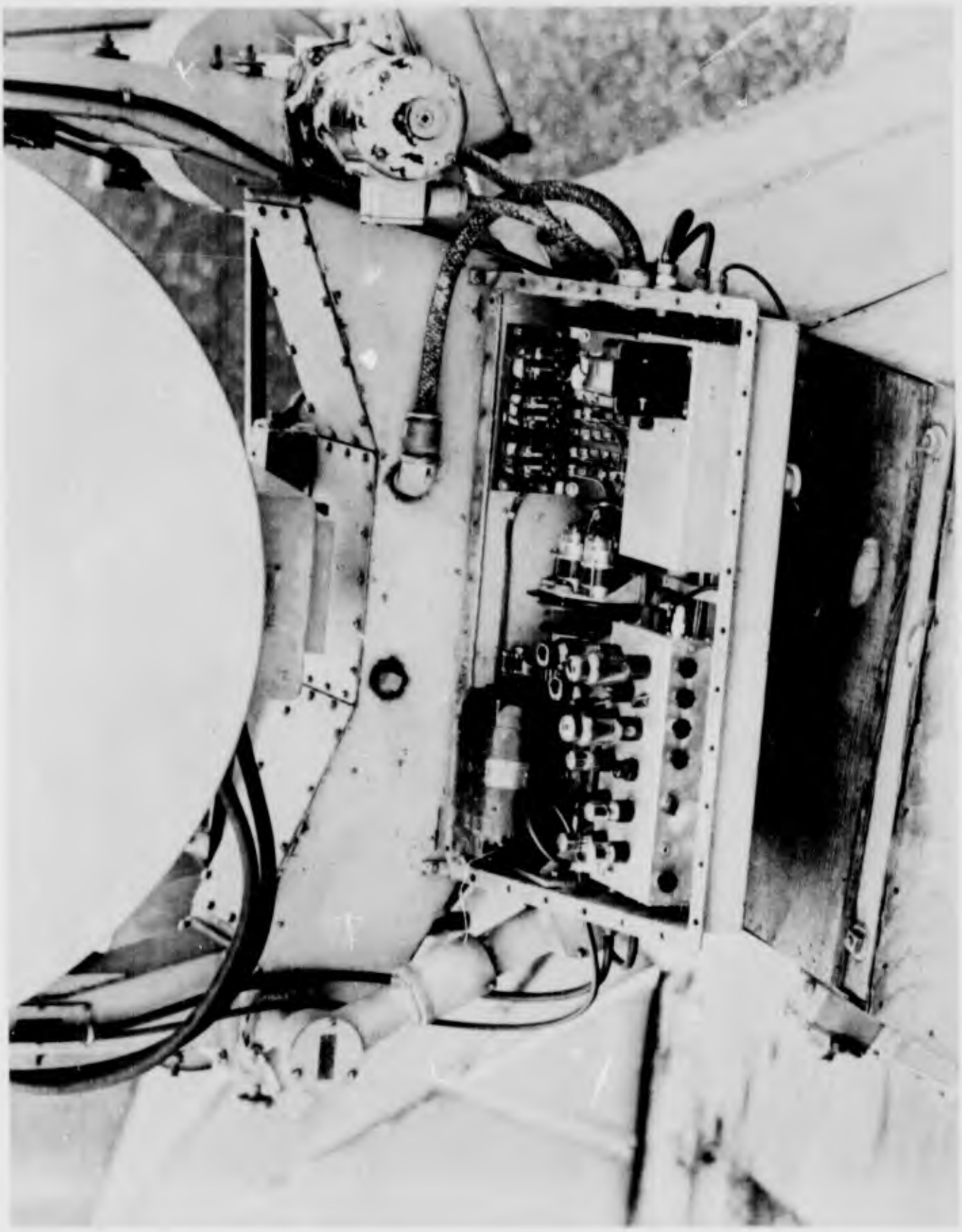

Figure 3.33 Control Box

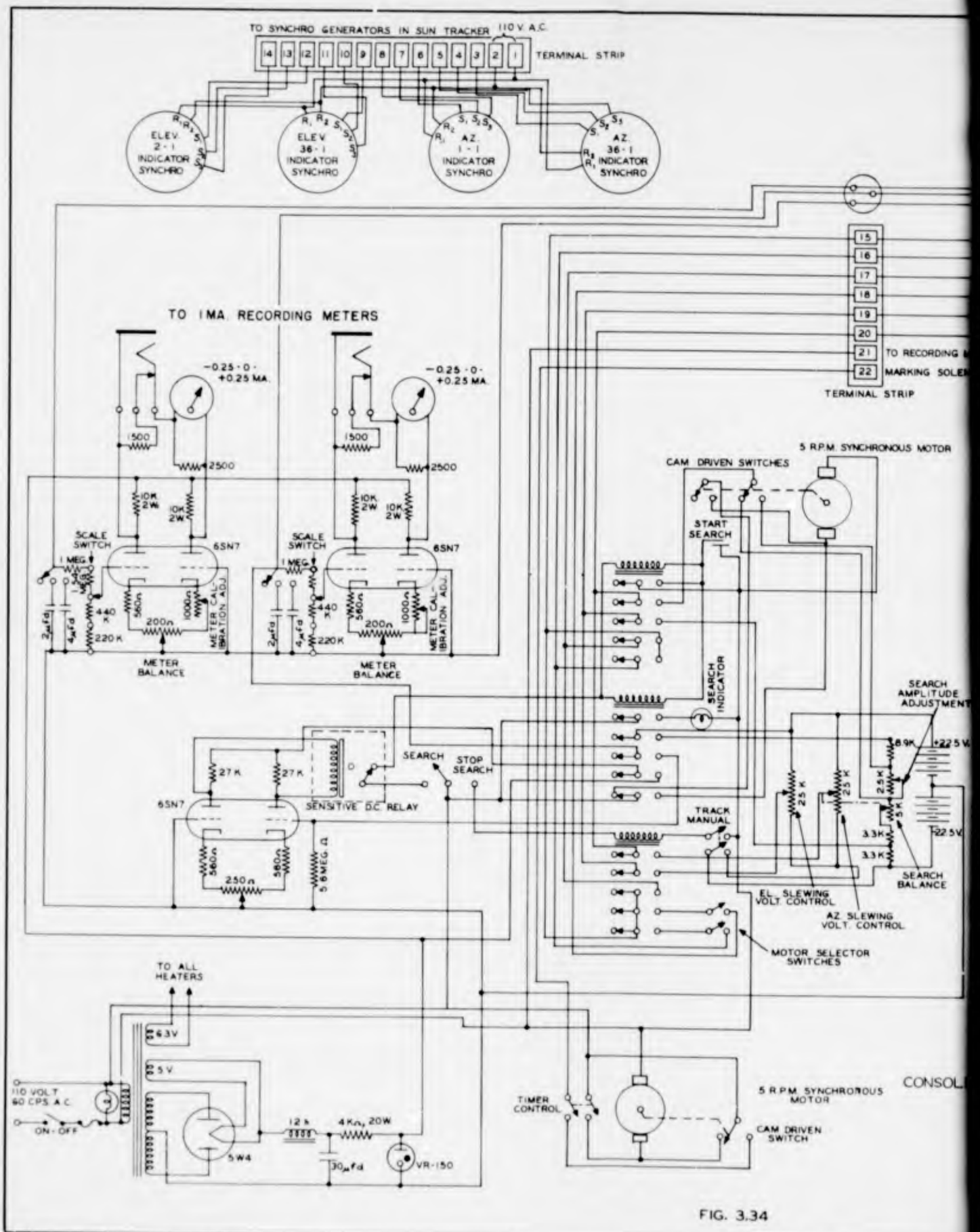
TO SYNCHRO GENERATORS IN SUN TRACKER
110 V. A.C.
TERMINAL STRIP
ELEV. 2-1 INDICATOR SYNCHRO
ELEV 36-1 INDICATOR SYNCHRO
AZ. 1-1 INDICATOR SYNCHRO
AZ. 36-1 INDICATOR SYNCHRO
TO 1MA. RECORDING METERS
-0.25-0-+0.25 MA.
1500
2500
10K 2W
SCALE SWITCH
1 MEG.
6SN7
2μfd
4μfd
440 K
220 K
560Ω
200Ω
1000Ω
METER CALIBRATION ADJ.
METER BALANCE
TERMINAL STRIP
TO RECORDING
MARKING SOLE
5 R.P.M. SYNCHRONOUS MOTOR
CAM DRIVEN SWITCHES
START SEARCH
SEARCH INDICATOR
SEARCH AMPLITUDE ADJUSTMENT
8.9K
+22.5 V.
25 K
2.5K
5K
3.3K
-22.5V.
SEARCH BALANCE
EL. SLEWING VOLT. CONTROL
AZ. SLEWING VOLT. CONTROL
MOTOR SELECTOR SWITCHES
TRACK MANUAL
SEARCH
STOP SEARCH
27 K
SENSITIVE D.C. RELAY
580Ω
250Ω
5.6 MEG. Ω
TO ALL HEATERS
6.3V
5 V
110 VOLT 60 CPS A.C.
ON-OFF
5W4
12 h
4 KΩ, 20W
30μfd
VR-150
TIMER CONTROL
5 R.P.M. SYNCHRONOUS MOTOR
CAM DRIVEN SWITCH
CONSOL

FIG. 3.34

EXP. NO. EP 1485-10-12 C

SCAN TITY	USED ON	QUAN-TITY	ITEM NO	QUANTITIES ARE FOR ONE ASSEMBLY: COLLINS PART NUMBER	GOVERNMENT PART NO	PART NAME

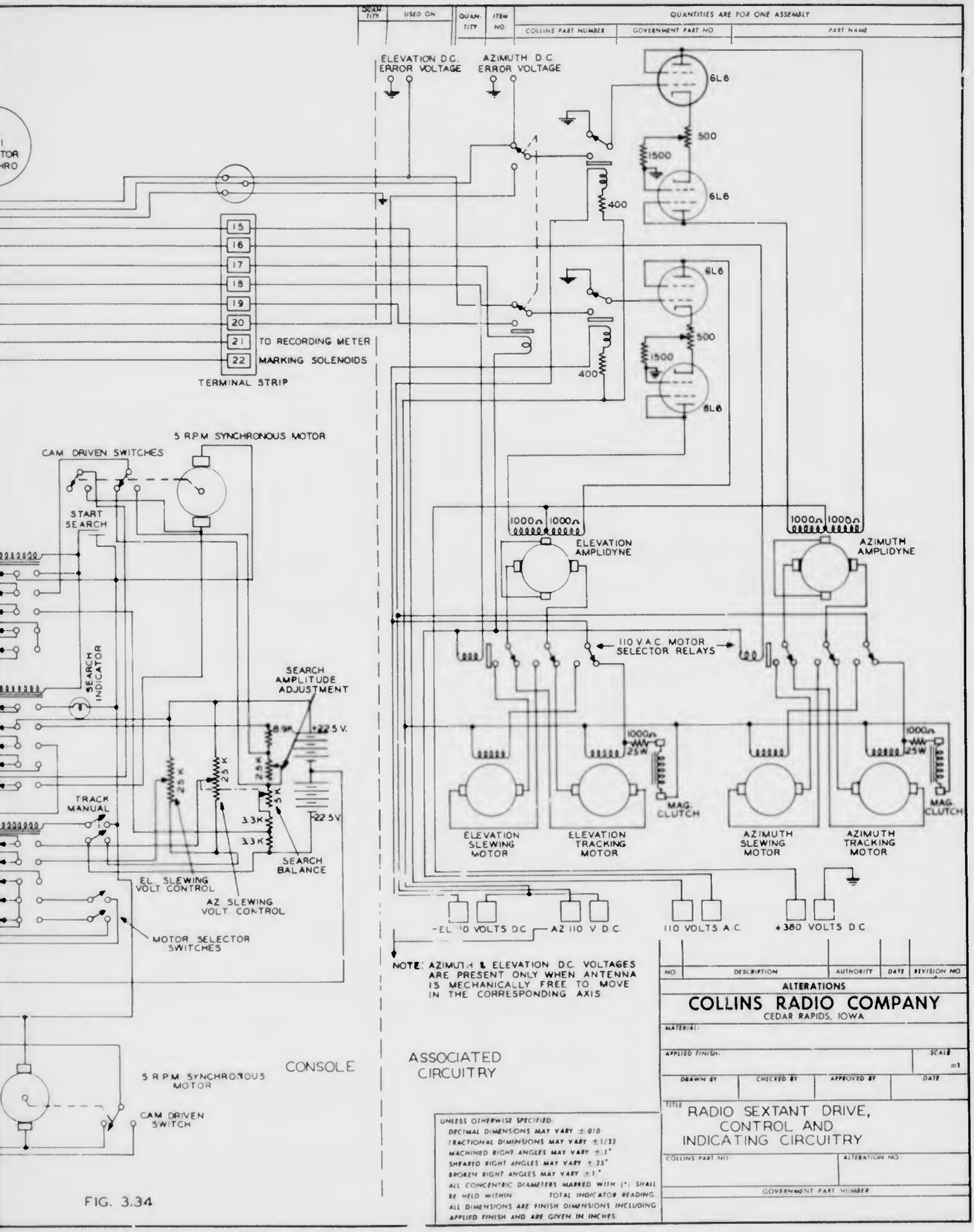

NOTE: AZIMUTH & ELEVATION D.C. VOLTAGES ARE PRESENT ONLY WHEN ANTENNA IS MECHANICALLY FREE TO MOVE IN THE CORRESPONDING AXIS.

NO.	DESCRIPTION	AUTHORITY	DATE	REVISION NO.

ALTERATIONS

COLLINS RADIO COMPANY
CEDAR RAPIDS, IOWA

MATERIAL:
APPLIED FINISH:
SCALE: =1

DRAWN BY	CHECKED BY	APPROVED BY	DATE

TITLE: RADIO SEXTANT DRIVE, CONTROL AND INDICATING CIRCUITRY

COLLINS PART NO. | ALTERATION NO.
GOVERNMENT PART NUMBER

UNLESS OTHERWISE SPECIFIED:
DECIMAL DIMENSIONS MAY VARY ± .010
FRACTIONAL DIMENSIONS MAY VARY ± 1/32
MACHINED RIGHT ANGLES MAY VARY ± 1°
SHEARED RIGHT ANGLES MAY VARY ± 2.5°
BROKEN RIGHT ANGLES MAY VARY ± 1°
ALL CONCENTRIC DIAMETERS MARKED WITH (*) SHALL BE HELD WITHIN ____ TOTAL INDICATOR READING.
ALL DIMENSIONS ARE FINISH DIMENSIONS INCLUDING APPLIED FINISH AND ARE GIVEN IN INCHES.

FIG. 3.34

2

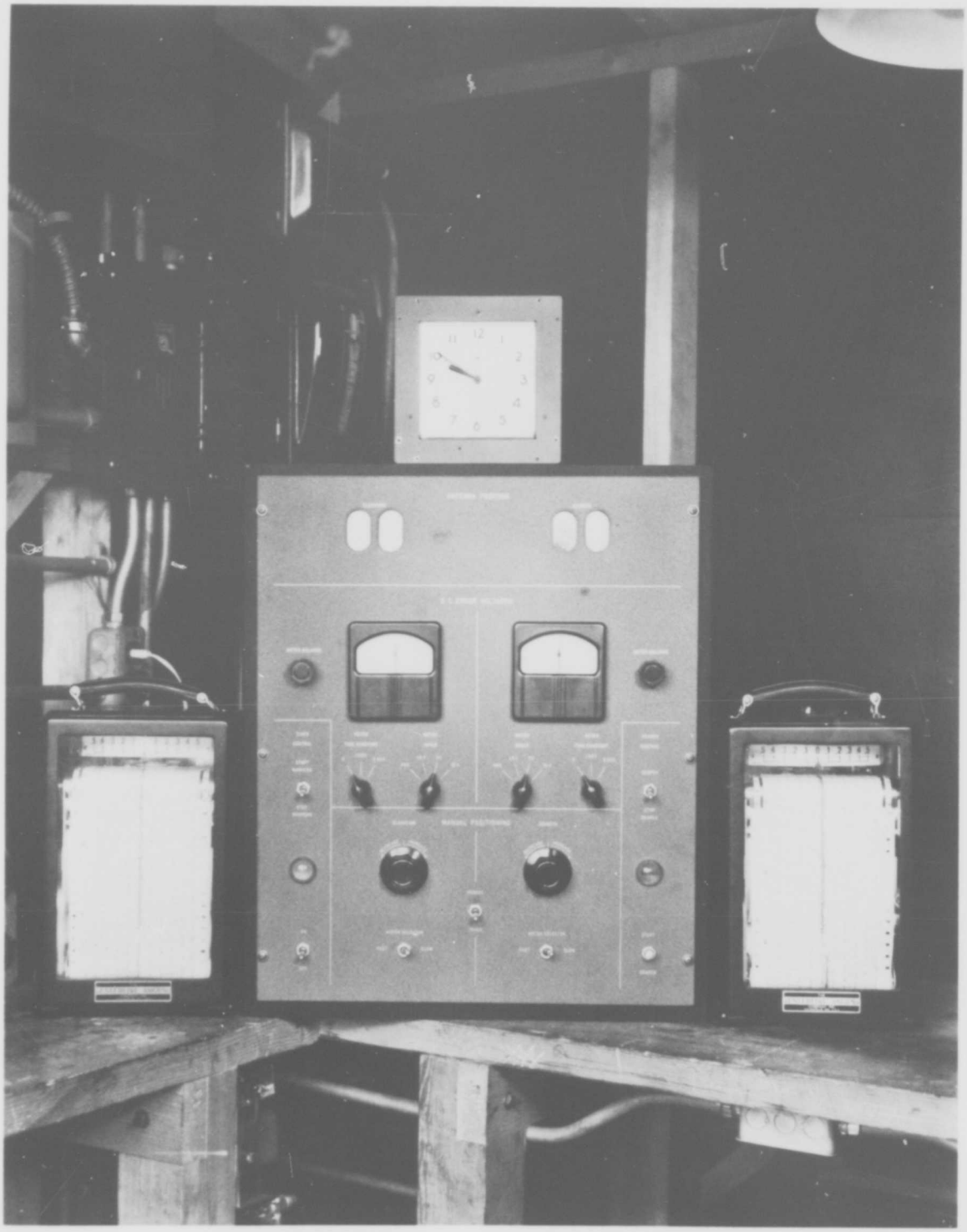

Figure 3.35 Radio Sextant Control Console

the tracking motors, slewing motors, or any combination of the two. The sextant may be made to search for the sun, and, if the sun is encountered during the search, the sextant will automatically lock on and start tracking the sun. Provisions are made for placing either a single timing mark or marks every 12 sec. on the recording meter charts.

The error voltage meters are d.c. vacuum tube voltmeters with an input resistance of 3.2 megohms. The meters are zeroed at the center of their scale and have three ranges - 1.5 to +1.5, -5 to +5 and -15 to +15 volts. As the phase detectors limit at 15 volts, no range higher than this is necessary. Zero, one, and two seconds time constant may be inserted into the meter input circuits. Synchronously driven Esterline Angus Meters with a rating of one milliampere were used to record the error voltages. They were inserted into the meter circuits through phone jacks in the rear of the console. The 0.1 ma. meters in the console were shunted so that they would read the same as the 1.0 ma. recording meters.

The control transformers in the searchlight were replaced by synchro generators. These are used to drive the synchro motors which are mounted near the top of the console. The synchro motors drive 4-1/4" diameter dials which are lighted to permit ease in reading. The dials and reference lines are mounted in such a way so as to minimize parallax, allowing the antenna position to be estimated to 0.02 degrees.

The tracking motors are so coupled to the searchlight that when driving the mount they also turn the armatures of the slewing motors. This meant that the slewing motors could not be used to position the sextant unless the tracking motors were first decoupled, due to the fact that the tracking motors cannot be driven back through their planetary gear trains. Magnetic clutches were installed to accomplish this decoupling. The tracking motors were mounted on the searchlight in the positions previously occupied by the seats for the operators, as shown in Figs. 3.20 and 3.25. The cylindrical housings enclose the magnetic clutches. The clutches were designed for an exciting voltage of 115 volts d.c., but they are operated at 24 volts in the sextant to permit them to slip before any damage is done to the gearing if excessive torques are encountered.

When manual positioning is desired, the track-manual switch, shown in Figs. 3.34 and 3.35, is thrown to "manual." This closes the lower relay in Fig. 3.34 which, in turn, closes the 110 volt a.c. relay, thereby giving control of the 616 grids to the console. If rapid positioning is desired, the motor selector switches are thrown to "fast." These switches close the motor selector relays which simultaneously disengage the clutches and connect the d.c.

field voltages and amplidyne outputs with the slewing motors. If vernier positioning is wanted in either or both axes, the motor selector switch or switches are thrown to "slow." This engages the magnetic clutches and gives control to the tracking motors. The sextant is manually positioned by adjusting the slewing voltage controls, Fig. 3.34, which place d.c. voltages on the 6L6 amplidyne control tubes in accordance with the desired motion. A 45 volt battery is used to supply these voltages. The sextant may be driven at a maximum angular velocity of 24 deg. per sec. in elevation and 28 deg. per sec. in azimuth by the slewing motors. The maximum angular velocities attainable with the tracking motors are 90 deg. per hr. in elevation and 144 deg. per hr. in azimuth.

A search mechanism was incorporated into the sextant control equipment. It was not deemed worthwhile to add control transformers to the sextant for extensive revisions and additions would have been required. Therefore, a simpler search system was designed.

In this system, a 5 R.P.M. synchronous timing motor, driving two cam operated microswitches, was used to control the sextant in azimuth during its search cycle. One microswitch with 180° operation places a voltage on the azimuth control tube grid. The amplitude of this voltage remains constant but its polarity is reversed every 6 sec. by the cam driven microswitch. This causes the sextant to oscillate in azimuth, completing one cycle every 12 sec. At the same time, a voltage is placed on the elevation control tube grid which constantly drives the sextant upwards in elevation. The azimuth slewing motor and the elevation tracking motor are used to execute the search.

To begin the search, the antenna is manually positioned to the suspected azimuth of the sun and to a few degrees below the suspected elevation of the sun. Then the search control switch is thrown to the "search" position and the "start search" button is depressed. This closes the upper two relays in Fig. 3.34 which lights the search indicator, selects the proper motors, and places the search voltages on to the control tube grids. During the search cycle, the antenna scans a 10° sector in azimuth while moving constantly upwards in elevation at 1.5 deg. per min. At the start of the search, the azimuth slewing voltage control may be adjusted to counteract any unbalance, dead zone or hysteresis effects present, and, therefore, cause the sector scanned to be vertical. If at any time during the search the sun is encountered and the signal received exceeds ± 4 volts, the search is automatically stopped, the search indicator is extinguished, and the relays return to their proper positions for automatic tracking.

This automatic lock on is accomplished through the use of a 1 ma. d.c. relay placed between the plates of a 6SN7 twin triode.

The azimuth error voltage is placed on the grid of one section while the other grid is grounded. When the error voltage exceeds ± 4 volts, a potential difference great enough to throw the relay exists between the two plates. After the search is stopped, the search timing motor continues to run until the 180° cam is in a position to start the next search at the midpoint of the sector. The second microswitch, with 1/2 second operation, then shuts off the motor. The sextant then cannot be positioned manually unless the search control switch is returned to the "stop search" position. During normal operation the sextant should automatically lock on to the sun if the axis of the antenna beam comes within a degree of the center of the sun.

3.2.4.7 Performance

a. Methods Used for Determination of Sextant's Accuracy

The tracking errors on which the radio sextant operates have been measured by two different methods. The first method centers about obtaining response curves for the system which express d.c. voltage output as a function of angular distance from the sun. These curves may then be applied to obtain the angular following error for a given operating error voltage. The second method is the direct measurement of the angular distance between the axis of the nutating antenna and the center of the sun by photographic means.

The response curves are obtained by allowing the sun to pass through the antenna beam. During the operation, one axis of the antenna is mechanically locked while the sextant is allowed to track in the other. The resulting d.c. signal in the channel corresponding to the mechanically locked axis is recorded against time. Knowing the velocity of the sun with respect to the axis in question, the recorded curve may be reduced to a plot of d.c. volts error signal vs. angular distance from the center of the sun. The slope of this curve in the region about the origin, measured in volts per degree error, is defined as the sensitivity of the system. Once this sensitivity is known, the angular tracking errors may be determined by dividing the operating error voltage by the sensitivity.

It is not at once obvious that this sensitivity may be applied under all operating conditions to both the elevation and azimuth channels in computing the tracking errors from their respective error voltages. Tests have shown the gain of the two channels to be the same up to the output of the phase detectors at which point the voltages are metered. Hence, a specific azimuth angular error will produce the same error voltage as an identical error in elevation. Therefore, a sensitivity measured for one axis will apply equally well to the other. Another factor must also be considered.

If an angular error in one axis affected the sensitivity in the other axis, this method could not be applied to determine the elevation and azimuth angular errors. However, it may be quite easily shown that the tracking errors in the two axes are independent for the operating angular errors encountered.

With reference to Fig. 3.24, the modulation produced by the nutating antenna is a linear function of the angular displacement of the axis of the antenna from the center of the sun up until the displacement exceeds 0.15 degrees. For all displacements less than 0.15 degrees, the modulation produced by the antenna may therefore be expressed by:

$$E_{ac} = CT_{sun}\sqrt{\epsilon_A^2 + \epsilon_h^2}$$ where

T_{sun} = black body temp. of sun

ϵ_h = elevation angular error

ϵ_A = azimuth angular error

C = antenna factor

The d.c. output of the phase detectors is equal to the a.c. signal input times the cosine of the phase angle between the signal and reference voltages.

As the two phases of the reference generator are 90° apart, it may be written:

$$E_A = CT_{sun}\mathcal{G}_s\sqrt{\epsilon_A^2 + \epsilon_h^2}\cdot\cos\theta$$

$$E_h = CT_{sun}\mathcal{G}_s\sqrt{\epsilon_A^2 + \epsilon_h^2}\cdot\sin\theta$$

where

E_A = azimuth error voltage

E_h = elevation error voltage

θ = phase angle between azimuth reference voltage and signal voltage

$\mathcal{G}_s$ = system gain from antenna to phase detectors

but: $\cos\theta = \dfrac{\epsilon_A}{\sqrt{\epsilon_A^2 + \epsilon_h^2}}$

$$\sin\theta = \frac{\epsilon_h}{\sqrt{\epsilon_A^2 + \epsilon_h^2}}$$

Hence: $E_A = CT_{sun}\mathcal{G}_s\ \epsilon_A$ volts

$E_h = CT_{sun}\mathcal{G}_s\ \epsilon_h$ volts

or

$$\epsilon_A = \frac{E_A}{CT_{sun}\mathcal{G}_s}$$

$$\epsilon_h = \frac{E_h}{CT_{sun}\mathcal{G}_s}$$

This brief analysis shows that up to 0.15 degrees the azimuth and elevation tracking errors for a given sensitivity, $CT_{sun}\,\frac{E_s}{S}$, are functions only of their respective operating error voltages. As will be indicated later, the tracking errors will never approach 0.15 degrees under normal conditions so this "sensitivity-error voltage" method of determining the tracking errors appears to be legitimate.

It is of interest to note that the sensitivity, $CT_{sun}\,\frac{E_s}{S}$ varies directly with the temperature of the source, assuming the receiver gain to be constant. This presents the possibility that the radio sextant may also be used as a radiometer.

Photographic methods were used to measure directly the radio sextant's tracking errors. For this purpose two modified 16 mm. magazine load movie cameras, synchronously driven from a camera control unit, were used. One camera was fitted with a low power telescope, containing cross hairs, whose field of view was a little over 1^{0}. This unit was mounted on the antenna mount, as shown in Fig. 3.36 and aligned with the axis of the antenna. The other camera, which is equipped with a wide angle lens, was used to photograph the error voltage meters and clock contained in the console. Fig. 3.37 shows the camera equipped with the wide angle lens on top of the camera control unit. The camera control unit consists of a 1/15 HP synchronous motor which drives a 7G synchro generator through a transmission which permits exposures at 10, 20 and 30 frames per second. The 5F synchro motors are driven by the 7G synchro generator. The two cameras are, therefore, synchronized and through proper marking at the start of each magazine of film, a frame taken of the sun through the telescope may be compared with a frame taken of the console at exactly the same time. The use of synchronized pictures of both the sun and the console allowed the previously discussed sensitivity measurements to be checked and the effect of a noisy signal on the instantaneous tracking error to be analyzed. The latter is of major importance in determining the maximum instantaneous tracking errors which occur. The sensitivity-error voltage method can be used only to determine the average tracking errors while the synchronized camera data allows the fluctutating angular errors to be measured. Incorporated into the camera control unit are provisions for remote operation, cyclic operation and for flagging the film for identification and reference purposes. A time indicator is also contained which may be used to indicate the time remaining on the magazines of film.

The telescope was aligned with the axis of the antenna permitting the position of the sun relative to the telescope's cross hairs to be filmed. This film data was reduced on a contour measuring projector on which relative positions on the film could

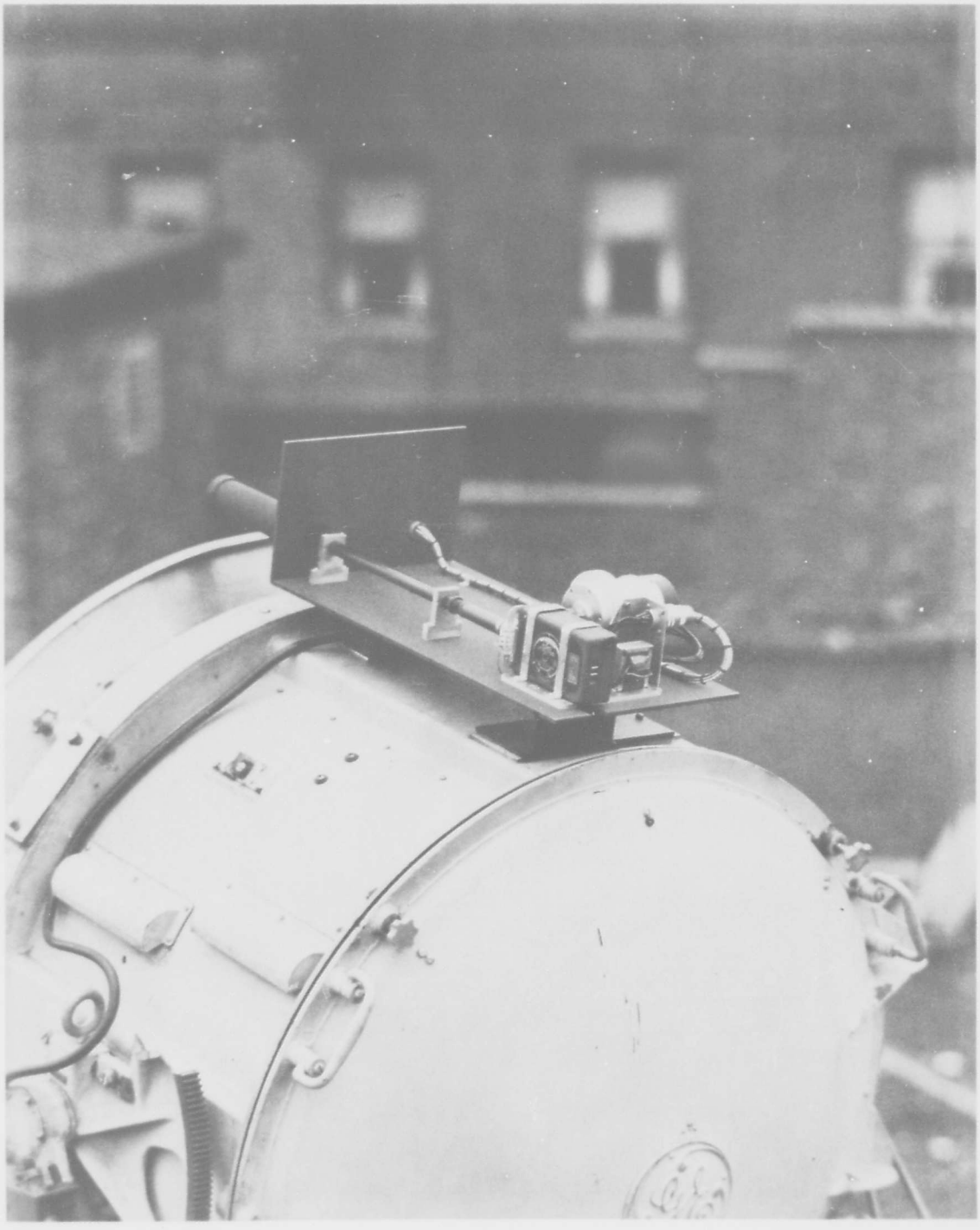

Figure 3.36 Telescope and Camera Assembly

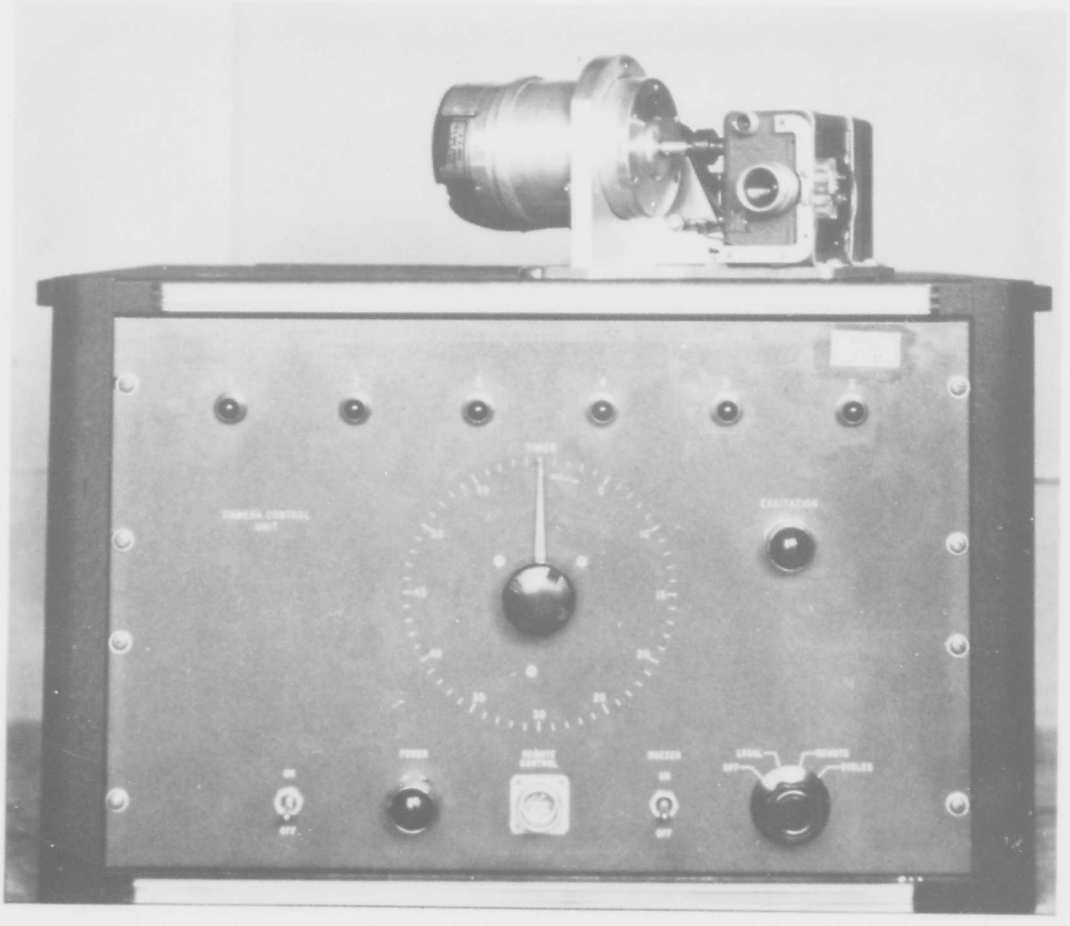

Figure 3.37 Camera Control Unit

be measured to 0.0001 inches. The screen of the projector was also equipped with cross hairs. A circular mask, the size of the sun's image, was placed on the screen with its center at the junction of the projector's cross hairs. This arrangement permitted the relative position of the center of the sun and the telescope's cross hairs to be measured. Knowing the angular diameter of the sun and the size of the sun's image on the film, the measurements thus obtained could be reduced to elevation and azimuth angular displacements between the center of the sun and the axis of the antenna.

An adaptor for holding and advancing the 16 mm. film, being reduced on the contour measuring projector, was constructed. This adaptor is shown in Fig. 3.38. The film drive arrangement permitted rapid and reliable selection of specific frames for reduction.

The finite resolution of the telescope and camera system and the inability to position the image of the sun exactly within the mask were the limiting factors in the accuracy of this method of reduction. All factors being considered, the resulting data was accurate to better than 0.001 degrees which is sufficient to determine the performance of the radio sextant.

The film taken of the console was reduced on a microfilm projector. The data of interest were the elevation and azimuth error voltages which could be read from the projector to 0.1 volts on the 5 volt meter scale, and 0.3 volts on the 15 volt meter scale.

In the beginning of this section a "sun velocity" method of measuring the sensitivity of the radio sextant was described. A more direct and also more complicated method of measuring the sensitivity would be to employ the synchronous camera equipment. The procedure would be identical to that described for the "sun velocity" method, except as the sun passes through the beam, its position with respect to the antenna axis would be photographed simultaneously with the d.c. error voltage meters. Then, the error voltages and sun positions, corresponding to the mechanically locked axis, could be plotted against each other. This would result in a response curve directly, the slope of which would be the desired sensitivity.

b. Average Following Error

The average following errors on which the radio sextant operates are most easily obtained by dividing the d.c. error voltages by the measured sensitivity. It was felt, however,

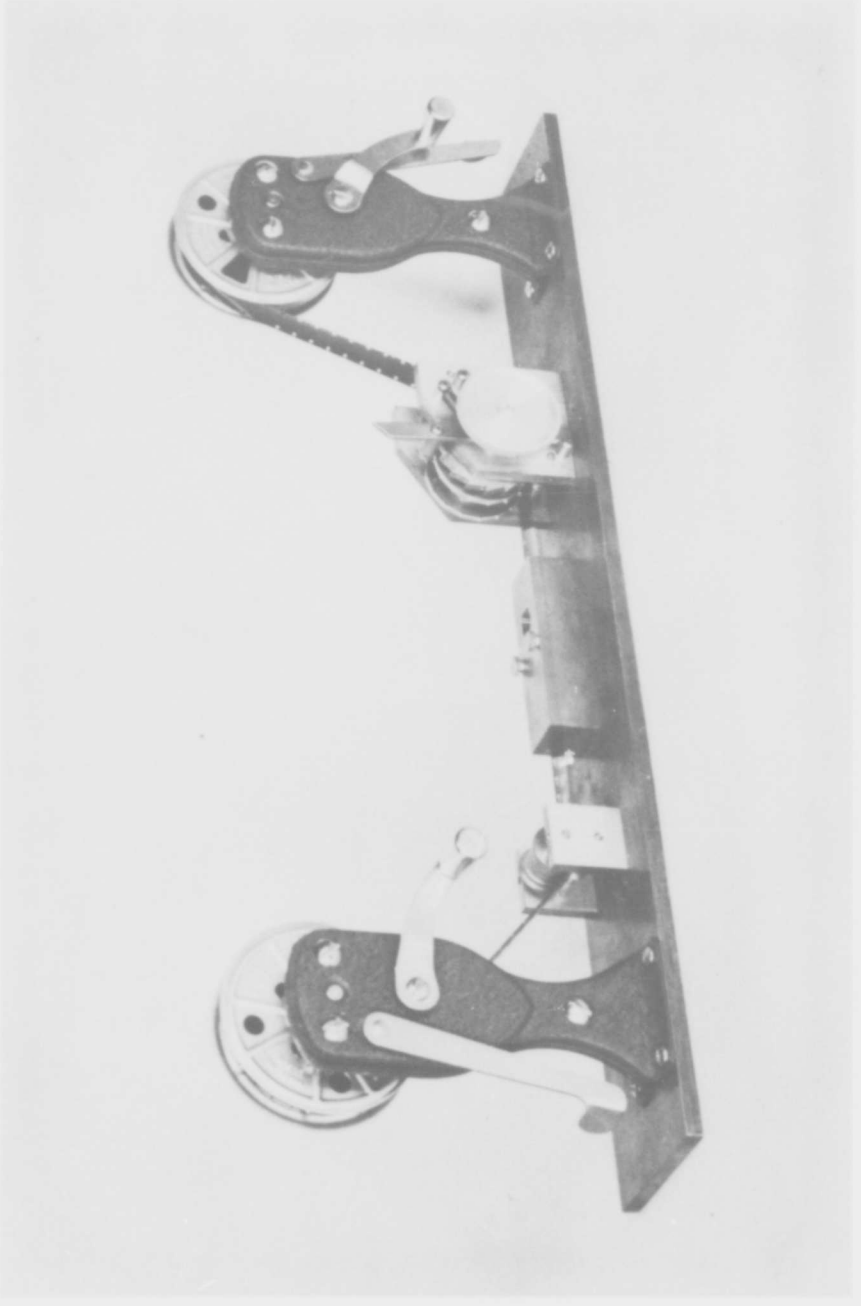

Figure 3.38 Adaptor for Reducing Film Data

that this sensitivity-error voltage method should be checked photographically to exclude any possibility of its being in error.

Response curves for the elevation and azimuth channels were taken simultaneously by the"sun velocity" and photographic methods described in the last section. Since the photographic method is considered to be the most accurate, the data obtained by the "sun velocity" method is compared with the photographic data to check the accuracy of the former method. This check is of interest since the "sun velocity" measurements are much easier to perform than the photographic measurements.

The comparison between the two methods is shown in Figures 3.39 and 3.40. The obvious agreement serves to justify the "sun velocity" method for obtaining the sensitivity of the radio sextant. The fact that the points do not fall exactly on a straight line is due primarily to noise on the error voltages.

Once the sensitivity of the sextant in the desired channel is obtained, it is a simple matter to compute the following error existing between the antenna axis and the sun. The following error voltage that exists while the sextant is tracking is always available on the meters which monitor both the elevation and azimuth channels. The average following error can be found by dividing the following error voltage by the measured sensitivity in volts/deg.

Since operation is at microwave frequencies, the oxygen and water content in the atmosphere contributes an attenuation factor which is a function of path length through the atmosphere as well as meteorological conditions. Obviously, then, the sensitivity of the sextant will be a function of time as well as meteorological conditions. The fact that meteorological conditions along the path from the observer to the sun are by no means predictable prevents the making of a theoretical analysis of the effect of atmospheric absorption on the sensitivity of the sextant. For this reason a program was started for measuring the reduction of sensitivity caused by atmospheric effects. Figure 3.41 is a plot of the measured sextant sensitivity as a function of the sun's elevation angle for weather conditions that were quite favorable. It is seen that for the particular day considered, the sensitivity is not reduced by a factor of 2 until the elevation angle has decreased to approximately 1-1/4 degrees. Comparing this curve with one for a less favorable day as shown in Figure 3.42, it can be seen that the sensitivity is reduced to one-half by the time the elevation angle has dropped to approximately three degrees. The effect of rain is shown in Figure 3.42. Heavy rains may not interfere seriously at high elevation angles, but for low elevation angles, the sensitivity will certainly be reduced by a large factor.

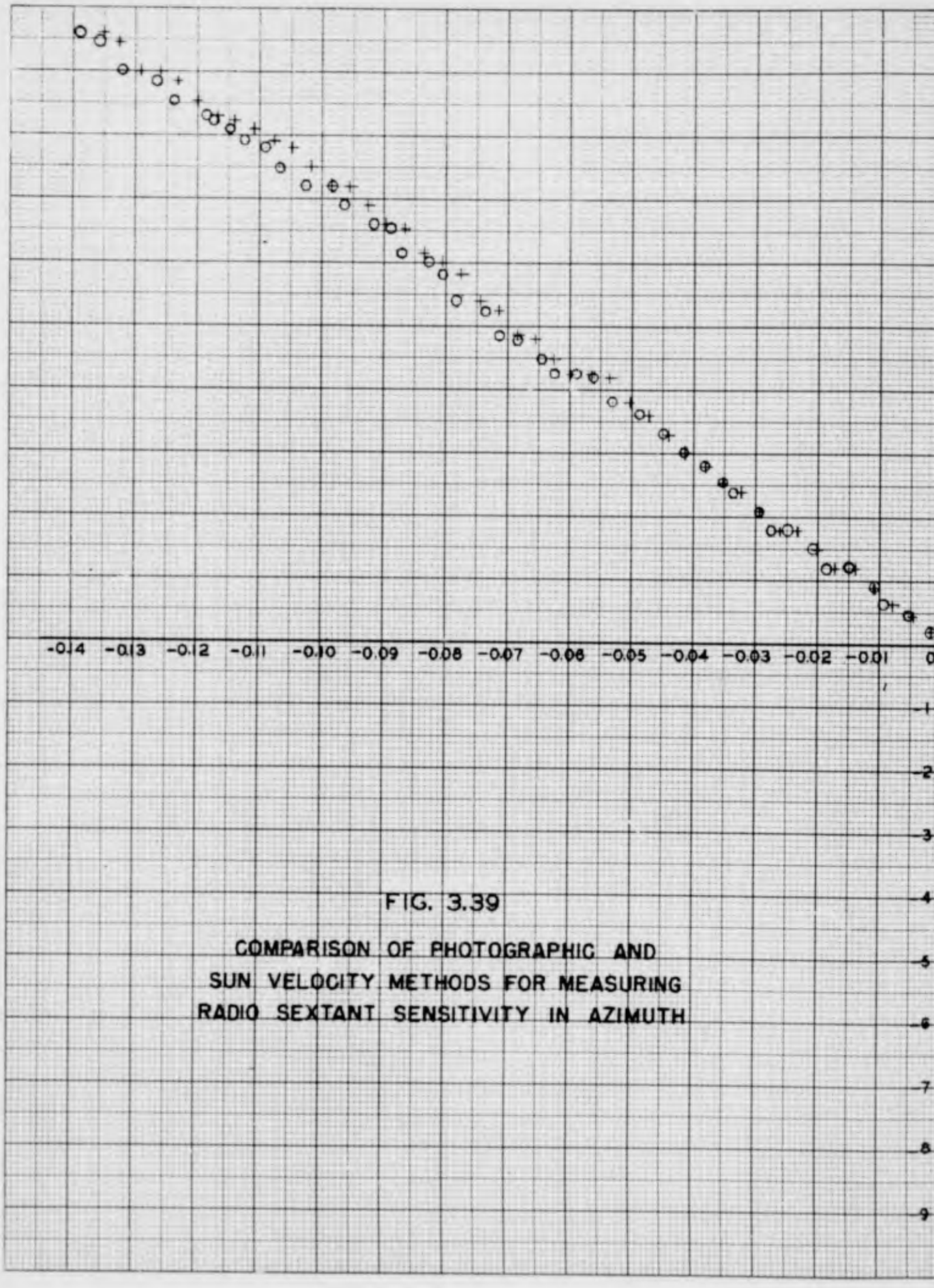

FIG. 3.39

COMPARISON OF PHOTOGRAPHIC AND SUN VELOCITY METHODS FOR MEASURING RADIO SEXTANT SENSITIVITY IN AZIMUTH

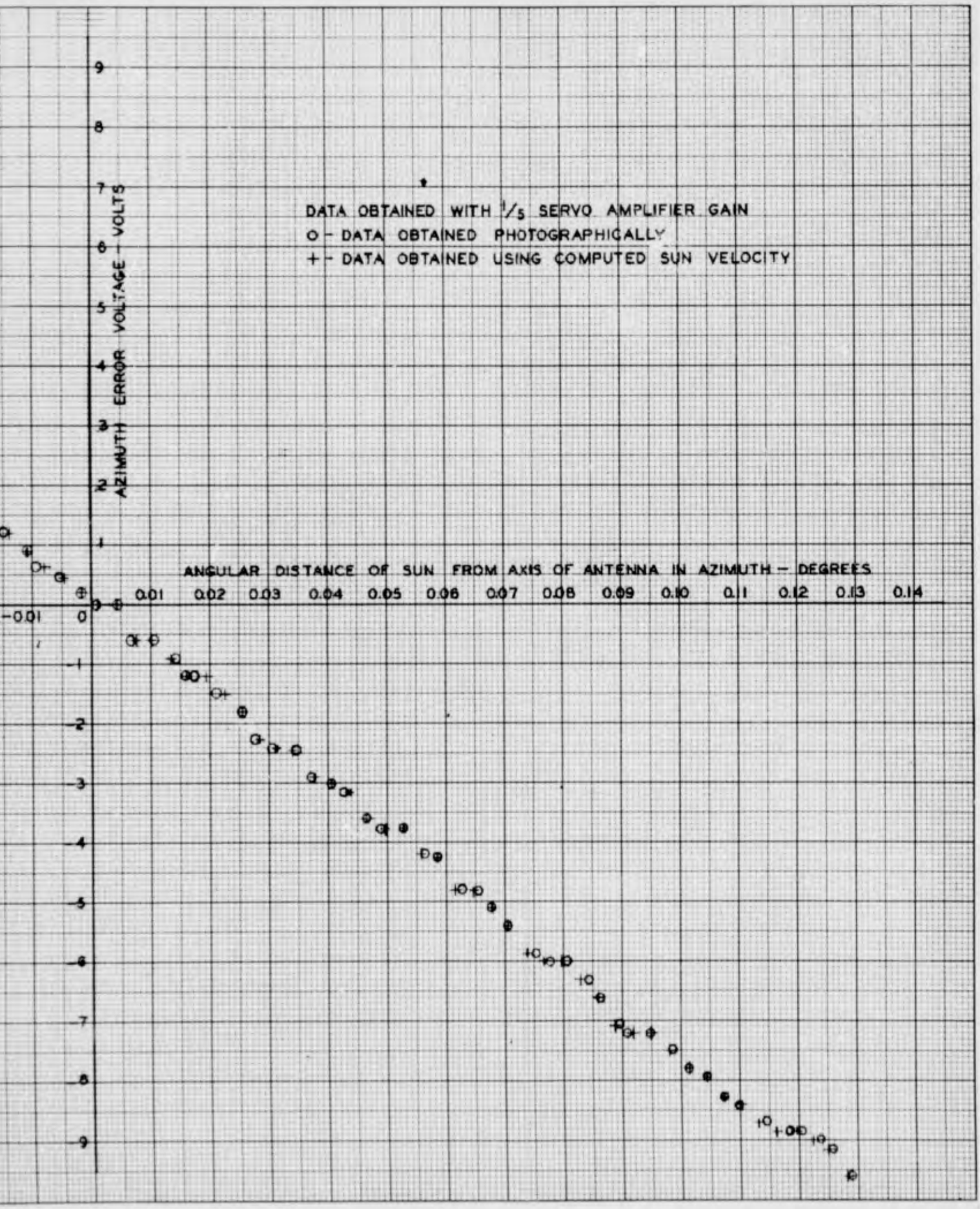
DATA OBTAINED WITH 1/5 SERVO AMPLIFIER GAIN
O - DATA OBTAINED PHOTOGRAPHICALLY
+ - DATA OBTAINED USING COMPUTED SUN VELOCITY
AZIMUTH ERROR VOLTAGE - VOLTS
ANGULAR DISTANCE OF SUN FROM AXIS OF ANTENNA IN AZIMUTH - DEGREES
9
8
7
6
5
4
3
2
1
0
-1
-2
-3
-4
-5
-6
-7
-8
-9
-0.01
0.01
0.02
0.03
0.04
0.05
0.06
0.07
0.08
0.09
0.10
0.11
0.12
0.13
0.14

2

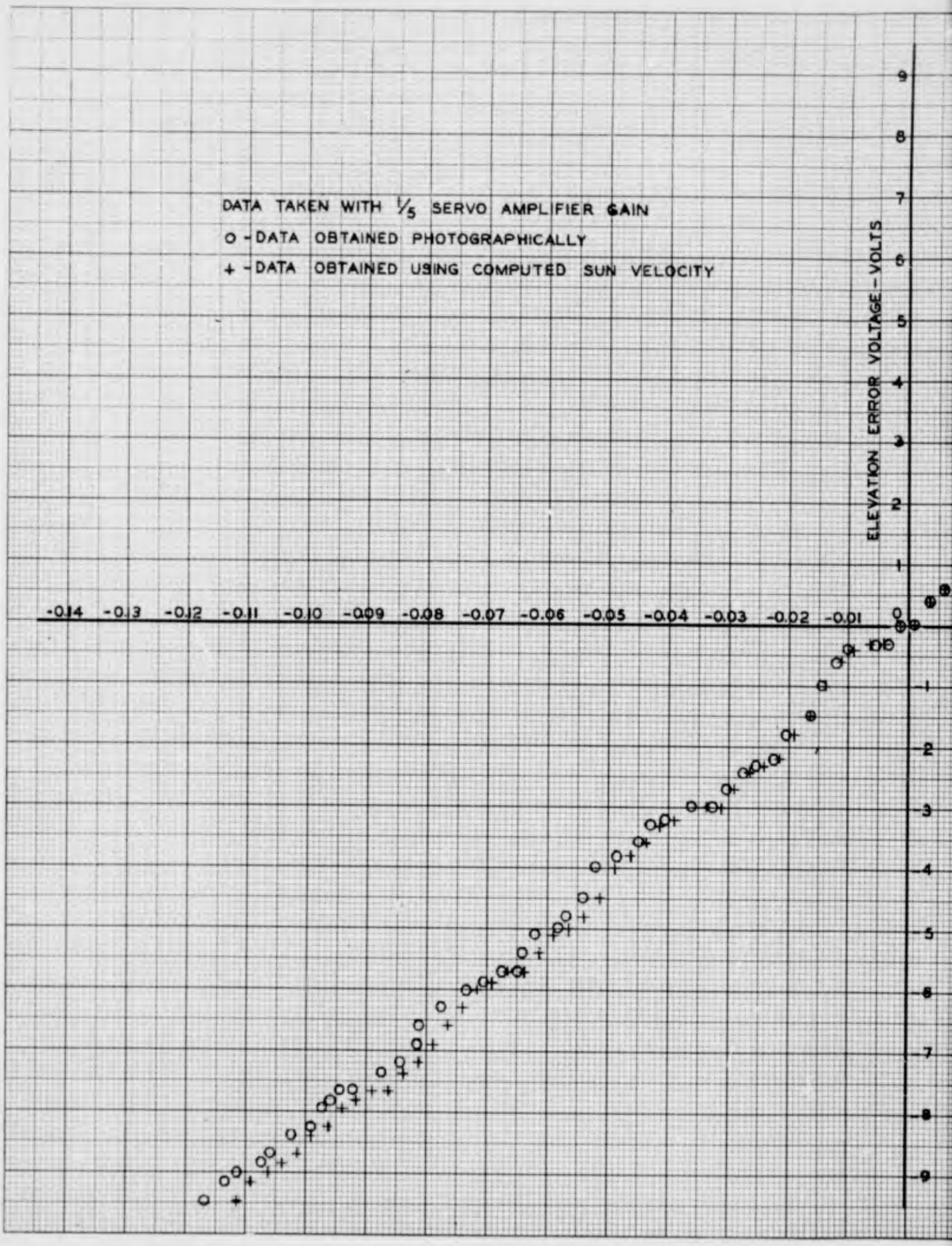
DATA TAKEN WITH 1/5 SERVO AMPLIFIER GAIN
O - DATA OBTAINED PHOTOGRAPHICALLY
+ - DATA OBTAINED USING COMPUTED SUN VELOCITY
ELEVATION ERROR VOLTAGE - VOLTS
-0.14 -0.13 -0.12 -0.11 -0.10 -0.09 -0.08 -0.07 -0.06 -0.05 -0.04 -0.03 -0.02 -0.01
9 8 7 6 5 4 3 2 1 -1 -2 -3 -4 -5 -6 -7 -8 -9

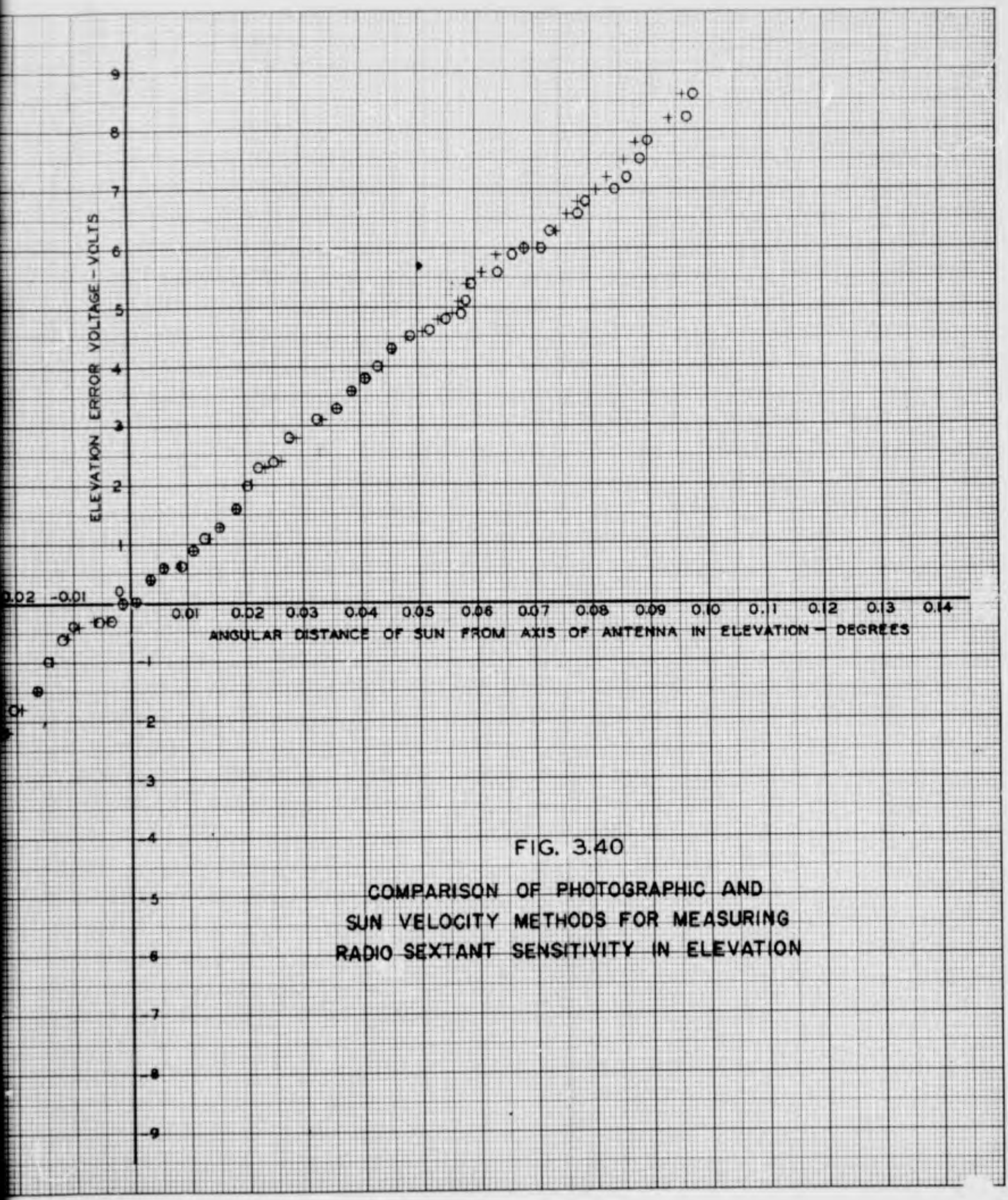

FIG. 3.40

COMPARISON OF PHOTOGRAPHIC AND
SUN VELOCITY METHODS FOR MEASURING
RADIO SEXTANT SENSITIVITY IN ELEVATION

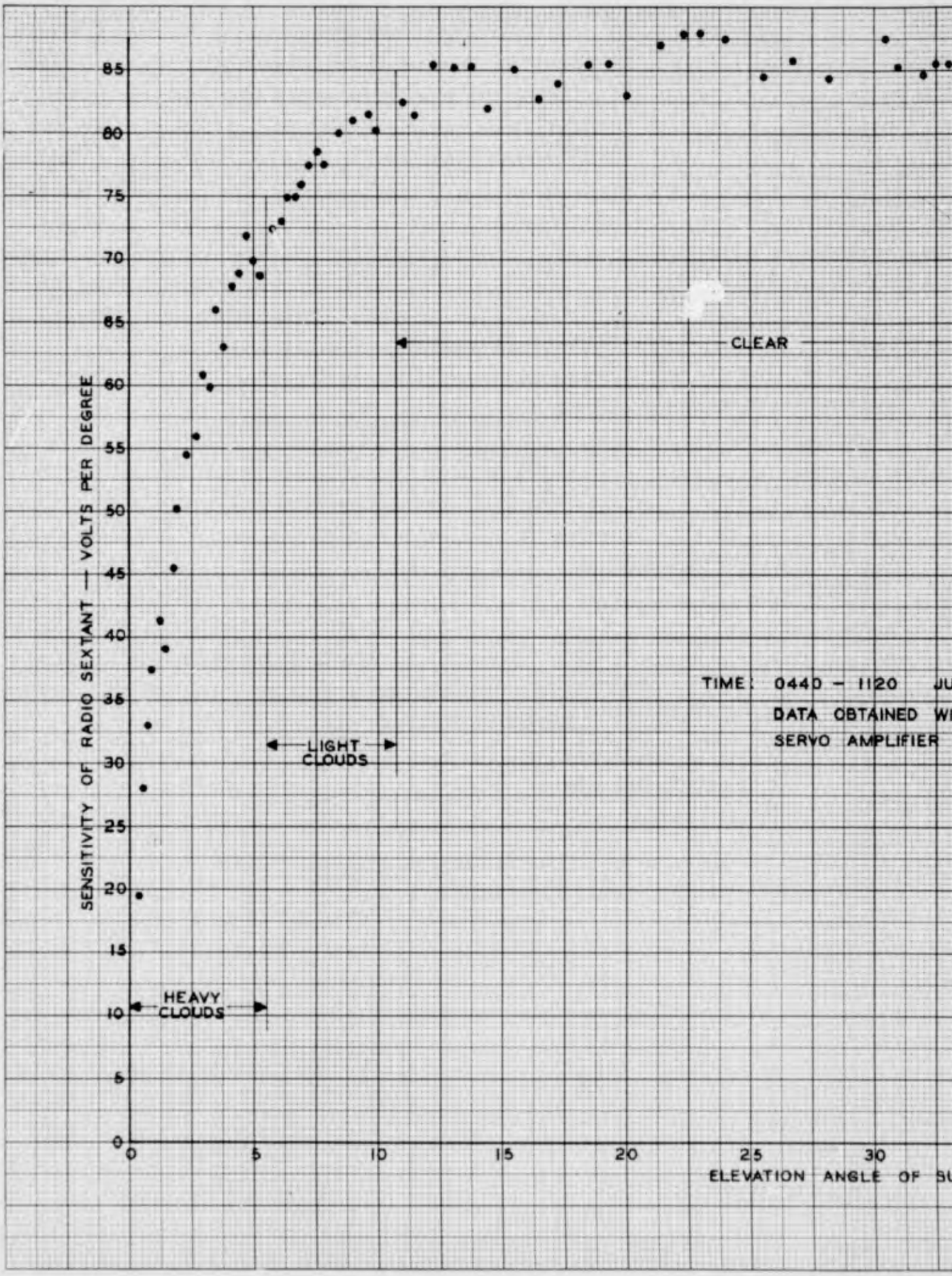
SENSITIVITY OF RADIO SEXTANT — VOLTS PER DEGREE
85
80
75
70
65
60
55
50
45
40
35
30
25
20
15
10
5
0
0
5
10
15
20
25
30
CLEAR
LIGHT CLOUDS
HEAVY CLOUDS
TIME: 0440 – 1120 JU
DATA OBTAINED WI
SERVO AMPLIFIER
ELEVATION ANGLE OF SU

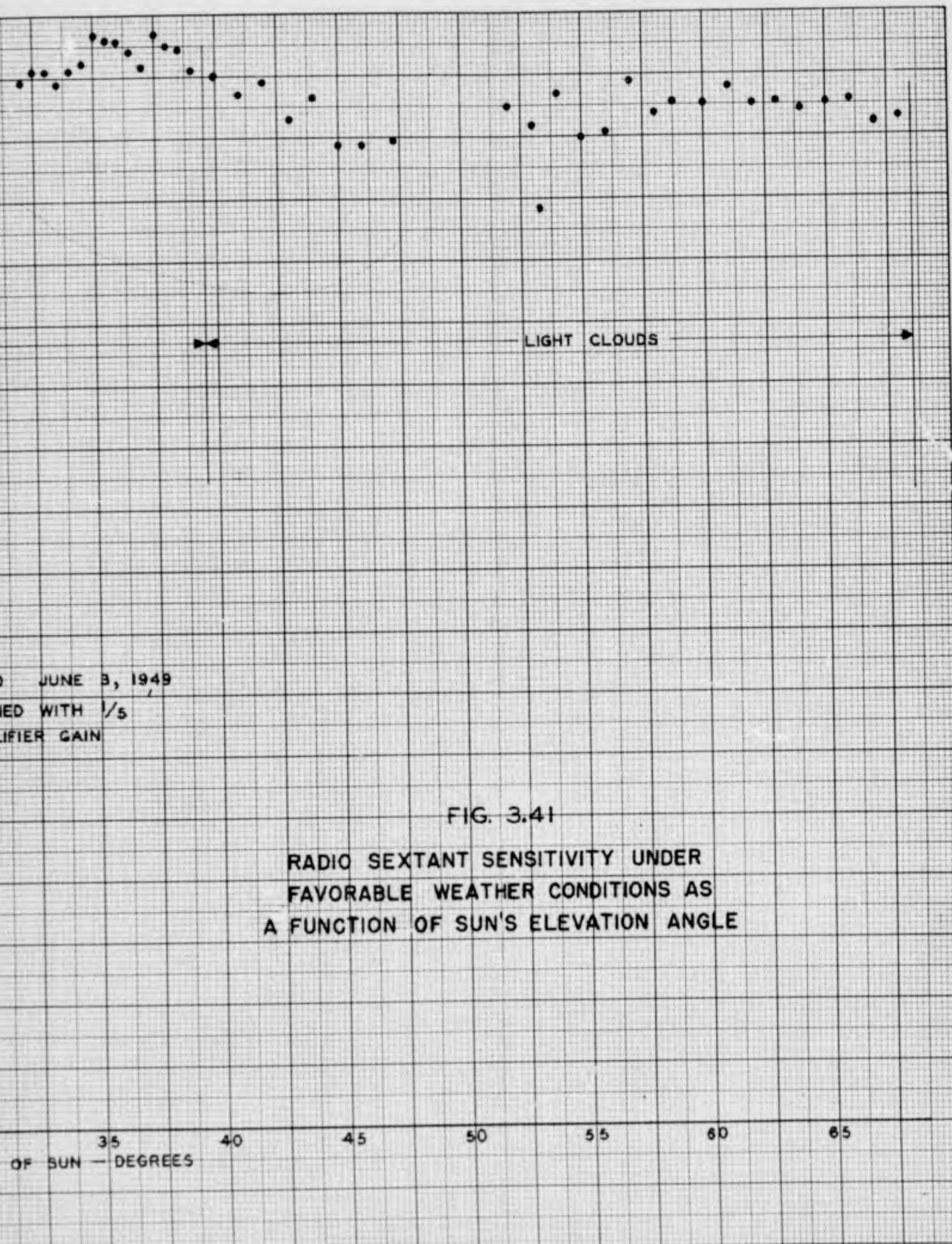

FIG. 3.41

RADIO SEXTANT SENSITIVITY UNDER FAVORABLE WEATHER CONDITIONS AS A FUNCTION OF SUN'S ELEVATION ANGLE

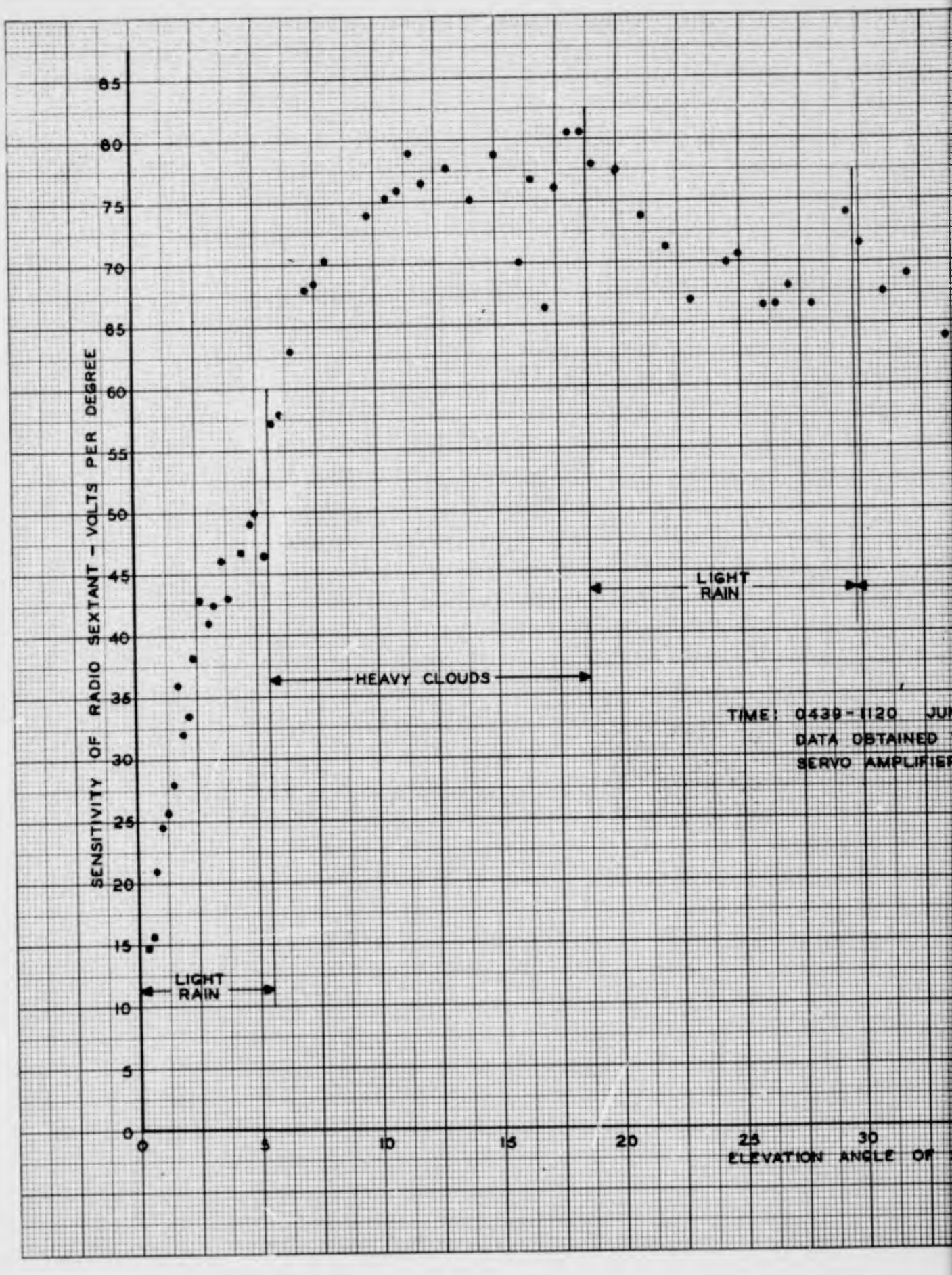
SENSITIVITY OF RADIO SEXTANT – VOLTS PER DEGREE
85
80
75
70
65
60
55
50
45
40
35
30
25
20
15
10
5
0
0
5
10
15
20
25
30
LIGHT RAIN
HEAVY CLOUDS
LIGHT RAIN
TIME: 0439 - 1120 JU
DATA OBTAINED
SERVO AMPLIFIE
ELEVATION ANGLE OF

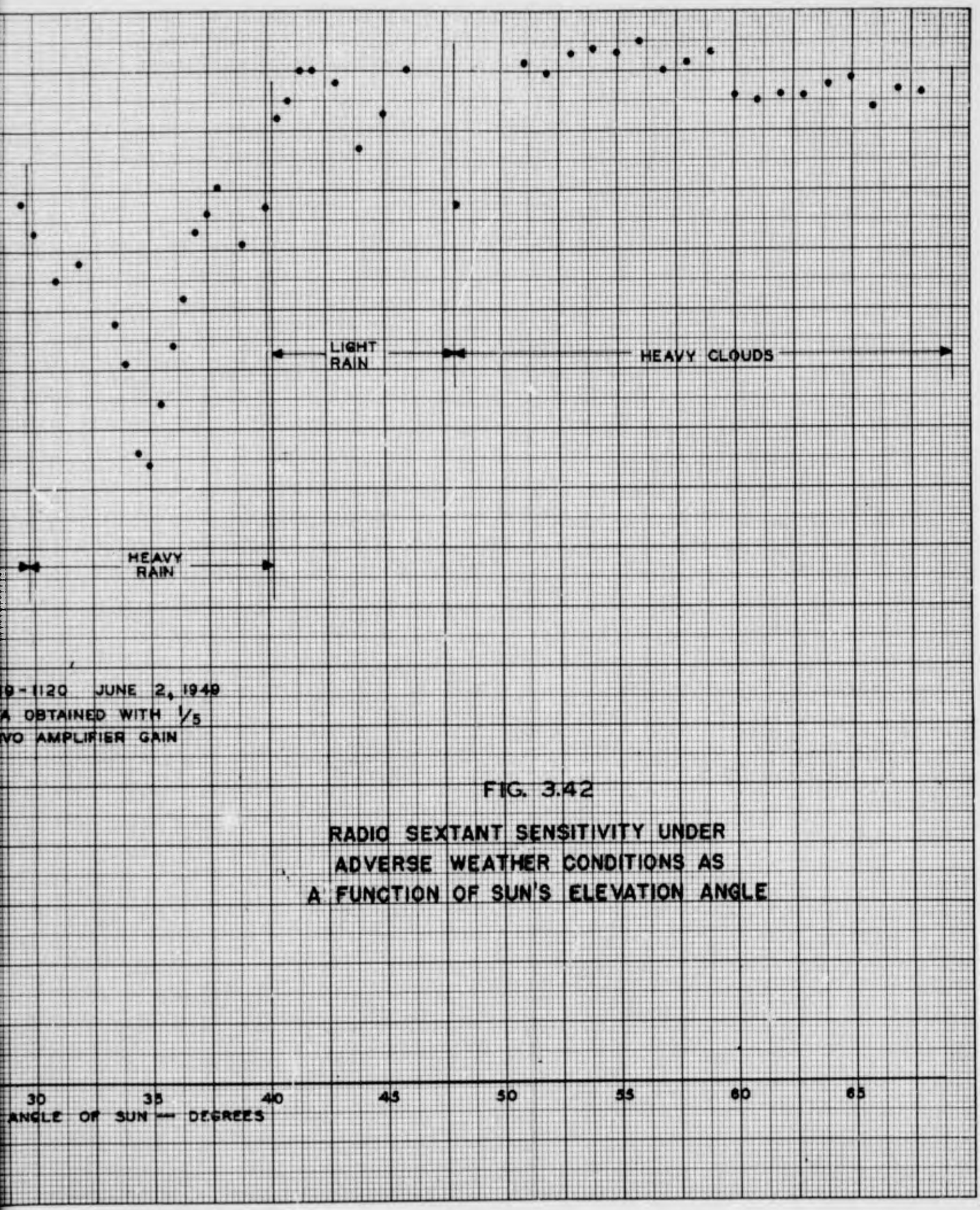

FIG. 3.42

RADIO SEXTANT SENSITIVITY UNDER ADVERSE WEATHER CONDITIONS AS A FUNCTION OF SUN'S ELEVATION ANGLE

All of the absorption data accumulated so far are shown in Figure 3.43. The absorption per unit atmosphere a_o, can be calculated from the results obtained during the period of heavy rain occurring at approximately 35° elevation. Using this value of a_o, the sextant sensitivity for other elevation angles can be obtained. This has resulted in the minimum sensitivity curve shown in Figure 3.43. If the rain covered the entire path from the antenna to the limit of the earth's atmosphere, the curve mentioned above would be correct for elevation angles above 20°. However, it is very unlikely that the rain would cover the entire path since heavy rains are usually localized over rather small areas. In view of this fact, the minimum sensitivity of the sextant can be reliably obtained only from actual measured data.

In view of the limitations imposed on the sextant by atmospheric absorption, any calculation of the following error must be properly qualified. An exception to this rule can be made for clear weather; in this case the absorption can be neglected for elevation angles above 10°. It must be pointed out, however, that the experimental radio sextant has never failed to track the sun to the horizon under all the weather conditions encountered during its operation.

Figure 3.44 is a record of the elevation and azimuth D.C. error voltages for an eight-hour period. The variation in the average azimuth error voltage during the period demonstrates the manner in which the sun's azimuth velocity reaches a maximum at local apparent noon. The discontinuity in the elevation track is due to the change in direction of the sun's elevation velocity, which occurs at local apparent noon. It takes an 0.8 volt change in error signal to reverse the elevation tracking motor; hence the 0.8 volt discontinuity.

During the eight-hour period, the sun's elevation was well above 10 degrees at all times. As weather conditions were favorable, the measured sensitivity, which was 70 volts per degree, is considered to have held throughout the run. The maximum angular tracking error in elevation was 0.027 degrees and the minimum was zero. The sextant was operated at only 1/5 gain during the period in which Figure 3.44 was recorded. The angular tracking errors were accordingly relatively large.

The average angular tracking errors for a given atmospheric absorption and sun velocity should vary inversely with system gain. Figure 3.45 shows the elevation and azimuth average following errors as a function of gain for the velocities and sensitivity indicated. Angular following errors obtained from direct photographic measurements and from the measured sensitivity and

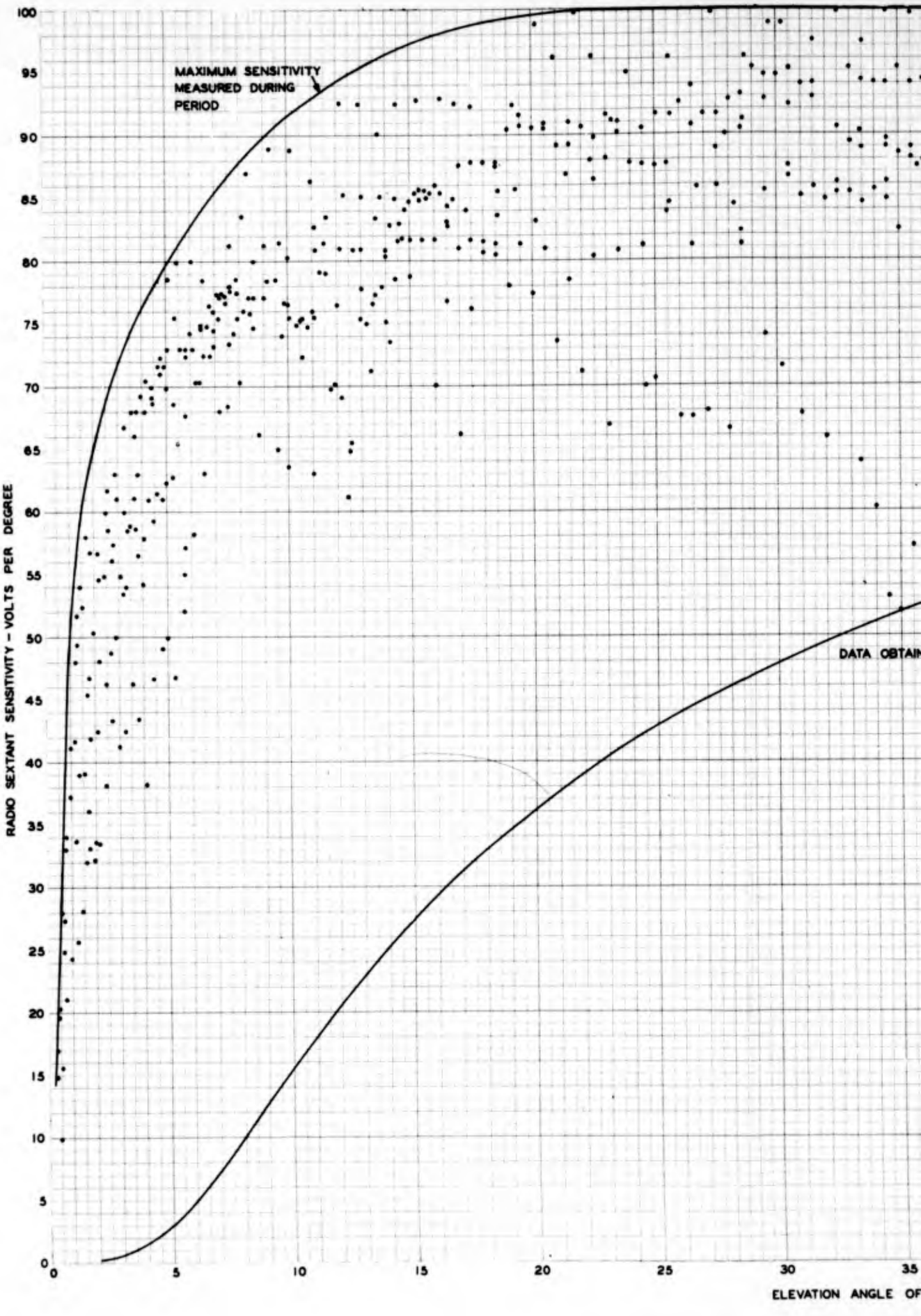
MAXIMUM SENSITIVITY
MEASURED DURING
PERIOD
DATA OBTAIN
RADIO SEXTANT SENSITIVITY - VOLTS PER DEGREE
ELEVATION ANGLE OF
100
95
90
85
80
75
70
65
60
55
50
45
40
35
30
25
20
15
10
5
0
0
5
10
15
20
25
30
35

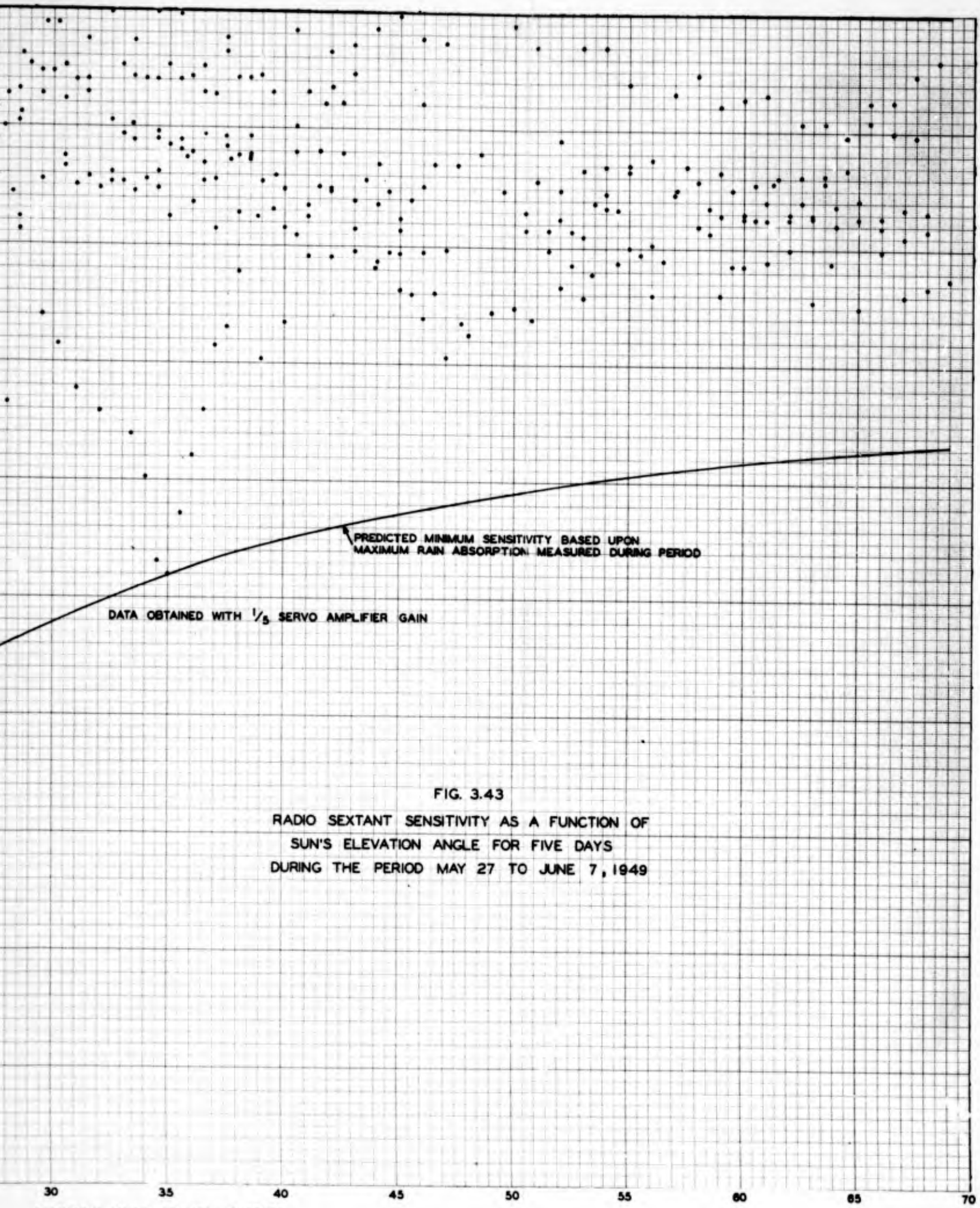

FIG. 3.43

RADIO SEXTANT SENSITIVITY AS A FUNCTION OF
SUN'S ELEVATION ANGLE FOR FIVE DAYS
DURING THE PERIOD MAY 27 TO JUNE 7, 1949

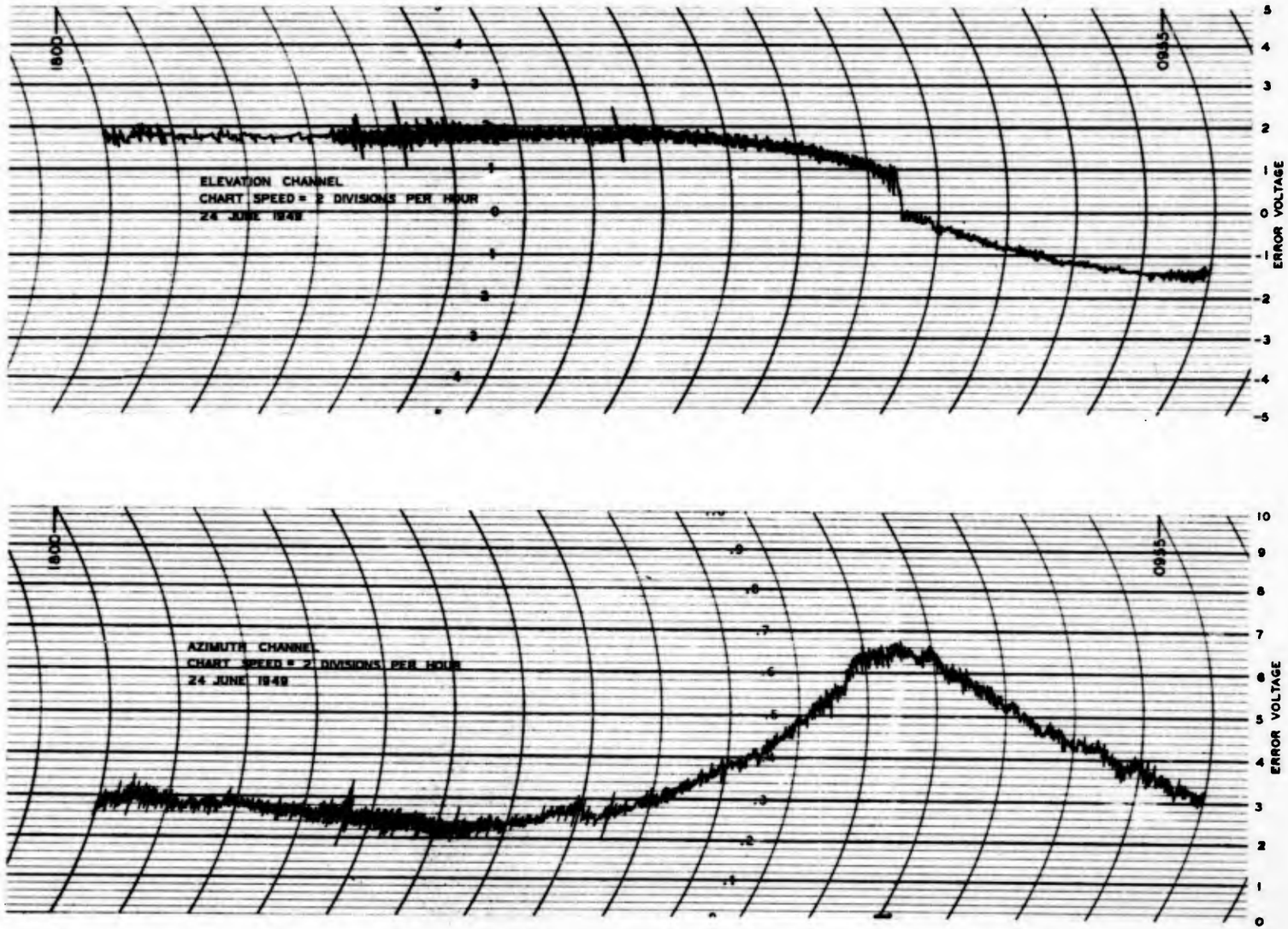

FIG. 3.44
RADIO SEXTANT TRACKING ERROR VOLTAGES

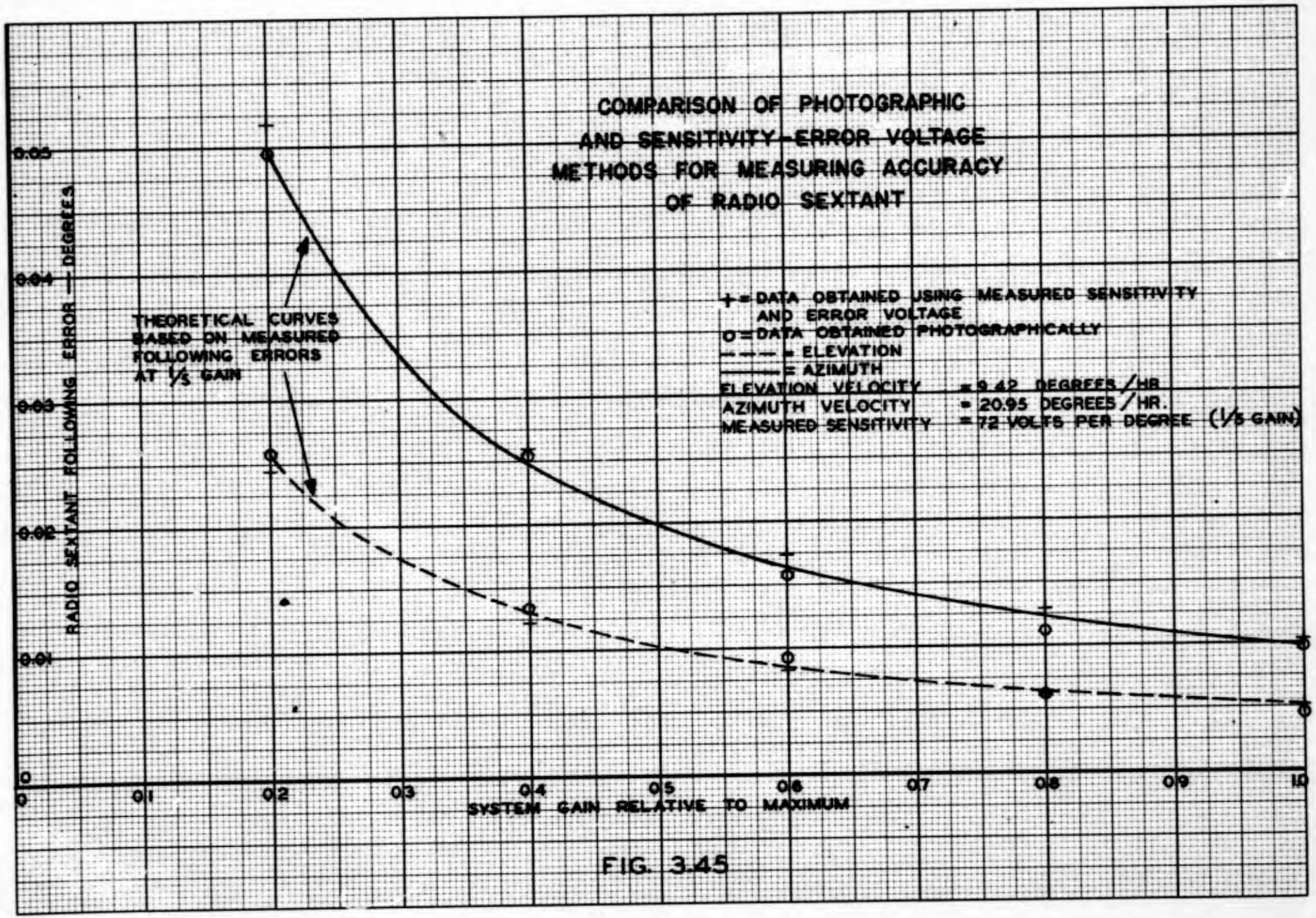
COMPARISON OF PHOTOGRAPHIC
AND SENSITIVITY-ERROR VOLTAGE
METHODS FOR MEASURING ACCURACY
OF RADIO SEXTANT
RADIO SEXTANT FOLLOWING ERROR — DEGREES
0.05
0.04
0.03
0.02
0.01
0
THEORETICAL CURVES BASED ON MEASURED FOLLOWING ERRORS AT 1/5 GAIN
+ = DATA OBTAINED USING MEASURED SENSITIVITY AND ERROR VOLTAGE
O = DATA OBTAINED PHOTOGRAPHICALLY
– – – = ELEVATION
——— = AZIMUTH
ELEVATION VELOCITY = 9.42 DEGREES / HR
AZIMUTH VELOCITY = 20.95 DEGREES / HR.
MEASURED SENSITIVITY = 72 VOLTS PER DEGREE (1/5 GAIN)
0
0.1
0.2
0.3
0.4
0.5
0.6
0.7
0.8
0.9
1.0
SYSTEM GAIN RELATIVE TO MAXIMUM

FIG. 3.45

error voltages are plotted. The theoretical curves were based on the photographically measured errors at 1/5 gain plus an inverse relationship between system gain and angular following error. The close agreement between the theoretical curves and the photographically measured errors further indicates that the photographic data, when reduced in the manner previously described, is accurate to better than 0.001 degrees. Furthermore, the excellent agreement between the errors calculated by the sensitivity-error voltage method and the photographically measured errors is further proof that accurate performance data may be obtained by measuring the sextant's sensitivity by the "sun velocity" method and applying this sensitivity to the following error voltages to determine the angular tracking errors.

The sun velocities at the time the data for Figure 3.45 were taken were relatively high when compared to the average velocities over a period of a day; yet increasing the gain from 0.5 to 1 decreased the angular following errors in elevation and azimuth only 0.005 and 0.01 degrees respectively. This fact illustrates that adding still more gain to the system could result in little reduction in the absolute average following errors. For maximum gain, the measured angular errors were about 0.005 degrees in elevation and 0.01 in azimuth. However, the effect of a fluctuating error signal is yet to be considered.

c. Fluctuations in Angular Tracking Errors

Since the d.c. error voltages for operating the servo system have noise components superimposed upon them, it is necessary to determine their effect upon the angular tracking errors before any absolute accuracies may be reported. Figures 3.46 and 3.47 are typical of the fluctuations encountered with maximum gain and a system time constant of approximately 4 sec. As seen from these figures, an increase in error voltage causes the angular tracking error to decrease. This is due to the fact that the larger voltage makes the motor run faster than needed to track the sun. The angular error will continue to decrease until the error voltage returns to the value necessary to track the sun, hence the peaks in the angular tracking error occur when the error voltage passes through the correct value for tracking.

For Figures 3.46 and 3.47 the average angular tracking error in azimuth was 0.0072 deg. with a maximum excursion of 0.0055 deg.; in elevation it was 0.0043 deg. with a maximum excursion of 0.0050 deg. These fluctuations are the maximum measured to date.

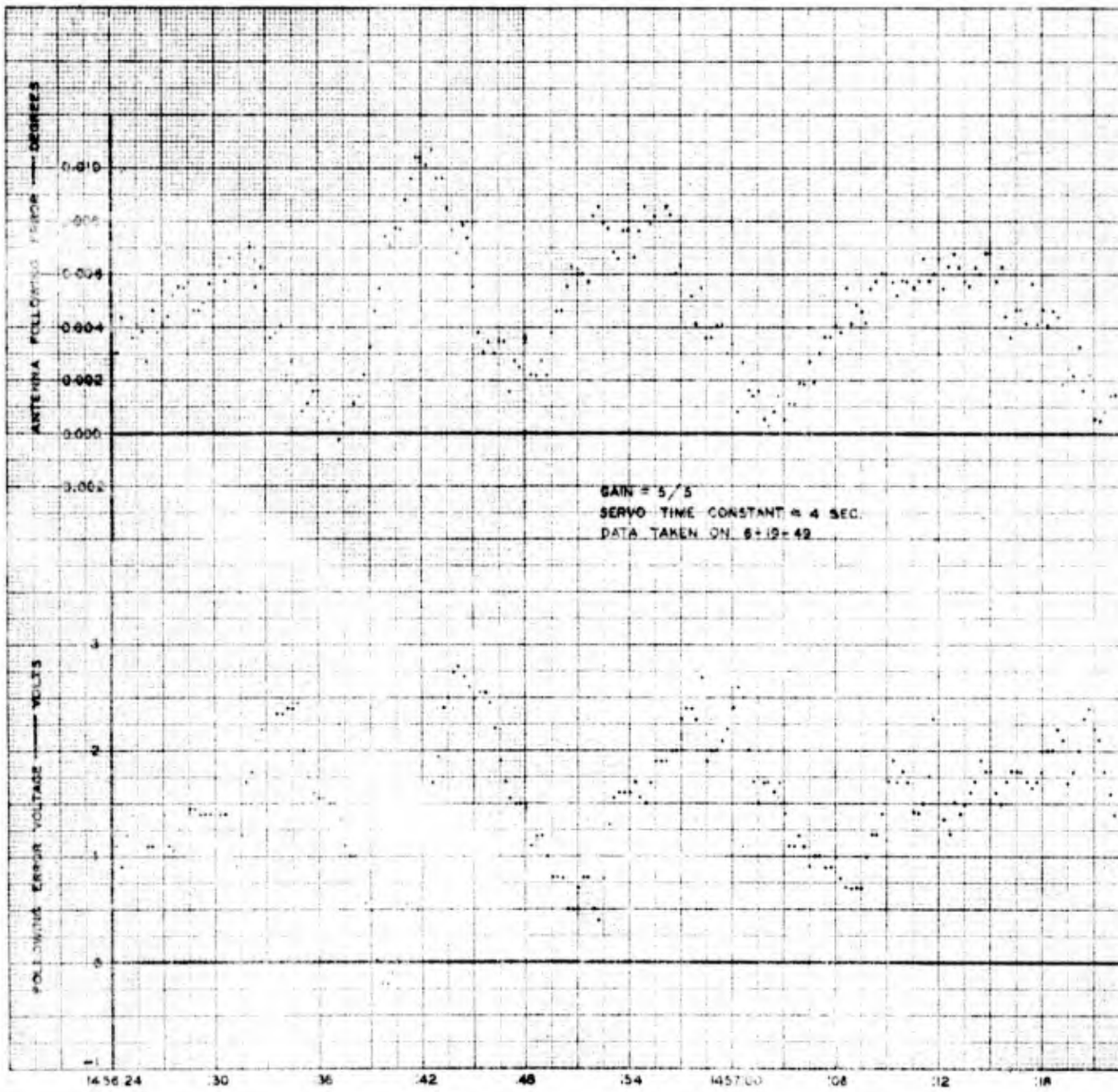
ANTENNA FOLLOWING ERROR — DEGREES
0.010
0.004
0.002
0.000
FOLLOWING ERROR VOLTAGE — VOLTS
3
2
1
0
-1
GAIN = 5/5
SERVO TIME CONSTANT = 4 SEC.
DATA TAKEN ON 6-19-62
14 56.24
.30
.36
.42
.48
.54
14 57.00
.06
.12
.18

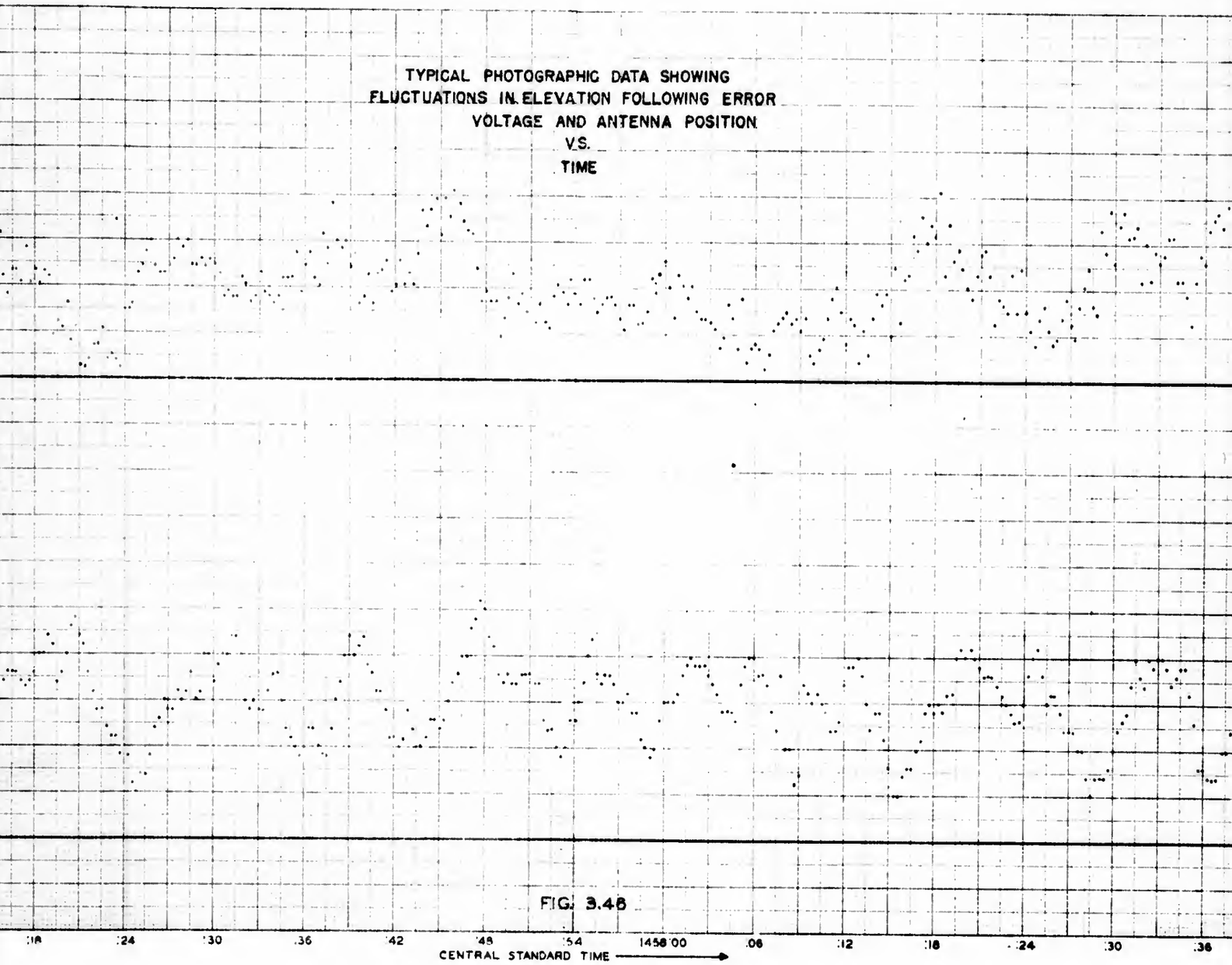
TYPICAL PHOTOGRAPHIC DATA SHOWING
FLUCTUATIONS IN ELEVATION FOLLOWING ERROR
VOLTAGE AND ANTENNA POSITION
V.S.
TIME
:18
:24
:30
:36
:42
:48
:54
1458:00
:06
:12
:18
:24
:30
:36
CENTRAL STANDARD TIME

FIG. 3.48

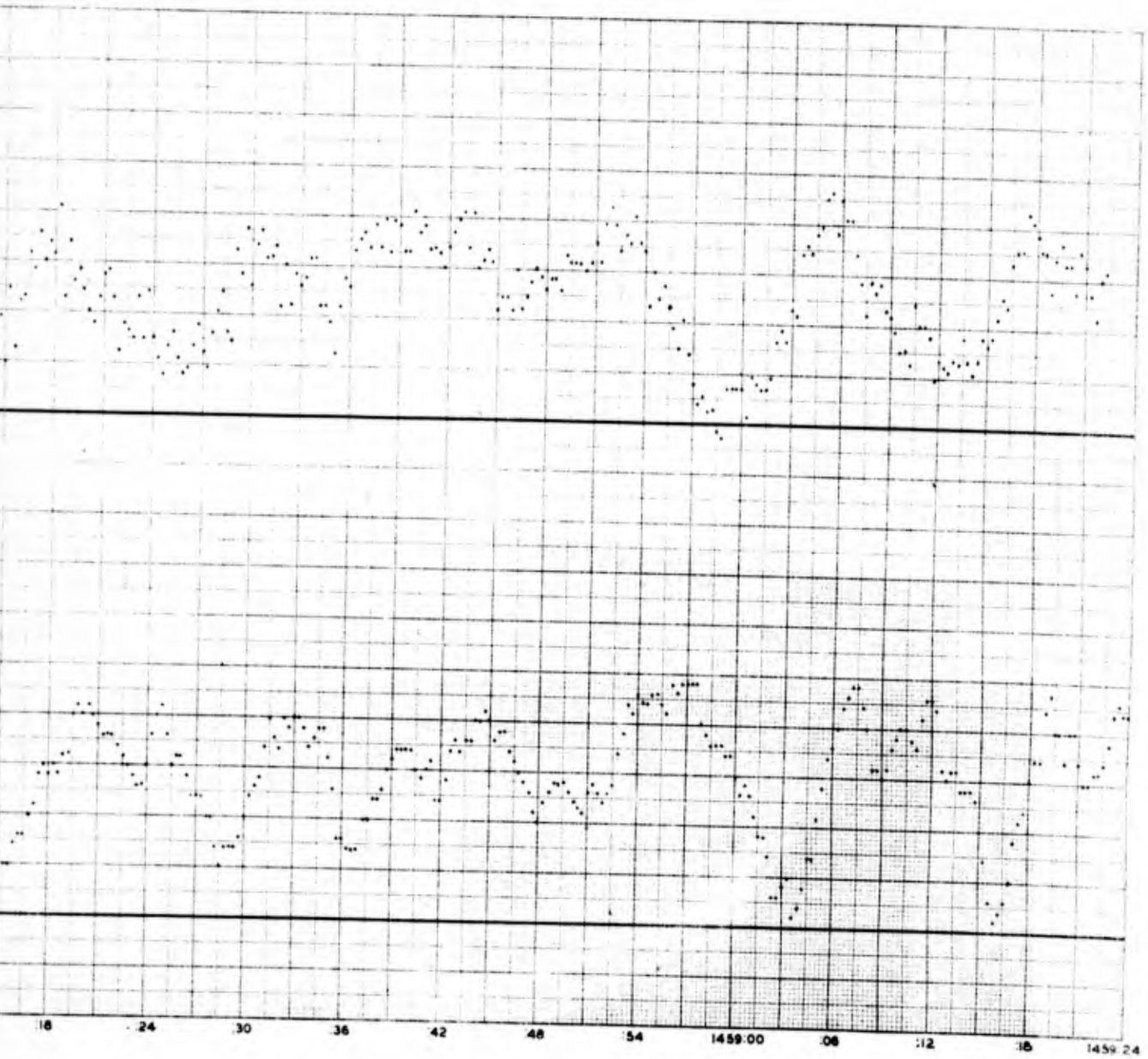
18
24
30
36
42
48
54
1459:00
06
12
18
1459:24

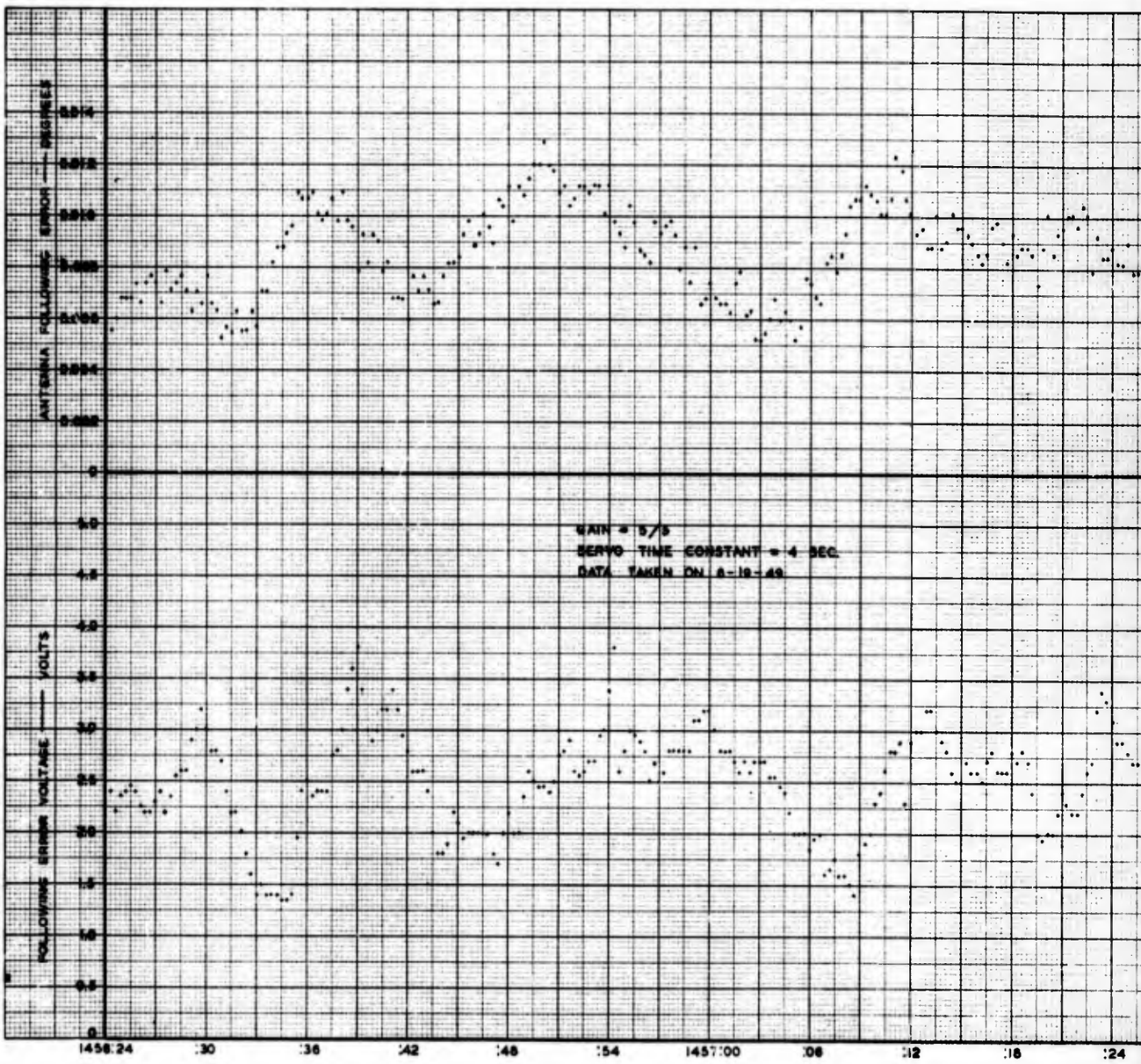
ANTENNA FOLLOWING ERROR — DEGREES
FOLLOWING ERROR VOLTAGE — VOLTS
GAIN = 5/5
SERVO TIME CONSTANT = 4 SEC.
DATA TAKEN ON 8-19-49
1456:24
:30
:36
:42
:48
:54
1457:00
:06
:12
:18
:24

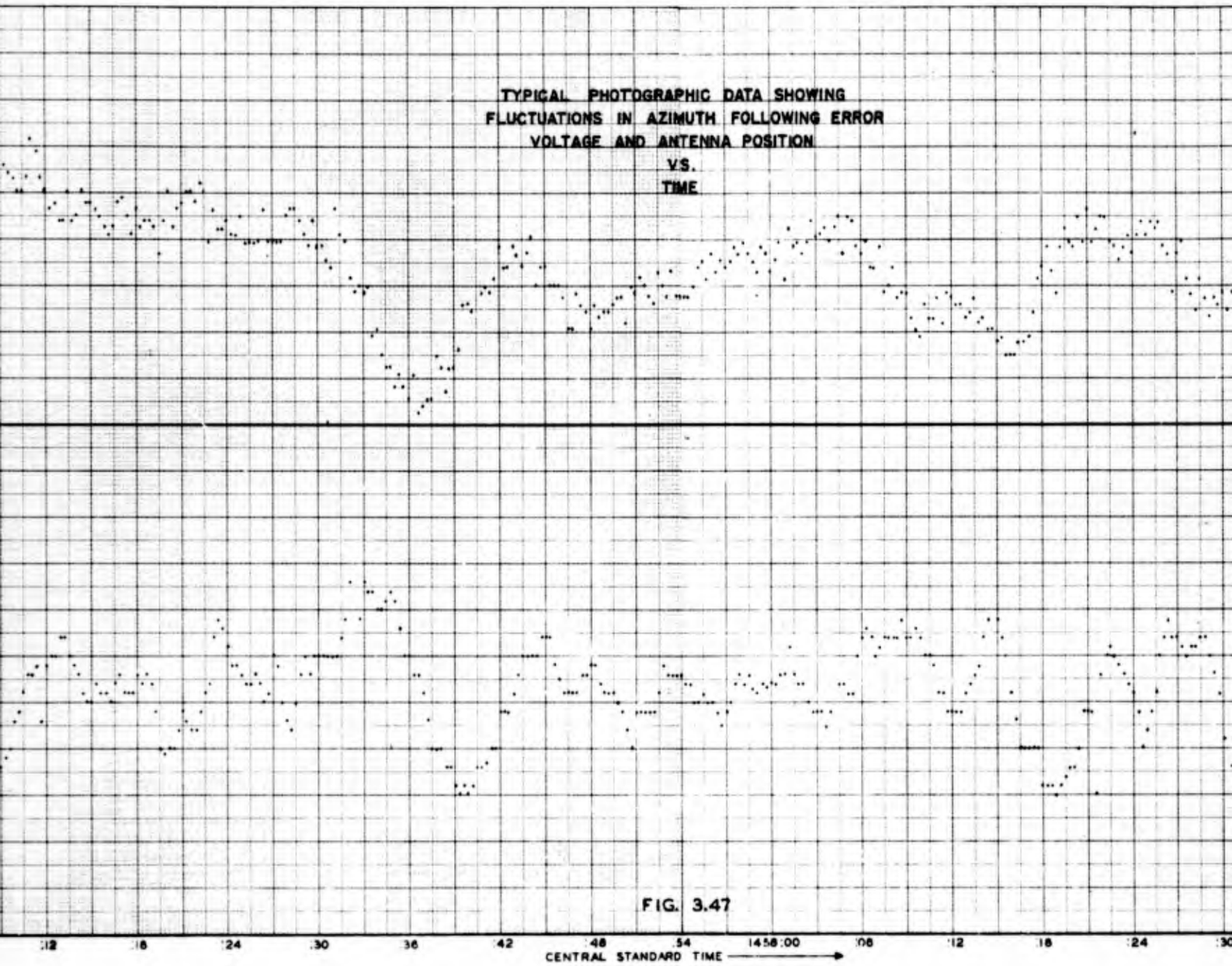
TYPICAL PHOTOGRAPHIC DATA SHOWING
FLUCTUATIONS IN AZIMUTH FOLLOWING ERROR
VOLTAGE AND ANTENNA POSITION
V.S.
TIME
:12
:18
:24
:30
:36
:42
:48
:54
1458:00
:06
:12
:18
:24
:30
CENTRAL STANDARD TIME

FIG. 3.47

2

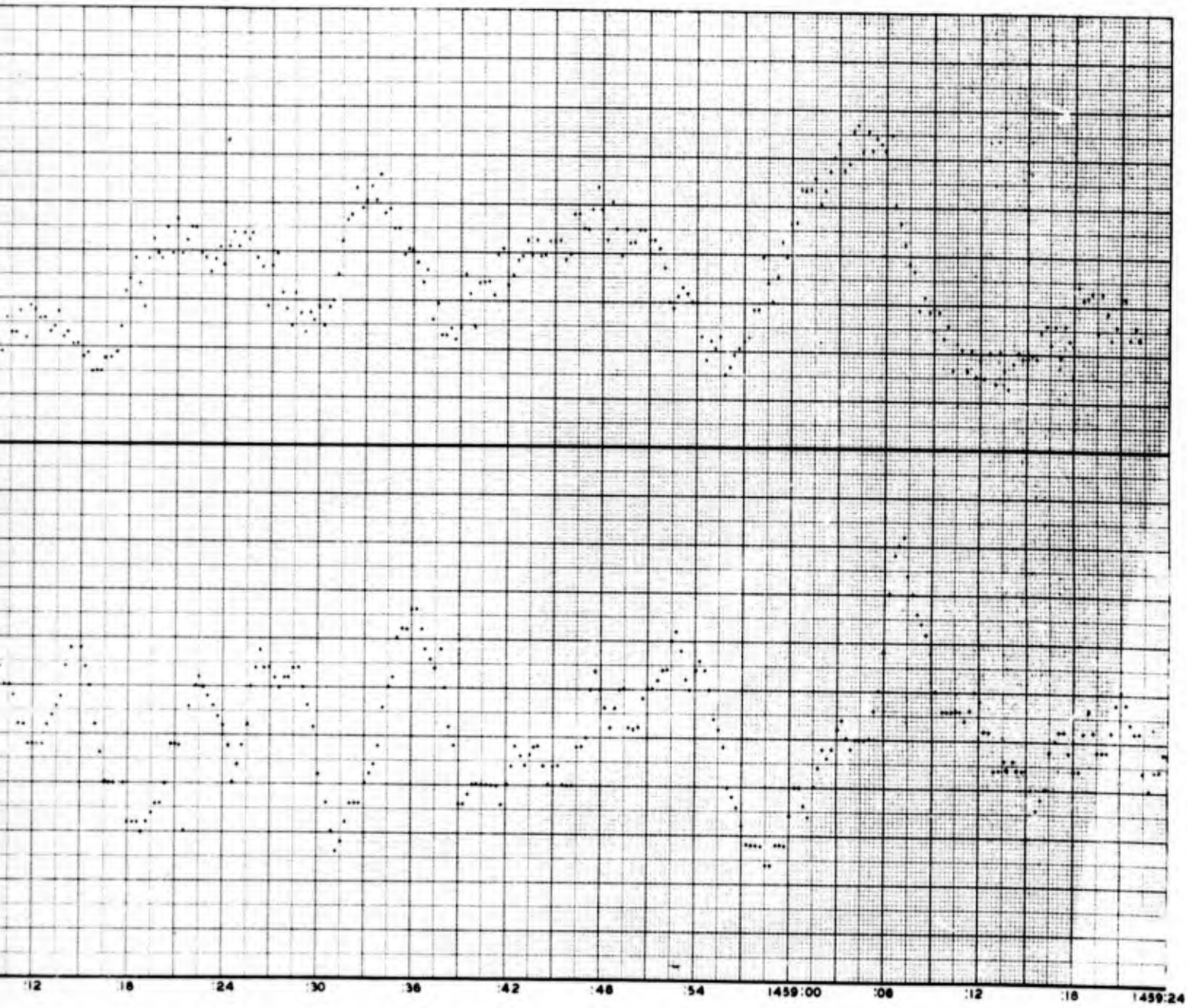
:12
:18
:24
:30
:36
:42
:48
:54
1459:00
:06
:12
:18
1459:24

Figure 3.48 shows the fluctuations in angular tracking errors and error voltages for azimuth and elevation when the system gain was 1/5 of maximum and the system time constant was again approximately 4 sec. The maximum excursion in the elevation and azimuth angular errors was about 0.0025 deg. This is a reduction of about a factor of two from the maximum excursion measured for maximum gain. The fact that increasing the gain by a factor of five increases the angular fluctuations by only a factor of two indicates that the higher gain allows the servo to obtain, rapidly, legitimate signals which counteract any fluctuations, thus resulting in relatively small angular excursions.

The measurements described in this section, together with those discussed previously, are sufficient to indicate that the greatest absolute accuracies are obtained with maximum gain for this system.

d. Predicted Performance

Figures 3.49 and 3.50 show the azimuth and elevation mount velocities as a function of signal volts on the grids of the amplidyne field control tubes. The maximum grid voltage applied in obtaining the data was 15 volts in accordance with the limit of the phase detectors. The average slope of the hysteresis loop about the origin for the elevation axis is 7.6 deg. per hour per volt, and for the azimuth axis it is 8.46 deg. per hr. per volt. The voltages necessary to overcome the static inertia and friction in the system as well as the saturation in the motor-amplidyne combinations are readily obtained from the curves. The addition of this data to the data previously presented permits the prediction of the performance of the sextant under various conditions.

The tracking errors, disregarding fluctuations, will be inversely proportional to the sensitivity. They will also vary directly with the sun's velocity divided by the slope of the velocity vs. 616 grid voltage curve plus the voltage necessary to overcome the static inertia, friction and saturation. Therefore, the predicted maximum angular errors can be expressed as:

$$\epsilon_A = \frac{1}{S}\left[\frac{\omega_A}{8.46} + E_1\right] + \Delta\epsilon_A$$

$$\epsilon_h = \frac{1}{S}\left[\frac{\omega_h}{7.6} + E_2\right] + \Delta\epsilon_h$$

where S = system sensitivity

ϵ_A = azimuth angular tracking error

$\Delta\epsilon_A$ = fluctuating azimuth angular error

ϵ_h = elevation angular tracking error

$\Delta\epsilon_h$ = fluctuating elevation angular error

ω_A = sun's azimuth velocity

ω_h = sun's elevation velocity

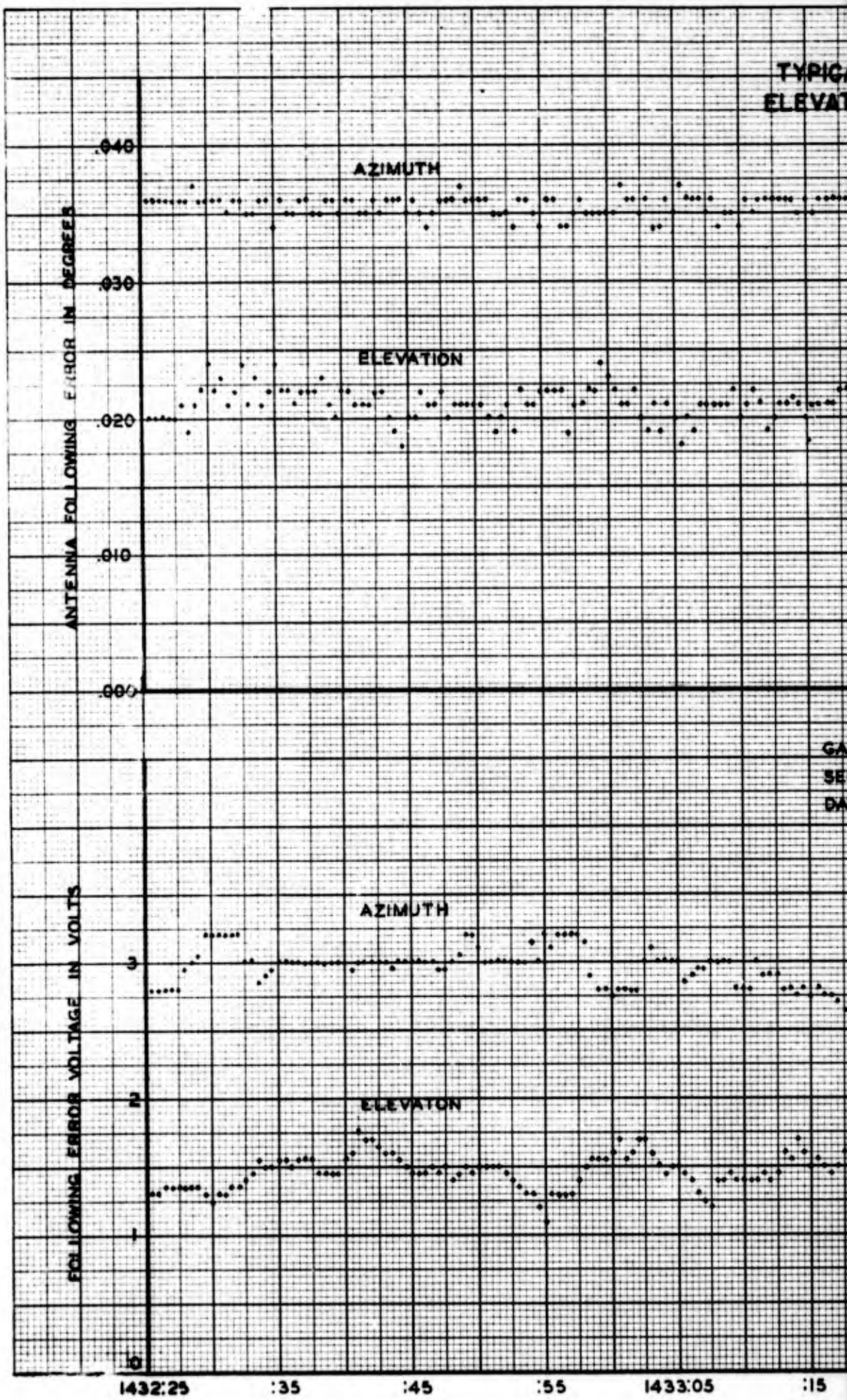
TYPIC
ELEVAT
.040
.030
.020
.010
.000
AZIMUTH
ELEVATION
ANTENNA FOLLOWING ERROR IN DEGREES
GA
SE
DA
3
2
1
0
AZIMUTH
ELEVATION
FOLLOWING ERROR VOLTAGE IN VOLTS
1432:25
:35
:45
:55
1433:05
:15

TYPICAL PHOTOGRAPHIC DATA SHOWING FLUCTUATIONS IN AZIMUTH AND ELEVATION FOLLOWING ERROR VOLTAGE AND ANTENNA POSITION VS. TIME

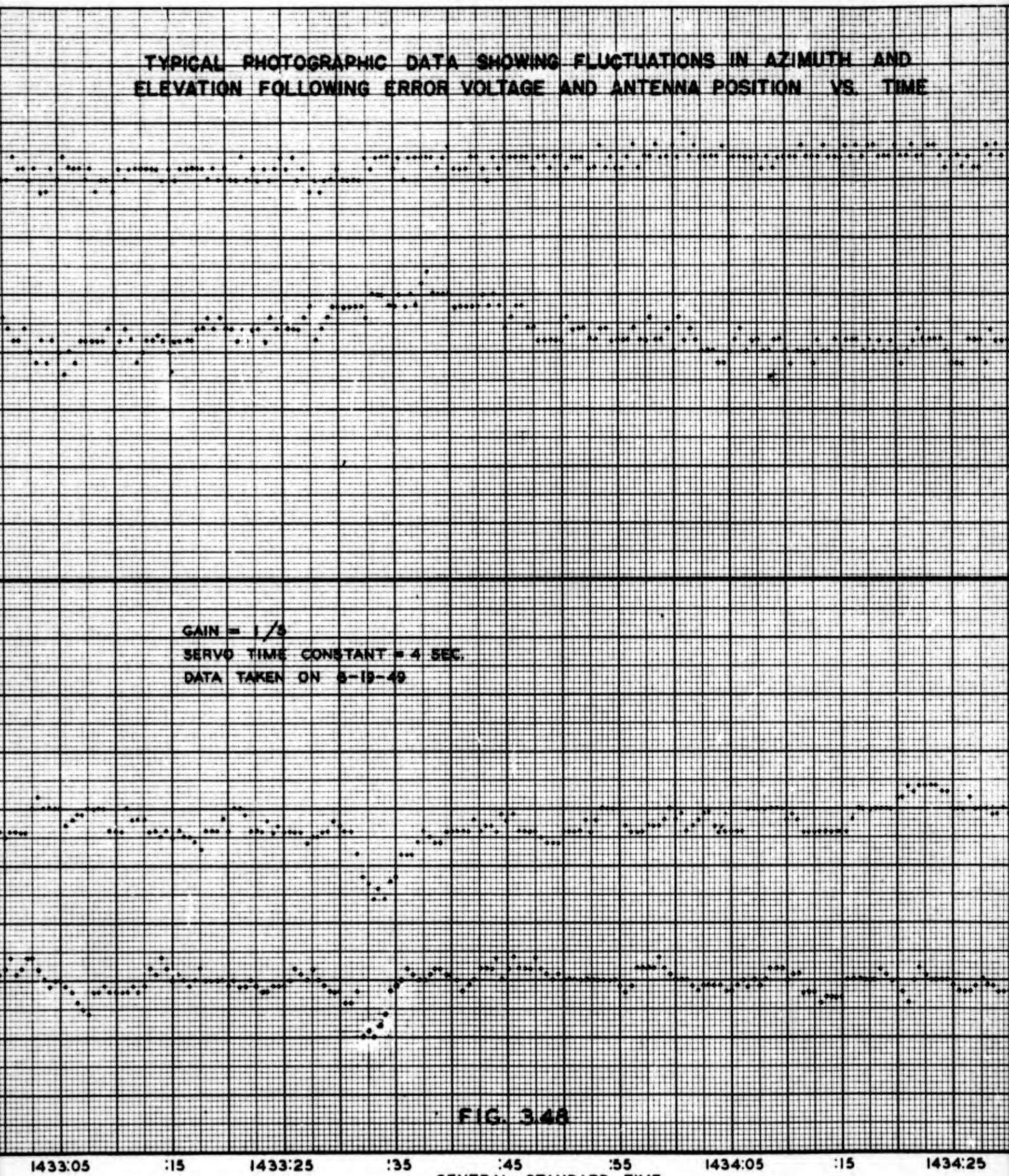

FIG. 3.48

2

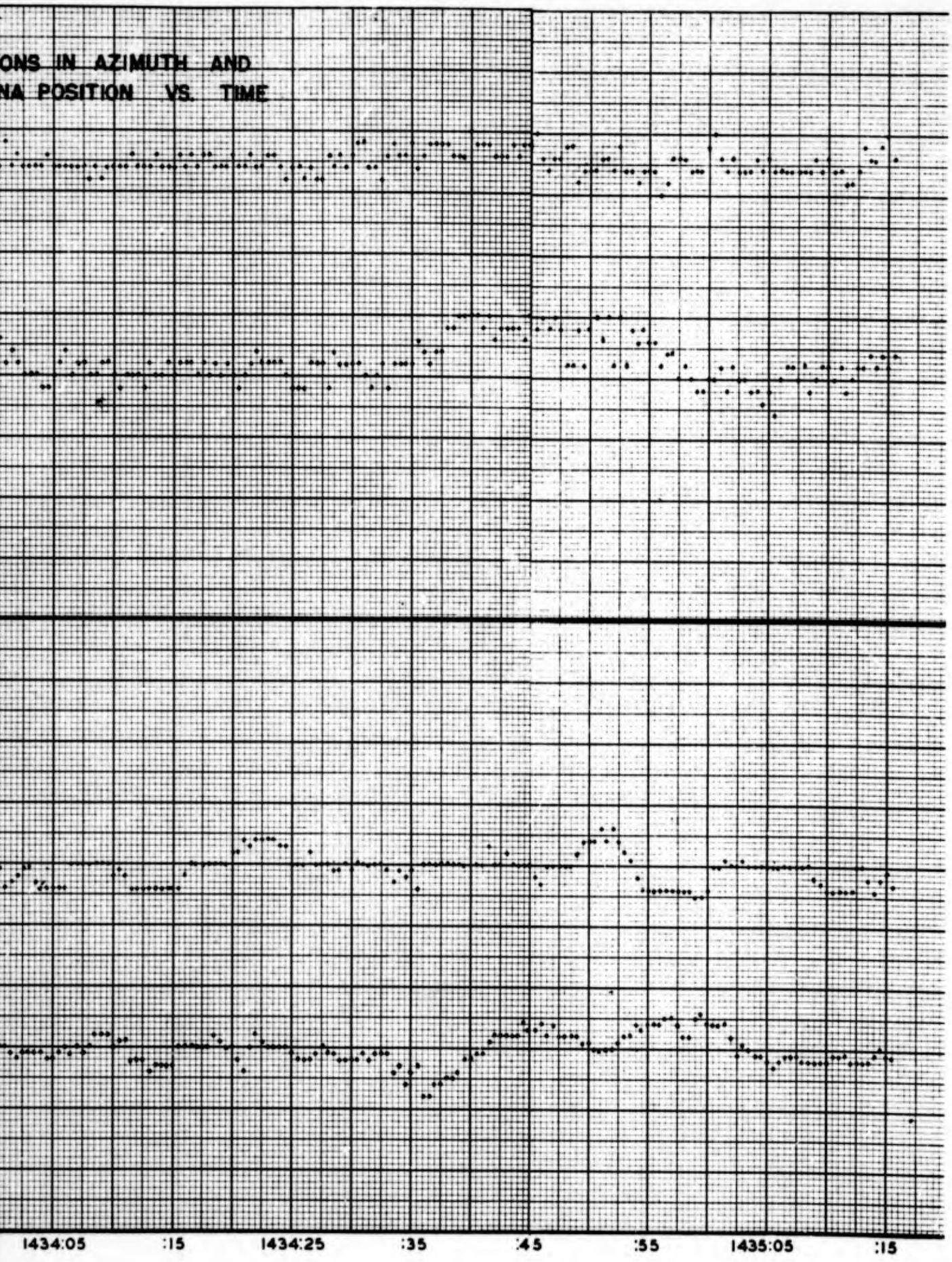
ONS IN AZIMUTH AND
NA POSITION VS. TIME
1434:05
:15
1434:25
:35
:45
:55
1435:05
:15

3

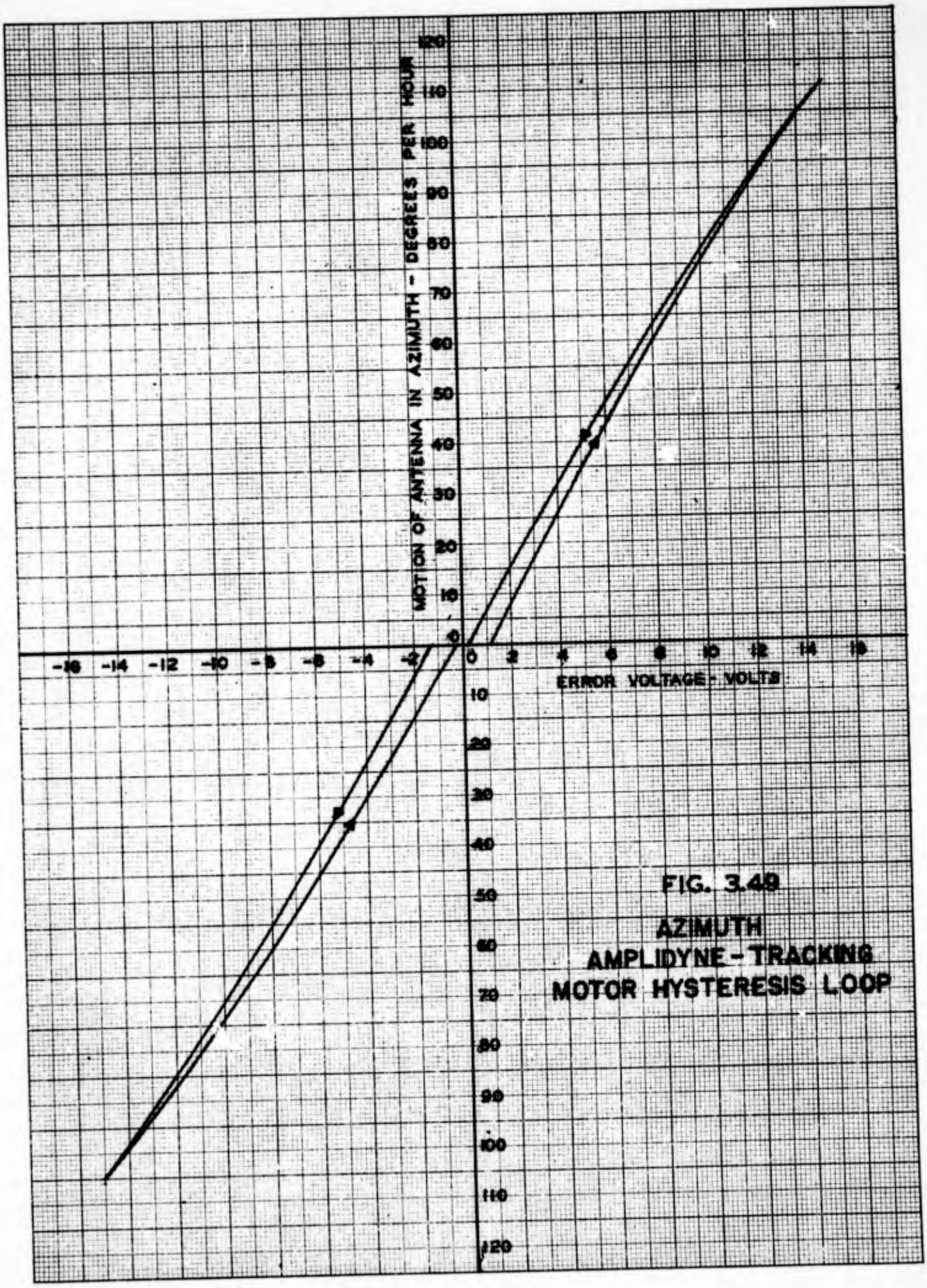

FIG. 3.48
AZIMUTH
AMPLIDYNE - TRACKING
MOTOR HYSTERESIS LOOP

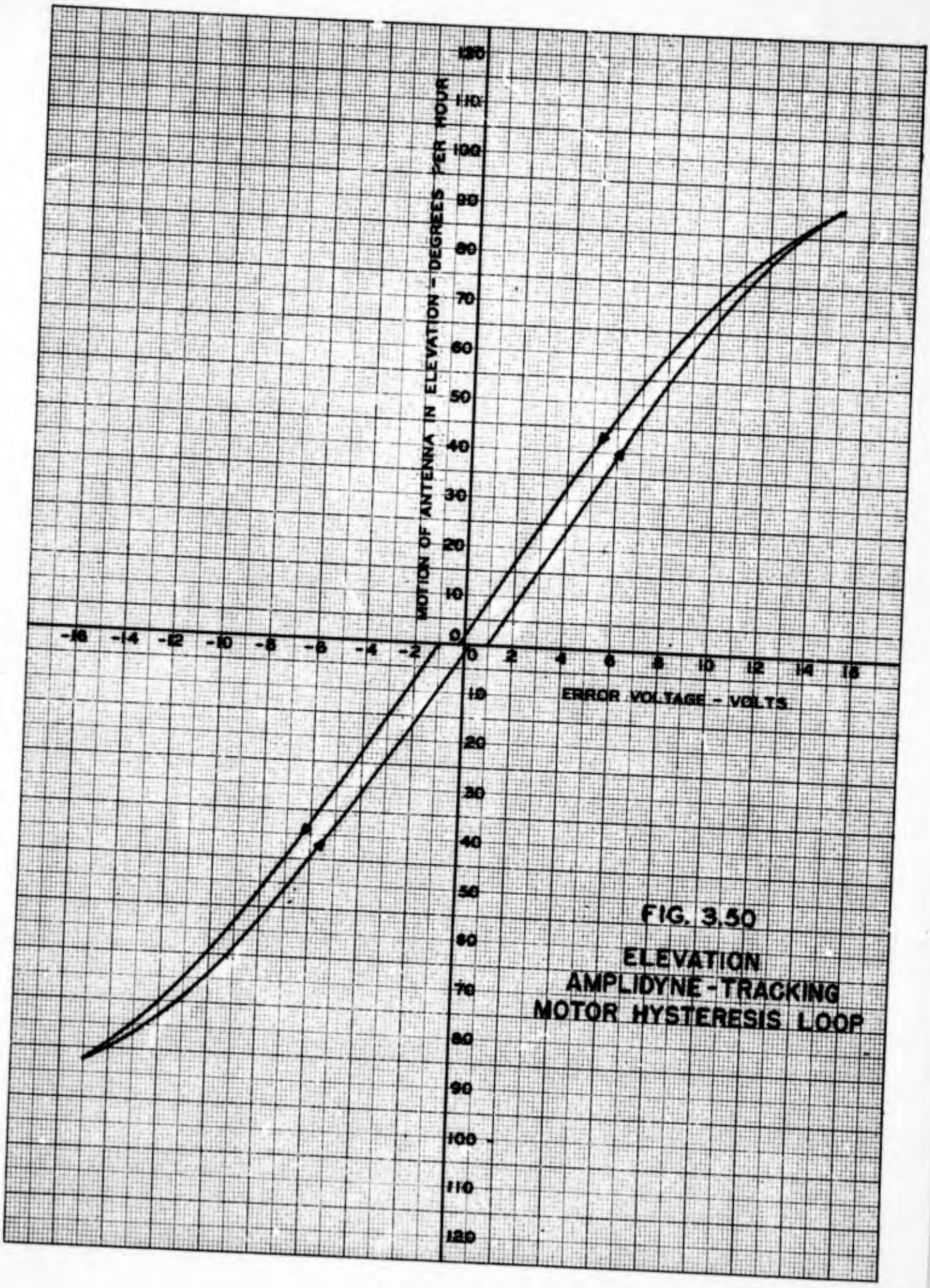

FIG. 3.50

ELEVATION AMPLIDYNE-TRACKING MOTOR HYSTERESIS LOOP

E_1 and E_2 are the voltages necessary to start the azimuth and elevation motors.

Limits on the various constants appearing in the equations above can now be expressed, thereby predicting the maximum and minimum tracking errors. The sextant's sensitivity will be considered for elevation angles above 5 deg., in accordance with the navigational practice of taking sights only on astronomical bodies which are above 5 degrees in elevation. Although rain was found to be absorbing at 1.8 cm., no conclusive data was obtained at 5° elevation to indicate that rain would cause the sensitivity to drop below 235 volts per deg. (the minimum measured for 5° elevation) for maximum system gain. The minimum sensitivity will therefore be taken as 235 volts per deg. and from Fig. 3.43 the maximum sensitivity is 500 volts per degree, again for maximum system gain.

For maximum gain, the maximum fluctuating error in azimuth, $\Delta\epsilon_A$, encountered during photographic tests was 0.0055°; and for elevation, the maximum value of $\Delta\epsilon_h$ was 0.005°. From Figures 3.49 and 3.50, the maximum and minimum values for E_1 were 1.2 and 0.3 respectively, and for E_2, 1.0 and -0.2. Thus:

$$\epsilon_{A\ max} = \frac{1}{235}\left[\frac{\omega_A}{8.46} + 1.2\right] + 0.0055$$

$$\epsilon_{A\ min} = \frac{1}{500}\left[\frac{\omega_A}{8.46} + 0.3\right] + .0055$$

$$\epsilon_{h\ max} = \frac{1}{235}\left[\frac{\omega_h}{7.6} + 1.0\right] + .005$$

$$\epsilon_{h\ min} = \frac{1}{500}\left[\frac{\omega_h}{7.6} - .2\right] + .005$$

These four equations were used to plot Figures 3.51 and 3.52 which show the maximum and minimum predicted tracking errors in elevation and azimuth. Fig. 3.45 was plotted for the average tracking error while Figures 3.51 and 3.52 have the fluctuating error, due to the noisy signal, taken into account. The maximum antenna excursions, mentioned before, were caused by voltage fluctuations of about 1.5 volts from the average. These fluctuations may be reduced to about 0.5 volts maximum by the insertion of 12 sec. time constant instead of 4 sec. into the output. This results, however, in the system being underdamped as indicated by Fig. 3.53. Nevertheless, the system remains stable with 12 sec. time constant for all velocities encountered at the latitude of Cedar Rapids. Hence, although no photographic

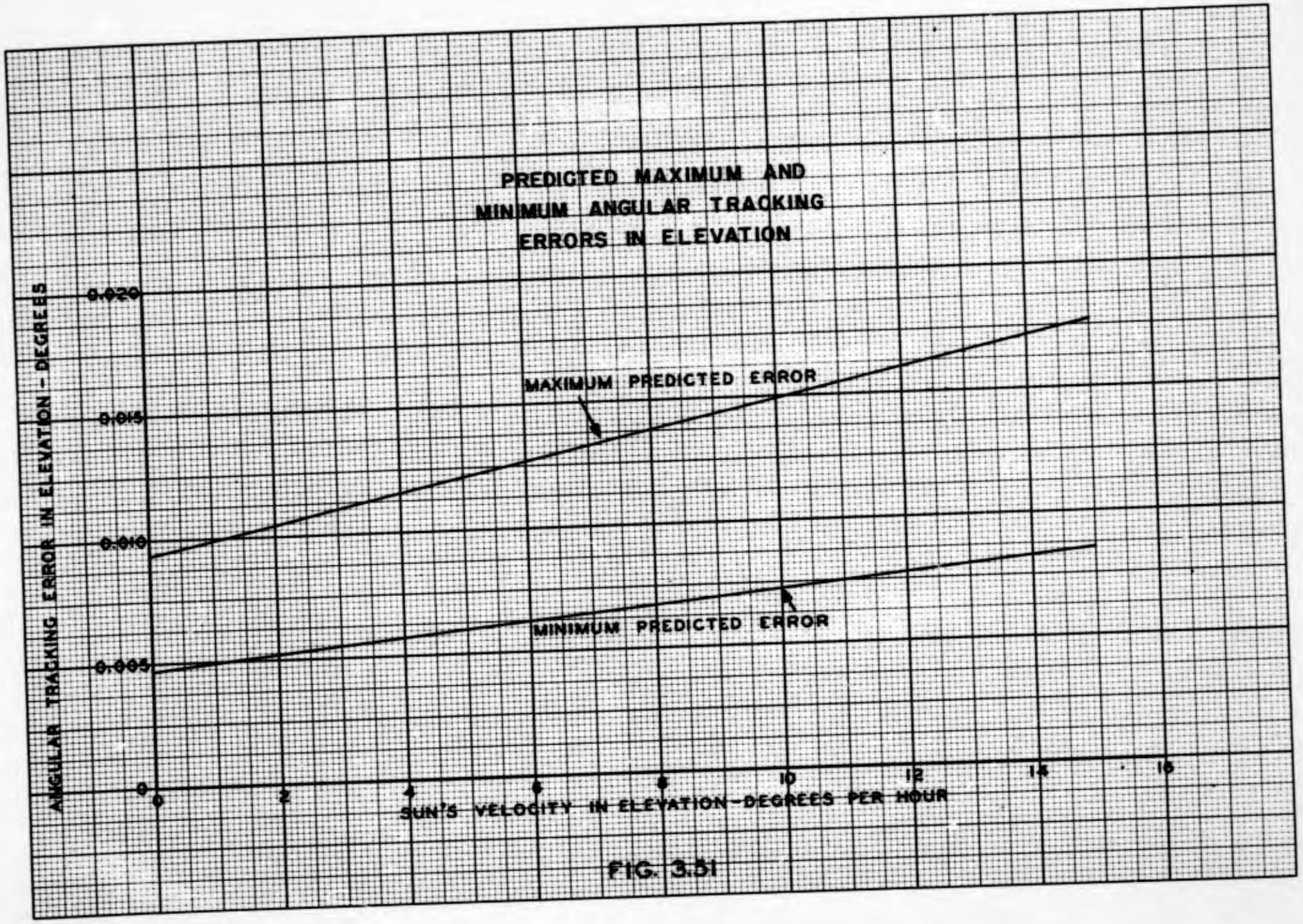
PREDICTED MAXIMUM AND
MINIMUM ANGULAR TRACKING
ERRORS IN ELEVATION
MAXIMUM PREDICTED ERROR
MINIMUM PREDICTED ERROR
ANGULAR TRACKING ERROR IN ELEVATION - DEGREES
0.020
0.015
0.010
0.005
0
0
2
4
6
8
10
12
14
16
SUN'S VELOCITY IN ELEVATION - DEGREES PER HOUR

FIG. 3.51

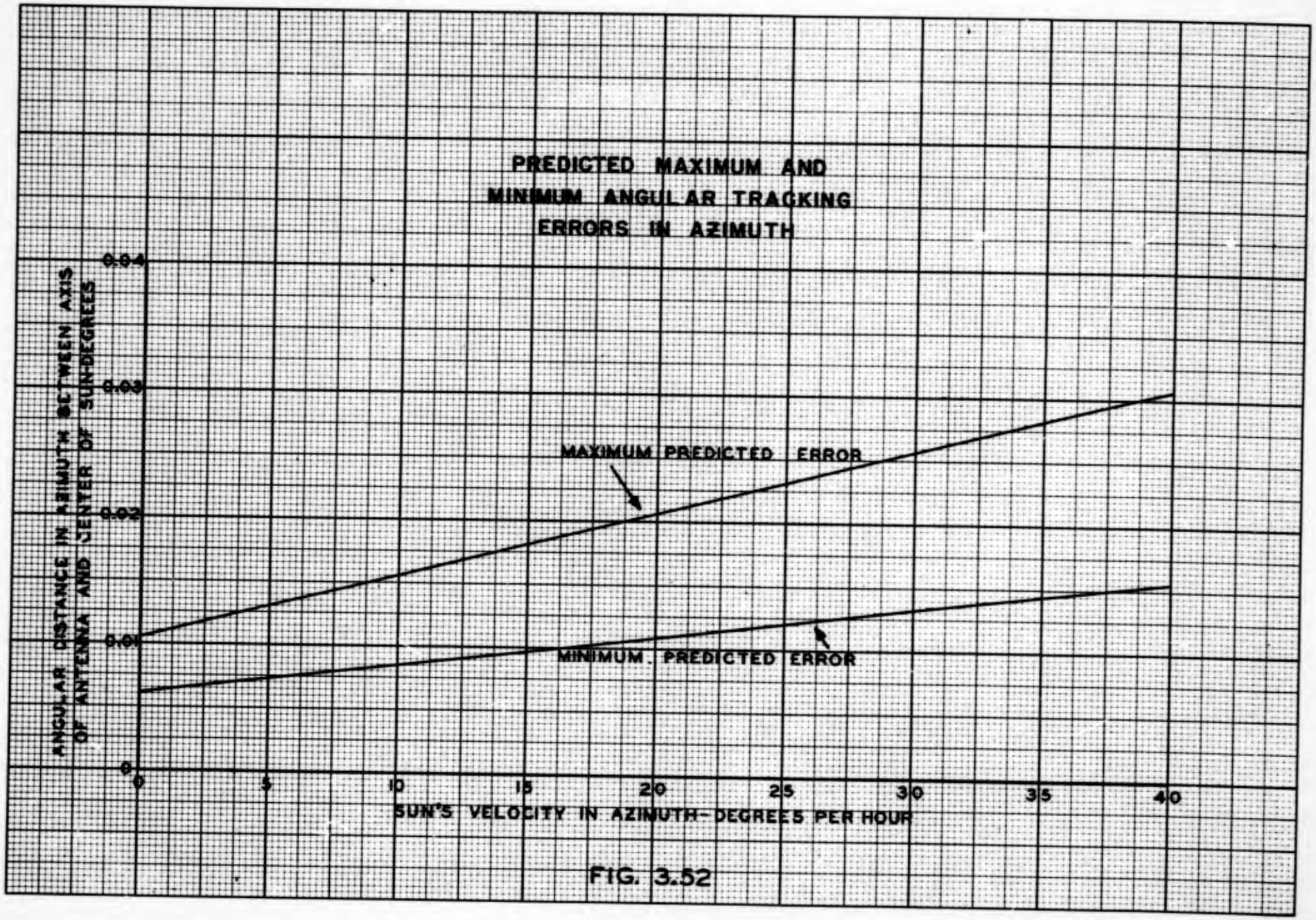
PREDICTED MAXIMUM AND
MINIMUM ANGULAR TRACKING
ERRORS IN AZIMUTH
ANGULAR DISTANCE IN AZIMUTH BETWEEN AXIS OF ANTENNA AND CENTER OF SUN-DEGREES
0.04
0.03
0.02
0.01
0
MAXIMUM PREDICTED ERROR
MINIMUM PREDICTED ERROR
0
5
10
15
20
25
30
35
40
SUN'S VELOCITY IN AZIMUTH-DEGREES PER HOUR

FIG. 3.52

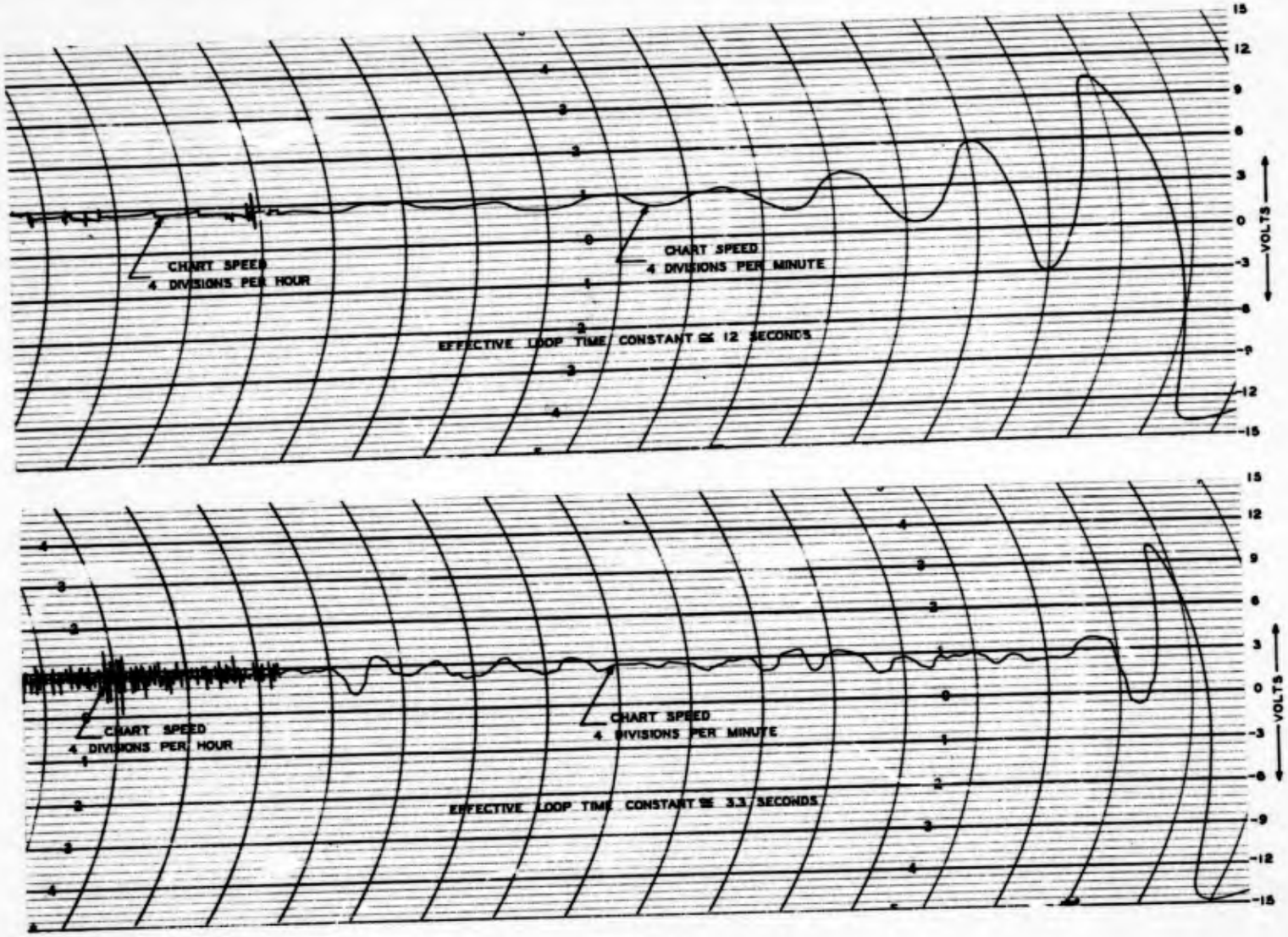

FIG. 3.53

CHARACTERISTICS OF ELEVATION CHANNEL PULLING IN ON SUN FOR TWO EFFECTIVE LOOP TIME CONSTANTS AND MAXIMUM LOOP GAIN

measurements have been made, it is felt that the fluctuating angular tracking errors may be reduced to a maximum of about 0.002 degrees. Also, in all probability the position indicators would be read at some time other than when the antenna was at the peak of its maximum excursion. The predicted errors in Figures 3.51 and 3.52 are accordingly felt to be excessive.

It is to be noted that Figures 3.51 and 3.52 are plotted for the angular distance between the axis of the antenna and the center of the sun. This is the same as the indicator error in elevation, but in azimuth, the error in the indicators will be the plotted value divided by the cosine of the sun's elevation angle at the time of interest. Since only elevation angles are of interest in celestial navigation, this situation is not elaborated upon nor is it considered important.

3.2.4.8 Conclusions and Suggestions

It is believed that the results of the measurements described in this report show conclusively that a radio sextant operating at a wavelength of 1.8 cm can be constructed which will measure the elevation angle of the sun as accurately as the navigator's sextant. Furthermore, it is believed that the radio sextant would exceed the navigator's sextant in value during daytime navigation, for it gives a continuous, automatic, and accurate presentation of the sun's elevation angle in all types of weather for elevation angles above 5°.

Refraction measurements are expected to show that valuable data may be obtained below 5° elevation, thereby increasing the radio sextant's value to navigation in the polar regions.

There are, however, two major limitations connected with this device. The radio sextant must be mounted on a stable platform for operational use, and the antenna dimensions required may be excessive for certain types of vessels or aircraft.

The antenna dimensions are governed by the required signal level to furnish reliable and accurate results. Smaller antennas could be used if shorter wavelengths were permitted, but the effect of rain on the propagation of power at wavelengths less than 1 cm is excessive. A comparison of performance, based on antenna dimensions, has been made for 1.8 cm wavelength. Figure 3.54 is a comparison of the modulation temperatures (proportional to error voltage) versus angular errors that would be measured with various parabolic reflector apertures. It is apparent that a 36" aperture would reduce the sensitivity by a factor of more than 2, and the accuracy would be decreased by the same factor. The fluctuating error, however, would be as large as before, and if

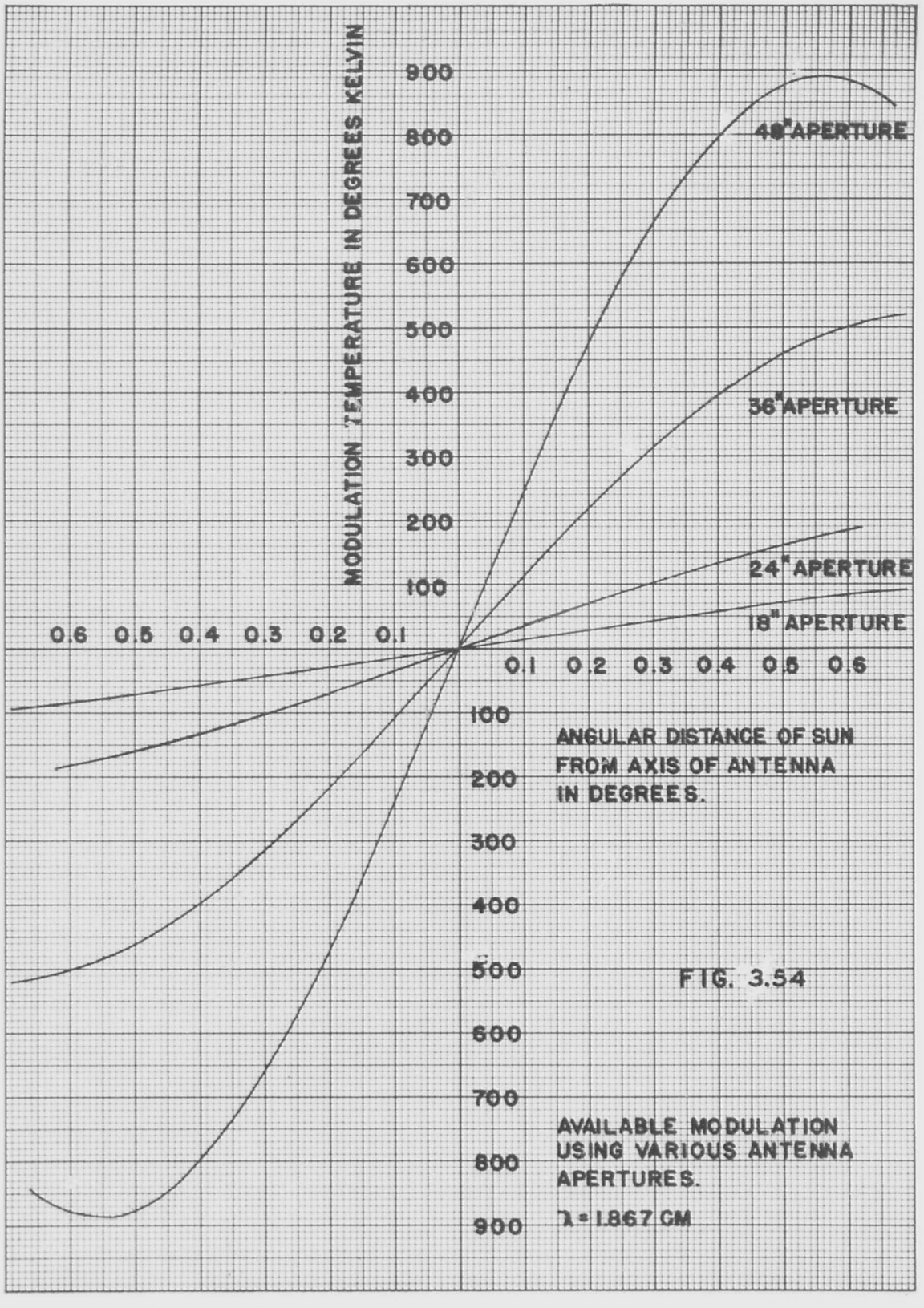

FIG. 3.54

AVAILABLE MODULATION USING VARIOUS ANTENNA APERTURES.

$\lambda = 1.867$ CM

the receiver gain were increased to compensate for the decreased antenna gain, the fluctuating error would also increase.

If the required accuracy of the sextant can be reduced from that shown in Figures 3.51 and 3.52, then the antenna aperture may be reduced accordingly, but if accuracy comparable to that of the navigator's sextant is required, a 48" diameter is the minimum diameter that can be used.

4. RESULTS AND CONCLUSIONS

4.1 Discussion of Applications and Astronomical Observations

4.1.1 Stars

Although they have very high black body temperatures, the stars subtend such minute solid angles that they cannot be detected in the microwave wavelength region. Recourse to equation 2.15 of the text demonstrates quickly that the useful component of the received power is directly proportional to the solid angle subtended by the source, for small solid angles.

There is a further complication in that the antenna looks at thousands of stars, rather than one. The present day antenna beam widths of from 0.1 to 1 degree enclose so many stars that even if detectable energy were received, the data may not be of any value.

4.1.2 Sun

The application of radiometry to the sun is discussed in detail in the section on the automatic radio sextant, Section 3.2.4. It was shown in this section that under the most unfavorable conditions encountered, the experimental model of the radio sextant tracked the sun with an error of only 0.018°. Under favorable conditions, the elevation errors ranged from 0 to 0.008 degrees.

4.1.3 Moon

The moon has been tracked with the radio sextant, with tracking errors from 0.2 to 0.4 of a degree. This is, of course, not sufficient for navigational purposes. In order for moon position data to be of any navigational value, the receiver would have to be improved or the antenna gain increased by at least a factor of four. Since compactness is desirable in this type of equipment, a moon tracker would be required to operate in the millimeter wavelength region. Because of the strong absorption

of mm. waves in rain, the possibilities of using the moon as a navigational aid in foul weather are somewhat limited.

4.1.4 Landmarks

Certain features of landmarks, such as skyscrapers and mountains, make them possible sources for warning devices operating on the radiometry principle. It is felt that a practical mountain detector could be constructed using a receiver similar to the K-band radiometer.

4.1.5 Vessels at Sea

To a radiometer there is no great contrast between a vessel and the sea. If the instrument is located at sea level, great difficulty would be encountered in distinguishing between radiation from the ship and the water. Also, at these very low elevation angles, atmospheric absorption would be considerable, reducing the contrast still more. An airborne radiometer might possibly be used to detect large vessels, in that metallic vessels would appear "cold" with respect to the water. However, it is doubtful that positive detection could be realized at very great ranges.

4.1.6 Aircraft Detection

Aircraft lend themselves to possible detection because they are surrounded by a medium at low temperature, giving them a contrast against their background. However, as will be shown, their own low black body temperature and small size greatly limit the range at which they may be detected. From the theory presented so far it is possible to predict theoretically the maximum range at which a given airborne target may be detected.

If any specific results are to be gained from an analysis of this problem, a specific target must be assumed. At the present time practically all aircraft are constructed with an outer metallic shell. The surface of aluminum or any fair conductor is so highly reflecting that the substance has a black body temperature of essentially zero. This is illustrated by the fact that the reflection coefficient for aluminum is about 0.9995. Therefore, it is evident that no appreciable thermal energy will be radiated from the metallic target itself.

However, the metallic targets are near perfect reflectors. This means that they will reflect any thermal radiation incident upon them. The principal source of this radiation is the earth itself. Radiation from the sun will contribute very little because of the small solid angle it subtends. A wavelength would have to be chosen where atmospheric absorption is small if the

target is to stand out against its background. Therefore, radiation from the atmosphere reflecting off the target need not be considered.

It will be assumed that the target is a perfectly reflecting isotropic reflector. Few target configurations approach isotropic reflection, but the assumption must be made in order to perform an analysis which is to be of any practical value. The fact that the earth subtends a solid angle of 2π steradians at the target makes the assumption more valid. For this case the amount an actual target will deviate from reflecting isotropically when illuminated from 2π steradians is not large enough to nullify the results of the analysis.

For the assumptions outlined, equation 2.25 may be applied to compute the energy received by an antenna from a reflecting target. Let aT for the earth be 300°K. To a good approximation, Ω_s will be 2π, $m_s = 0$ and $m_r = 1$. Hence equation 2.25 becomes:

$$P = \frac{k\,\Delta f\,300}{2}\,\frac{1}{4\pi}\int_{\Omega_r} G(\theta,\phi)\,d\Omega_r$$

which yields an equivalent antenna temperature of

$$T_r = 150\cdot\frac{1}{4\pi}\int_{\Omega_r} G(\theta,\phi)\,d\Omega_r$$

At the present state of the art, a change of at least 25° in antenna temperature from free space to the target is needed for positive detection. This value is somewhat larger than the three degrees quoted for the sensitivity of the K-band radiometer because the permissible time constants for an airborne target detector are less than the ten seconds used in the K-band radiometer. Using this temperature, the minimum value for the integral is found to be:

$$\frac{1}{4\pi}\int_{\Omega_r} G(\theta,\phi)\,d\Omega_r \Bigg|_{min} = 0.167$$

Some computations which will indicate the possibilities of radiometer detection of aircraft can now be made. The target may be reduced to an equivalent circular reflector. Then CER #149 may be used to solve equation 2.25 for various wavelengths, angular target diameters and antenna sizes. Figure 4.1 is a plot of the results of these computations. In the following table the maximum range at which a ten square yard target could be detected is listed for various wavelengths and parabolic reflector diameters.

FIG. 4.1

PREDICTED RADIOMETER PERFORMANCE AS A PASSIVE DETECTOR OF METALLIC AIRBORNE TARGETS

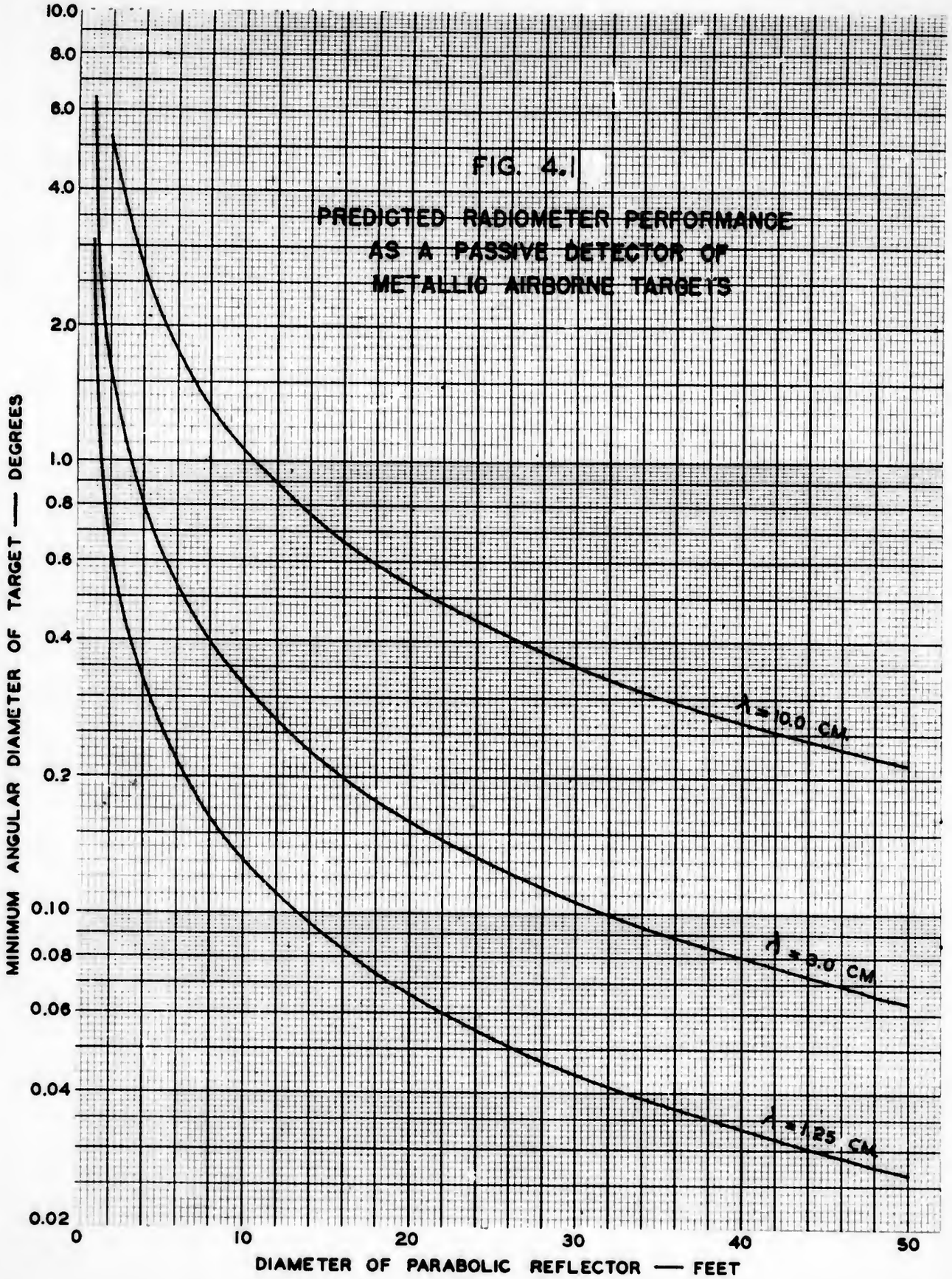

In reality, these values are optimistic because higher efficiencies were used in CER #149 than can usually be obtained in practice.

Wavelength (Centimeters)	Antenna Diameter (Feet)	Maximum Range (Yards)
1.25	2.5	390
1.25	10.	1560
1.25	50.	7800
3.	10.	648
3.	50.	3240
10.	10.	195
10.	50.	975

Inspection of Figure 4.1 and the preceding table reveals that a radiometer, in its present state of development, could not serve capably as a passive detector of aircraft. Its performance would probably be much poorer than that indicated because of atmospheric absorption, which would serve to reduce the target's contrast with its background. (Atmospheric absorption would be high for the low elevation angles involved; also, at these angles an increasing fraction of the antenna beam would intercept the ground, further reducing any contrast). For the present at least, it is evident that detection of metallic airborne targets by this method is impractical, if not impossible.

4.1.7 Determination of the Vertical.

A device which can locate the vertical by radiometry methods could be constructed. The fact that the "antenna temperature" as measured by the radiometer is a function of the angle between the vertical and the "line of sight" of the antenna is of value here. If the antenna is rotated so the antenna beam describes a cone, the "antenna temperature" will be constant throughout the rotation providing the axis of the cone is vertical. If the axis of rotation is tipped from the vertical, the "antenna temperature" will be modulated. The phase and amplitude of this modulation can be used to correct the error between the axis of rotation and the vertical.

It is estimated that the vertical can be located with an accuracy of $\pm$0.2 degrees neglecting the difficulties introduced by the sun and non-homogeneity of the earth's atmosphere. The effect of the latter may be quite serious.

4.2 Astronomical Aspects of Radiometry

4.2.1 Sun Studies

No systematic program of sun measurements was undertaken; however, measurements were made to determine the apparent black body temperature of the sun at a wavelength of 1.25 cm. It is very well known, of course, that this wavelength is very near the maximum of the first water absorption band; therefore, all sun measurements must be corrected for the absorption occurring in the earth's atmosphere. The effect of atmospheric absorption is shown in Figure 4.2. These measurements were made by following the sun with the K-band radiometer for approximately ten minutes and then setting the antenna back in hour angle so that it retraced the previous path of the sun. In this manner the radiometer first measured the radiation from the sun as attenuated by the atmosphere, plus the radiation from the atmosphere. The second measurement was simply the radiation from the atmosphere for the equivalent path of the previous sun measurement. As shown in Section 2.1.3, these two conditions can be stated mathematically as follows:

$$T_r = (1 - e^{-2a_o \sec\theta})\, T_m + e^{-2a_o \sec\theta} T_{sun}\, C \qquad 4.1$$

$$T_\theta = (1 - e^{-2a_o \sec\theta})\, T_m \qquad 4.2$$

where T_r is the antenna temperature when the antenna is pointing toward the sun and T_θ is the antenna temperature pointing away from the sun; a_o is the attenuation of a vertical path through the atmosphere in nepers; θ is the zenith angle of the sun; T_m is the absorption weighted temperature of the atmosphere; T_{sun} is the apparent black body temperature of the sun; and C is the antenna factor. The two expressions cited do not hold for very large zenith angles, since $\sec\theta$ is not proportional to the path length for values of θ that are in excess of 70°.

Subtracting equation 4.2 from equation 4.1,

$$T_r - T_\theta = e^{-2a_o \sec\theta} T_{sun}\, C$$

$$T_{sun} = \frac{T_r - T_\theta}{e^{-2a_o \sec\theta} C}$$

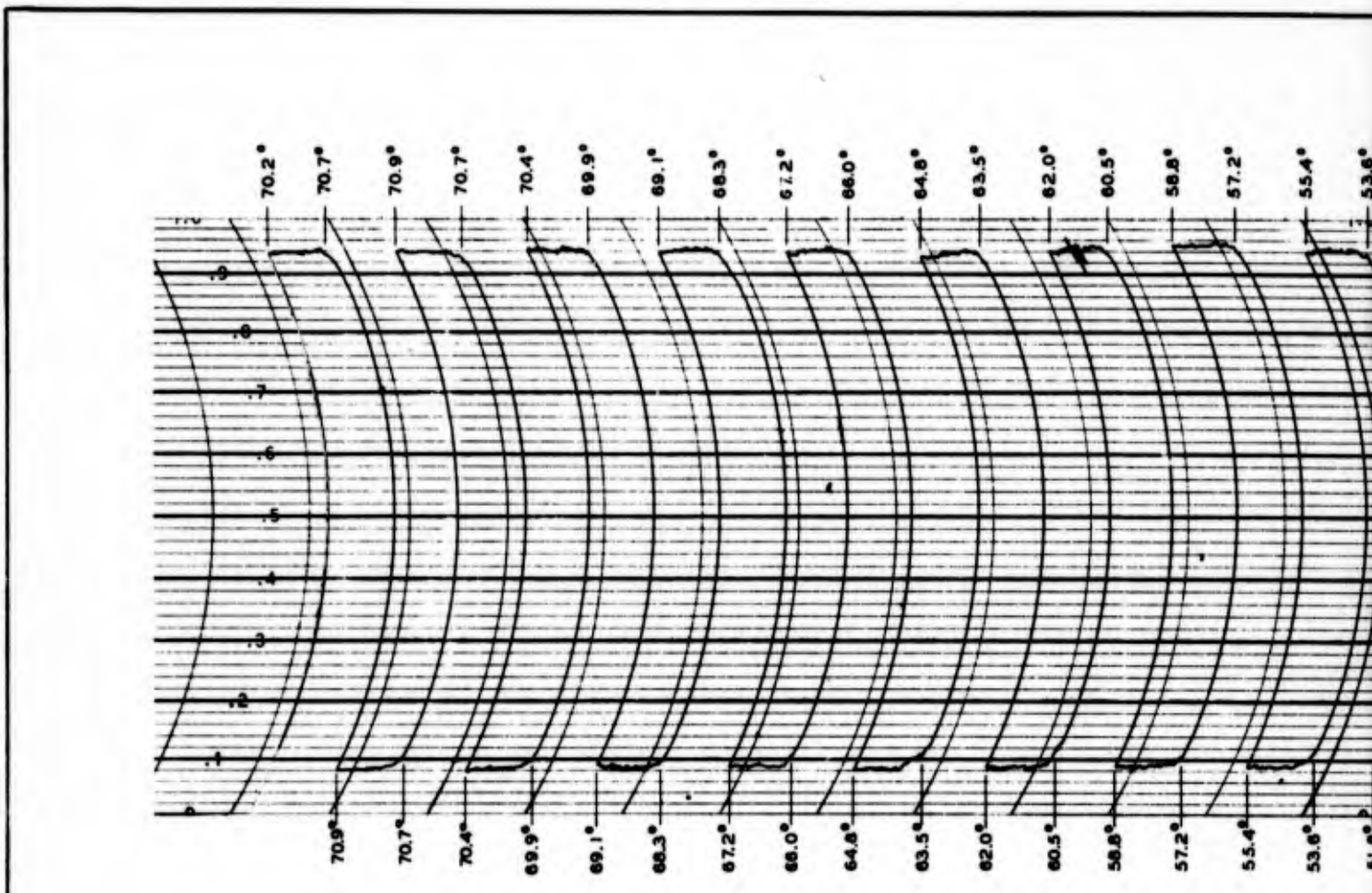

COMPARISON OF RADIATION RECEIVED FROM

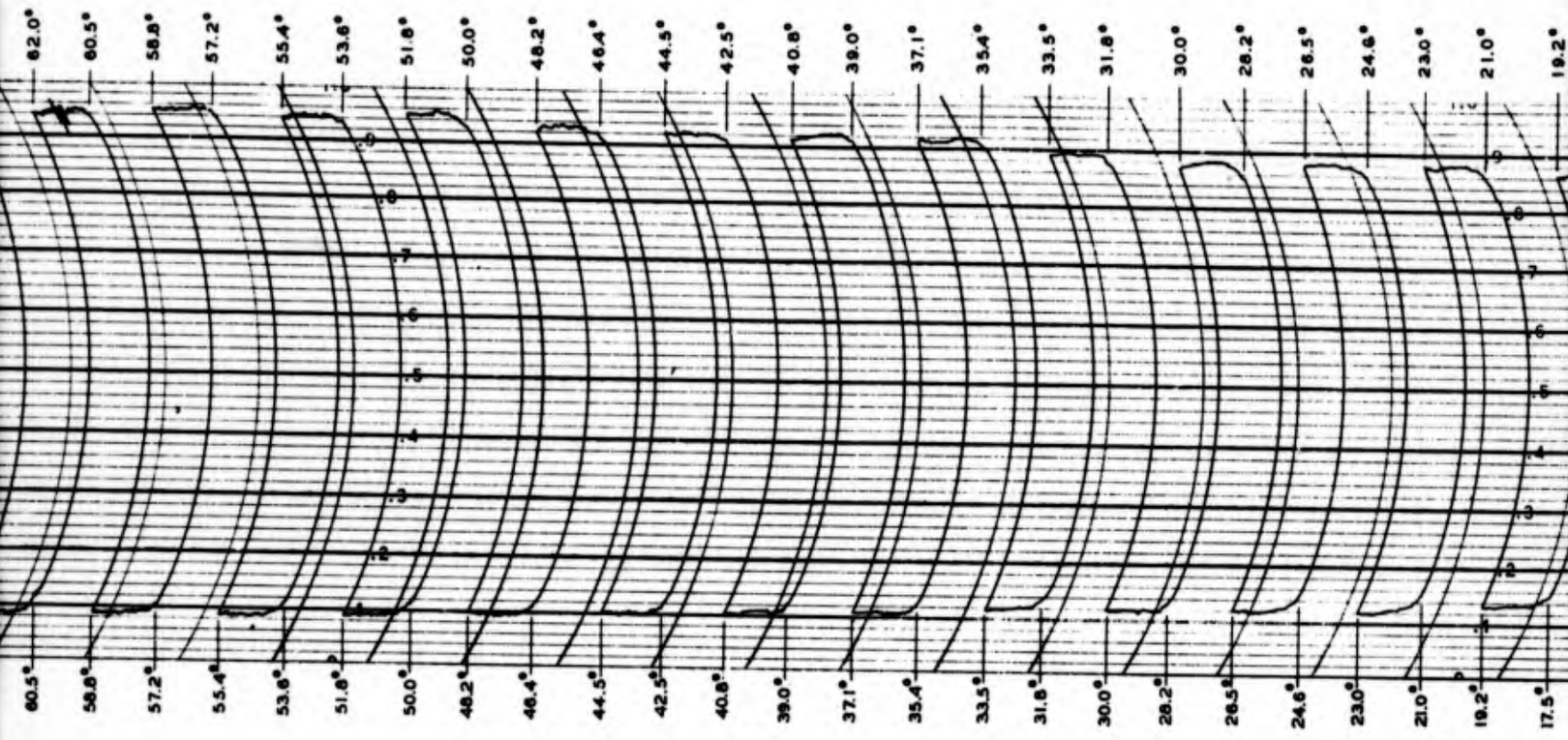

FIG. 4.2

DIATION RECEIVED FROM SUN AND RADIATION RECEIVED FROM FREE SPACE FOR IDENTICAL PATHS THROUGH EA

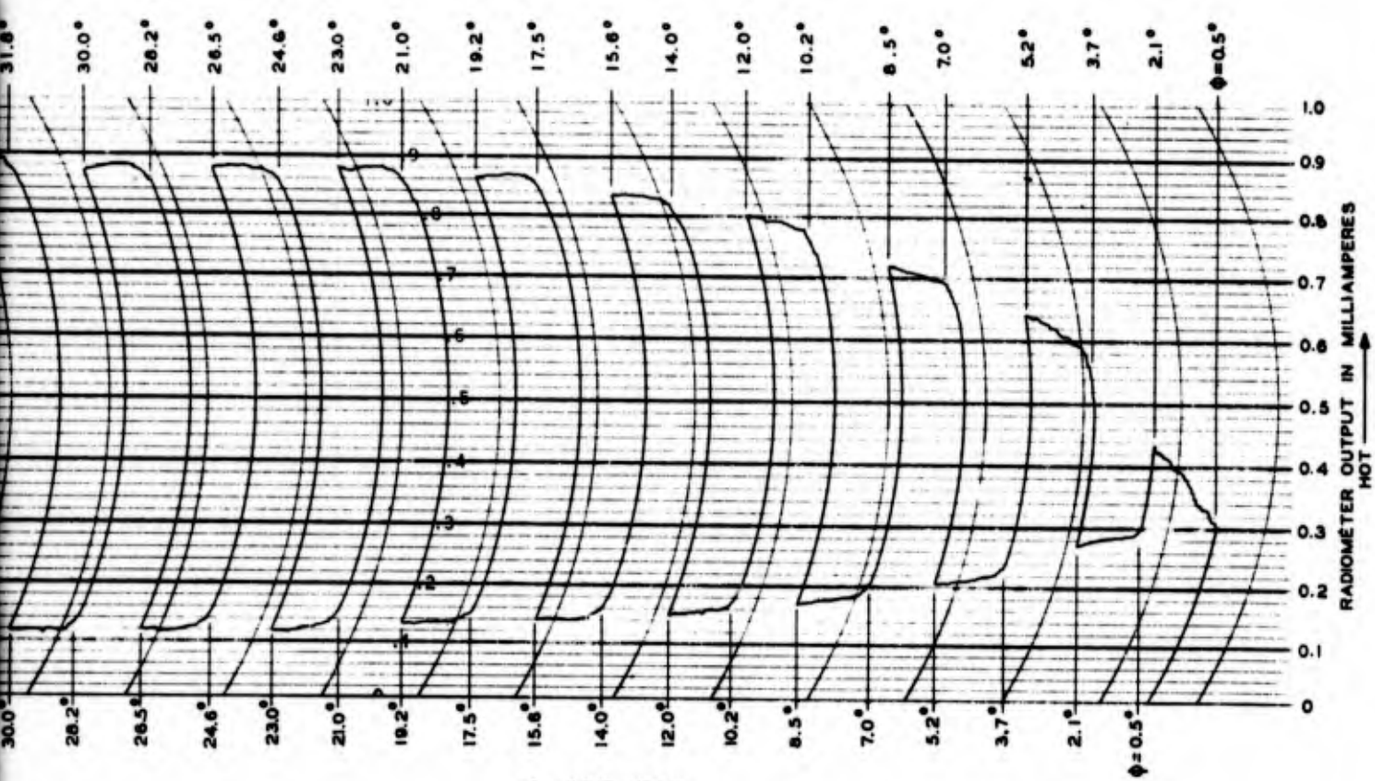

7 JUNE 1949

Φ = ELEVATION ANGLE

R IDENTICAL PATHS THROUGH EARTH'S ATMOSPHERE

The antenna factor, C, is $\frac{1}{4\pi}\int_{sun} G d\Omega$. The peak gain of the antenna (30" diameter paraboloid) was measured by comparing it with a standard horn. Then $\int_{sun} G d\Omega$ was evaluated graphically from the measured antenna pattern and peak gain. The absorption, a_o was evaluated by the first method discussed in Section 2.1.3.

The hot load for calibrating the radiometer is substituted for the antenna feed. Therefore, since the measured antenna gain includes the feed losses, no correction for waveguide losses in the radiometer is required.

The results of several measurements of the black body temperature of the sun are shown in the following table.

SUN TEMPERATURE DATA

λ = 1.25 cm.

Antenna Gain = 42.3 db.

Date	Loss Due to Atmosphere (nepers)	$T_r - T_\theta$ ($^\circ$K.)	Apparent Sun Temperature ($^\circ$K.)	Solid Angle Subtended by Sun-Steradians
7 June 1949	0.04	1040	13,400	6.60×10^{-5}
21 July 1949	0.113	576	10,100	6.60×10^{-5}
22 July 1949	0.04	966	12,600	6.60×10^{-5}
25 July 1949	0.071	734	10,300	6.60×10^{-5}

It is seen from the preceding table that the sun temperatures are not constant. Whether this is due to experimental errors or not is difficult to say. At any rate, there is certainly room for error in determining the atmospheric absorption, although this determination has been made as carefully as possible. The difficulty may lie in the fact that the atmosphere may be lumpy; consequently, the method of measuring absorption by tipping experiments may be in error.

The average of all measurements is 11,600°K. This figure is somewhat higher than that quoted by Dicke and Southworth.

Dicke[15] quoted two measurements of 10,000°K. and 11,000°K. respectively for 9 July 1945 and 12 July 1945. Southworth[16] reports temperatures of approximately 5000°K. neglecting absorption effects.

No definite reason for the discrepancies can be advanced, although the greatest possibility for error may be in the measurement of the antenna gain and the determination of the atmospheric absorption.

4.2.2. Moon Studies

A number of measurements on the moon have been made at wavelengths of 1.8 cm. and 1.25 cm. The 1.25 cm. measurements were made with the K-band radiometer described in Section 3.2.3. The radiation received from the moon is small due to the fact that the moon is not very hot, and the antenna accepts only part of the total radiation. For this reason the gain required in the radiometer was high and it was necessary to "balance out" the "cold" background reading which was 8 or 9 times as large as the desired temperature difference between the moon and its fore and background.

4.2.2.1 Moon Temperature Measurements

The results of several measurements indicate that the moon radiates at a wavelength of 1.25 cm. as much energy as a black body would at a temperature of 260°K.

The measurements were made in the same manner as the sun measurements described in Section 4.2.1. As before, the apparent black body temperature of the moon, T_{moon}, was found from the difference of the antenna temperature measured when the antenna was pointed first at the moon and then at free space at the same elevation angle. Thus:

$$T_{moon} = \frac{4\pi\,(T_r - T_\theta)}{\int_\Omega G\,d\Omega \cdot e^{-2a_0 \sec\theta}} \qquad 4.3$$

Ω is the solid angle subtended by the moon

The average experimental values obtained are given below:

$$\frac{T_r - T_\theta}{e^{-2a_0 \sec\theta}} = 24^\circ \text{ K.};$$

[15] Dicke and Beringer, "MICROWAVE RADIATION FROM THE SUN AND MOON," The Astrophysical Journal, May, 1946.

[16] Marton, "ADVANCES IN ELECTRONICS," Academic Press, Inc., Book 6, 1948, p. 377.

peak gain of antenna = 42.3 db. relative to isotropic;
and $\int_{\text{solid angle subtended by moon}} G d\Omega = 1.16$

$$\therefore T_{moon} = \frac{4\pi\,(24)}{1.16} = 260^{\circ}\ \text{K.}$$

This value is less than that measured by Dicke et. al.[17] which was 293° K. However, for a difficult measurement such as this, the agreement can be considered quite good. Much better data could be obtained with larger antennas, providing the gain of the larger antenna can be measured accurately.

4.2.2.2 Moon Eclipse Measurements

The radiation from the moon at a wavelength of 1.25 cm. was also measured during the total eclipse of 12 April 1949. Figure 4.3 is a photograph of the actual data obtained.

The effects of "balance" changes in the radiometer which occur over fairly long periods of time were eliminated by continuously comparing the antenna temperatures measured when the antenna is pointed alternately at the moon and then away from the moon. In this particular case the antenna followed the moon for approximately a seven-minute period; then the declination was increased by five degrees and the antenna allowed to follow a path in space for seven minutes. The hour angle axis of the antenna mount was driven at constant speed with corrections made during the seven-minute period when the antenna was not following the moon to compensate for the difference between the motion of the moon and the antenna.

Since the molecular absorption due to water vapor in the earth's atmosphere is appreciable at this wavelength, the antenna temperature measured for a path five degrees in declination above the moon had to be corrected to the value which would have been obtained if the antenna were pointing along the path traveled by the moon in the previous seven-minute interval.

[17] Dicke and Beringer, "MICROWAVE RADIATION FROM THE SUN AND MOON", The Astrophysical Journal, May, 1946.

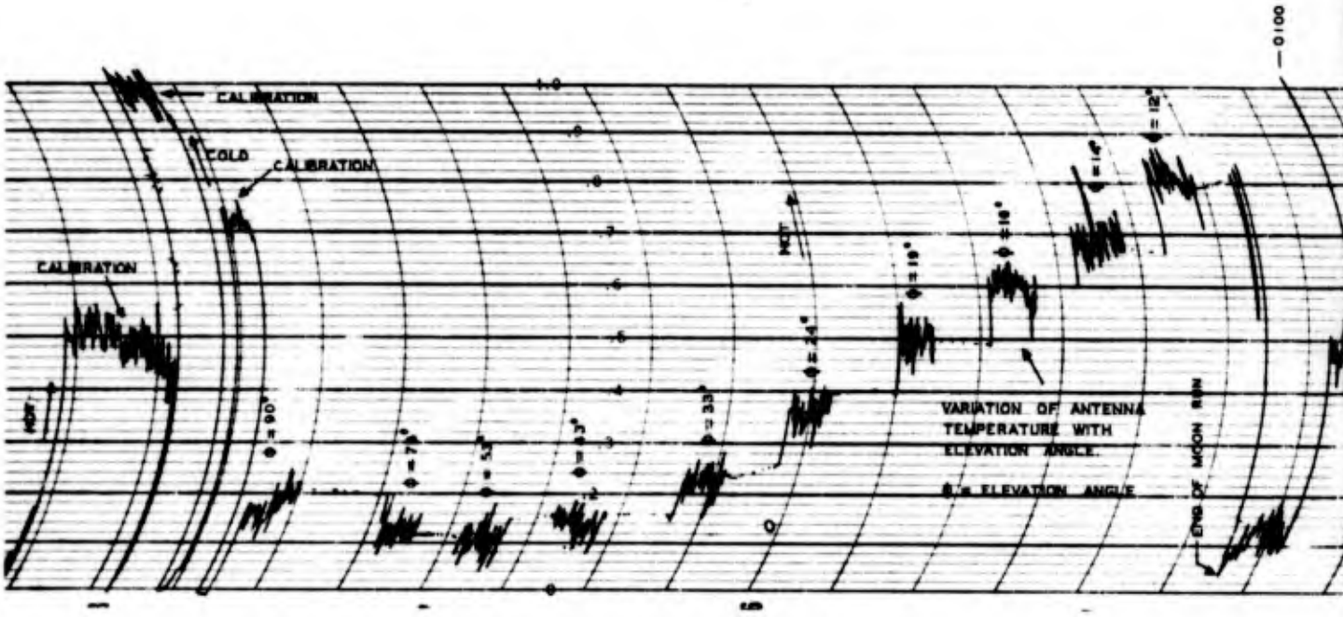
CALIBRATION
COLD
CALIBRATION
CALIBRATION
1.0
.9
.8
.7
.6
.5
.4
.3
.2
.1
0
NOT
VARIATION OF ANTENNA
TEMPERATURE WITH
ELEVATION ANGLE.
θ = ELEVATION ANGLE
END OF MOON RUN
0100

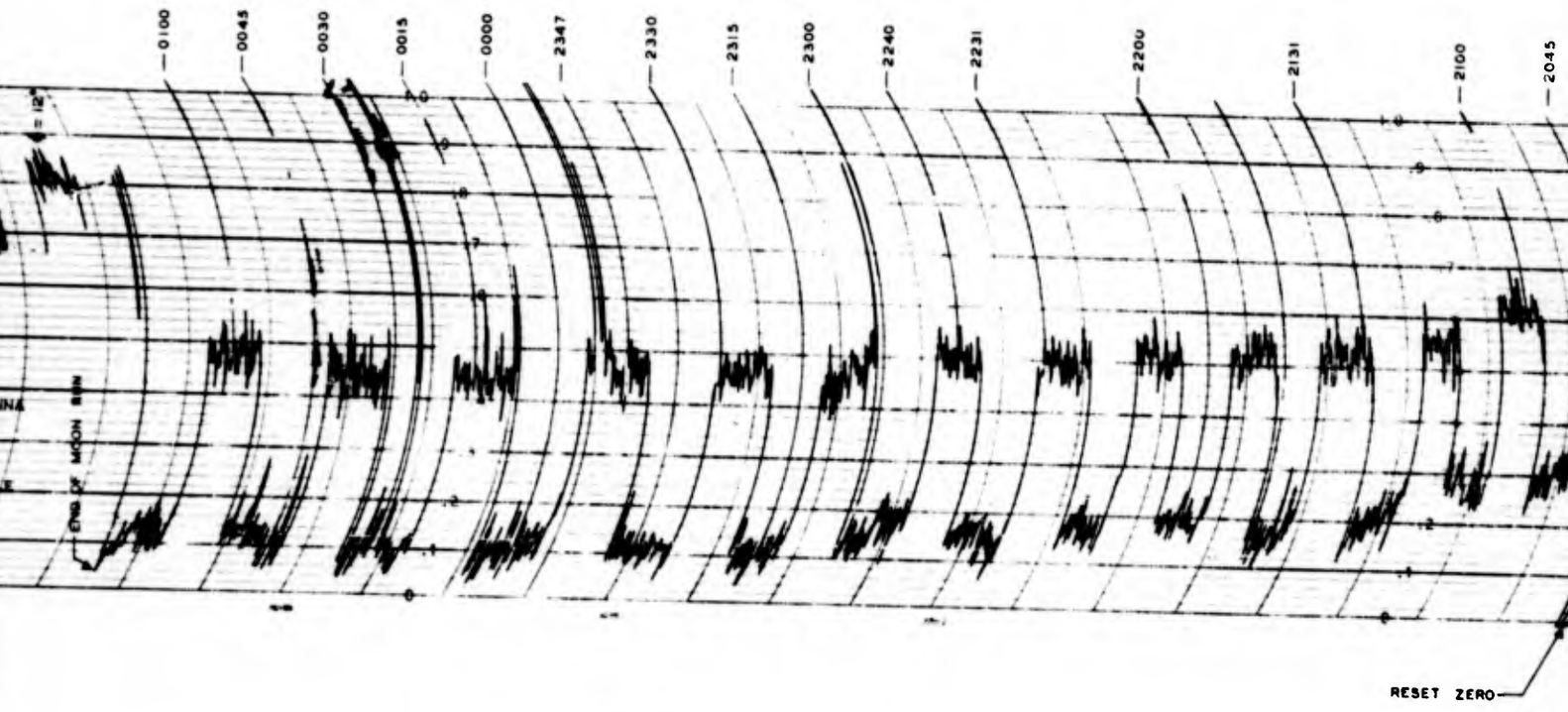

FIG. 4.3

MOON ECLIPSE DATA

12 APRIL 1949

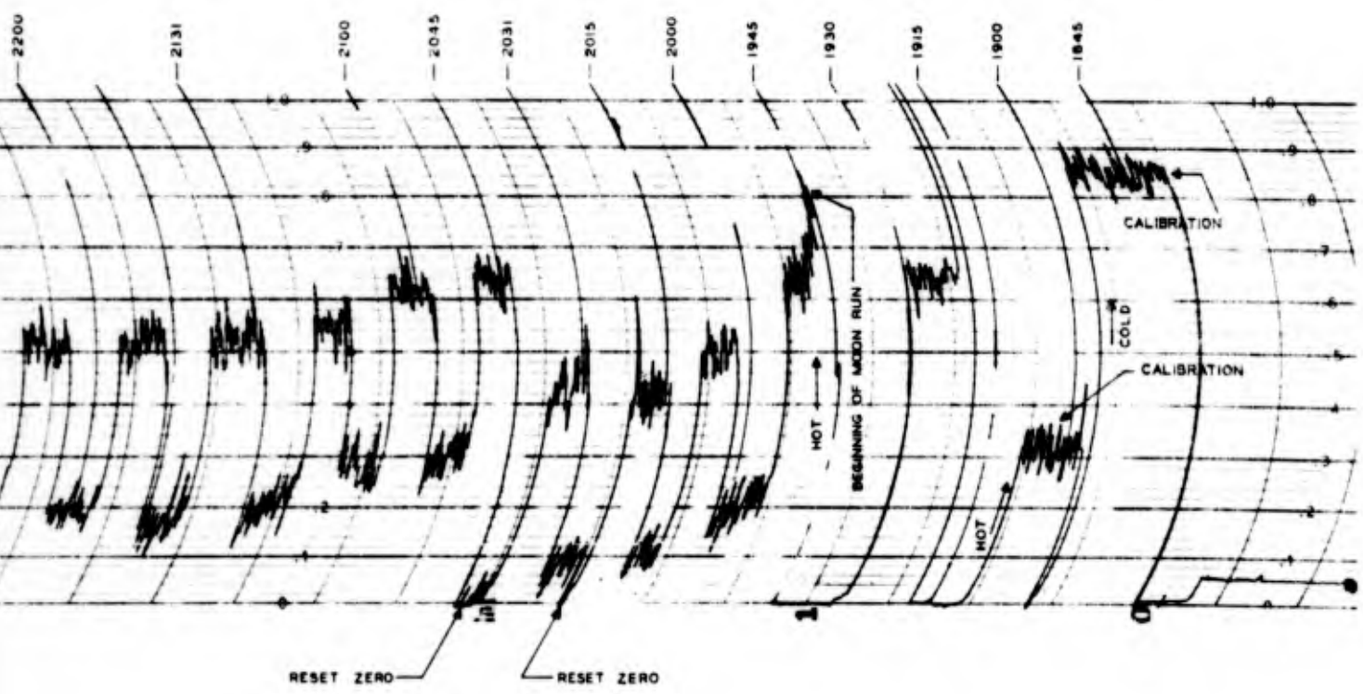
2200
2131
2100
2045
2031
2015
2000
1945
1930
1915
1900
1845
CALIBRATION
COLD
CALIBRATION
HOT
BEGINNING OF MOON RUN
HOT
RESET ZERO
RESET ZERO

The data shows that the fluctuations were appreciable compared to the total temperature difference being measured. In general, the maximum fluctuation was ± three degrees compared to a total temperature difference of 23 degrees. The large spikes on the chart, exclusive of the time markers, were due to external interference.

Reduction of the data was accomplished by averaging the meter readings in the immediate vicinity of each discontinuity representing the time when the antenna was changed from the moon to space. The differences of these readings were converted to temperature differences by means of the calibrations taken at the beginning and end of the run. The temperature differences after correction for different path lengths and atmospheric absorption yield a temperature which is equal to the apparent K-band temperature of the moon multiplied by the antenna constant.

The reduced data is shown in Figure 4.4. The average value appears to be constant, indicating within the limits of experimental error, that the radiation from the moon was no different during the total eclipse than when fully illuminated by the sun.

Figure 4.5 is a similar set of data taken at a wavelength of 1.87 cm. This data was taken with the radio sextant. Since the radio sextant output is not a direct function of incident power, it was necessary to measure the error voltage as a function of angular distance between moon and antenna. In Section 3.2.4 it is shown that the slope of the error voltage curve is proportional to the source temperature which, in this case, is the moon. Due to equipment difficulties the observations at this wavelength were not started until after the eclipse began.

Neither set of data indicates a significant change when the moon is obscured from the sun by the earth. This, however, is about the only conclusion that can be drawn, in view of the spread in the measured data.

Resorting to the theory of thermal radiation, it is possible to arrive at some expressions which show that the moon's radiation at these wavelengths should not decrease greatly during the eclipse.

4.2.2.3 Analysis of Expected Energy from the Moon at One Centimeter

The received energy from the moon is of two distinct types; energy from the sun reflecting from the moon's

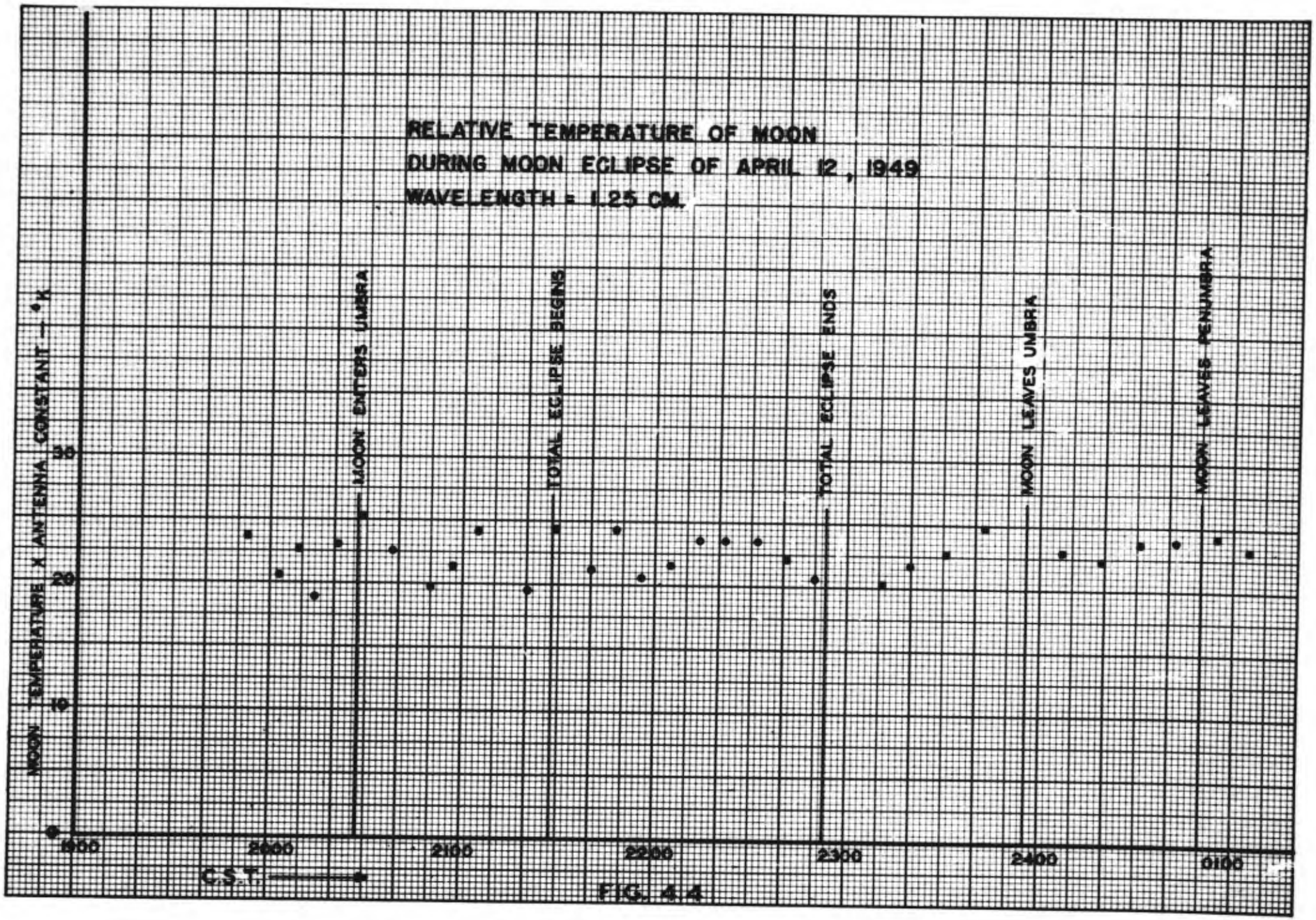
RELATIVE TEMPERATURE OF MOON
DURING MOON ECLIPSE OF APRIL 12, 1949
WAVELENGTH = 1.25 CM.
MOON TEMPERATURE X ANTENNA CONSTANT — °K
30
20
10
MOON ENTERS UMBRA
TOTAL ECLIPSE BEGINS
TOTAL ECLIPSE ENDS
MOON LEAVES UMBRA
MOON LEAVES PENUMBRA
1900
2000
2100
2200
2300
2400
0100
C.S.T.

FIG. 4.4

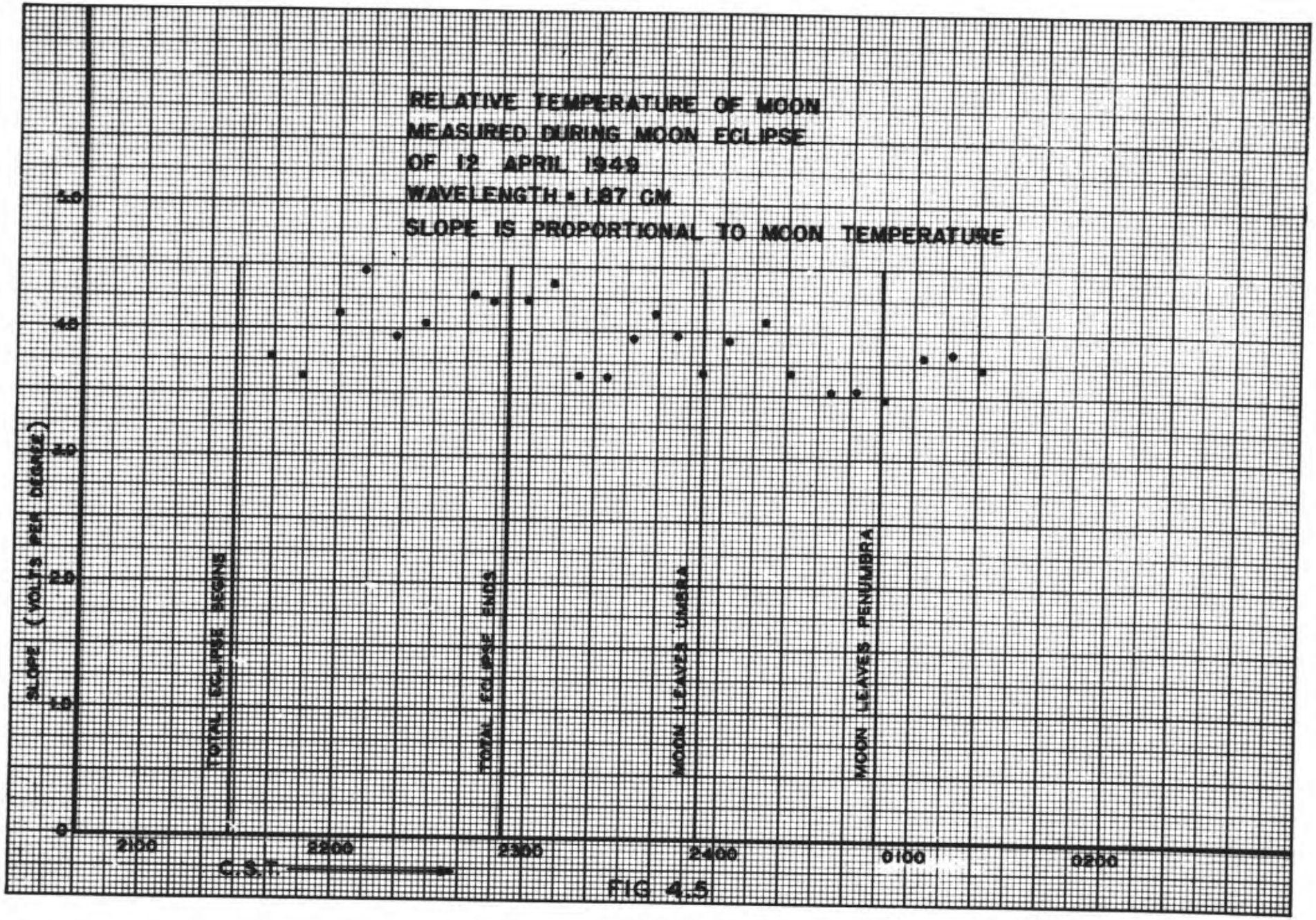
RELATIVE TEMPERATURE OF MOON
MEASURED DURING MOON ECLIPSE
OF 12 APRIL 1949
WAVELENGTH = 1.87 CM.
SLOPE IS PROPORTIONAL TO MOON TEMPERATURE
SLOPE (VOLTS PER DEGREE)
50
40
30
20
10
0
TOTAL ECLIPSE BEGINS
TOTAL ECLIPSE ENDS
MOON LEAVES UMBRA
MOON LEAVES PENUMBRA
2100
2200
2300
2400
0100
0200
C.S.T.

FIG 4.5

surface and thermal radiation from the moon itself due to its own temperature. The former will be considered first.

Enough is known about the surface of the moon to predict how the moon will reflect one cm. energy. If the moon were assumed to be a perfectly smooth sphere, the reflected energy received by an antenna on the earth would be expected to come from a single small area at the nearest surface. This is obviously not the case for reflections in the light spectrum, and it most probably is not the case for reflections in the one cm. region. Due to the lack of atmosphere the surface of the moon is probably even rougher and more irregular than that of the earth, which is usually considered to act much like an isotropic reflector. Therefore, the reasonable assumption seems to be that the moon acts as an isotropic reflector for one cm. energy; i.e., it presents a disk equal in area to the projected area of the sphere when fully illuminated by the sun.

For this case, equation 2.25 may be used to compute the reflected energy that an antenna would receive when directed at the moon.

For the sun, assume $M_s = 0$ and $aT = 10,000^\circ$ K. The sun subtends a solid angle of 0.68×10^{-4} steradians at the moon. Thus, equation 2.25 becomes:

$$P_r = \frac{K\Delta f}{4\pi} (m_r)(10^4)(0.68 \times 10^{-4}) \frac{1}{4\pi} \int_\Omega G(\theta, \phi)\, d\Omega$$

$$= K\Delta f\ m_r\ (0.0541) \frac{1}{4\pi} \int_\Omega G(\theta, \phi)\, d\Omega$$

This yields an equivalent antenna temperature of

$$T_r = (m_r)(0.0541) \frac{1}{4\pi} \int_\Omega G(\theta, \phi)\, d\Omega \quad (^\circ K)$$

The maximum value that the antenna factor and the reflectivity of the moon's surface can assume is unity. Hence, the maximum antenna temperature possible due to reflected energy from the moon is 0.0541°K., which is far below the maximum sensitivity of 3° K for the K-band radiometer.

From the numerical result above, it may be concluded that no moon temperature change should be detected due to the change in reflected energy at different degrees of illumination, and that the energy received from the moon is due to thermal radiation from the moon itself.

Some assumptions must of necessity be made in computing the total energy received from the moon due to thermal radiation from the surface material. Equation 2.13 will be used for this computation. Obviously not enough is known about the moon's surface to predict how n, a, and T will vary with θ and ϕ. Therefore, it will be assumed that they are constants with respect to these variables. Also, it must be assumed that a does not vary with z. With these assumptions equation 2.13 becomes:

$$P_r = 2K\Delta f\ (1 - m) \left[\int_0^d e^{-2az} aT(z)dz\right] \frac{1}{4\pi} \int_\Omega G(\theta, \phi)d\Omega$$

This yields an equivalent antenna temperature of

$$T_r = 2(1 - m) \left[\int_0^d e^{-2az} aT(z)dz\right] \frac{1}{4\pi} \int_\Omega G(\theta, \phi)d\Omega \qquad 4.4$$

The formulation of $T(z)$ for the moon can be done only on a hypothetical basis. Temperature measurements of the moon's surface have been made during different degrees of illumination. The surface temperature has been measured to vary from +100°C at noon to -50°C at sunset and to -150°C at midnight. Measurements made during eclipses of the moon indicate that the surface temperature may fall 150°C in an hour and as much as 220°C during a total eclipse. Such rapid cooling of the surface when sunlight is withdrawn is due partly to the absence of an atmospheric blanket, and partly to the low heat conductivity of the surface material. In fact the cooling of the surface is rapid enough to indicate that the heat conductivity of the surface material is so low that the temperature a foot under the surface of the moon remains at about 0°C, regardless of the surface temperature. This fact gives some insight into what function $T(z)$ follows.

From theoretical work employing the heat flow equation and assumed boundary conditions, it appears that during full illumination the temperature will vary approximately exponentially with depth. Assuming this to be the case:

$$T(z) = (T_s - T_d)\, e^{bz} + T_d \qquad 4.5$$

where T_s = surface temperature

T_d = temperature at a considerable distance beneath surface

b = factor in the exponential giving the rate of decay of temperature with depth

Substituting equation 4.5 for $T(z)$ in equation 4.4 and performing the integration yields,

$$T_r = 2(1-m)\left[\frac{(T_s - T_d)\, a(1 - e^{-(2a+b)d})}{2a+b} + \frac{T_d}{2}\,(1 - e^{-2ad})\right] \frac{1}{4\pi}\int_\Omega G(\theta, \phi)\, d\Omega \qquad 4.6$$

"d" is any distance inside the moon where the absorption from the surface to "d" is essentially complete. Hence, e^{-2ad} and $e^{-(2a+b)d}$ are zero and equation 4.6 reduces to

$$T_r = (1-m)\left[\frac{(T_s - T_d)2a}{2a+b} + T_d\right] \frac{1}{4\pi}\int_\Omega G(\theta, \phi)\, d\Omega \qquad 4.7$$

Although many assumptions have been made in its derivation, equation 4.7 should represent the true situation with sufficient accuracy to permit the derivation of some conclusions from it. In view of the temperatures mentioned before, T_s must vary from about 393°K to 173°K during an eclipse of this duration, while T_d is constant at about 273°. The fact that no appreciable temperature change could be detected at 1.8 cm. and at 1.25 cm. during the eclipse of 12 April 1949 therefore indicates that b is much larger than a.

If, as suggested before, the temperature a foot under the moon surface remains essentially constant at about 273° K., b must be in the neighborhood of 0.1 nepers per centimeter. In other words, this value of b decreases the temperature from 393°K. to within 5.7° of 273°K. in one foot. An estimate of the value of a can be made by comparing the attenuation constants of like substances on earth, taking into account the absence of moisture in the moon's surface layer.

At these wavelengths, it is felt that a value between 0.005 and 0.01 nepers/cm. is representative. Thus, it is concluded that b should be larger than a, perhaps by a factor of ten.

Equation 4.7 may be used to compute, approximately, the effective black body temperature of the moon in the one-centimeter region. For a = 0.01 nepers per centimeter, b = 0.1 nepers per centimeter, T_s = 393°K. and T_d = 273°K, equation 4.7 gives:

$$T_r = (1 - m)\ 293\ \frac{1}{4\pi} \int_\Omega G(\theta, \phi)\, d\Omega$$

Some insight may be gained on choosing a value for "m" by appealing to astronomical data. The albedo of the moon has been measured to be 0.07. Undoubtedly for one-centimeter wavelengths, "m" will not be exactly equal to the moon's albedo, but this is the best estimate available. Accordingly, "m" will be taken as 0.07. This yields:

$$T_r = 272 \cdot \frac{1}{4\pi} \int_\Omega G(\theta, \phi)\, d\Omega$$

This temperature (272°K.) compares favorably with the 260° measured at 1.25 cm. However, the result was gained only to show that equation 4.7 gives moon temperatures in the correct range.

Another factor must be considered in analyzing the temperature variation with depth during an eclipse. When illuminated for a long period of time, the temperature should decrease approximately exponentially with depth. However, when the moon is shadowed, the surface temperature drops rapidly below the temperature a short distance under the surface. The heat flow equation may be solved for this case. The general shape of the resulting curve is indicated in Figure 4.6.

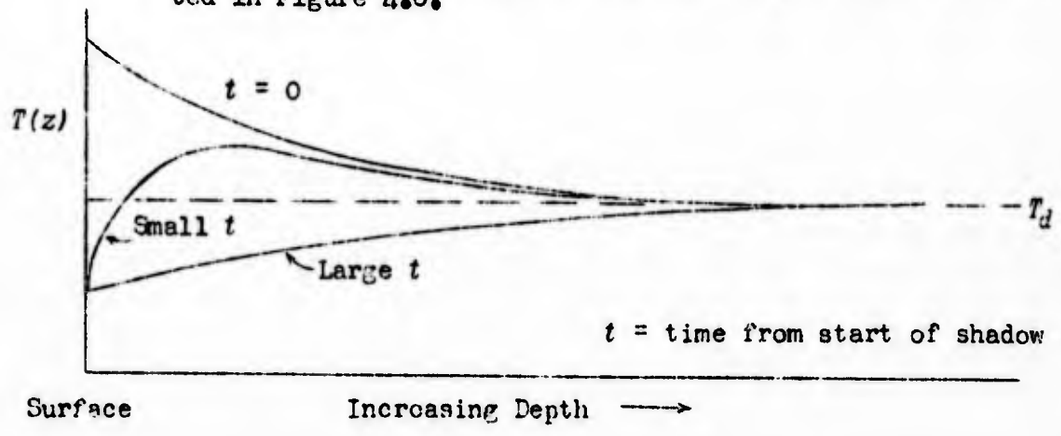

Figure 4.6

A temperature variation such as indicated for "small t" does not lead to a marked decrease in black body temperature of the moon in the one-centimeter wavelength region during an eclipse, due to the existence of higher temperatures than the surface temperature only slightly beneath the surface. However, for long periods of shadow, the "large t" curve of Figure 4.6 is approached, presenting the possibility that the temperature of the moon at a wavelength of one-centimeter might change slightly from new to full moon.

This analysis has not been intended to be rigorous in all respects. It was intended to theoretically justify the inability to detect a temperature change during the moon eclipse of 12 April 1949. Equation 4.7, although its derivation involved many approximations, shows that the black body temperature of the moon may be relatively independent of the surface temperature for wavelengths one centimeter and longer. This condition is approached by a surface layer which is a very low loss dielectric and a good heat insulator.

REFERENCES

Baker, R. H., "Astronomy", VAN NOSTRAND, New York, 1938

Beers, Yardley, "Noise Figure and Measurement", MIT. RAD. LAB REPORT 746, July, 1945

Bergman and Fett, "Theory and Application of the Parallel T Resistance Capacitance Network", ELECTRICAL ENGINEERING DEPARTMENT, University of Illinois, Urbana, Illinois, 27 April 1948

Beringer, R.E., "The Absorption of One-Half Centimeter Electromagnetic Waves in Oxygen", THE PHYSICAL REVIEW, 1 July 1946

Burgess, R. E., "Ground Absorption with Elevated Vertical and Horizontal Dipoles", WIRELESS ENGINEER, Vol. 26, April 1949

Dicke, R. H., "The Measurement of Thermal Radiation", REVIEW OF SCIENTIFIC INSTRUMENTS, July 1946

Dicke, R. H. and Beringer, R. E., "Microwave Radiation from the Sun and Moon", THE ASTROPHYSICAL JOURNAL, May 1946

Dicke, R. H., Kyhl, Vane and Beringer, "The Absorption of Atmospheric Water-Vapor in the K-Band Region", McGRAW-HILL BOOK COMPANY, January 1946

Dutton, B., "Navigation and Nautical Astronomy", UNITED STATES NAVAL INSTITUTE, 1943

Friis, H. T., "Noise Figures of Radio Receivers", PROCEEDINGS OF THE I.R.E., July 1944

Graham, R. E., "Linear Servo Theory", BELL SYSTEM TECHNICAL JOURNAL, October 1946

Greenwood, Holdam and MacRae, "Electronics Instruments", Vol. 21, McGRAW-HILL BOOK COMPANY, New York, 1948

Hopper and Miller, "Design of Radar I.F. Amplifiers", PROCEEDINGS OF THE I.R.E., November 1947

Krauss, H. L., "Graphical Solutions for Cathode Followers", ELECTRONICS, January, 1947

Marton, L., "Advances in Electronics", ACADEMIC PRESS INC., 1948

North, D. O., "Fluctuations in Space-Charged Currents at Moderately High Frequencies", RCA REVIEW, 1941-42

North, H. Q., "A Comparison of Silicon and Germanium Crystals as Harmonic Generators of 4 mm and 6 mm Waves", G.E. REPORT, January 1946

North, H. Q., "Properties of Welded Contact Germanium Rectifiers", JOURNAL OF APPLIED PHYSICS, November 1946

Pound, R. V., "Microwave Mixers", Vol. 16, McGRAW-HILL BOOK COMPANY, New York, 1948

Reber and Greenstein, "Radio Frequency Investigations of Astronomical Interest", OBSERVATORY, London, February 1947

Richtmeyer and Kennard, "Introduction to Modern Physics", McGRAW-HILL BOOK COMPANY, New York, 1942

Russell, Dugan and Stewart, "Astronomy I: The Solar System", GINN AND CO., 1945

Southworth, G. S., "Microwave Radiation from the Sun", JOURNAL OF THE FRANKLIN INSTITUTE, April 1945

Torrey, Whitmer, "Crystal Rectifiers", Vol. 15, McGRAW-HILL BOOK COMPANY, New York, 1948

Valley and Wallman, "Vacuum Tube Amplifiers", Vol. 18, McGRAW-HILL BOOK COMPANY, New York, 1948

Van Voorhis, "Microwave Receivers", Vol. 23, McGRAW-HILL BOOK COMPANY, New York, 1948

Wallman, Macnee and Gadsden, "A Low Noise Amplifier", PROCEEDINGS OF THE I.R.E., June 1948